

**Studies of Cryothermal Ablation for the Treatment of Atrial
Fibrillation**

A DISSERTATION
SUBMITTED TO THE FACULTY OF THE GRADUATE SCHOOL
OF THE UNIVERSITY OF MINNESOTA
BY

Ryan Patrick Goff

IN PARTIAL FULFILLMENT OF THE REQUIREMENTS
FOR THE DEGREE OF
DOCTOR OF PHILOSOPHY

Paul Anthony Iaizzo

April 2014

© Ryan Patick Goff 2014

Acknowledgements

The works included in this thesis would not be possible with support from many others, including family, friends, and colleagues. One of the things that first drew me to the lab during first year laboratory rotations was the team atmosphere and the creativity of the members. I have been privileged to work alongside and collaborate with this bright group of people, whom despite the occasional long hours maintain a positive attitude and amazing sense of humor. I feel very lucky to call you my colleagues and even more importantly, my friends: Mike Bateman, Chris Rolfes, Julianne Spencer, Steve Howard, Steve Quallich, Brian Howard, Asish Singal, and Mark Benscoter.

I would like to offer my sincere gratitude to the Visible Heart Lab staff and students for their invaluable input during my tenure in the lab. Particularly, I would like thank Monica Mahre for her expertise in manuscript preparation and keeping the lab running like a well-oiled machine. Gary Williams, I am grateful for your technical expertise and assistance with all things electronic and digital. Bill Gallagher, Charles Soule, and Tinen Healy thank you for your experimental input, dedication to the students in the lab, tireless hours conducting studies, and endless patience.

To my family I dedicate this work. Without your unwavering support of my endeavors from a young age I would not be where I am today. No matter where I go in life I will always be thinking of you.

I would like to extend a very special thank you to Paul Iaizzo. As a mentor, you are without a doubt unparalleled. This simple thank you cannot express the gratitude I have for my time in your laboratory. You have been a great role model academically, creatively, and personally. Your tireless efforts and great sense of humor have made working with you an amazing, enjoyable experience. Thank you.

Dedication

This work is dedicated to my family whom have always supported my endeavors and nurtured my curiosity.

Katie, my little sister who I'll always try to watch after, but has truly taught me about living and the need to do what you love.

Erik, you've always been my big brother and led with big shoes to fill. I've always looked up to you and admired you, your pursuits, and great family.

Linda, you've always been there for me and offered positive, loving advice. You truly are the best mother a son could have and I aspire to be like you in so many ways both personally and professionally.

Pat, you taught me so much as a child that no doubt has shaped who I am and what I do today. You always fostered my love of science and mechanics.

Abstract

Atrial fibrillation (AF) remains as the most prevalent tachyarrhythmia, with a prevalence in the U.S., of 1% in the general population. The current therapeutic/treatment paradigm for the patient with atrial fibrillation, is to first attempt to restore normal rhythm via anti-arrhythmic pharmaceuticals. If this does not ameliorate the problem, or the patient does not well tolerate the drug side-effects, a transcatheter ablation is usually performed. The relatively recent introduction of cryoballoon based ablation has provided the electrophysiologist with an easier method of treating AF via pulmonary vein isolation. However, despite current clinical use research questions regarding anatomy, dosing, and device-tissue interactions have remained unanswered.

Anatomical studies of the phrenic nerve, coronary sinus, left atria, and pulmonary vein anatomy were performed using high-resolution MRI and direct measurements on heart specimens. These novel anatomical studies may guide future device iterations and the computer based models used for numerical simulation. The amount of cooling required to injure and/or kill cardiac tissue, lung tissue, and the phrenic nerve was quantified using novel in-vitro models. These data may be used for procedural modeling and dosing optimization. Device-tissue interactions were studied using a functional, isolated heart-lung bloc model and a patent has been filed for this methodology. Using this model infrared imaging was performed to quantify the level of cooling being achieved by cryoballoon catheters. A separate study was performed using MRI to quantify ice dynamics and to our knowledge is the first cardiac cryoablation performed in an MR environment. This collection of work will aid the clinical, scientific, and engineering communities in further optimization of cardiac cryoablation.

Table of Contents

List of Tables.....	vii
List of Figures	viii
Introduction:.....	1
I- Section 1 Anatomical Aspects of Ablation:	7
I.I- Chapter 1: Phrenic Nerve Anatomy	8
I.I.I- High-Resolution MRI Reconstructions of Human Phrenic Nerve Anatomy in Relation to the Pulmonary Veins and Computational Modeling of Cryoballoon Ablative Therapy	9
Introduction	9
Methods.....	11
Results.....	13
Discussion	18
Conclusion.....	19
I.II- Chapter 2: Coronary Sinus Anatomy.....	20
I.II.I- Anatomical considerations that contribute to applied ablations in the coronary sinus and/or mitral isthmus for the treatment of atrial fibrillation	21
Executive Summary	22
Introduction	23
Methods.....	24
Results.....	28
Discussion	31
Conclusions	33
I.III- Chapter 3: Anatomy of the Human Heart of AF Versus Non-AF Patients	35
I.III.I- Cardiac remodeling as a consequence of atrial fibrillation: An anatomical study of perfusion-fixed human heart specimens	36
Executive Summary	36
Introduction	36
Methods.....	39
Results.....	41
Discussion	46
Conclusion.....	48
I.IV- Chapter 4: Imaging of balloon based catheters using Visible Heart methodologies	49
I.IV.I- The Path of a Swan Ganz Catheter Visualized through a Beating Human Heart.....	50
I.IV.II- Multimodal imaging of a cryoballoon ablation within a reanimated hearts.	55
I.V- Concluding Remarks	59
II- Section 2 Assessment of Cryothermal Injury.....	60
II.I- Chapter 5: Determination of Cryothermal Injury Thresholds in Tissues Impacted by Cardiac Cryoablation	61
Background	61
Methods.....	63

	v
Results	67
Discussion	72
Conclusions	73
II.II- Chapter 6: Development of a high-throughput, in-vitro model to assess ablation parameters and modalities	74
Introduction	74
Methods	75
Results	76
Discussion	80
II.III- Chapter 7: In Vitro Assessment of Induced Phrenic Nerve Cryothermal Injury	83
Executive Summary:	84
Introduction	84
Methods	90
Results	94
Discussion	96
Conclusions	96
II.IV- Concluding remarks	97
III- Section 3 Investigation of Device-Tissue Interactions	98
III.I- Chapter 8: The Novel In-vitro Reanimation of Isolated Human and Large Mammalian Heart-Lung Blocs	99
Executive Summary	99
Background	100
Method	101
Results	104
Discussion	110
Acknowledgements	112
III.II- Chapter 9: Infrared imaging of cryoballoon ablation therapy applied to reanimated swine and human heart-lung blocs	113
Introduction	113
Methods	115
Results	118
Discussion	124
III.III- Chapter 10: Magnetic Resonance Imaging of Ice Dynamics During Cryoballoon Ablation	127
Introduction:	127
Methods:	127
Results:	129
Discussion:	132
III.IV- Concluding Remarks	134
Thesis Summary	135
References	137
Appendices	151
Appendix A: Published or Accepted Conference Abstracts	151
In-Vitro Assessment of Phrenic Nerve Cryothermal Injury	151

In-Vitro Characterization of Myocardial Cryothermal Injury.....	153
Direct Visualization of Pulmonary Vein Ablations within Reanimated Swine Hearts to Investigate Recent Advances in Cryo-balloon Technologies.....	155
External Infrared Visualization of an Endocardial Cryoablation: Performed on a Reanimated Swine Heart.....	156
Novel visualization of iatrogenic atrial septal defects and ablation lesions in a reanimated human heart	158
MRI Reconstruction of Human Hearts and Their Relationship to Direct Measurements taken from Hypertensive Specimens	160
Left-sided Epicardial Pacing Via A Transvenous Lead Delivery	161
Functional In-Vitro Cardiac Tissue Model For The Evaluation of Ablation Parameters and/or The Use of Adjuvant Therapies.	164
Development of an Endocardial Cryoablation Catheter for Concomitant Delivery of Cryogenic Treatments and Adjuvants.....	165

List of Tables

Table 1: Donor specimen profiles.....	14
Table 2: Results of Tukey pairwise comparisons. Results shown graphically in Figure 9.	17
Table 3: Study population demographics for 30 perfusion-fixed human hearts presented as the mean \pm standard deviation.....	25
Table 4: Coronary Sinus Anatomical Parameters (n=30)	28
Table 5: Patient information from atrial fibrillation and their corresponding control hearts. For all but two AF hearts suitable matches were found as controls based on subject genders, ages, weights and heights for these collected specimens.	40
Table 6: The mean and median values of the pulmonary vein ostia between AF and control heart specimens.....	42
Table 7: Muscle bundle length and mass characteristics between treatment groups.	77
Table 8: Published incidences of PN injury occurring clinically. Studies are ordered from greatest number of patients to least. Entries left blank were not specified in the journal publication.	87
Table 9: Hemodynamic performance of reanimated swine heart-lung blocs.....	119

List of Figures

Figure 1: General anatomical course of the phrenic nerve. (Image from Gray’s Anatomy33, public domain).	8
Figure 2: Anatomical course of the phrenic nerve.	11
Figure 3: Computer models of ArticFront 23 mm (left) and 28 mm (right) geometry during an ablation. The 23 mm balloon is transparent so that the three measurement splines at the tip, middle, and equator can be seen.	12
Figure 4: An example 3D reconstruction of heart 226 showing the right phrenic nerve (A) in relation to a 23 mm cryoballoon in the RSPV (B) and 28 mm cryoballoon in the RIPV (C). The left phrenic nerve is shown as well (D).	13
Figure 5: Average distance with standard deviation from ipsilateral PN to indicated measurement spline of the 23 mm cryoballoon. The number of measurements averaged appears above the bars. (LSPV=left superior pulmonary vein, LIPV= left inferior pulmonary vein, LCPV=left common pulmonary vein, RSPV=right superior pulmonary vein, RIPV= right inferior pulmonary vein, RCPV=right common pulmonary vein).....	15
Figure 6: Average distance with standard deviation from ipsilateral PN to indicated measurement spline of the 28 mm cryoballoon. The number of measurements averaged appears above the bars.....	15
Figure 7: Distribution of distances between ipsilateral PN to mid measurement spline of the 23 mm cryoballoon.....	16
Figure 8: Distribution of distances between ipsilateral PN to mid measurement spline of the 23 mm cryoballoon.....	16
Figure 9: The results from the general linear model demonstrating the min effects on the distance to the phrenic nerve.....	17
Figure 10: Images of a perfusion-fixed human heart specimen. The image on the left shows the anterior surface and the one on the right shows the posterior view.....	24
Figure 11: An anatomical reconstruction of the left atrium (LA), coronary sinus (CS), and the left inferior pulmonary vein (LIPV) derived from one of the perfusion-fixed human hearts. The light blue line depicts the centerline of the CS and the yellow line depicts the area of the mitral isthmus (MI).	26
Figure 12: Shown in this image is the method used to analyze the relative amounts of fat present adjacent to the coronary sinus at the mitral isthmus. The 0 to 180 degree line was drawn parallel to the mitral annulus. Using the center of the coronary sinus, 45, 90, and 135 degree lines were created using 0 degrees as the starting point and rotating counterclockwise. The left atrium (LA) and left ventricle (LV) were labeled for reference.....	27
Figure 13: Images obtained for one of the human heart specimens: on the left is an MRI image and on the right is a photograph of the same human heart specimen sectioned to represent the same physical plane. The left atrial endocardial space is labeled. One can observed that the	

specimen section includes the coronary sinus and immediately inferior to it is a deposit of fat that is visible on both the MRI and photograph.....	27
Figure 14: (A) Shown here is a bar graph indicating the relative presence of fat around the perimeter of the coronary sinus. The graph compares the percentage of non-AF (n=15, blue) and AF hearts (n=15, red) where fat was present at different locations around the perimeter of the coronary sinus (CS). (B) Distances between different points around to the coronary sinus and the left atrial space for non-AF (blue) and AF (red) hearts were provided. An asterisk* indicates a significant difference ($p < 0.05$) between these non-AF and AF specimens.	30
Figure 15: Illustration of the half circumference measurements taken to obtain diameters and area measurements of the various PVs.	41
Figure 16: Comparisons of the paired left, right and total atrial volumes between the matched AF and control hearts. Note that the AF hearts had greater variability of volumes compared to the controls.	42
Figure 17: The relative variation in pulmonary vein ostia sizes between the two groups of heart specimens. The histograms provide the corresponding areas of these ostia. Top: the relative distributions of pulmonary vein sizes of the right pulmonary veins; with means of 24.2mm ² and 21.6 mm ² and medians of 23.1 mm ² and 19.9 mm ² respectively. Bottom: the left pulmonary vein areas, means of 18.7 mm ² and 19.0 mm ² and medians of 18.4 mm ² and 17.7 mm ² respectively. The trend lines depict the two point moving averages of the distributions and illustrate the relative differences between these two heart populations.	44
Figure 18: Relative distribution of thicknesses of the left atrium between the AF and control hearts. These thicknesses values were determined by taking measurements from each of the four pulmonary vein junctions in each heart, as well as the center of the posterior walls of the left atria. The trend lines depict the two point moving averages of the population distributions.	45
Figure 19: Average widths and heights of the fossa ovalis sizes between the two populations of hearts. The relative widths of the fossa ovalis were designated as the fossa ovalis anterior-posterior (FOAP) measurements and the heights were designated as the fossa ovalis superior-inferior (FOSI) measurements (error bars represent the SEs). It was observed that there were no significant differences between the calculated averages of the measurements taken of and the distributions of the sizes showed similar trends between the AF and control hearts (data not shown).....	46
Figure 20: A representative screen shot of the video as the Swan Ganz catheter is passing through the tricuspid valve. On the top left a fluoroscopic image is presented with a computer animation found below to aid the viewer in navigation. On the right, using endoscopy and Visible Heart® methodologies ¹¹ , direct visualization of the balloon is shown with the beginning of the characteristic transition in pressure waveform found bottom right.	51
Figure 21: A screen shot similar in description to Fig. 1, but of the pulmonary valve. Note characteristic change in diastolic pressure as the balloon passed through the valve found on the bottom right.	53

Figure 22: (A) Dilator and FlexCath advancement through the swine fossa ovalis visualized from the right atria (top left), under fluoroscopy (top right), and from the left atria (bottom right). Note, a guidewire has already been exchanged for the Brockenbough needle shown in bottom left of B. A view from the right atrium (top left) is also shown in B with a view of left pulmonary veins (top right), fluoroscopic position (bottom right), and fossa ovalis with right pulmonary veins in view (bottom left). 56

Figure 23: Position of the ArticFront as seen from within the left pulmonary vein (top left A, top right B), fluoroscopy (top right A, bottom right B), and within the left atria (bottom right A, bottom left B). The Cryo Console screen is shown top left in B. These images are during the beginning of an injection of fluoroscopic contrast, with blue or green dye for direct visualization. Darkening of the vein distal to the balloon on fluoroscopy demonstrates good occlusion of the vein..... 57

Figure 24: Near the end of a four minute ablation ice can be seen within the left pulmonary vein (top left A, top right B). The temperature profile on the console screen is displayed (bottom left A, top left B). An endocardial view of the balloon and ice formation in the tissue can be seen as well (bottom right A, bottom left B). The fluoroscopic position is displayed top right in A and bottom right in B..... 57

Figure 25: Infrared imaging apparatus shown left and resultant isotherms shown left. The samples are impaled onto the cryoprobe and imaged from the top down. A resultant isotherm from an ablation performed with the Galil system is shown right with white indicating temperatures less than -20°C, blue -20°C to -10°C, green between -10°C to 0°C, and red greater than 0°C..... 64

Figure 26: Examples of TTC stained myocardium (left), kidney (center), and lung (right) with central ablation lesions. 65

Figure 27: Shown left is a plot of the normalized gray values of a TTC stained image plotted radially outward from the cryoprobe. Shown right is how the data is classified after picking the two critical points (blue stars) on the sigmoid curve..... 67

Figure 28: Swine kidney tissue viability response to ablation with Galil Seednet probe. (n=6)... 68

Figure 29: Swine atrium tissue viability response to ablation with Medtronic FreezorMax. (n=8) 69

Figure 30: Swine ventricle tissue viability response to ablation with Medtronic FreezorMax. (n=14) 69

Figure 31: Swine myocardium tissue viability response to ablation with Medtronic FreezorMax. (n=22) 70

Figure 32: Swine myocardium tissue viability response to ablation with Galil Seednet. (n=17) .. 70

Figure 33: Human myocardium tissue viability response to ablation with Medtronic and Galil cryoprobes. (n=6)..... 71

Figure 34: Swine lung tissue viability response to ablation with Medtronic and Galil cryoprobes. (n=5)..... 71

Figure 35: Human lung tissue viability response to ablation with Medtronic and Galil cryoprobes. (n=6).....	72
Figure 36: Shown left an illustrated schematic of experimental apparatus consisting of a water jacketed chamber, force transducer, platinum field stimulation panels, and gassing chamber. Shown right is a photograph of the actual system while a muscle bundle (A) is held in place by the force transducer and lower ring (B) during an ablation (C). The field stimulation panels (D) are used to elicit contraction.....	76
Figure 37: Effect of varying duration cryoablation treatments on normalize maximum force generated.....	78
Figure 38: Effect of high NaCl buffer during ablation application as a proposed adjuvant therapy.	78
Figure 39: Performance of cardiac tissue compared to skeletal muscle tissue.	79
Figure 40: Example of pre- (Left) and post-TTC stained (Right) control (Top) and ablated tissues (Bottom). Samples 5, 6,7, and 8 were ablated for 2, 1.5, 1, and 0.5 minutes respectively.	80
Figure 41: General anatomical course of the phrenic nerve. (Image from Gray's Anatomy33, public domain).	85
Figure 42: Nerve recording chamber displaying recording and stimulating electrode configuration. The white Styrofoam thermocouple array can be seen in the middle of the chamber. The nerve is stimulated at the left of the picture and evoked CAPs are recorded along the length of the nerve as they travel towards the right.	91
Figure 43: An example of a CAP recorded proximal (top) and distal to ablation (bottom). The dotted line (A) indicates time at which stimulus was applied. The magnitude (B) and latency to peak (C) were determined and average conduction speed (D) calculated based upon the distance the signal traveled.....	92
Figure 44: Shown left is the cryoprobe relation to the nerve, thermocouple array (*), and skeletal muscle segment to reduce cooling power experienced by the nerve. On the right is an example of the cooling profile experienced by the nerve.	93
Figure 45: Relationship between cooling and recovery of phrenic nerve CAPs. Note that two extreme cooling cases are shown bottom left and off the scale of this graph to enable better visualization of the data.	94
Figure 46: Phrenic nerve pre- and post-ablation CAP magnitude and nadir temperature relationship. Note that temperature is displayed as 1/10th the actual temperature to fit within the scale of the CAP magnitude.....	95
Figure 47: Latency to CAP onset pre- and post-ablation.	95
Figure 48: An external view of human heart 277 in systole and attached to the system is shown inset top right. Displayed center is a flow diagram for a functional heart and lung reanimation consisting of: (1) a respirator connected to the cannulated trachea and thus attached to the lung(s), (2) a pre-load chamber for the right side of the heart, (3) an aortic after-load chamber which mimics the resistance that the left ventricle works against, (4) a left pre-load chamber employed when only one lung is present, and (5) an oxygenator reservoir for pooling fluid	

expelled by any cannulated branch of the pulmonary artery. (6 & 7) fluid pumps to maintain the pre-load pressures, (8) hemostasis valves that allow access for delivery of cameras, instruments, and assorted devices, (9) valves that may also be used to redirect flow as physiologically appropriate, while (10) cannulation of the pulmonary vein(s) are shown here for a right lung preparation, but are absent or translated when either both lungs or the left alone respectively are used..... 103

Figure 49: An image series obtained from reanimated human heart-lung bloc 284 (A,B) and 277 (C,D) showing the path through the distal pulmonary arteries and veins, respectively. The corresponding fluoroscopic images (B,D) in each case show the relative locations of the videoscopes (A,C). A supplemental video of the journey through the vasculature can be viewed as well..... 108

Figure 50: Provided here is a time series of images from human heart 277 showing tricuspid valve closure from the right ventricle (A) and right atria (B). Images are displayed 1/15th per second apart in time. Panel C displays ice formation on the distal portion of a cryoballoon ablation catheter (Artic Front, Medtronic, Inc., Minneapolis, MN) as seen from within the pulmonary vein. The images are spaced post-ablation 30 seconds, 1, 2, and 3 minutes apart.. 109

Figure 51: Shown above (A) the heart-lung bloc, with overlaid thermograph, attached to the Visible Heart[®] apparatus with heart held laterally to best image area of therapy. Panel B shows a close up view of the resultant thermograph with the temperature scale ranging from -18 to 37 °C in this example. 117

Figure 52: ArticFront 28 mm balloon cryoablation catheter with colored markings for optimizing the alignments of catheter position between ablations. The blue band corresponds to the top of the catheter handle and the red band corresponds to the left side of the handle (i.e., the operator’s perspective)..... 118

Figure 53: Relative area cooled by employing ArticFront (blue) and ArticFront Advance (red) catheters. Above each bar is the number of ablations in which the indicated level of cooling was achieved. For each the ArticFront and ArticFront Advance catheters, 24 and 25 ablations were analyzed, respectively. Ablations which did not achieve cooling to the measured temperature were averaged with the other ablations performed that day as zero area cooled. (*= p<.05) . 120

Figure 54: Relative area cooled during therapy application by ArticFront (blue) and ArticFront Advance (red) catheters excluding cases in which the measured temperature was not achieved (e.g., if -5°C was not achieved, that ablation was not analyzed in the -5°C group). The number of ablations measured is displayed above the error bars. (*= p<.05) 120

Figure 55: Time to reach indicated epicardial temperatures from beginning of ablation. Note that differences between treatments delivered with ArticFront (blue, n=16) versus ArticFront Advance (red, n=20) catheters were not found to be significant..... 121

Figure 56: Distribution of nadir temperatures achieved following treatments with either catheter system: ArticFront (blue) and ArticFront Advance (red). Note, accuracy of temperatures less than -30°C may be decreased as denoted by an *. No temperatures fell within the 50°C bin and therefore it was omitted. 122

Figure 57: Minimum temperature achieved by treatment applications with ArticFront (blue) and ArticFront Advance (red) catheters (p=0.036).....	122
Figure 58: Area cooled by ArticFront 23 mm catheter in human (blue) and swine (red). The number of ablations measured is displayed above the error bars. (*= p<.05)	123
Figure 59: Time progression of ablation at MRI slice number 24. The top four images are during the active ablation period. The bottom three images are after the balloon has deflated and coolant injection has stopped. Measurements are displayed because the images are not the same magnification.....	130
Figure 60: Three dimensional reconstruction of the first scan at the beginning of ablation and following deflation of the balloon. These reconstructions are from scan one and scan five from Figure 59.....	130
Figure 61: Volume of balloon and ice reconstruction over time. Ablation 3 was slightly delayed in time. Each scan is one minute.	131
Figure 62: Volume of ice versus time. The balloon volume was subtracted from the balloon/ice reconstruction for the time points at which the balloon was inflated. Scan sequence time of 1 minute.....	131
Figure 63: Results from fitted ellipse measurements from a cross section slice in center of balloon running from distal tip to the shaft. Examples of the measurements can be seen in Figure 59.....	132

Introduction:

Atrial fibrillation (AF) remains as the most prevalent tachyarrhythmia, with a prevalence in the U.S., of 1% in the general population ¹. However, prevalence is age related and for persons over age 40 it increases 2.3% and for those over age 65 to 5.9% ². It is characterized by uncoordinated electrical and mechanical myocardial activity, termed fibrillation. In its observed appearance, the heart looks as though it is quivering. One of the startling findings of this arrhythmia is its self-perpetuating nature. In general, if left untreated, paroxysmal AF (self-terminating episodes) eventually turns into persistent AF (not self-terminating) and then permanent AF (i.e., a constant state of fibrillation) ³⁻⁵. In other words, the longer an AF patient waits for therapeutic intervention, be it drugs, an ablation procedure, or both, the harder it is to restore a normal rhythm. Such difficulties in the restoration/treatment are in part due to both structural and biomolecular remodeling of the myocardial tissues that provides a sustaining substrate for maintenance of AF. Structural remodeling refers to physical changes, such as dilation of the atria and the formation of interstitial fibrosis. The biomolecular remodeling of primary concern in such patients is electrophysiologic in nature: this results the shortening of the atrial effective refractory periods, thus aiding perpetuation and also preventing natural termination of fibrillation. This self-perpetuation becomes especially disturbing when a given patient's prognosis is taken into account: mortality rates double and stroke occurrences increase by 5% per year in such patients with AF (i.e., 2 to 7 times the rate of people without AF) ⁵. The current therapeutic/treatment paradigm for the patient with atrial fibrillation, is to first attempt to restore normal rhythm via anti-arrhythmic pharmaceuticals. If this does not ameliorate the problem, or the patient does not well tolerate the drug side-effects, a transcatheter ablation is usually performed. However more recently, this treatment paradigm is beginning to shift, due to promising research showing that patients have better outcomes with ablative treatments or a combination of drugs and ablation, versus drugs alone ⁶. Although transcatheter ablation therapy generally requires more than one procedure, it offers the unique benefit of being a potentially "curative" treatment for cardiac dysfunction.

Atrial fibrillation requires both a substrate and a trigger for maintenance and initiation, respectively. Through non-contact or contact mapping of the atria, the electrophysiologist in the catheterization laboratory can electrically and/or anatomically map a patient's heart. This type of mapping helps not only to better identify the potential sources of triggers and provides a visual reconstruction for intravascular navigation of therapeutic catheters, but aids the physician to efficiently performing such procedures. From here, the physician can attempt to ablate and destroy focal triggers or create linear lesions that will electrically isolate given areas of the heart; i.e., due to creation of non-conductive scar tissue. The linear lesions are typically used to help create a modified Cox-Maze lesion set, that serves to guide electrical activity, as if it were traveling through a maze and the lesions are the walls of the maze (hence part of the name). Since Haissaguerre's⁷ seminal paper, published in 1998, established that the pulmonary veins (PV) were a substantial source of AF triggers, electrically isolating the PVs has become a cornerstone of the typical patient ablative procedure. Other common atrial triggers also exist, that lead to better outcomes when ablated, such as the neuronal autonomic ganglia plexus found epicardially near the pulmonary vein ostia⁸. It should be noted, that often pulmonary vein isolations may directly or indirectly modify these plexus triggers.

The modern cardiac electrophysiologist has a wide range of energy sources to select from for creating transcatheter ablation lesions, including: radiofrequency (RF; irrigated and non-irrigated), cryothermal (cryo), chemical, and/or laser. Further, high-intensity focused ultrasound, electroporation (IRE), and microwave are currently under development, but not yet in clinical use⁹. All of these later modalities, except electroporation, have benefits and drawbacks related to functioning on a thermal basis; they either increase or decrease temperature to destroy tissue and create an isolating lesion of fibrosis. Today, RF ablation remains as the current gold standard being used most frequently. It offers the benefit of faster procedural times due to faster thermal treatment and also better catheter manipulation. Yet, cyoablation has the unique ability to adhere to the tissue upon energy application, ensuring the catheter does not change position during the therapy delivery. Therefore, the physician does not need to apply constant pressure, possibly reducing the risk of perforations, which may lead to cardiac tamponade (fluid in the space around the heart that prevents complete filling and can lead to death). Cryoablation also offers the

option of cryomapping which involves a short application of energy (focal cooling), so to test a lesion location before making it permanent. Cryomapping aids in avoiding damage to the native conduction system because when problems present, the treatment is stopped and the tissue can typically recover. Further, when comparing heating (RF) versus cooling (cryo): 1) cryo has been found to better preserve the structure of associated tissues, by not causing hyperthermal fixation of proteins¹⁰, 2) cryo has a lower incidence of thrombus^{11,12}, 3) cryo does not create charring or popping of tissue, and 4) until recently cryo has not been reported to cause pulmonary vein stenosis¹³. Interestingly, although RF is the current clinical “gold standard”, both cryo and RF have been shown to be relatively equal in therapeutic efficacies¹⁴.

More recently, the utilization of new cryoballoons, devices that go into the pulmonary veins, are inflated, and then simultaneously cools the whole vein annulus, have the potential for creating circumferential lesions. In other words, this approach isolates the whole vein at once and thus has shown promise in helping to reduce procedure times for therapeutic cryoablation¹⁵⁻¹⁷. Nevertheless, cardiac cryothermal cellular and tissue effects remain relatively unstudied compared to hyperthermal treatments.

To date, transcatheter ablation has proven to be effective therapy, resulting in AF elimination rates as high as 90% for some centers, while being relatively safe with a procedural mortality rate of 2 to 3%⁵. However, transcatheter ablation is not without potential complications and these have been highly related to spatial anatomical orientations of tissue adjacent to the atria. For examples, two such tissues, the phrenic nerve and esophagus, have been found using 3D reconstruction to be 2.1±0.4 mm and 10±6 mm from the atria, respectively^{18,19}. Currently, with the available technologies, the highest complications in such procedures is phrenic nerve palsy (PNP), with reported rates as high as 11.2%¹⁶: this may even result in hemiparalysis of the diaphragm. It has been generally reported that PNP will generally resolve within a year, but occasionally it is permanent¹⁶. Further, patients have reported varying degrees of decreased quality of life, with diaphragm hemiparalysis in some severe cases mechanical ventilation has been required. Atrioesophageal fistula is another potential AF procedural complication, described as the formation of a hole from the atria to the esophagus, resulting in much graver consequences, with associated mortalities higher than 75%. Yet, it is reported to

only occur in <.1% of cases, but appears to be more prone to occur with RF treatment^{20,21}. Nevertheless, esophageal damage is probably much higher than reported because patients are not screened for this postoperatively²⁰. In addition, pulmonary vein stenosis has only been recently reported in the literature to be caused from cryoballoon treatment and surprisingly the first rate reported was 3%¹⁶. Furthermore, lung injury and esophageal hypomotility have also been reported, but fortunately, most of such patients are generally asymptomatic.

It has been suggested that the tolerances of tissues to cryoenergy can vary widely²² and there is virtually no data on the tolerances for cardiac and/or surrounding tissues. Despite this fact, cryoablation is being performed clinically: in other words, there is little information regarding the relative sensitivities of tissues involved. On the other hand, numerous cell viability studies have been performed extensively in the field of oncology so to determine the biophysical response to freezing and have found large differences between tissue and cell types^{23,24}. There are a wide range of techniques available to investigate thermal effects, such as: cryomicroscopy, differential scanning calorimetry, histology, and viability assays. Yet to date, there have been virtually no published data on the thermal tolerances of cardiomyocytes themselves, and much less on the adjacent tissue types. Many of the related studies found in literature focus on the feasibility of creating a lesion, not the physical processes that are actually happening to the tissues and cells²².

Importantly, there has been an increased interest in clinically monitoring the previously discussed adjacent tissues during ablative procedures, but due to temperature monitoring limitations, high variability in anatomy, and variability of cryoenergy applications; it has not been possible to draw conclusions about individual tissue thermal tolerances. One of the greatest limits of the currently available clinical research is the lack of associated temperature monitoring during the delivery of therapy. Thus, without understanding what is actually happening to these tissues, in terms of a thermal dose, it is very difficult to predict the outcomes, or qualitative tissue tolerances. For example, recent studies on the properties of the esophagus have shown that performing luminal temperature monitoring, and power monitoring for RF ablation, does not correlate with the ultimate formation of a fistula^{20,25}. These studies used a single thermal sensor while it has been shown that using

multiple sensors better results can be attained²⁶. However, this does not remedy the fact that the endoluminal temperature is lower than the intramural temperatures, and the operator needs to use caution when making decisions based on such measurements²⁷. Interestingly, it has also been suggested that the clinical use of temperature probes may actually interact with applied RF energies and actually increase the risks for esophagus damage²⁸.

If a better overall knowledge of thermal injury thresholds for the heart and its surrounding tissues can be obtained, it will not only be immediately useful for both clinician and medical device designers, but will become increasingly valuable when MRI and ultrasound thermography gain greater use. It has been shown that thermometry using both of these modalities is possible for use during ablation procedures, thereby eliminating the need of primitive thermal sensors and providing the whole picture “thermal dose” that the tissues are receiving²⁹⁻³¹. It should be considered that with the ever increasing uses and availability of MRI, it is only a matter of time until clinical ablation procedures will utilize MRI or 3D ultrasound rather than fluoroscopy. In fact, MRI compatible RF ablation catheters have already been developed by various groups³² as well as by our laboratory. Such novel monitoring techniques will provide physicians with the benefits of: limited radiation exposure, loss of the requirement to wear lead, and/or high resolution temperature monitoring. Additionally, it can easily be envisioned that software packages could be designed to have temperature thresholds and thermal dose limits as presets, so to help prevent procedural complications. Nevertheless, to accomplish such goals, a thorough understanding of what these doses and thresholds should be, still need to be attained.

For the preceding reasons the focus of the studies in my thesis falls into three main categories: anatomy, thermal injury thresholds, and device-tissue interactions. As mentioned previously the collateral injury that occurs due to ablation procedures can be in a large part considered as anatomical interactions (i.e., close proximities of adjacent tissues causes them to experience energy meant for the myocardium). For this reason, studies were undertaken to fill the field of cardiac ablations’ gaps of knowledge on the relative thoracic anatomy in the atrial fibrillation patient. For example, the data obtained in the phrenic nerve anatomical project can also be used for future computer modeling to

treatments. In the second section of my thesis, on thermal injury thresholds, the primary aims were to determine to what degree of cooling is necessary to achieve complete cardiac lesions. These studies not only fill another gap in basic knowledge, but may be subsequently used to titrate dosing and therefore reduce collateral injury. Further, the output from these studies could potentially be used for future predictive computer modeling of cryo ablative therapies applied not only in the heart. The third section of my thesis focuses on the system level interactions between the ablation devices and tissues. To date, it is unknown to what degree ice, and accompanying injury, extends outside the myocardium. Using MRI and infrared thermometry novel insights were gained as to how far the cooling extends outside the desired treatment area and at what rates. To create the most anatomically appropriate environment a novel heart-lung preparation has been developed. The preceding chapters will also include respective introductions to familiarize the reader with their exact context and purpose.

I- Section 1 Anatomical Aspects of Ablation:

The focus of this section of my thesis is anatomical aspects of cardiac ablation for the treatment of atrial fibrillation: it consists of three published or in submission manuscripts on anatomy related to AF. The three specific anatomical topics include: the phrenic nerves, anatomy of the coronary sinus, and general cardiac anatomy of AF versus non-AF patients.

The importance of thorough understanding of cardiac anatomy cannot be understated in the context of ablation for both the practicing clinician and the medical device design engineer. Originally, in the clinical setting a mental representation of the anatomy was absolutely critical for proper catheter navigation. Today, with the introduction of the latest technologies, such as three dimensional electroanatomical mapping and merging of realtime catheter navigation systems with pre-procedural imaging, this intimate knowledge of anatomy takes on differing utilities. Nonetheless, understanding a given patient's thoracic anatomy remains a requisite knowledge for the electrophysiologist so to optimize therapeutic results. For the medical device designer, the environment and use conditions of such systems of interest, will ultimately guide the design of components from start to finish. Further, precise anatomical geometry in a computational design environment can cut developmental times and prototype generations to yield a more efficient product development cycle. It is for these reasons that the first chapter of this thesis seeks to expand the current thoracic anatomical knowledge found in the literature.

1.1- Chapter 1: Phrenic Nerve Anatomy

The topic of phrenic nerve anatomy was chosen for investigation because there is very little published data available in this area, despite phrenic nerve injury being the most common procedural complication of cryoballoon ablation¹⁷. In general, the right phrenic nerve in general follows the posterior or posterolateral aspect of the superior vena cava and the left phrenic nerve passes over the marginal veins of the left ventricle (Figure 1). The right and left phrenic nerves travel within or encapsulated by the pericardium.

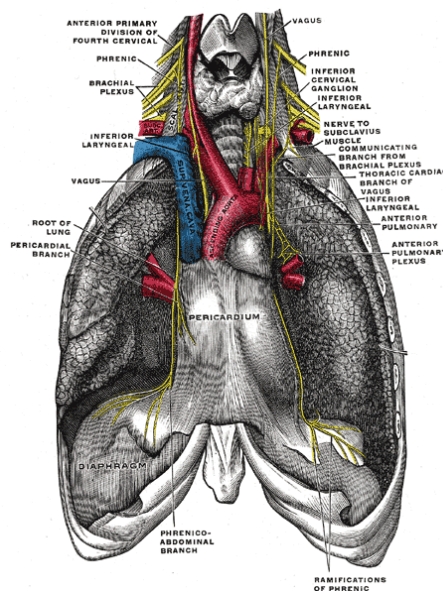


Figure 1: General anatomical course of the phrenic nerve. (Image from Gray's Anatomy33, public domain).

A primary goal of the phrenic nerve anatomical MRI studies was to determine with relation of cryoballoon ablation positioning relative to where exactly the phrenic nerves were located. As described in the subsequent article there are only a handful of previously reported anatomical studies on phrenic nerve anatomy related to ablation. Here I describe how using the perfusion fixed heart/lung blocs allowed for high resolution MRI to identify where the actual nerves are located relative to the potential locations of cryoballoon placements. I believe that this is the first such anatomical study to utilize such an approach.

1.1.1- High-Resolution MRI Reconstructions of Human Phrenic Nerve Anatomy in Relation to the Pulmonary Veins and Computational Modeling of Cryoballoon Ablative Therapy

Ryan P. Goff BS^{1,2,3}, Julianne H. Spencer PhD^{1,2,3}, Paul A. Iaizzo PhD^{1,2}

Introduction

Today, phrenic nerve injury is the highest non-access site related complication of cryoballoon ablation for the treatment of drug refractory atrial fibrillation (AF): this was recently reported in the pivotal US trial STOP-AF¹⁷ as well as other multi center trials³⁴. This form of injury is not unique to cryoballoon ablation, but a recent systematic literature review suggests it may occur more frequently in cryoballoon ablations than in radiofrequency ablations³⁵.

The right phrenic nerve in general follows the posterior or posterolateral aspect of the superior vena cava and the left phrenic nerve typically passes over the marginal veins of the left ventricle (Figure 2). The right and left phrenic nerves (PN) terminate on the superior surface of the diaphragm. Injury to a phrenic nerve may result in diaphragmatic hemi-paralysis or palsy^{36,37}. Usually, only the right phrenic nerve has been reported to be injured during cryoballoon ablation and most frequently during ablation of the right superior PV^{38,39}. However, recent case reports have been published on left PN injury^{36,40} and this occurrence may rise with increased cryoballoon adoption.

Reported rates of phrenic nerve injury due to cryoballoon ablation vary in the literature, in the range of 2%⁴¹ to 24%⁴². The reported time course of phrenic nerve functional recovery may be highly variable for each patient⁴³. However, with the use intraprocedural phrenic nerve pacing, many times these complications are being reported as only transient, implying recovery even before procedure end⁴⁴. Yet, the noted shortest

¹ Department of Biomedical Engineering, University of Minnesota (Minneapolis, MN)

² Department of Surgery, University of Minnesota (Minneapolis, MN)

³ Medtronic Inc., Mounds View, MN

recovery time periods reported are on the order of hours³⁸ and the longest on the order of months⁴⁵.

Previous anatomical studies of the phrenic nerves have been performed using multi-slice CT^{46,47} and human cadavers¹⁸. Studies by Sanchez-Quintana and colleagues determined that the distance between the right superior (RSPV) and inferior pulmonary veins to the right PN is 2.1 ± 0.4 and 7.8 ± 1.2 mm, respectively. However, it was noted that studies on whole body preserved cadavers may have slightly distorted anatomy due to the deflation of the lungs and heart. Thus, it would also be unclear what size vessel the measurement was being made and whether or not these measurements were being correlated to positions where ablation catheters would actually be placed (i.e., measurements may be made to the distal vein and not the antral or ostial areas where ablations are typically applied. Further, a study carried out by Horton *et al.*, reported that the RSPV was 15.2 ± 8.3 mm from the pericardiacophrenic artery using CT angiography. Yet, one needs to consider that the aforementioned points may account for the discrepancy in measurements between the two studies.

The proximity of the phrenic nerves to the pulmonary veins, and therefore the placement of a cryoballoon during a clinical ablation procedure, is largely thought to be the determinant of whether or not injury will likely occur. Further, deep seated balloon catheters have also been suggested to distort the cardiac and PV anatomy and thereby further reducing the distances these catheters are from a given nerve⁴⁸. Interestingly, the use of smaller balloons has been suggested to be more likely to cause injuries, due to the fact that it may be inserted further into the PVs^{34,49}. It has been recently noted that the proximity of the left phrenic nerve to the left pulmonary veins is largely unstudied in comparison to the anatomy of the right^{18,38,47}.

The aim of the current study was to employ high-resolution MRI to further quantify the anatomic relationships between the human pulmonary veins and phrenic nerves. To date, the authors believe this is the first such quantitative study of the left phrenic relationship to the PVs in the context of ablation.

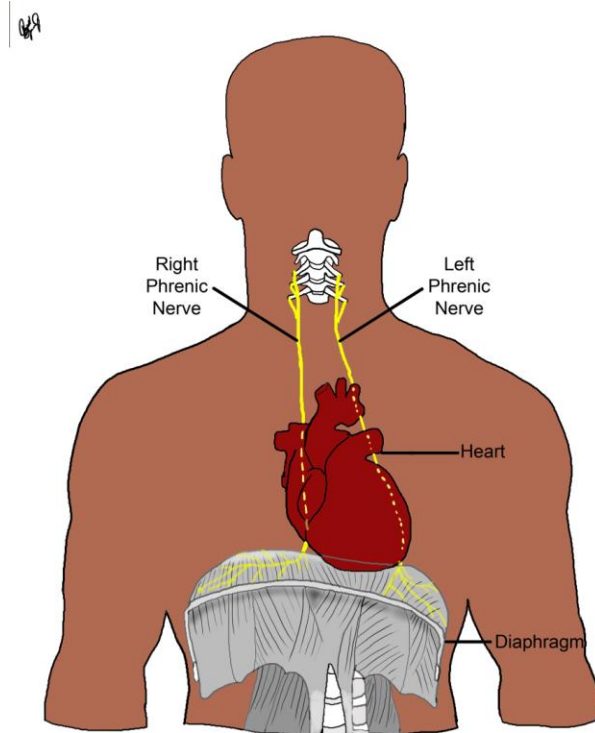


Figure 2: Anatomical course of the phrenic nerve.

Methods

Anatomical Specimen Preparation and Scanning

Human heart-lung blocs were obtained through the University of Minnesota Bequest Program. Specimens were dissected from unpreserved donors. These donor bodies were stored at 4°C until the heart-lung blocs were procured and the procurement was typically performed within 24 hours of death. The aorta, trachea superior vena cava, and the inferior vena cava (when possible on a given specimen) were cannulated and attached to a perfusion fixation chamber as described previously^{50,51}. This approach preserved each heart in a modified end-diastolic state (fully expanded atria and ventricles) and also dilated the lungs. The pericardium and phrenic nerves were left intact. These hearts were fixed with 10% formalin in PBS solution for at least 24 hours, under 40-50 mmHg pressure and then stored in formalin.

In order to increase visibility the phrenic nerves on MRI scans, samples were prepared by gluing a thin gauge polymer tube to each phrenic nerve. In order to ensure anatomically accurate scans, small incisions were made in the atria and cotton gauze was stuffed into

the atria and pulmonary veins to maintain dilated shapes: all incisions were closed by use of sutures. To maintain the close approximation of the lung to the heart during preparation, specimens were wrapped in polymer film (Seran Wrap, Johnson Co., Racine, WI). Samples were then imbedded in 7% agar gel to stabilize the samples during scanning and decrease artifact as described previously⁵². Scans were performed in a 3T machine (Seimens TRIO) using an mprage (T1 weighted) protocol and base resolution of 512.

Anatomical Reconstructions and measurements

Datasets (N=10) were analyzed using Mimics (Materialise, Leuven Belgium) to derive anatomical measurements. To do so, each cardiac image set was imported using the native DICOM data files generated from the MRI scan and then converted into three dimensional renditions (i.e., each 2D DICOM image was layered together to create a 3D model). The left atria and pulmonary veins were segmented from the 2D data and then volumes were created. To analyze the phrenic nerve locations, a spline was created at the tissue/fiducial marker interface (i.e., on the nerve).

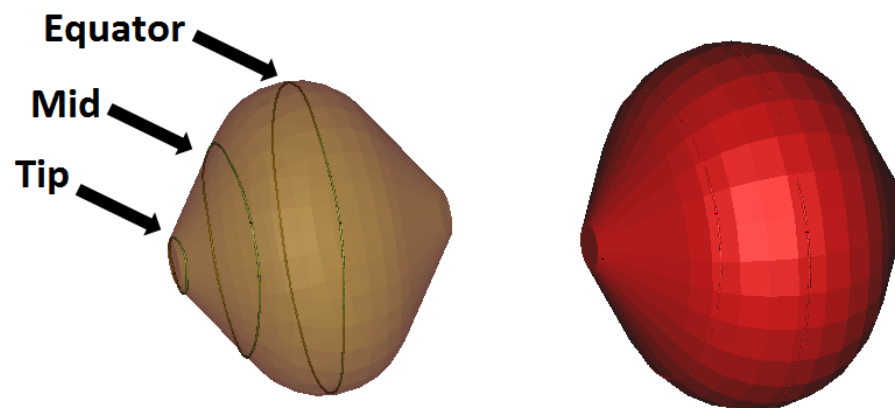


Figure 3: Computer models of ArticFront 23 mm (left) and 28 mm (right) geometry during an ablation. The 23 mm balloon is transparent so that the three measurement splines at the tip, middle, and equator can be seen.

To determine the PN distance from the PV in the context of balloon PV isolation, 23 and 28 mm ArticFront cryoballoon computer models were obtained from Medtronic, Inc. (Minneapolis, MN). These models were then mated with the reconstructed PV ostias by alignment in the software package 3-Matic (Materialise). This was done by aligning the

tip of a given balloon so that it was coaxial with the pulmonary vein in multiple viewing planes. Each balloon reconstruction was then advanced such that a small portion was showing through the shell of the pulmonary vein (Figure 4) at more than one point. This was done because the veins are not perfectly round, like the model balloon, and therefore when back pressure would be applied to the balloon to wedge it in place, as is done clinically, they would conform to the balloon. The model balloons had three measurement splines at the tip, equator, and midway between the two (Figure 3). The minimal distance between the splines on the balloon and the nerve were then measured. This was done by comparing the spline distances using the Part Comparison feature 3-Matic .

To analyze significant effects on the measurement of distance a general linear model ($\alpha=.05$) was created using Minitab 16 (Minitab Inc., State College, PA) with the factors: balloon size, balloon measurement spline, pulmonary vein, and heart specimen as a random variable. Pairwise comparisons of the factors were performed using the Tukey method with a 95% confidence interval.

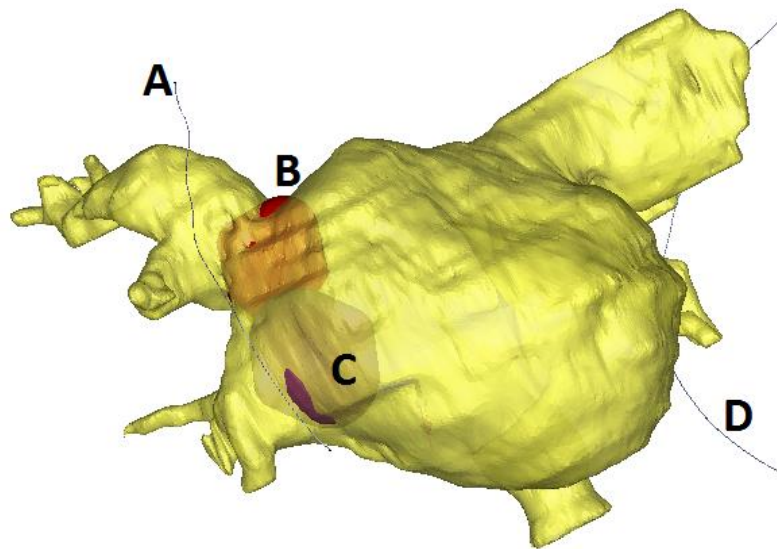


Figure 4: An example 3D reconstruction of heart 226 showing the right phrenic nerve (A) in relation to a 23 mm cryoballoon in the RSPV (B) and 28 mm cryoballoon in the RIPV (C). The left phrenic nerve is shown as well (D).

Results

Using the described technique, ten heart-lung blocs were scanned, modeled and then assessed. The study population characteristics are detailed in Table 1. Note, in specimen

five the right phrenic nerve could not be clearly identified due to the nerve being heavily encapsulated in fat and was therefore not used. Specimen two was of a particularly small stature donor and would not accommodate the 28mm balloon in its left common PV and thus was not used for this measurement. Specimens two and three demonstrated right common PVs, defined as a right common trunk, that accommodated both balloons, which branched to distinct superior and inferior branches distal that accommodated neither balloon.

Interestingly, the difference in placement of the 23 and 28 mm cryoballoons was quite small. The difference between the mid spline distance to the phrenic nerve between the two cryoballoon sizes was 1.7 ± 1.2 mm. This can be attributed to the fact the distal portion of the balloon generally came into contact with the antrum before the waist of the balloon. This caused the 23 mm size balloon usually only be slightly positioned deeper within a given vein.

Table 1: Donor specimen profiles.

Specimen	Sex	Age	Weight (kg)	Height (cm)	History
1	M	77	86.2	152	Myocardial infarction, hypertension
2	F	74	24.9	152	No cardiac history
3	F	65	68	163	No cardiac history
4	M	81	74.8	165	Arrhythmia, leaky heart valve
5	F	70	63.5	165	Congestive heart failure, coronary artery disease
6	F	94	49.8	160	Atrial fibrillation, congestive heart failure
7	F	96	70	155	Atrial fibrillation, coronary artery disease, hypertension
8	M	97	72.7	178	Atrial fibrillation, hypertension, heart failure
9	M	79	95	188	Atrial fibrillation
10	F	81	104.3	168	Atrial fibrillation, hypertension, congestive heart failure

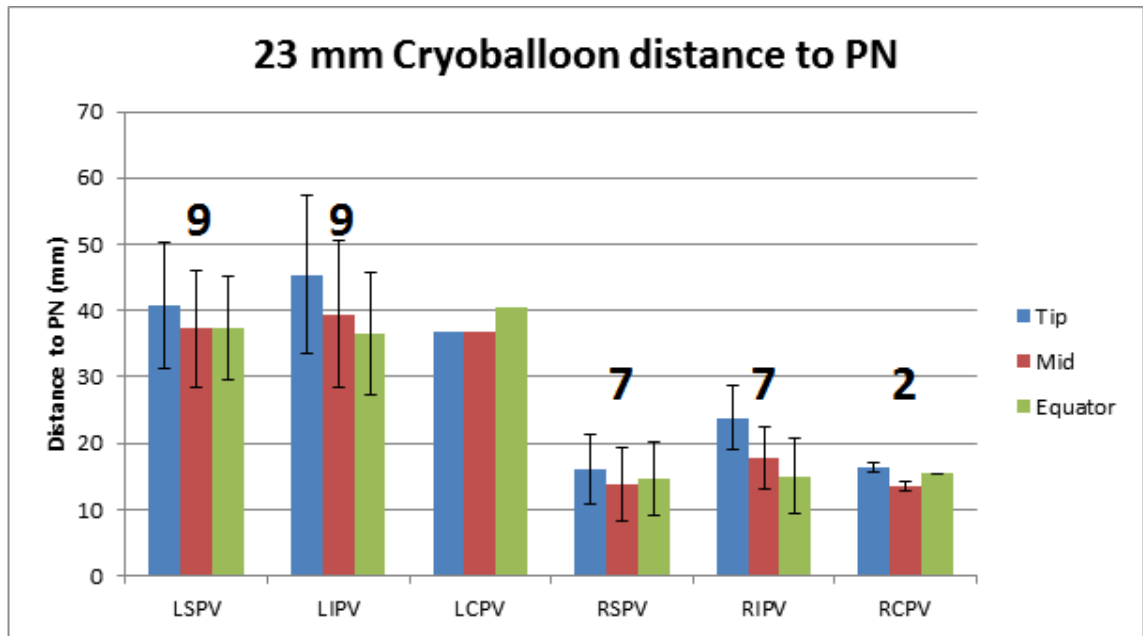


Figure 5: Average distance with standard deviation from ipsilateral PN to indicated measurement spline of the 23 mm cryoballoon. The number of measurements averaged appears above the bars. (LSPV=left superior pulmonary vein, LIPV= left inferior pulmonary vein, LCPV=left common pulmonary vein, RSPV=right superior pulmonary vein, RIPV= right inferior pulmonary vein, RCPV=right common pulmonary vein)

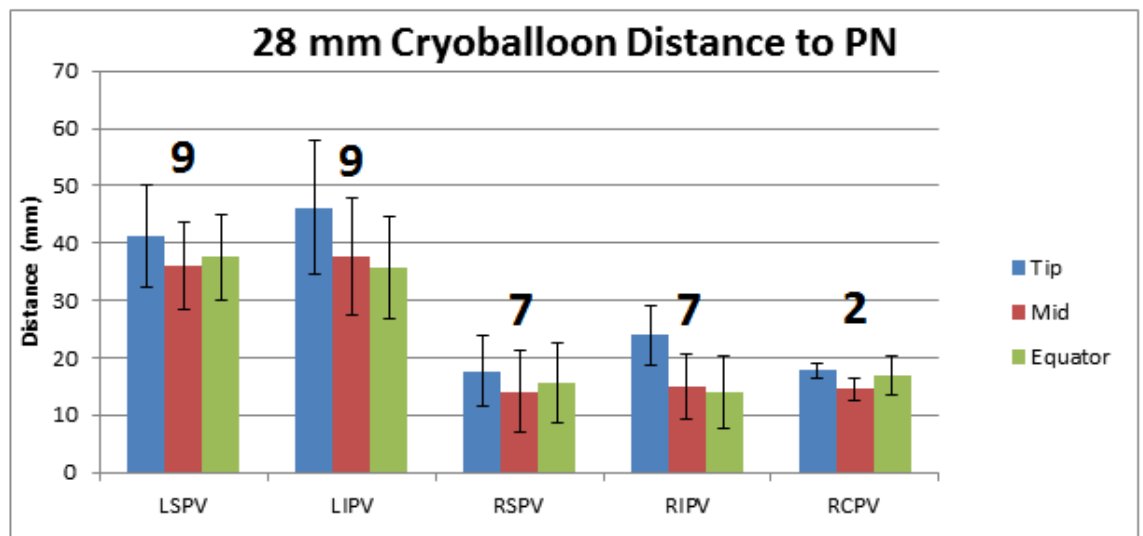


Figure 6: Average distance with standard deviation from ipsilateral PN to indicated measurement spline of the 28 mm cryoballoon. The number of measurements averaged appears above the bars.

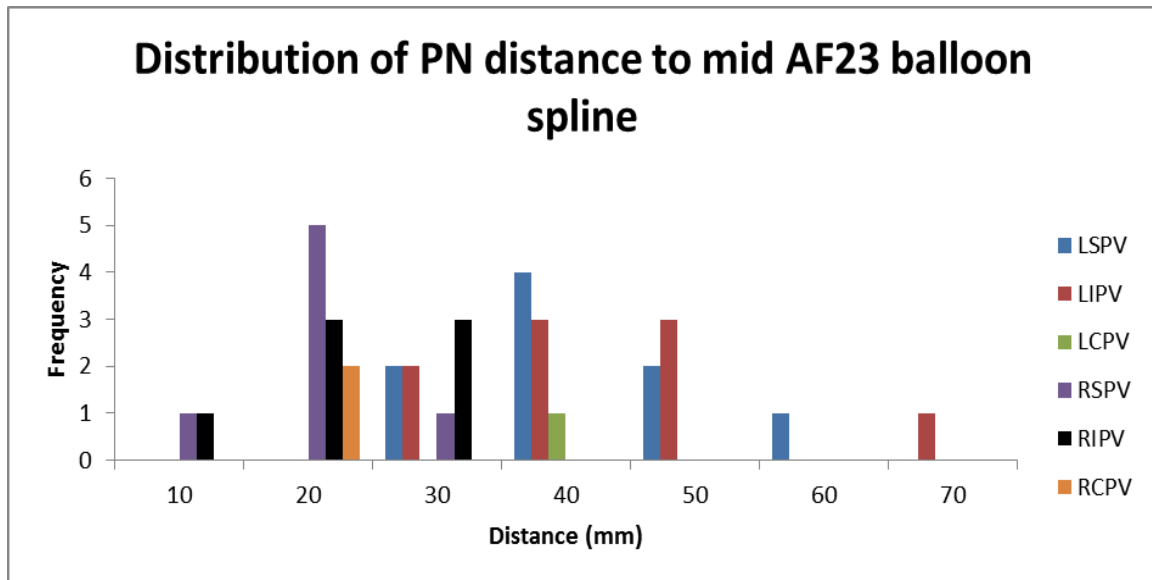


Figure 7: Distribution of distances between ipsilateral PN to mid measurement spline of the 23 mm cryoballoon.

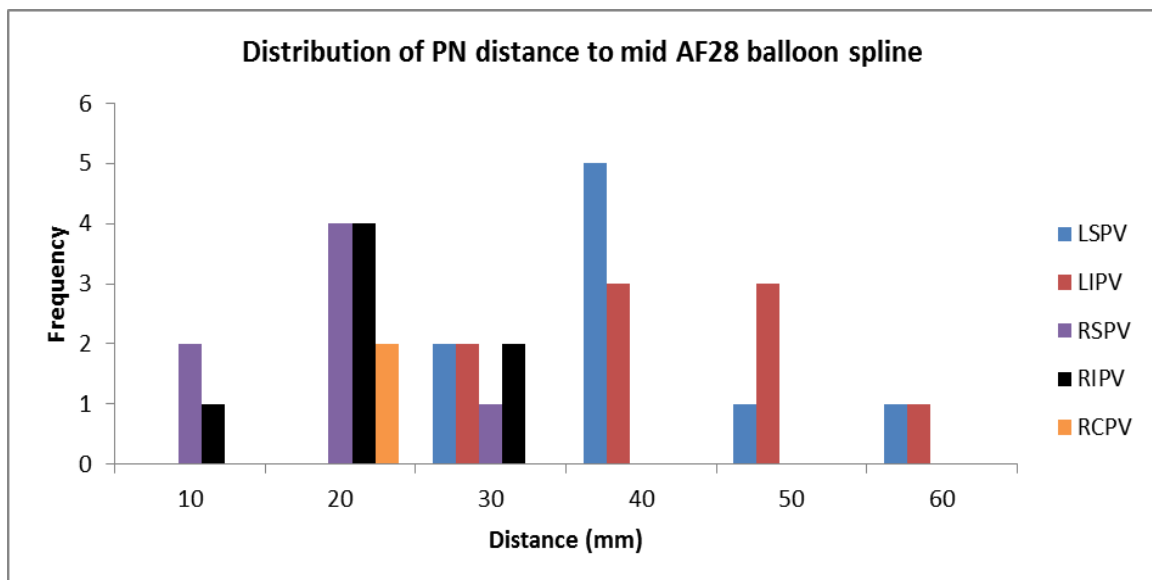


Figure 8: Distribution of distances between ipsilateral PN to mid measurement spline of the 23 mm cryoballoon.

The general linear model yielded a good fit to the data with an adjusted R-squared of 81.48. It was determined that the factors balloon spline, pulmonary vein, and heart would significantly affect the distance to the phrenic nerve ($p < 0.0005$ for all cases, see Figure 9). The factor balloon size was found to be non-significant ($p = 0.965$). The Tukey pairwise comparison results are shown in Table 2.

Table 2: Results of Tukey pairwise comparisons. Results shown graphically in Figure 9.

	N	Mean	Grouping
Balloon			
AF23	103	26.8	A
AF28	104	26.8	A
Pulmonary Vein			
LIPV	54	40.2	A
LSPV	54	38.5	A
LCPV	3	36.2	A
RIPV	42	18.3	B
RSPV	42	14.1	C
RCPV	12	13.5	B,C
Balloon Measurement Spline			
Tip	69	30.5	A
Mid	69	25.1	B
Equator	69	24.7	B

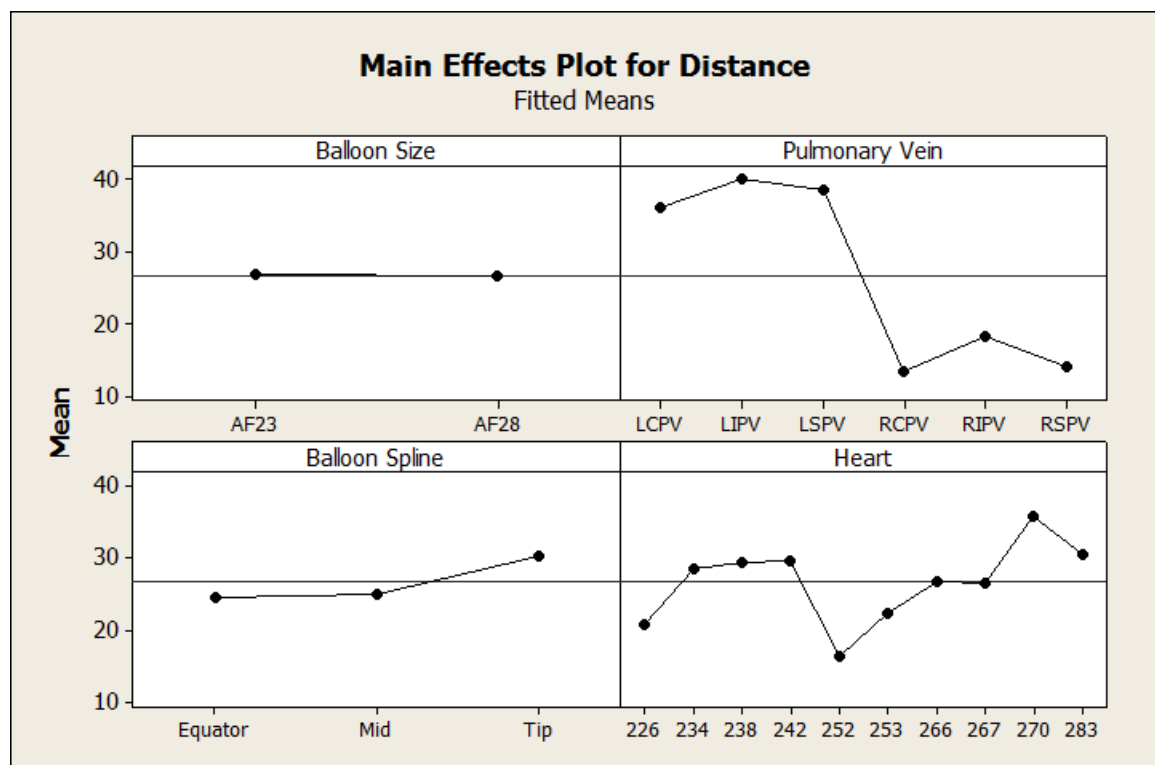


Figure 9: The results from the general linear model demonstrating the main effects on the distance to the phrenic nerve.

Discussion

To the author's knowledge, this is first such study to examine the anatomical relation of the phrenic nerves to the projected locations of cryoballoon therapy application in the pulmonary vein antrum. Due to the complexity of this study and the desire to utilize fresh human heart/lung bloc specimens, our sample size was modest. Further, because this being a human anatomical study, we note that there existed a high degree of variability within this dataset. Yet, our approach of employing a static imaging of the heart-lung blocs, provided very high resolution images for analysis without motion artifact.

In general, the right phrenic nerves in these human specimens were in significantly closer approximations to projected zones of cryoablation versus the left phrenic nerves. These computational results fit with reported clinical data that phrenic nerve palsy more frequently occurs following ablative therapy on the right side of the left atrium and also has only been reported on the left side rarely. This may imply that improper balloon placement is the root cause of the left nerve palsies reported or possibly unique patient anatomy not encountered in the current anatomical investigation. Regardless, proper balloon placement should be strived for therapeutic applications, so to avoid phrenic nerve or other collateral tissue injury. Interestingly, the proximity of balloon tip, middle, and equatorial interfaces with the atrium differed little, yet the tip was significantly closer, as somewhat expected, from the projected distances to a given phrenic nerve. This suggests that the changing of the cooling profile of the balloon from the first to second generation may not have a drastic effect on the rate of phrenic nerve injury. This is not to say that a change in cooling power may not effect injury rates.

We note here that the current study is not without potential experimental limitations.

First, the placements of the cryoballoon model within the reconstructed pulmonary veins was accomplished by having multiple, small portions of the balloon breaching the shell of the reconstructed PV. Yet, it was considered here that this in turn would lead to the best approximation of the true balloon placement in compliant anatomy. In the future, it may be of value to consider developing a morphing algorithm that could possibly reduce subjectivity and optimize placement. The sample size is relatively small given the complex nature of the data acquisition and analysis performed. As expected, the random factor of heart specimen was found to have a significant effect on distance to the phrenic

nerves. This also speaks to the general anatomical variation that may exist between patients, suggesting that individual, patient specific imaging may be necessary to assess risk of phrenic nerve injury. It is somewhat unknown to what extent imaging a dynamic structure, such as the one investigated here, in a static approach may alter the measurements being made (i.e., one must also consider both respiratory and cardiac cycle movements). Finally, the computational models developed here were derived from anatomical measurements made here from MRI diacom data set that were obtained in a diastolic-like state and therefore may be somewhat overestimating these distances.

Conclusion

The purpose of this computational modeling study was to better quantify the distances of the phrenic nerves to areas where cryoballoon ablations may be applied. This study has found that the right phrenic nerves are closer to the pulmonary veins than left, the tip of the balloon is closer to the nerves as expected, and balloon size does not alter distance to the nerves. A better understanding of human anatomical phrenic nerve proximities to the endocardial surfaces in the context of ablation may lead to the optimization of therapeutic treatments. The model anatomy created and described here may also be used for future experimental studies of associated therapies and hence may aid both clinician and medical device designers.

I.II- Chapter 2: Coronary Sinus Anatomy

The coronary sinus has been well noted to be the main venous return of the coronary circulation. Importantly, ablation catheters are commonly placed in the coronary sinus and navigated to the section of this vein that lie in close proximity to the mitral annulus, as well as to the left inferior pulmonary vein. At such locations, ablations may be performed to create transmural mitral isthmus lesions. The thought being that performing these ablations endocardially and within the coronary sinus, will help to ensure clinical transmurality.

The purpose of following manuscript was to quantify the unique anatomy of the coronary sinus and associated structures with respect to transcatheter ablation. Parameters that may ultimately influence lesion creation and a comparison of AF to non-AF hearts were examined. It should be noted, that other investigators have examined the coronary sinus anatomy in the context of ablation ^{53,54}, but to our knowledge this is the first such study that was performed using high-resolution MRI scans of perfusion fixed human hearts.

I.II.I- Anatomical considerations that contribute to applied ablations in the coronary sinus and/or mitral isthmus for the treatment of atrial fibrillation

Mark A. Benscoter, MS^{4,5,6}; Julianne H. Spencer, PhD^{4,5,6}; Ryan P. Goff, BS^{4,5};
Stephen A. Howard, PhD^{4,5,6}; Paul A. Iaizzo, PhD⁵

Brief Title: Variations in left atrial human heart anatomy

Relationship with Industry: Research contract with Medtronic, Inc.

⁴ Department of Biomedical Engineering, University of Minnesota (Minneapolis, MN)

⁵ Department of Surgery, University of Minnesota (Minneapolis, MN)

⁶ Medtronic Inc., Mounds View, MN

Executive Summary

Objective: To identify morphologic characteristics of the mitral isthmus and coronary sinus that may influence how focal ablation catheters are operated and how lesions are generated within the atrial tissues at or near the mitral isthmus and coronary sinus.

Background: Ablations within the coronary sinus (CS) are conducted to treat atrial fibrillation (AF). This study investigates the anatomy around the CS in a set of isolated human hearts with specific implications for coronary sinus and mitral isthmus ablation techniques.

Methods: The coronary sinus of thirty perfusion-fixed human hearts were assessed at the CS ostium and at the mitral isthmus. Specifically, the CS diameter, circumference, length, and shape; distance to the left atrial space; and the amount of fat around the CS were measured. Human hearts were classified as patients without a history of atrial fibrillation (non-AF) or with AF.

Results: On average, the distance along the coronary sinus to the mitral isthmus was 50.4 ± 14.1 mm in non-AF specimens and 66.8 ± 14.6 mm in AF specimens ($p < 0.01$). The CS was 3.4 ± 1.3 mm away from the left atrial space in non-AF hearts and 5.6 ± 2.0 mm away in AF hearts ($p < 0.01$). The ostial circumference of the coronary sinus was 31.2 ± 10.7 mm in non-AF hearts and 35.2 ± 15.3 mm in AF specimens ($p = 0.63$). The coronary sinus circumference at the mitral isthmus was 21.3 ± 7.8 mm in non-AF hearts and 18.1 ± 4.1 mm in AF hearts ($p = 0.09$).

Conclusions: A detailed understanding of coronary sinus anatomy and how it differs for patients with AF is valuable for those who design or use catheter ablation devices.

Significant differences in the anatomy of AF and non-AF hearts. Further, the cardiac features assessed in this study are critical to consider for both optimal catheter placement and the selection of proper ablation parameters to achieve successful transmural lesions.

Keywords: Atrial fibrillation, catheter ablation, magnetic resonance imaging, mitral isthmus, coronary sinus

Abbreviation List

AF = atrial fibrillation

CS = coronary sinus

LA = left atrium

MI = mitral isthmus

Introduction

Catheter based ablation of atrial fibrillation is a well-established approach for treatment and the devices and techniques used to treat the disease continue to evolve.^{55,56} More specifically, the application of ablative therapies within the coronary sinus and the left atrial mitral isthmus, have been shown to effectively treat many patient's eliciting atrial fibrillation^{57,58}. Today, the creation of a linear lesion at the mitral isthmus is both a common practice and a challenge to complete: i.e., while attempting to achieve electrical isolation^{54,59-61}. For example, ineffective ablation applications within this region have been reported to be subsequently pro-arrhythmic^{60,62-64}. Thus, new approaches/techniques are continually being explored to decrease such occurrences. When properly performed, ablations of the coronary sinus and mitral isthmus are able to create a linear set of lesions that can terminate conduction pathways for these atrial fibrillation (AF) patients⁶⁵⁻⁶⁹.

In order to carry out effective ablative therapies within the coronary sinus and mitral isthmus, physicians must be able to navigate through a highly variable region of cardiac anatomy^{58,70,71}. Thus, a detailed understanding of all associated anatomical structures and their relationships to adjoining structure is critical (i.e., the circumflex artery, atrial myocardial tissue, and/or the endocardial ridgeline between the left pulmonary vein and the mitral annulus)^{59,60}. Previous studies have used CT or fluoroscopy images to attempt to characterize the morphologies and anatomy in this area: i.e., during the course of ablation procedures^{58,60,72}. Additionally, several other reports studied the endocardial surface shape of the mitral isthmus. However, they did not identify changes associated with cardiac remodeling due to AF^{52,59,60}.

The purpose of this study was to further characterize the anatomy that may impact ablative therapies delivered at the mitral isthmus. To do so, we utilized a unique set of MRI anatomical reconstructions of perfusion-fixed human hearts, including both with and without a known history of atrial fibrillation. Controls had no known history of

cardiac disease. The high spatial resolution we could obtain via static MR imaging of these specimens allowed for precise analyses of coronary sinus and left atrial anatomy. As noted above, it is clinically important to investigate the potential variations in this regional cardiac anatomy attributed to the consequences of atrial fibrillation, so to perform more effective ablation therapies.



Figure 10: Images of a perfusion-fixed human heart specimen. The image on the left shows the anterior surface and the one on the right shows the posterior view.

Methods

Study Population

Data were gathered from 30 human hearts that were considered non-viable for transplantation via LifeSource (St. Paul, MN) or from the Bequest donation program at the University of Minnesota: these specimens were obtained fresh, with all chambers intact and with the great vessels attached. Each heart specimen was then perfusion-fixed to elicit an end-diastolic state (see below): i.e., including those from both patients diagnosed with AF (n=15) as well as those from individuals with no known cardiac clinical diagnoses (n=15). These specimens and the individuals from which they came were characterized in Table 3: i.e., genders, ages, clinical histories, body weights and heart sizes. A Wilcoxon rank sum test was performed to determine significant ($p < 0.05$) differences between the histories of the AF and non-AF specimens (Table 3). It is important to note that the AF population was older and had a larger male to female ratio, but had similar body weights relative to the control group.

Table 3: Study population demographics for 30 perfusion-fixed human hearts presented as the mean \pm standard deviation.

	Control (n=15)	Atrial Fibrillation (n=15)	P-Value
Age (years)	52.8 \pm 18.9	71.8 \pm 11.1	0.01*
Gender (male/female)	4/11	9/6	N/A
Patient Weight (kgs)	76.8 \pm 21.8	81.2 \pm 24.8	0.65

- indicates significant difference ($p < 0.05$)

Specimen Preparation and Imaging

Heart specimens were carefully prepared by cannulating the great vessels, positioning them in a specialized chamber and then perfusion-fixing them with a head pressure of approximately 50mmHg with 10% formalin, as previously described [21]. This allowed the hearts to maintain a pseudo end-diastolic shape and thus elicit a realistic anatomical form, so to allow us to obtain these morphometric measurements (Figure 10). Subsequent to fixation each heart was embedded with and positioned in a 7% agar solution: this allows one to decrease motion artifacts during magnetic resonance scanning⁵². Scans of these 30 human hearts were performed with a 3T scanner (Magnetom TRIO 3T MRI scanner, Siemens Corp., Munich, Germany) using an mprage (T1 weighted) protocol with a base resolution of 512.

Anatomical Reconstructions and Measurements

The dicom datasets obtained from the magnetic resonance imaging (MRI) were then imported into Mimics Software (Materialise, Leuven, Belgium) to create 3D models and then subsequently make digital measurements. Each cardiac image set was imported and segmented into three-dimensional reconstructions of the left atrium and the coronary sinus (Figure 11). The left atrial reconstruction was used to define the mitral isthmus area that would be accessed via a catheter through the coronary sinus by using the mitral annulus and left inferior pulmonary vein as references. A centerline was generated for the coronary sinus. Anatomical measurements relevant to ablation in the coronary sinus (CS) or a mitral isthmus ablation line were assessed. These measurements included:

- CS ostial diameters and circumference
- Distance along the CS from its ostium to the mitral isthmus

- CS diameters, circumference, and cross-sectional shape at the mitral isthmus
- Distance to the left atrium from the CS at the mitral isthmus
- The presence of fat around the coronary sinus

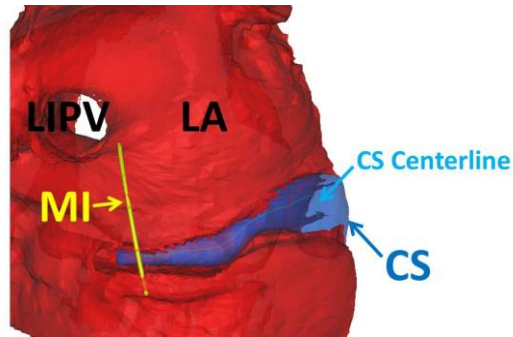


Figure 11: An anatomical reconstruction of the left atrium (LA), coronary sinus (CS), and the left inferior pulmonary vein (LIPV) derived from one of the perfusion-fixed human hearts. The light blue line depicts the centerline of the CS and the yellow line depicts the area of the mitral isthmus (MI).

The 3D models were then re-sliced into 2D data sets to make the CS ostium visible in plane. The CS ostial diameters and circumference were measured on this plane. The CS centerline was used to determine the distance a catheter would have to travel within the CS to reach the mitral isthmus. Next, the 3D models were again re-sliced so that the cross section of the CS at the mitral isthmus was in plane. The diameters, circumference, and shape of the CS were assessed in this plane as well as the distance to the left atrium and presence of fat around the vessel.

The presence of fat and the distance to the left atrial space was also investigated at different positions around the coronary sinus at the mitral isthmus. To do so, a line was drawn across the mitral annulus as a reference. Next, a line parallel to the mitral annulus was drawn across the center of the CS cross-section and defined as 0° . Finally, three additional lines were created through the center of the CS cross-sections at 45° , 90° , and 135° to the 0° line (Figure 12). The presence of fat between the intersection of these lines with the boundary of the CS and the left atrium (LA) was assessed as a binary parameter. Then the distance from the coronary sinus to the left atrial space was measured at each location around the CS.

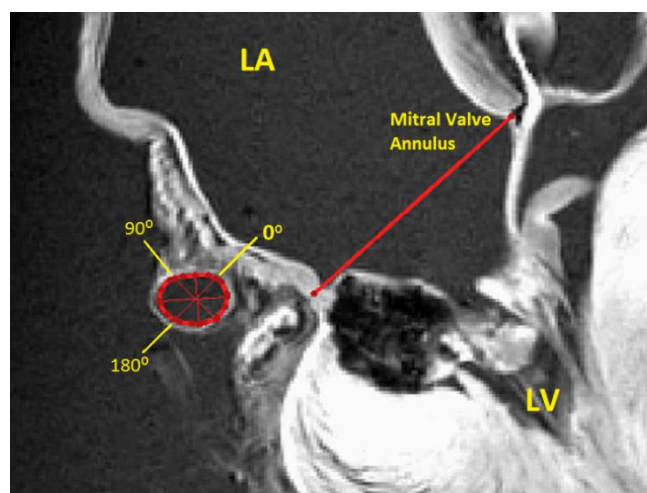


Figure 12: Shown in this image is the method used to analyze the relative amounts of fat present adjacent to the coronary sinus at the mitral isthmus. The 0 to 180 degree line was drawn parallel to the mitral annulus. Using the center of the coronary sinus, 45, 90, and 135 degree lines were created using 0 degrees as the starting point and rotating counterclockwise. The left atrium (LA) and left ventricle (LV) were labeled for reference.

The location of fat was identified by the variation in contrast seen within the MRIs. This was subsequently verified by physically sectioning a heart into 3-5mm thick sections following fixation (Figure 13). Finally, these fixed tissue slices were re-scanned by MRI to verify that the grayscale of the fat around the CS considered to be present in the scans did well correlate to the fat seen on the physical inspection.

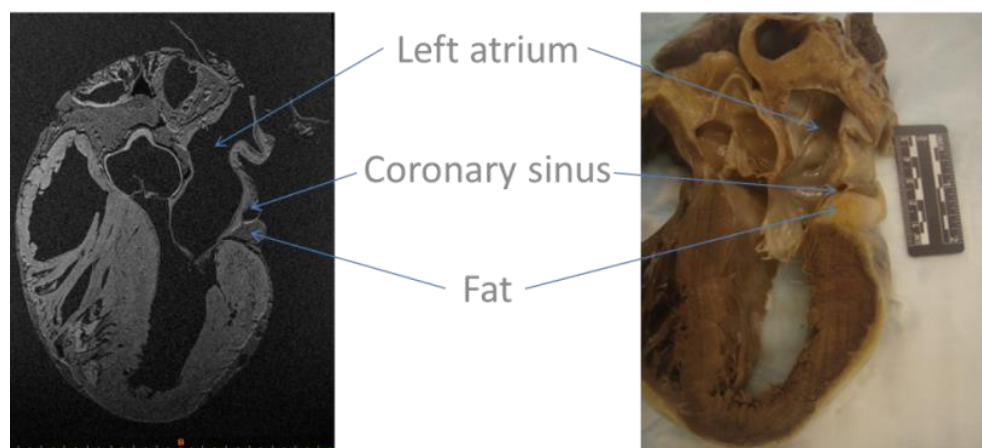


Figure 13: Images obtained for one of the human heart specimens: on the left is an MRI image and on the right is a photograph of the same human heart specimen sectioned to represent the same physical plane. The left atrial endocardial space is labeled. One can observe that the specimen section includes the coronary sinus and immediately inferior to it is a deposit of fat that is visible on both the MRI and photograph.

Statistical Analysis

Data were presented as the means \pm standard deviations. Nonparametric Wilcoxon rank sum tests ($\alpha=0.05$) were performed to determine if there were statistical differences between the AF and non-AF hearts for the various parameters of interest.

Results

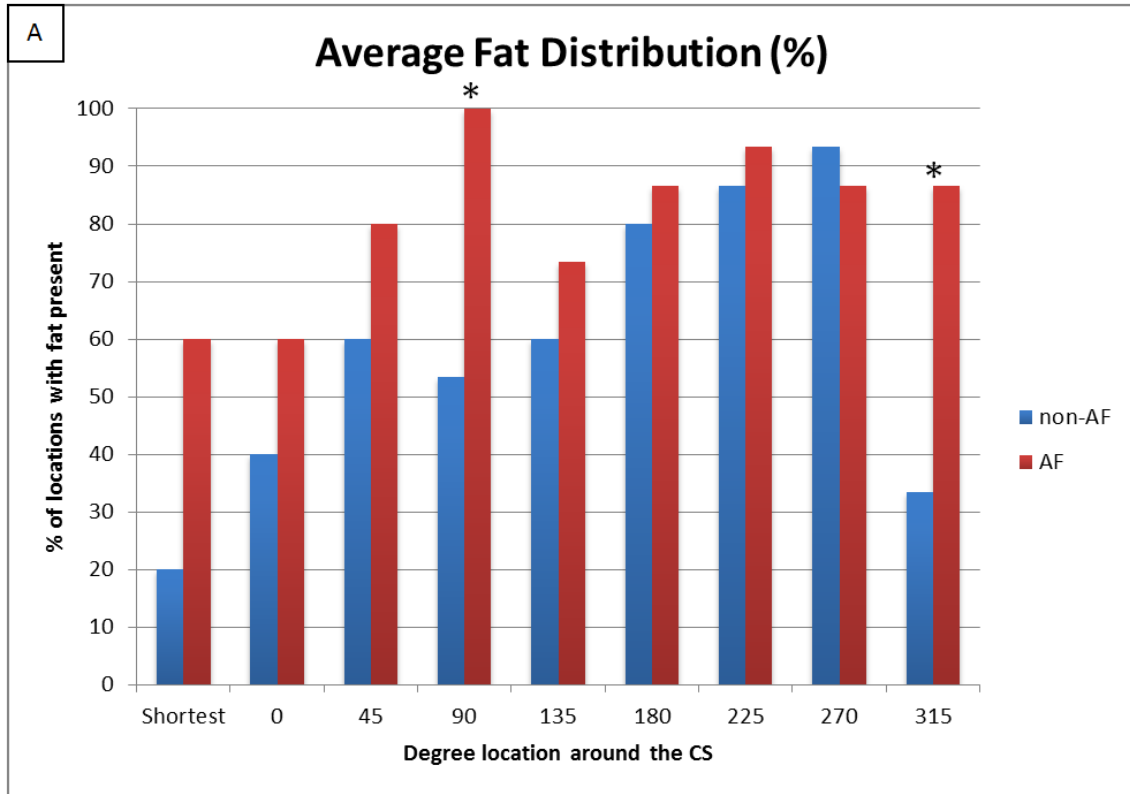
Table 4 summarizes many of the observed anatomical differences between the AF and non-AF patient hearts (n=30). In terms of diameters and circumferences, the coronary sinuses were on average larger at the ostium and smaller at the mitral isthmus for AF specimens relative to non-AF specimens. Significant differences between the AF and non-AF hearts were identified for: 1) the distances along the coronary sinus to the mitral isthmus ($p < 0.01$), 2) the CS long axis diameters at the mitral isthmus ($p = 0.03$), and 3) the shortest distance from the CS to the left atrium at the mitral isthmus ($p < 0.01$) (see Table 4).

Table 4: Coronary Sinus Anatomical Parameters (n=30)

	Non-AF Hearts (n=15)	AF Hearts (n=15)	p- values ($\alpha =$ 0.05)
CS Ostial Plane Measurements:			
<i>CS circumference</i>	31.2 \pm 10.7mm	35.2 \pm 15.3mm	0.63
<i>CS long axis</i>	11.2 \pm 4.1	12.3 \pm 6.9	0.92
<i>CS short axis</i>	6.8 \pm 2.6	7.3 \pm 3.0	0.69
Distance from Ostium to Isthmus along CS	50.4 \pm 14.1	66.8 \pm 14.6	<0.01*
CS at the Mitral Isthmus Plane:			
<i>CS circumference</i>	21.3 \pm 7.8	18.1 \pm 4.1	0.09
<i>CS long axis</i>	8.1 \pm 3.1	6.4 \pm 1.7	0.03*
<i>CS short axis</i>	4.7 \pm 2.0	4.5 \pm 1.4	0.97
<i>CS to LA distances at Isthmus</i>	3.4 \pm 1.3mm	5.6 \pm 2.0mm	<0.01*
<i>General CS shapes:</i>			
<i>Round</i>	4	6	NA
<i>Oval</i>	8	7	NA
<i>Slit</i>	3	2	NA

AF=atrial fibrillation; CS=coronary sinus; LA=left atrium

Figure 5 summarizes the measurements taken at locations around the CS. The overall presence of fat was higher at every position around the CS for the AF specimens with the exception of the 270° position. In addition, the 90° and 315° locations were found to be significantly different ($p=0.03$ and $p=0.01$ respectively). The smallest percentage of fat for the AF patients was observed to be at the 0° location. Altogether, fat was observed in 79 out of 135 locations (59%) in non-AF hearts and 109 out of 135 locations (81%) in hearts with a history of AF. The average distances from the CS to the left atrial space was also larger for the AF specimens at every location assessed around the CS. The 0° and 315° locations were significantly different ($p<0.01$ and $p=0.02$ respectively). The shortest distances to the left atrium were the smallest at the 0° and 45° locations.



Distance (mm) from the coronary sinus to the left atrial

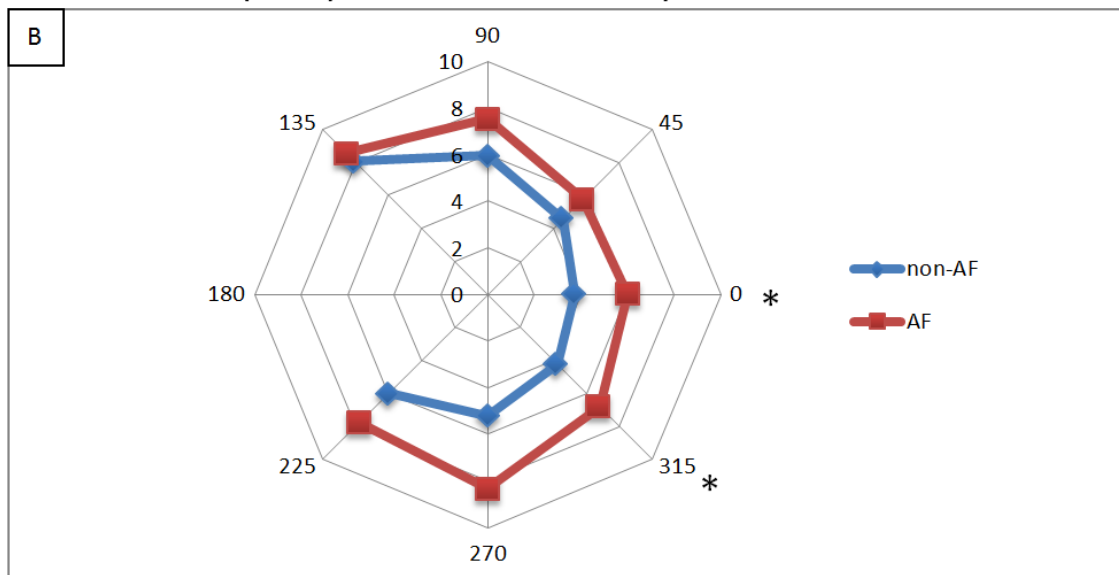


Figure 14: (A) Shown here is a bar graph indicating the relative presence of fat around the perimeter of the coronary sinus. The graph compares the percentage of non-AF (n=15, blue) and AF hearts (n=15, red) where fat was present at different locations around the perimeter of the coronary sinus (CS). (B) Distances between different points around to the coronary sinus and the left atrial space for non-AF (blue) and AF (red) hearts were provided. An asterisk* indicates a significant difference ($p < 0.05$) between these non-AF and AF specimens.

Discussion

The present study was performed so to identify morphologic characteristics of the mitral isthmus and coronary sinus that may influence how focal ablation catheters are operated and how lesions are generated within the atrial tissues at or near the mitral isthmus and coronary sinus. Currently, ablations within the regional anatomy of the coronary sinus (CS) are commonly performed to treat atrial fibrillation (AF). Our novel study investigated this important cardiac anatomy in a set of isolated human hearts. These intact human heart specimens were obtained fresh and then carefully prepared (perfusion-fixed) to allow us to obtain high resolution MRI datasets which were then analyzed. Finally, we sectioned these specimens visually studied them as well as re-scanned them. In general, we observed notable anatomical differences between the hearts with AF relative to those from individuals with no known cardiac histories. We consider here that these detailed analyses will provide important insights not only to the practicing cardiac electrophysiologist and medical device designers as well.

Major Findings

The average dimensions of the CS at its ostium were larger in AF patients than in the hearts with no clinical presentation of AF, but smaller at the plane of the mitral isthmus. The average distance a catheter would have to travel to the mitral isthmus via the coronary sinus in AF specimens was 5.6 ± 2.0 mm, which was significantly ($p < 0.01$) longer than non-AF specimens (3.4 ± 1.3 mm). The perfusion-fixed hearts that were obtained from AF patients had a higher rate of fat present around the CS compared to hearts with no history of AF. The distance between the CS and the left atrial space was larger in AF hearts than the non-AF group at every location around the CS. Interestingly, the short axis diameter of the CS in the region of the mitral isthmus (4.7 ± 2.0 mm) was larger than the commonly available 7 Fr (2.3 mm) ablation catheter tip.

Clinical Implications

The use of traditional anatomical landmarks around the mitral isthmus commonly aids the cardiac electrophysiologist in the location of an ablation catheter tip within the coronary sinus. However, they may be an insufficient approach to ultimately achieve an effective

lesion necessary for electrical isolation⁵⁹. Thus the clinical implications of the present anatomical study are quite relevant to such ablation procedures. We presented anatomical information regarding CS size, CS length, the presence of fat around the CS, and distance relative to the endocardial surface of the mitral isthmus. Each of these parameters can affect the ablation catheter placements, the tip orientations, and/or resultant energy delivered. The data presented in this study also suggest that the ability to create a lesion for AF patients could be impacted by an increased presence of fat and a larger distance between the CS and the endocardial wall. Consistent with such a notion, Wong et al. previously reported that when diameters of the CS at the mitral isthmus are larger than the catheter tip, the catheter tip will need to be manipulated many times in order to achieve tissue contact. The relatively large average diameter found in this study (short axis: 4.7 ± 2.0 mm for AF specimens) suggests that it will be challenging to place the catheter tip on the desired tissue to achieve a successful ablation therapy.

The human heart data provided here also indicated that placement of the catheter tip aimed towards the LA in a parallel direction to the mitral valve annulus may increase the potential for delivery of a successful transmural lesion. More specifically, the 0° position around the CS resulted in the lowest percentage of fat presence (60%) and the second shortest distance to the left atrium at 6.0 ± 2.0 mm (after the 45° position at 5.8 ± 2.0 mm). It is well recognized, that the ability to generate an effective lesion requires that catheters be placed on viable tissue. We suggest here that better understanding of these parameters will allow for planned manipulations of catheters to ensure contact with the desired tissue. In other words, this CS-to-device relationship and the knowledge that there are regions around the CS more susceptible to the presence of fat suggest that catheter placement within CS makes a difference in the creation of an effective lesion set.

It should be noted that the focus of this study did not include lesion characterizations. However, previous work by Yokokawa et al. demonstrated that changes in the ablation settings may be required to achieve a transmural lesion. The results of our study showed that there is an increase in the tissue thickness between the CS and the left atrium in the area of the mitral isthmus for specimens with a history of AF (3.4 ± 1.31 mm for non-AF

hearts versus 5.6 ± 1.97 mm for AF hearts). This, in turn, supports the notion that changes to ablation durations and settings may be required to result in lesion transmural.

Limitations

It may be considered that a potential limitation of our present study is that we did not specifically investigate the device-tissue interface. Hence, we acknowledge that additional work is needed to further understand how to optimize catheter placement and/or designs, along with the corresponding ablation settings, to generate transmural lesions in these anatomical locations most effectively and thus improve single procedure success. Another potential limitation of this study is that the findings may have been affected by the average age of the AF patients, i.e., being significantly higher than our non-AF population. Additionally, it is not fully understood what effects long-term formalin storage of tissues has on the morphology when such high resolution measurements are being made. Ideally, a subset of hearts would undergo fresh analysis followed by preserved analysis to determine the effects. Finally, although we would like to note that it was a major undertaking to obtain this sample of specimens and perform all scans and model generation, it may have not been large enough to achieve statistical power for some parameters due to the inherent high anatomical variability found in humans. Yet, one also has to consider that no difference may typically exist.

Conclusions

Ablation procedures performed within the CS with an aim to alter the function within the left atrium can be very important to the overall efficacy and completeness of overall arrhythmia therapy. Thus, a better understanding this specific regional cardiac anatomy and how it may be altered within the AF patient population can help the physician better utilize (as well as the device designer to optimize) the next generation of ablation systems. The outcomes from this study suggest that additional consideration is required to create lesions in these anatomy which are affected by disease states. Specifically, the slightly longer lengths of the CS in the hearts obtained from AF patients may suggest that the volumes of the left atrium are predicatively larger^{59,62}. In addition, there are clear differences in the thicknesses of the myocardial tissues in the regions of the isthmus in the AF hearts. Finally, the circumferences of the CS indicate that the ability to affix a

catheter in the distal areas of the CS may require specific manipulations to ensure the catheter tip is in contact with atrial tissue.

I.III- Chapter 3: Anatomy of the Human Heart of AF Versus Non-AF Patients

The Visible Heart® laboratory here at the University of Minnesota has created a unique collection of perfusion fixed human hearts. These hearts are being received through a research collaboration with LifeSource (St. Paul, MN), the regional organ procurement organization. Hearts that are deemed not viable for transplant are acquired at the time of acquisition of other organs that are being used for transplant. All such specimens are delivered to the lab within 24 hours, usually within 4 hours of organ cross-clamp time. The hearts are then fixed in formalin in an end diastolic shape. This overall process described in more detail in the article that follows, which was published in the Journal of Geriatric Cardiology.

Briefly, using this unique human heart library we sought to quantify differences between the hearts of donors with and without AF. Parameters relevant to AF were measured, such as: PV sizes, chamber sizes, tissue thickness, and fossa ovalis dimensions.

Specifically, I contributed to all aspects of this publication, including data collection, data analysis, manuscript preparation and submission. I also have aided in the preservation of specimens in the human heart library throughout my stay in the laboratory: when I began my graduate work we had ~150 perfusion dilated heart specimens and at the time of writing there are 300+.

The following is a copy of the published manuscript.

I.III.I- Cardiac remodeling as a consequence of atrial fibrillation: An anatomical study of perfusion-fixed human heart specimens

Christopher D. Rolfes, PhD^{7,8,9}; Stephen A. Howard, PhD^{8,9,10}; Ryan P. Goff, BS^{8,9}; Paul A. Iaizzo PhD^{8,9}

Executive Summary

Background Atrial fibrillation (AF) causes a continuum of atrial anatomical remodeling.

Methods Using a library of perfusion fixed human hearts, specimens with atrial fibrillation were compared to controls. During this preliminary assessment study, direct measurements were taken of atrial volume, pulmonary vein (PV) circumference, and left atrial wall thicknesses.

Results Hearts with AF typically had larger atrial volumes, as well as a much larger variation in volume compared to controls (range of 59.6-227.1mL in the AF hearts compared to 65.1-115.9mL in control). For all hearts, right PVs were larger than left (mean 171.4 ± 84.6 for right and 118.2 ± 50.1 for left, $p < 0.005$). Left atrial wall thicknesses ranged 0.7-3.1mm thick for both AF and control hearts.

Conclusions Hearts with AF had a large range of sizes which is consistent with the progression of atrial remodeling during AF. The large range of thicknesses will influence the amount of energy needed to create transmural lesions during ablation procedures.

Keywords: Left atrial dimensions, volumes, pulmonary vein ostia, atrial fibrillation

Introduction

Atrial fibrillation (AF) is the most prevalent tachyarrhythmia, with a prevalence of 1% in the general population¹. One of the particular clinical features of this arrhythmia is its self-perpetuating nature. Paroxysmal AF (self-terminating episodes) may eventually turn into persistent (> 7 days) and then even permanent AF³⁻⁵. This progression is considered in part, due to both structural and electrophysiological remodeling of the tissue that

⁷ Department of Biomedical Engineering, University of Minnesota (Minneapolis, MN)

⁸ Department of Surgery, University of Minnesota (Minneapolis, MN)

⁹ Medtronic Inc., Mounds View, MN

provide substrates for maintenance of such arrhythmias. Structural remodeling associated with AF refers to physical changes, such as dilation of the atria and interstitial fibrosis. The electrophysiologic remodeling results the shortening of the atrial effective refractory periods, thus aiding the perpetuation of an arrhythmia and/or limiting the ability to terminate fibrillations. More specifically, the self-perpetuation is especially disturbing symptom when patient long-term prognosis is taken into account: mortality rate doubles and stroke occurrence averages up to 5% per year in patients with AF, which is 2 to 7 times the rate of individuals of similar ages whom are uninflected with AF⁵.

The prevalence of atrial fibrillation in relation to age and associated risks

The clinical treatment of AF is an especially relevant topic in geriatric cardiology due to the well documented increasing prevalence with age. When considering an overall general population, the relative prevalence of AF is 1%, yet in persons over 40 years of age the prevalence reaches 2.3% and then climbs to 5.9% for individuals over 65². The geriatric population, defined by the WHO as persons with age greater than 65, contains over 75% of people suffering from AF¹. It should also be noted that AF has also been found to be more common in men than women (1.1% versus .8%)¹.

Atrial fibrillation is well known to be associated with decreases in quality of life: as reported by as many as 68% of patients with paroxysmal AF⁷³. Interestingly the psychological, not physical, quality of life may be impacted more⁷⁴. In addition to stroke⁵, AF has also been associated with many other health problems that would cause decreases in quality of life such as depression, professional and sex life complications⁷⁵, etc. However, it is debated whether or not AF is or is not associated with cognitive decline⁷⁶⁻⁷⁸. It is highly probable that because AF causes an increased risk of stroke and emboli, that cognitive decline in part be linked to the potential for multiple small and transient cerebral infarcts, yet this will also be dependent on the given patient and their anticoagulation management⁷⁹.

In addition to the above detrimental effects of AF, anatomical remodeling of the atria can occur within the heart. Patients who have AF tend to have larger left atria and larger pulmonary veins which could potentially lead to the further propagation of AF⁸⁰. Alternatively, the reverse has also been shown: upon return to sinus rhythm after radiofrequency ablation, there is a measureable reduction in left atrial size^{81,82}. Depending

on the length of AF and the stage of remodeling, patients with the arrhythmia may have large variation in their anatomy.

Left Atrial volume measurements

Heart left atrial (LA) volumes have been selected here to be measured in this sample of perfusion fixed human hearts, due to reported AF related atrial remodeling (dilations). For example, the work by Leung et al. found that increases in LA volumes could be used to independently predict the increased risks of cardiovascular death, heart failure, AF, stroke, or MI⁸³. Further, subsequent reductions in LA volumes (reverse remodeling) has been found to be a strong predictor of the successful treatment of AF using either catheter based⁸⁴ or surgical⁸⁵ ablations. Relative LA volumes for a given patient have also been found to predict the potential for recurrence of AF after cardioversion⁸⁶ and conversion of atrial flutter to AF after successful ablation⁸⁷. More specifically, the probability of relapse after catheter ablation was found to be significantly higher for LA volumes greater than 145 ml⁸⁴. LA volume index greater than 135 ml/m² was found to have 100% specificity and LA diameter greater than 60mm was found to have 100% sensitivity for prediction of surgical Maze failure⁸⁵. Not surprisingly, normal LA volumes have been found to be associated with absence of thrombus⁸⁸ and relative LAA dimensions have been found to be a positive predictor for stroke/TIAs in patients with AF⁸⁹.

Pulmonary vein sizes

Since the clinical discovery that the pulmonary veins (PVs) can be substantial site-sources of ectopic beats⁷, PV anatomy has attracted increasing attention. A patient's pulmonary vein sizes are useful measurements when planning for an ablation since some procedures, such as cryoballoon ablation, offer multiple sized devices to optimize PV isolation. The PV circumference was chosen because even though the PVs (especially the left PVs) are typically oval in shape⁹⁰, they are also considered as compliant and a balloon pushed against the ostium will slightly change its shape. In other words, using simply the long or short axis for planning may lead to the decision to use a balloon that is too big or small, respectively.

Left Atrial Wall Thicknesses

Left atrial wall thicknesses are also commonly assessed and were done so here as well. The area on the posterior wall near each of the PVs was measured as well as the center of the posterior wall. These locations were selected not only because they are smooth in comparison to the left atrial appendage, but they are often areas of therapeutic focus during AF ablation procedures. Variation in LA wall thicknesses is also important to consider during radiofrequency ablation procedures, since it should influence the amount of energy to be applied⁹¹.

One of the primary goals of this preliminary assessment study is to present our ongoing investigations as to human cardiac anatomy. Our Visible Heart® Laboratory has a current library of over 200 human heart perfusion fixed specimens that we can uniquely employ for such investigations. In addition, many of our obtained images and videos of functional cardiac anatomy are available to the general public, via our free-access web site, “The Atlas of Human Cardiac Anatomy” (<http://www.vhlab.umn.edu/atlas>).

Methods

Human hearts deemed not viable for transplantation were donated for educational and research purposes. Following similar guidelines for transplantation, the hearts were stopped, cooled and transported to our lab. Within 24 hours of being excised, these specimens were weighed and the aorta, superior vena cava, pulmonary artery, pulmonary veins and the inferior vena cava (when possible on a given specimen) were cannulated and attached to a perfusion fixation chamber as described previously⁵⁰. This approach will preserve the hearts in a modified end-diastolic state (fully expanded atria and ventricles). These hearts were fixed with 10% formalin in PBS solution for at least 24 hours under normal physiologic pressure and then stored in formalin.

Heart specimens have been collected and added to our library since 1997 and to date the library has grown to over 200 in the collection. Anatomical studies can be performed on this large collection so to better understand the variation in anatomy between different hearts. For most of such specimens, pertinent clinical histories are also available, thus allowing us to assess the variation in anatomy with respect to the relative disease state of the heart. In the present study, we identified and used hearts that had a clinical diagnosis

of AF and compared them to hearts with no indication of AF or mitral/tricuspid regurgitation (normal anatomy). The AF hearts were sex, age, weight, and height matched to control hearts. For all but 2 of this sample of 10 AF hearts, acceptable control hearts were found and/or were measureable (Table 5).

	AF	Control
n	10	8
age (sd)	69.9 ± 11.6	63.9 ± 12.5
male (%)	6 (60)	4 (50)
weight (kg)	80.8 ± 21.8	93.5 ± 31.5
CAD (%)	2 (20)	0 (0)
HTN (%)	4 (40)	5 (62.5)
Valve insufficiencies	0	0

Table 5: Patient information from atrial fibrillation and their corresponding control hearts. For all but two AF hearts suitable matches were found as controls based on subject genders, ages, weights and heights for these collected specimens.

To measure the volumes of the atria, the hearts were oriented such that the annulus of the atrioventricular valves would be parallel to the ground while measuring their respective side. To measure the volume of the left atrium (LA), the aorta and all but one PV were clamped off and the LA and left ventricle were filled with deionized water. After the LA was completely filled the water was drawn out and collected until the water level reached the level of the annulus of the mitral valve, which was determined by visualization using a fiberscope. The weight of the water was taken and this process was repeated a minimum of three times. The right atrium (RA) was measured the same way; however the pulmonary artery, inferior vena cava, coronary sinus and posterior interventricular vein were closed up and the water was drawn out to the level of the tricuspid valve. The siphoned water was weighed and repeated three times. Note, that since deionized water was used, the weight of the fluid is equivalent to the volume of the chamber.

All of the other anatomical measurements that were recorded were obtained using standard calipers or a C-clamp micrometer. The thicknesses of the LA were determined using the C-clamp at five distinct locations: the center of the posterior LA wall and the junction of the right superior, right inferior, left inferior and left superior PVs. The

junction of a PV was defined as the location in which the vein transitioned into the wall of the left atrium. To determine the relative areas of the PVs, the opening of each vessel was pinched together to measure half of the circumference (Figure 15) and obtain an area assuming the vessel is circular. Although it has been found in the literature that the PVs are generally oval in shape, it was decided that comparing the vessels as circular would alleviate the problem of re-approximating the oval shape of the pulmonary veins. Furthermore, in some of these cases, the PV can be slightly distorted due to the nature of the fixation process.



Figure 15: Illustration of the half circumference measurements taken to obtain diameters and area measurements of the various PVs.

The size of the fossa ovalis (FO) in each specimen was also measured; it should be noted that since the FOs were not collapsed during the fixation process, we were able to obtain accurate assessment of these structures. These areas were determined by measuring the diameters along the superior/inferior and the anterior/posterior direction of each FO. Values presented are mean with standard error unless otherwise noted. For comparisons of continuous variables between two groups a Student's t test was used.

Results

Within these investigated hearts, as expected the AF hearts had larger LA, RA and total atrial volumes compared to the controls hearts (Figure 16). However when we compared

individual AF heart to their specific sex, age, weight and height matched control, there was no clear correlation as to which types of heart had larger atrial chamber sizes. Yet, the data did suggest that there was a higher variability within the hearts from the AF patients compared to the controls: with a range of 59.6ml to 227.1ml in the AF hearts compared to 65.1ml to 115.9 ml in the control hearts. Note that the differences in ranges for both atria are over 3 times larger in the AF group than in the control group.

	All PVs		Right PVs		Left PVs	
	Mean (mm ²)	Median (mm ²)	Mean (mm ²)	Median (mm ²)	Mean (mm ²)	Median (mm ²)
AF	152	139	193	170	116	109
Control	138	120	156	126	121	100

Table 6: The mean and median values of the pulmonary vein ostia between AF and control heart specimens.

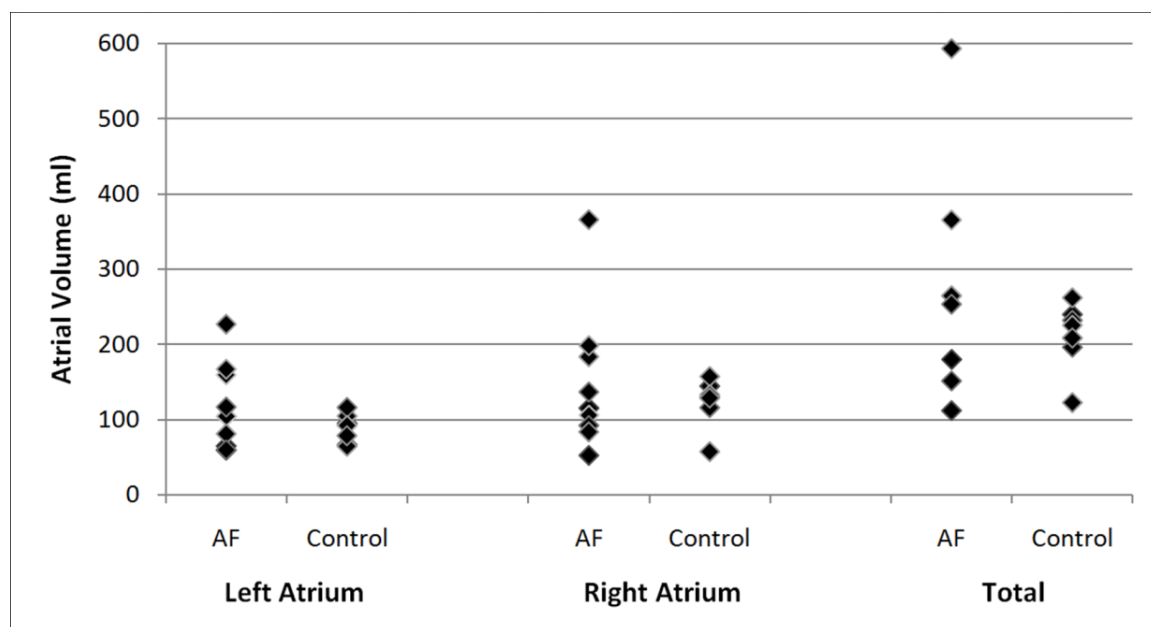


Figure 16: Comparisons of the paired left, right and total atrial volumes between the matched AF and control hearts. Note that the AF hearts had greater variability of volumes compared to the controls.

As noted above, the sizes of the pulmonary veins were assessed by assuming all as circular openings (Figure 17). Between the two groups, the control hearts had smaller PV ostia for both the left and right veins. One can observe two different peaks on these histograms; with the higher peak associated with the data from the AF hearts. This

finding was consistent also when the right and left PVs were compared separately (Figure 17). Interestingly, there was also the observed trend that the left PVs were smaller than the right PVs in both the control and AF specimens (Table 6). Further, when trying to determine that the right PVs were larger than the left, while looking at the whole population of hearts, there was a significant difference seen between the two (mean 171.4 ± 84.6 for right and 118.2 ± 50.1 for left, $p < 0.005$).

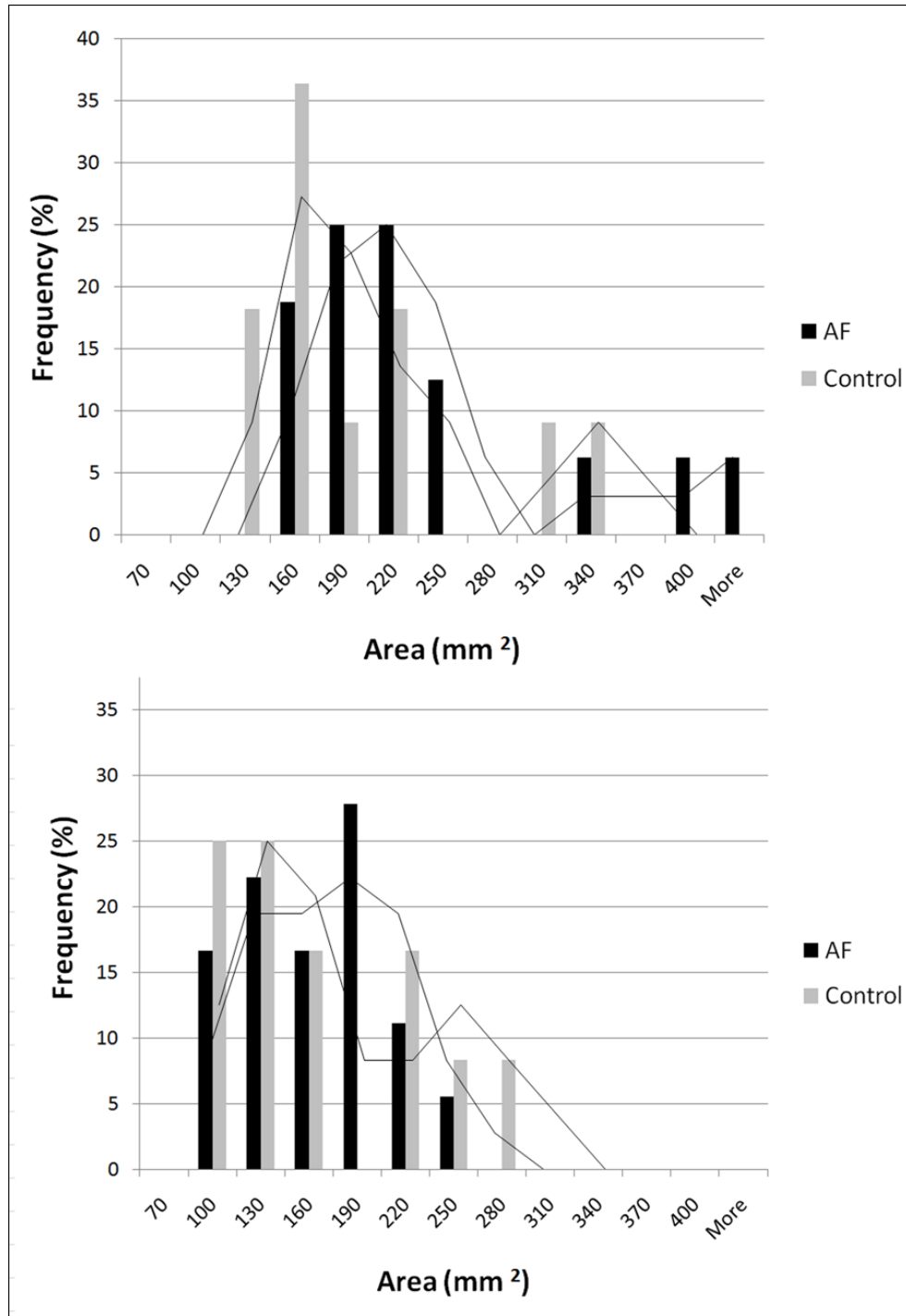


Figure 17: The relative variation in pulmonary vein ostia sizes between the two groups of heart specimens. The histograms provide the corresponding areas of these ostia. Top: the relative distributions of pulmonary vein sizes of the right pulmonary veins; with means of 24.2mm² and 21.6 mm² and medians of 23.1 mm² and 19.9 mm² respectively. Bottom: the left pulmonary vein areas, means of 18.7 mm² and 19.0 mm² and medians of 18.4 mm² and 17.7 mm² respectively. The trend lines depict the two point moving averages of the distributions and illustrate the relative differences between these two heart populations.

Although there were observed trends between the relative areas of the PV ostia of these two groups, in contrast there were minimal differences in the thicknesses of the LA walls within our samples: the means and medians were 1.19mm and 1.24mm for the AF population and 1.26mm and 1.21mm for the control population, respectively. The histograms and population spreads between the AF and control groups appear to elicit a fair amount of overlap; in other words, they appeared similar between the groups and were not dependent upon the diagnoses of AF (Figure 18). Similar findings were also observed when examining the relative sizes of the FO in these hearts. The FO dimensions only had slightly larger sizes in the anterior-posterior (AP) vectors, whereas they elicited minimal or no differences in the superior-inferior vectors (SI) (Figure 19).

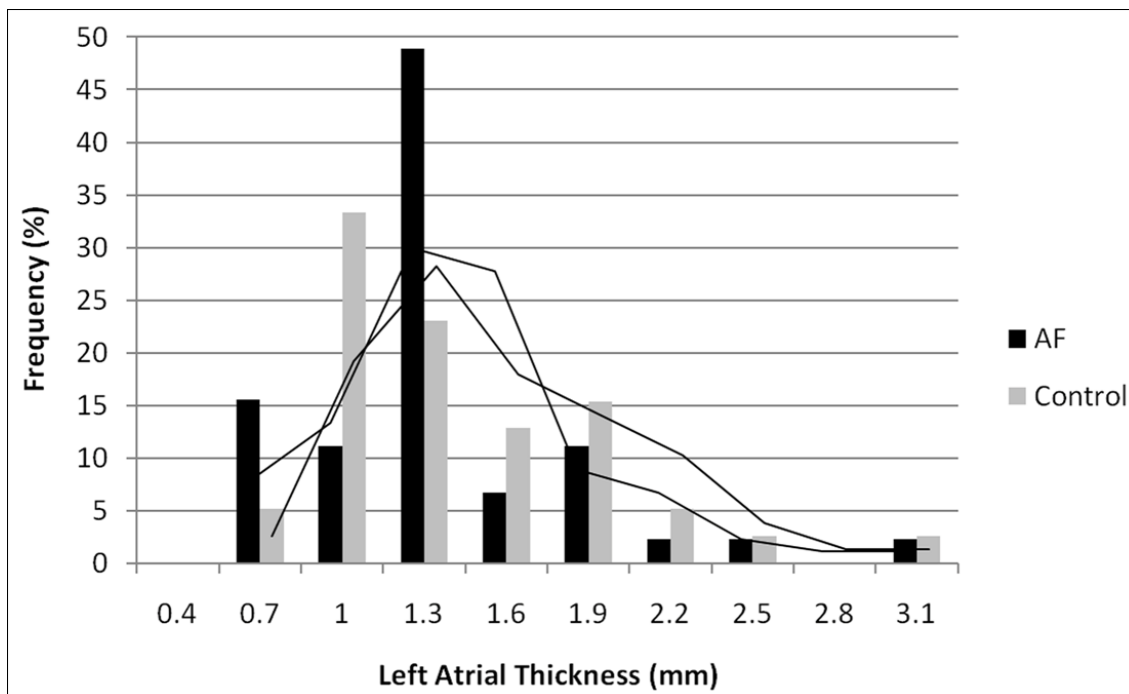


Figure 18: Relative distribution of thicknesses of the left atrium between the AF and control hearts. These thicknesses values were determined by taking measurements from each of the four pulmonary vein junctions in each heart, as well as the center of the posterior walls of the left atria. The trend lines depict the two point moving averages of the population distributions.

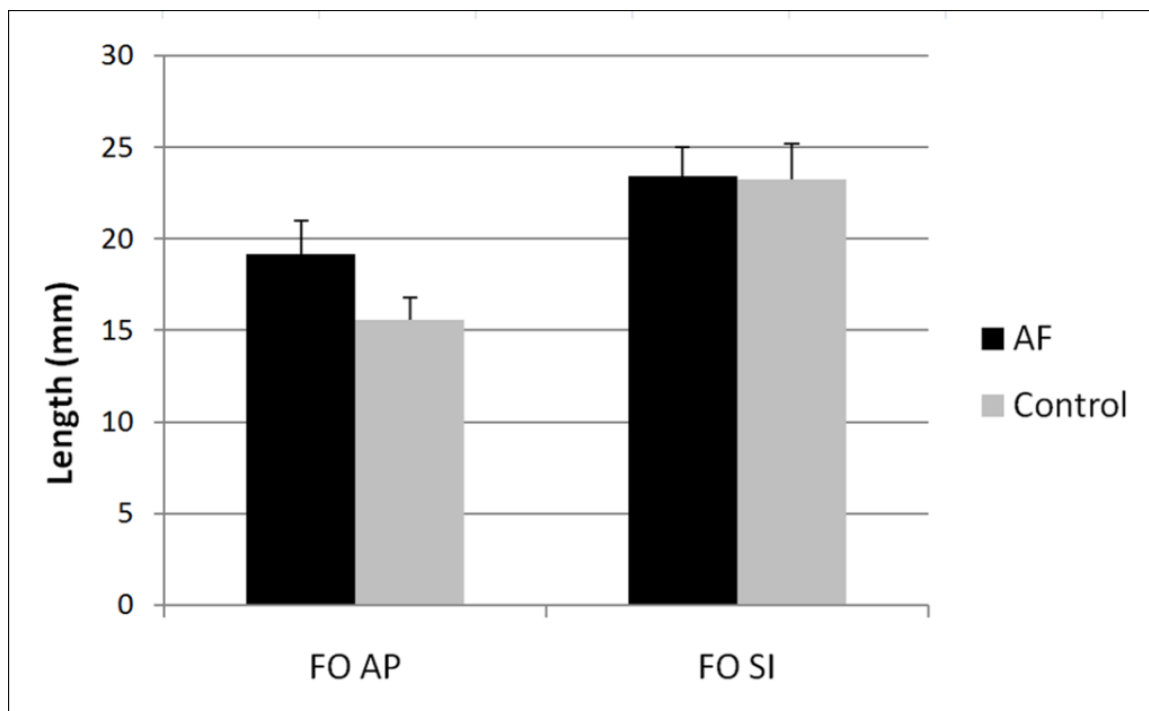


Figure 19: Average widths and heights of the fossa ovalis sizes between the two populations of hearts. The relative widths of the fossa ovalis were designated as the fossa ovalis anterior-posterior (FOAP) measurements and the heights were designated as the fossa ovalis superior-inferior (FOSI) measurements (error bars represent the SEs). It was observed that there were no significant differences between the calculated averages of the measurements taken of and the distributions of the sizes showed similar trends between the AF and control hearts (data not shown).

Discussion

In the present study we describe novel measurements of relevant cardiac anatomy obtained from our unique library of perfusion fixed human hearts. In this preliminary assessment study, we describe approaches to allow for the detailed quantifications of specific atrial anatomy. The presented information provides useful insight as to the changes in structure that may occur when the human heart remodels following the development of AF, and we plan to continue these studies as our relevant library of specimens grows.

Current imaging modalities, including MRI, ultrasound, and CT scans, allow for relative approximations of the volumes and sizes of the LA and RA using algorithms available in various software packages or by simply estimating diameters. Yet, it is considered that measurements of LA volumes are more accurate than diameter data, especially as a given

heart dilates, i.e., small increases in diameter will provide for larger increases in derived LA volumes^{50,92}. Our volume measurements take into account the variability of chamber anatomies from heart to heart, and thus resulted in a more accurate representation of the total chamber sizes. Therefore, these chamber volumes, along with thickness measurements of the LA, were considered to better point to variations in anatomy due to a given pathological state. However based on our data on this somewhat small sample size, we could not make correlations as to the clinical state based solely on these measurements. Yet, it should be noted that even in the absence of AF, large atria are often indicative of other cardiovascular issues⁹³, thus in these hearts we studied from this elderly population of subjects it was likely that the non-AF hearts, or so-called controls, may have been not truly normal.

Our initial characterization of these AF hearts confirmed various trends that have been reported within current literature, such as the increased sizes of right PVs compared to the left PVs⁸⁰. However, as with most anatomical studies a large sample set is required so to potentially produce statistically significant results. With our growing library of these perfusion-fixed human hearts, we will be able to perform ongoing anatomical studies so to better assess the differences within various populations of heart disease states or demographics. Our collection of specimens to date has allowed us to obtain useful insights as to the common anatomical features of the atria from patients with AF with a high degree of accuracy. The variety of physical specimens also allows for physician education and therapeutic device feedback as any number of devices can be placed within the hearts. The continued study of the details of human cardiac anatomy will provide further insights as to the changes in structure that may occur when the human heart remodels or reverse remodels due the presence of disease or following treatment, respectively. Though above study shows that PV measurements are not sufficient to diagnose AF, it illuminates the variety of anatomies that accompany the arrhythmia within the population. This large variation observed in the diseased patients is important for the physicians who treat AF, the educators, and engineers who must design medical devices to fit the whole range of anatomies. Using the fixed hearts we plan to continue to employ the study methods described here to further build an anatomical database, which we hope to compare to MRI, CT and 3-D models derived from each.

Conclusion

Atrial fibrillation comes with a great deal of anatomical and physiological changes. Anatomically, the size of the atria can vary greatly, but the pulmonary veins and vena cavae do not remodel significantly. The variation in anatomy has great importance and should be considered when treating and designing devices for AF.

Acknowledgements

The authors would like to thank Krista Rothstein, Scott Pearson for their help collecting measurements as well as LifeSource, the donors, and their families for contributing to the collection of human hearts at the University of Minnesota.

I.IV- Chapter 4: Imaging of balloon based catheters using Visible Heart methodologies

One of the unique opportunities available for our lab's use is the imaging capabilities of the Visible Heart® methodologies. In other words, the isolated heart system described in detail previously⁹⁴⁻⁹⁶ allows for a simultaneous multimodal imaging. This is especially useful for the medical device designer and physician for the testing of prototypes, education, practice, and mental visualization of various clinical procedures/techniques. With the end goal of producing educational publications on cryoballoon ablation I began by partnering with a colleague, Dr. Oliver Bandschapp, on imaging of a pulmonary artery catheter. Commonly referred to as the Swan-Ganz catheter, this device is a balloon tipped catheter, similar to the ArticFront (Medtronic, Inc.) cryoballoon catheter. A shortened version work was published in the American Journal of Respiratory and Critical Care Medicine (impact factor 11.04) in 2012. This video begins with footage filmed in the clinic of placement of a pulmonary artery catheter and ends with endocardial journey into the distal pulmonary artery wedge position.

After working with Medtronic and Professor Iaizzo, I was able to procure a Cryo Console for permanent use in the laboratory and from there I produced an imaging piece detailing the visualized cryoballoon ablation procedure. In brief, this work demonstrates the commonly employed endocardial procedure, with accompanying fluoroscopic views that the electrophysiologist would normally see. A similar piece of work which compared the new generation cryoballoon to the previous was selected for a poster presentation at the 2013 Transcatheter Therapeutics conference. The accepted abstract can be found in the appendix. Videos are also included on the Atlas of Human Cardiac Anatomy website. This preliminary work was followed up with more advanced imaging and quantitative work utilizing reanimated heart-lung blocs, see section 3. These novel, initial studies allowed us to optimize imaging of balloon catheters and also brought to light shortcomings that were later improved upon (i.e., including the lung in the preparation for imaging of pulmonary vein isolation).

I.IV.I- The Path of a Swan Ganz Catheter Visualized through a Beating Human Heart

Oliver Bandschapp, MD^{10,11}, Ryan Goff¹¹, George Mallin¹¹, Michael Loushin, MD¹², and Paul A. Iaizzo, PhD^{11,12}

Reprinted with permission of the American Thoracic Society. Copyright © 2014 American Thoracic Society. *Am J Respir Crit Care Med.* 2012;186(4):385

In 1967 cardiologist Dr. Jeremy Swan envisioned placing a catheter into the pulmonary circulation via the right heart by using a catheter with an inflatable balloon at its tip to assist navigation without the use of fluoroscopy, which was standard practice at the time. His concept predicted that the movement of the balloon would be assisted by the blood flow, to direct the catheter through the right atrium, past the tricuspid valve, through the right ventricle, past the pulmonary valve, and into the pulmonary circulation. The story has been told that Dr. Swan observed sailboats off-shore on a sunny day in Santa Monica; all boats were becalmed, except for one, a sailboat with a large spinnaker that made reasonable speed, despite only calm winds. This observation stimulated the idea of a balloon-tipped catheter.⁹⁷ Together with Dr. William Ganz, Swan planned to measure the intracardiac pressures at the distal lumen of this balloon catheter. By doing so, they reasoned that even without visualization, they would know where the tip of the catheter was located at any given moment. In essence, they would be able to ‘monitor’ the whole procedure and deliver their special catheter safely through the heart. Swan and Ganz were right.⁹⁸ Their procedure proved feasible and reasonably safe to be performed at the bedside, with only conventional monitoring in place (i.e., ECG, blood pressure, SpO₂ and intracardiac pressure readings through the distal lumen). The relative ease of performance and the substantial amount of information gathered (i.e., assessment of cardiac output, wedge pressure) quickly made their flexible balloon catheter an essential diagnostic tool in intensive care units worldwide.⁹⁹ However, a wealth of new data now show that the use of these catheters in critically ill patients has not always been

¹⁰ Department of Anesthesiology, University of Basel, Basel, Switzerland

¹¹ Departments of Surgery, Biomedical Engineering, and Integrative Biology and Physiology University of Minnesota, Minneapolis, USA

¹² Department of Anesthesiology, University of Minnesota, Minneapolis, USA

associated with improved clinical outcome.^{100–103} So, there is substantial controversy about the use and indications of Swan Ganz catheters at the moment, and the discussion is ongoing.^{104–106} It is not the intention of this video publication to add to the discussion, but rather to give a reprise of Dr. Swan’s vision of ‘sails in the wind’. Here we employed Visible Heart® methodologies to reanimate a human heart (male, 45 years) with a clear perfusate and make such stunning catheter placement images possible.⁹⁴ Although this heart was not deemed viable for transplant, we were able to elicit viable function of the heart in vitro; it sustained a normal sinus rhythm and cardiac outputs over 4 L/min. Thus, what started in Dr. Swan’s mind and what we all are imagining ourselves, while staring at the pressure curves during Swan Ganz catheter placement, is visible in this actual video footage – a balloon catheter traveling through the valves and chambers of a right human heart into a wedge position in the pulmonary circulation, in synchrony with typical pressure readings from the distal lumen and a timed computer animation.

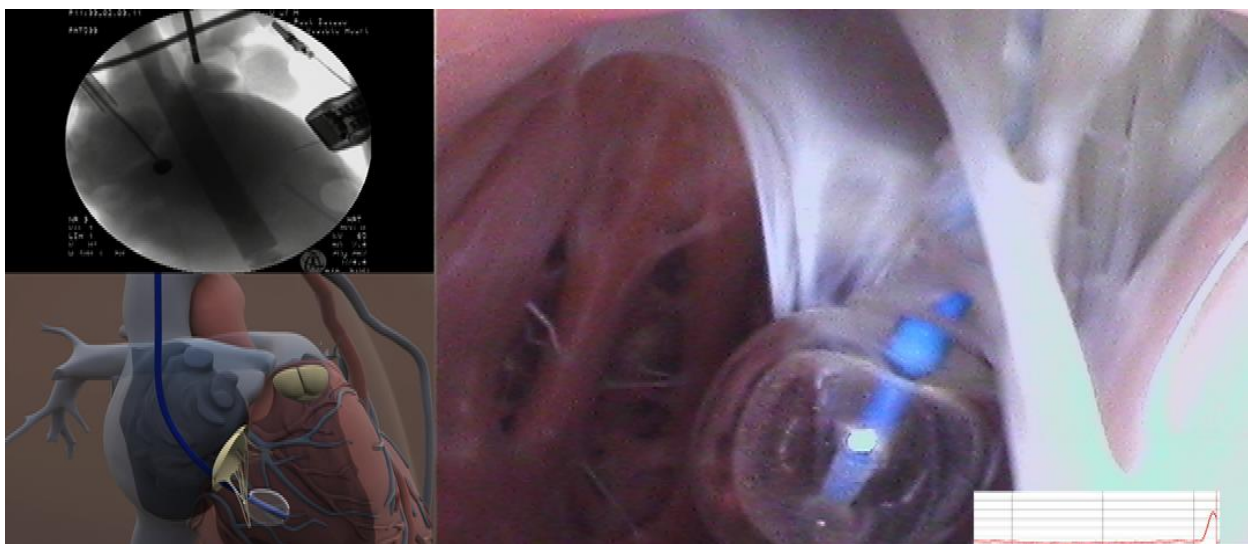


Figure 20: A representative screen shot of the video as the Swan Ganz catheter is passing through the tricuspid valve. On the top left a fluoroscopic image is presented with a computer animation found below to aid the viewer in navigation. On the right, using endoscopy and Visible Heart® methodologies¹¹, direct visualization of the balloon is shown with the beginning of the characteristic transition in pressure waveform found bottom right.

Advancing the Swan Ganz catheter through the heart into wedge position

The following is a synopsis of a typical catheter deployment: after central venous (i.e., internal jugular vein or subclavian vein) cannulation, the flexible balloon catheter is

placed intravascularly through an introducer. Before placing the catheter through this port, the operator confirms correct pressure readings from the distal lumen, by gently swinging the catheter tip. The movement of the catheter should appear on the monitor as a swinging pressure curve. Additionally, the balloon is inflated to make sure no leak is present and then deflated prior to placement. Of note, the balloon should be inflated prior to advancing the catheter forward and should be fully deflated prior to withdrawing or pulling back on the catheter. Patients should be monitored with ECG, blood pressure, and SpO₂ at all times, as severe arrhythmias can occur during placement of the catheter and/or even later on.^{107,108} Then, the catheter is advanced 10-15cm into the vessel and the balloon is inflated. By connecting the distal lumen with a pressure transducer, one can observe the actual pressure present at the tip of the catheter during the whole procedure. As the catheter is advanced further into the right atrium, the measured pressure remains constant at low levels and the waveform stays flat, consistent with the components of a central venous pressure waveform. As soon as the tip of the catheter enters the right ventricular chamber, ventricular pressure readings appear, indicating the intraventricular position of the catheter tip. The typical pressure reading of high systolic pressures together with near zero diastolic pressures is present, as long as the tip of the catheter is located in the blood pool within the ventricle. If, despite further advancement of the catheter, the pressure curve does not change this characteristic, the catheter needs to be redrawn. This could signify that the catheter is looping inside the ventricle; catheter knots have been described.¹⁰⁹ However, once the balloon passes the pulmonary valve, the pressure curve shows an abrupt increase of the diastolic pressure together with a stable systolic pressure. This increase of diastolic pressure signals that the balloon has just passed the pulmonary valve. The catheter is now advanced further into one of the pulmonary arteries. As soon as the balloon arrives in the wedge position – the balloon obstructs the entire lumen of the vessel – a characteristic decline of the pressure waveform occurs and the pulsatile pressure waveform ceases. The obtained pressure readings (‘wedge pressure’) can now be used to assess the fluid status of the patient and give indirect information about the filling pressures of the left heart chambers.^{110,111} Importantly, as soon as the actual wedge pressure readings are taken, the balloon should be deflated, as lung infarction could occur if it is left inflated and wedged for a duration of time. If the balloon is deflated, there

should always be a pulsatile waveform in the distal pressure reading on the screen. If not, the catheter has migrated too far into the pulmonary circulation and needs to be redrawn immediately; fatal vessel rupture or lung infarction could occur otherwise.^{112,113}

Additionally, the Swan Ganz catheters can be used for cardiac output assessments, either by thermodilutionary methods with cold saline or, as presented in the actual video footage, with a balloon catheter capable of continuous cardiac output monitoring.

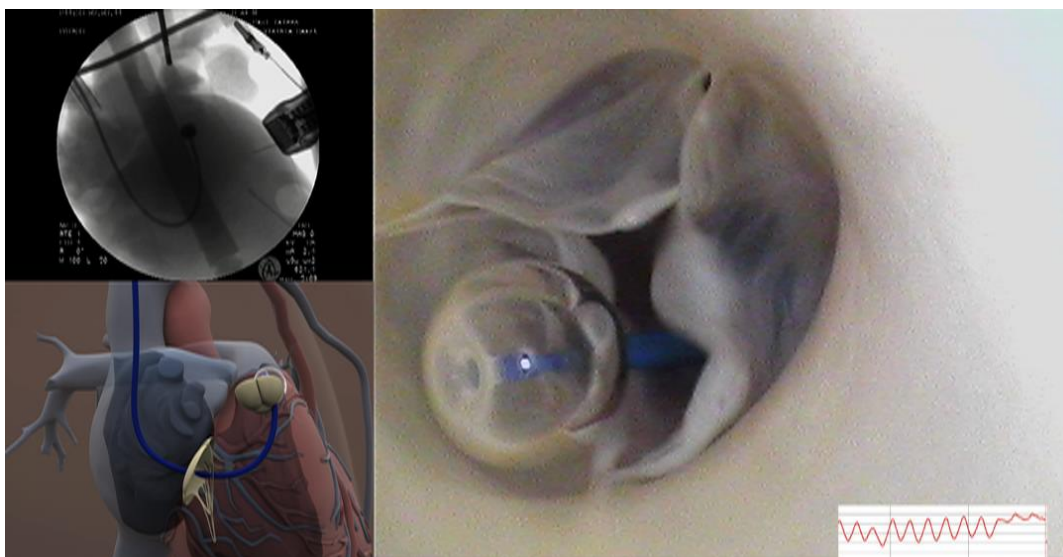


Figure 21: A screen shot similar in description to Fig. 1, but of the pulmonary valve. Note characteristic change in diastolic pressure as the balloon passed through the valve found on the bottom right.

The insertion and application of Swan Ganz catheters requires meticulous care and attention to detail. The intervention is, by its nature, invasive; grave complications during such action can and do occur.¹¹⁴ To bring the best care to patients, the anatomy and physiology of events need to be thoroughly understood. This video provides a novel visual perspective of the critical events that occur while inserting a Swan Ganz catheter and shows the resistant yet fragile intracardiac structures. We also refer readers to the ‘Pulmonary Artery Catheter Education Project’, which can be found at www.pacep.org for additional theoretical and educational coverage.

Financial support: This research was supported in part by the Department of Surgery at the University of Minnesota and LifeSource. The computer animations of Swan Ganz catheter footage were provided by Medtronic, Inc..

Acknowledgements:

We would like to thank this organ donor and family for the generous gift of this heart for research; the patient was a cardiac resuscitation victim whose heart was not deemed viable for transplant. Additionally, we would like to thank LifeSource for performing the organ recovery and transport to the University of Minnesota. We thank the staff at Medtronic, Inc. for their continuous support of the Visible Heart® project. Furthermore, we thank Michael Leners for his computer animated Swan Ganz catheter footage. Lastly, the authors thank Monica Mahre for editorial assistance and help with manuscript submission, as well as Gary Williams for his support with video footage.

I.IV.II- Multimodal imaging of a cryoballoon ablation within a reanimated hearts.

Background:

Cryoballoon ablation is a relatively new ‘single-shot’ treatment modality for pulmonary vein (PV) isolation in patients with drug refractory recurrent symptomatic paroxysmal atrial fibrillation (AF).

Treatment using the cryoballoon for pulmonary vein isolation has been reported in the literature to have comparable efficacies and safeties to the widely practiced radiofrequency ablation³⁵.

Despite the ease of a ‘single-shot’ approach, there can remain technically difficult maneuvers needed to successfully access the right inferior pulmonary vein: e.g., the hockey stick, C-loop, inversed C-loop, and pull-down techniques¹⁶. This, along with the suspicion that undersizing balloons increases risk of procedural complications³⁵, warrants further study of the device-tissue interaction. To date, these interactions and procedural workflow has yet to be reported on using isolated large mammalian hearts that allow direct visualization of the procedure.

Methods and Results:

Human hearts and 75-85 kg Yorkshire cross swine hearts were procured using anesthetic and surgical procedures of cardiac transplant^{95,115}. The hearts were then reanimated using Visible Heart® methodologies described previously¹¹⁵. Following catheter placement in the right atrium, via the inferior vena cava, a transseptal puncture was performed using a Brockenbough needle (Medtronic, Inc., Minneapolis, MN) to catheterize the left atria. The ArticFront® cryoballoon and a FlexCath® steerable sheath (Medtronic, Inc.) were introduced to the left atria using an over the wire method. Subsequently, the cryoballoon was positioned in the left pulmonary vein ostium and inflated. Fluoroscopic contrast mixed with blue or green dye, for videoscope visualization, was injected into the PV to verify proper placement. Leakage of the

contrast around the balloon indicates poor initial placement. After repositioning and confirming occlusion, a four minute ablation was performed.

Images obtained from human heart 271 are shown below right (B) and images from swine below left (A). Human heart specimen 271 is from a 68 year old female with BMI of 23.8 who died of anoxia and had no relayed relevant cardiac history.

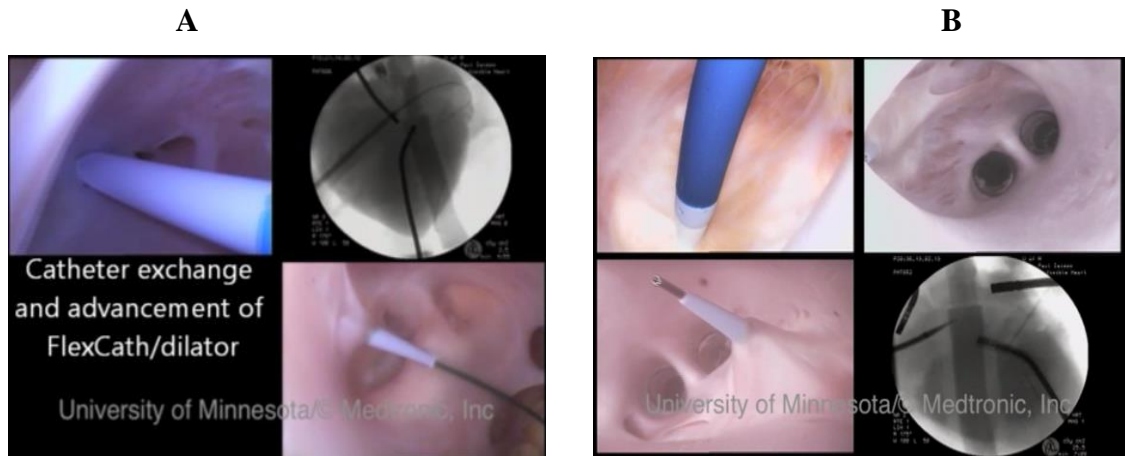


Figure 22: (A) Dilator and FlexCath advancement through the swine fossa ovalis visualized from the right atria (top left), under fluoroscopy (top right), and from the left atria (bottom right). Note, a guidewire has already been exchanged for the Brockenbough needle shown in bottom left of B. A view from the right atrium (top left) is also shown in B with a view of left pulmonary veins (top right), fluoroscopic position (bottom right), and fossa ovalis with right pulmonary veins in view (bottom left).



Figure 23: Position of the ArticFront as seen from within the left pulmonary vein (top left A, top right B), fluoroscopy (top right A, bottom right B), and within the left atria (bottom right A, bottom left B). The Cryo Console screen is shown top left in B. These images are during the beginning of an injection of fluoroscopic contrast, with blue or green dye for direct visualization. Darkening of the vein distal to the balloon on fluoroscopy demonstrates good occlusion of the vein.

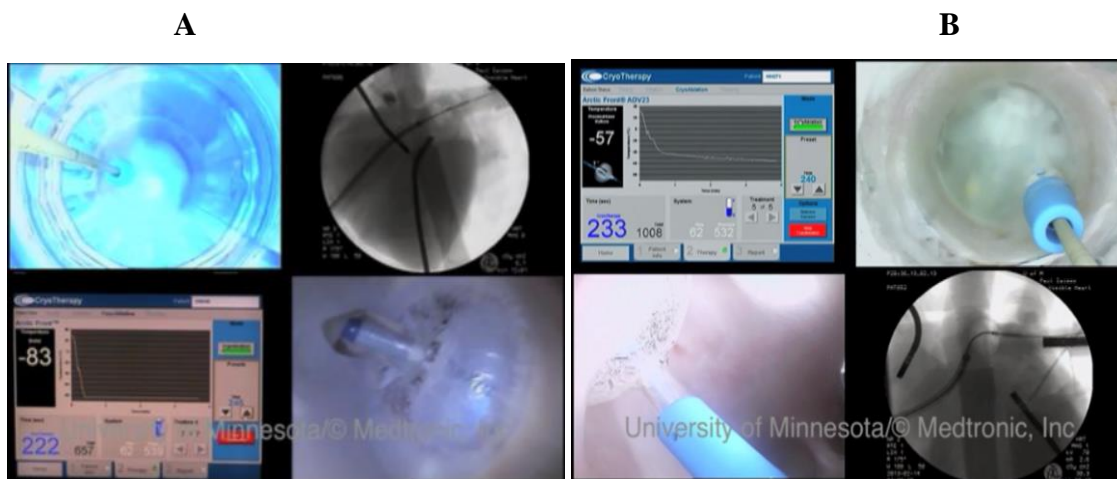


Figure 24: Near the end of a four minute ablation ice can be seen within the left pulmonary vein (top left A, top right B). The temperature profile on the console screen is displayed (bottom left A, top left B). An endocardial view of the balloon and ice formation in the tissue can be seen as well (bottom right A, bottom left B). The fluoroscopic position is displayed top right in A and bottom right in B.

The images yielded from this study demonstrate the procedural workflow using a 28mm cryoballoon visualized from within the heart using videoscropy and fluoroscopy. The degree of ice formation was inspected at both the endocardial surface and from within the PV.

Conclusions:

To date, six human specimens and over 30 swine specimens have been animated and had balloon cryoablations performed and imaged within them. Direct visualization of cryoballoon ablation has led to the creation of novel videos showing the endocardial view of this treatment. These videos can be used to inform and educate physicians and patients on the use of cryoballoon ablation. This model can be further used by device designers to improve current products or test next generation devices.

Several limitations of the swine animal model do exist. Swine generally have only two pulmonary veins and smaller left atria. Yet, this may prove of value when trying to simulate difficult human patient anatomies: e.g., those with common left or right pulmonary veins or small patient stature. Being this footage was captured utilizing an isolated heart, the heat transfer situation is very different from that found clinically. This, coupled with the fact that part of the cryoballoon was within the pulmonary vein cannula, leads to the authors' opinion that ice formation and duration after the ablation has been stopped may differ significantly from the clinical situation. Our laboratory also has the capability to reanimate human, non-viable organ donor hearts, and similar studies are underway using these specimens. A video publication is in preparation of these works.

Funding Sources:

This work has been supported by the Institute for Engineering in Medicine at the University of Minnesota and a contract for Visible Heart® research with Medtronic.

I.V- Concluding Remarks

To summarize the findings of the various studies presented in this section of my thesis, I have:

- Further elucidated the remodeling that occurs in the AF patient versus non-AF patient.
- Quantified phrenic nerve anatomy using a novel, high resolution technique that may also be used for further computer modeling.
- Quantified coronary sinus anatomy in the context of isthmus lesion creation and catheter navigation.
- Developed preliminary methodologies of imaging balloon based catheters that were later expanded and improved upon in my graduate studies. (see Chapter 3, Heart-lung bloc reanimation)

I consider here that these studies not only fill in gaps in knowledge in the literature, but provide novel experimental approaches that can be built upon in the future. For example, the medical device developer may use these findings to: 1) design application specific ablation tools for the coronary sinus, 2) make recommendations on therapy dosing and/or 3) use such information for future product designs by using computer models that can be constructed. Additionally, from these presented studies, I believe that the clinician has been provided with new and confirmatory information on anatomy and remodeling related to ablation and AF, respectively, that may help guide clinical practice. For example, knowledge of the true distances of the phrenic nerves from sites of ablation application have yet to be studied in the context of cryoballoon ablation, but are now better understood.

II- Section 2 Assessment of Cryothermal Injury

Upon familiarization with the literature in cardiac cryothermal ablation it became apparent that there existed a critical knowledge gap or at least not thoroughly investigated as it enhances therapeutic delivery. For example, very few, if any, reported studies examined the tolerances of the tissues that may be impacted by such aforementioned procedures. Nevertheless, in order to eventually predict therapeutic outcomes it is necessary to understand what will lead to those outcomes. Therefore, the following portion of my thesis will describe experiments I performed to elucidate the viability and/or physiologic responses of tissues that may be impacted during cardiac cryothermal ablation.

In this section of my thesis I detail the work of three individual studies. In the first I will describe, an in-vitro system that can be feasibly used with any muscular tissue and I developed using rectus abdominis and myocardium. The developed experimental approach is currently being extensively by other graduate students in the lab to examine esophagus and other tissues response to various ablation modalities. Secondly, I sought to further understand phrenic nerve cryothermal tolerances, because this is highest reported procedural complication of cardiac cryoballoon ablation. This also involved developing a unique system to monitor nerve function and record nerve temperature changes during therapeutic applications. Lastly, understanding myocardium and lung viability response to cryoablation was pursued. These two tissues for study were selected because the myocardium is the tissue of target and therefore, understanding how much cooling is necessary to obtain a complete lesion is highly valuable for potential predictive modeling of therapy. Finally, the methods used for assessing myocardium thermal tolerances were determined to work with lung tissue as well and thus I performed a secondary study on lung tissue: note that plural tissues have been reported to be collaterally injured as well during such clinical procedures.

II.I- Chapter 5: Determination of Cryothermal Injury Thresholds in Tissues Impacted by Cardiac Cryoablation

Ryan P. Goff, BS^{13,14,15}; Steve Quallich BS^{13,14,15}; Robert Buechler MS^{13,14,15};
 Jeunghwan Choi PhD¹⁶;
 John Bischof PhD^{13,16}; Paul A. Iaizzo PhD^{13,14,15}

Background

Cardiac balloon cryoablation for the treatment of atrial fibrillation has been gaining attention as an approach for isolation of the pulmonary veins (PV) since its first reported use in 2003¹⁵ and in the current clinical form in 2005¹¹⁶. Focal cryoablation has been used surgically for many years¹¹⁷ with transcatheter devices becoming available in more recent decades. An advantage of cryoballoon ablation is that it is a ‘single-shot’ approach, which aids in accelerating the slow nature of freezing compared to RF energy (i.e., not point-by-point ablation). The currently available ArticFront (Medtronic, Minneapolis, MN) cryoballoon has been shown to have comparable success rates to RF ablation with low adverse events^{34,118}. The recent STOP-AF trial concluded similar findings to the observational European studies, that being an acceptable safety profile and superiority to antiarrhythmic drugs in those who have failed to respond to them¹⁷. Despite widespread and growing clinical use there are still questions regarding dosing and treatment times for cryoablation, which may affect both efficacy and collateral injury^{119,120}. Parameters affecting RF ablation lesions are thoroughly characterized, and temperatures of 50°C or higher are required for the creation of myocardial scars¹²¹. For instance, the effects of power, ablation durations, catheter orientations, catheter sizes, usage of irrigation, and contact forces on lesion size have been thoroughly studied for RF¹²²⁻¹²⁵. This is particularly relevant given the release of a second generation cryoablation device with a different cooling profile that may affect operation¹²⁶. The

¹³ Department of Biomedical Engineering, University of Minnesota (Minneapolis, MN)

¹⁴ Department of Surgery, University of Minnesota (Minneapolis, MN)

¹⁵ Medtronic Inc., Mounds View, MN

¹⁶ Department of Mechanical Engineering, University of Minnesota (Minneapolis, MN)

highest regularly detected clinical complication is phrenic nerve palsy at rates of 4-8%^{17,118}. The esophagus may be incurring even higher rates of injury, but this is not normally detectable unless specifically searched for using endoscopy^{44,127}. Given that the phrenic nerve and esophagus are in intimate contact with the right PVs and posterior wall of the LA, respectively, one can see how adjusting dosing may lead to better outcomes. It is recommended by the manufacturer that two separate four minute ablations are applied per PV.

The literature is largely lacking on data of hypothermal injury to the myocardium and surrounding tissues that may be impacted. This is the first study to the authors' knowledge to report myocardium tolerance limits for cryo ablation. These data are particularly useful for numerical modeling of therapies that may influence decisions regarding optimal treatment times or even patient specific recommended treatments. Optimization of treatment time may potentially lead to shorter treatments, which still lead to transmural lesions, and reduce collateral injury.

Conversely, in the hyperthermal (i.e., RF, laser, etc.) treatment area there are data regarding injury to the myocardium. Work by Pearce and colleagues^{128,129} exploited cardiac tissue's unique, native birefringence to detect protein denaturation after thermal ablation. Protein denaturing is thought to be the main mechanism leading to necrosis from hyperthermal treatments¹³⁰. However, this same approach cannot be used to determine completely necrotic zones caused by freezing because birefringence changes potentially prior to actual cell death occurring when cooling. Intracellular ice crystal formation and dehydration are the main mechanisms of injury to cells during freezing^{24,131}. Cooling below the actual freezing point of tissue is necessary for complete necrosis, as shown in studies of the kidney^{117,132} and liver¹³³ where cooling to -15°C was required for necrosis.

It is therefore the goal of this series of experiments to determine what cooling regimes lead to necrosis, injury, or have no detectable effect on myocardium. Infrared (IR) thermography was selected because of the large amount of data produced (i.e., every pixel produces a thermal profile). Additionally, it is a non-contact measurement technique, which is particularly beneficial given the large thermal gradients produced during cryoablation (i.e., 100 C/cm), and has been used previously for hypothermal¹³⁴

and hyperthermal¹³⁵ studies in the cancer arena (bischof ref?). The drawback of IR thermography is that the accuracy of the measurement is not that of other techniques (i.e., +/- 2C or 2%) and that the system used was limited to detection down to -20C. The authors hypothesize that injury to tissue will begin to occur when tissue is cooled to the phase change temperature (~0 or -.5 C for most tissues). The authors also hypothesize that in order to obtain complete necrosis more substantial cooling to the levels found to be necessary in other tissues, such as the aforementioned temperatures for liver and kidney, will be required.

Methods

To first benchmark this novel approach a small sample of swine kidney (n=6, two animals) were evaluated and compared to the literature. Kidney cortex is homogenous with a smooth, flat surface making it easier to work with. Once it was determined the approach was technically sound myocardium and a smaller set of lung samples were evaluated.

Sample preparation

Human heart(n=3) and lung(n=3) specimens were obtained from non-viable cardiac transplant organ donors through the regional organ procurement organization, LifeSource (St. Paul, MN) within 6 hours of cross-clamp time. Female Yorkshire Cross swine hearts (n=15), lungs (2 animals, n=5), and kidneys, were chilled and stored in modified Krebs-Henseleit buffer within 30 minutes post-mortem from the University of Minnesota Meat Sciences Laboratory. Swine hearts were then transported to our laboratory within an hour. Human and swine samples were dissected from the atria and ventricles to nominal thicknesses of five millimeters. Locations were selected that were relatively 'flat' with low degree of invaginations to provide a uniform surface for infrared (IR) imaging as to avoid out of focus effects and non-symmetrical ablation lesions. Samples were placed in individual petri dishes with room temperature phosphate buffered saline.

Dissected samples were placed in an infrared imaging apparatus shown in Figure 25, consisting of a plastic petri dish with central ablation probe and 2 millimeters of Sylgard (Dow Corning, Midland, MI) polymer formed to the bottom. The system was designed to accommodate two cryoablation probes with different cooling powers. One being the Galil

Medical (St. Paul, MN) SeedNet system designed for prostate cryoablation using an argon refrigerant with cooling rates and end temperatures approximately $400\text{ }^{\circ}\text{C}/\text{minute}$ and $-120\text{ }^{\circ}\text{C}$. The second system is the Medtronic Cryocath (Minneapolis, MN) system using the FreezorMAX catheter with cooling rate and end temperatures approximately $300\text{ }^{\circ}\text{C}/\text{minute}$ and $-84\text{ }^{\circ}\text{C}$. The samples ablated using the Galil system were impaled on the needle like catheter and the samples ablated using the Medtronic system had a two millimeter biopsy punch hole placed in the center of the sample and then advanced onto the catheter. Using this technique approximates a situation that is easy to model numerically, removes the variability of catheter contact pressure, and creates uniform, axis-symmetric lesions (i.e., round. Figure 25, right).

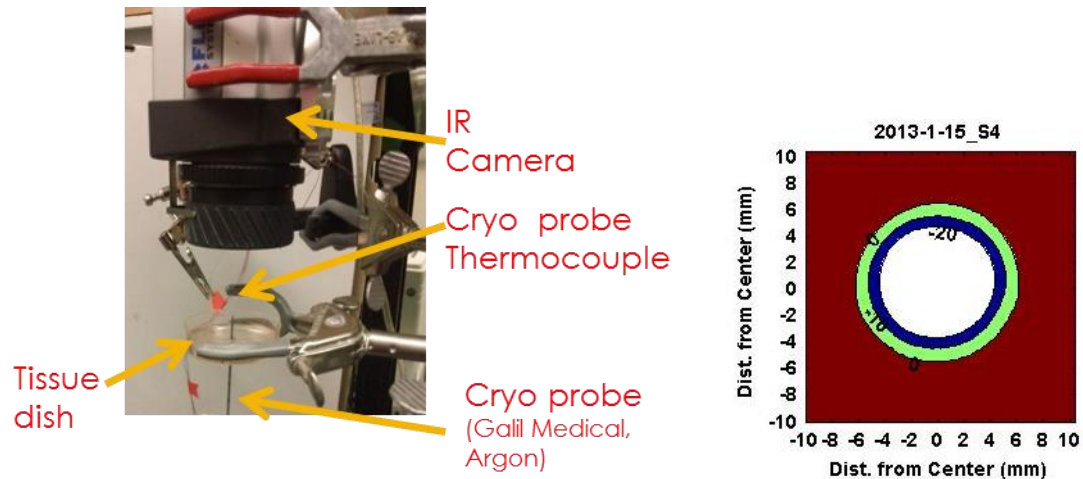


Figure 25: Infrared imaging apparatus shown left and resultant isotherms shown left. The samples are impaled onto the cryoprobe and imaged from the top down. A resultant isotherm from an ablation performed with the Galil system is shown right with white indicating temperatures less than $-20\text{ }^{\circ}\text{C}$, blue $-20\text{ }^{\circ}\text{C}$ to $-10\text{ }^{\circ}\text{C}$, green between $-10\text{ }^{\circ}\text{C}$ to $0\text{ }^{\circ}\text{C}$, and red greater than $0\text{ }^{\circ}\text{C}$.

Infrared imaging and viability assessment

Prior to sample placement in the sample dish ~ 5 milliliters of ultrasound gel was distributed uniformly about the bottom of the dish. After placement of the sample another volume of ultrasound gel was added to surround the sample. Ultrasound gel has been shown to have very similar thermal properties as myocardium⁽¹³⁶⁾ and unpublished data) and by surrounding the sample with ultrasound gel we seek to minimize the thermal effects that variation in sample size, inherent with biological samples, may have.

After sample placement the emissivity and appropriate environmental parameters were input to the infrared software (ThermaCAM Researcher Pro 2.9, FLIR Systems, Inc., Boston, MA). Emissivity was determined by comparison of IR temperature to a 0.040" T-type thermocouple temperature (5SRTC, Omega Engineering) being read by a Fluke 51II thermometer (Everett, WA). A T-type thermocouple with data logging was affixed to the active cooling metal portion of the cryoprobe with Kapton (3M, St. Paul) tape for later computer modeling. Ablations of desired durations were subsequently performed.

After the ablation samples were washed with phosphate buffered saline, incubated with 60 milliliters of cell culture media (DMEM/F12, 10% fetal bovine serum, and 1% penicillin/streptomycin), and placed in a cell culture incubator. Myocardium samples were incubated for 22-24 hours to allow full cryo injury to manifest. Incubation of 4 hours were necessary for lung and kidney samples. Samples were then stained with 1% triphenyltetrazolium chloride (TTC) in Trizma buffer (7.4 pH) at 37°C for 1 hour. TTC functions by reduction of the compound (i.e., electron donation from NADH oxidation from metabolism) and forms a red formazan derivative when in contact with viable tissue¹³⁷. Non-viable tissue turns pale or white after incubation as shown in Figure 26. This stain has been validated and widely used previously for identification of infarct regions in artery occlusion models^{138,139}. The discrepancy in incubation time between tissues is believed to be due to the higher mitochondrial content (i.e., more metabolic enzymes remaining active for longer periods) of cardiac tissues.

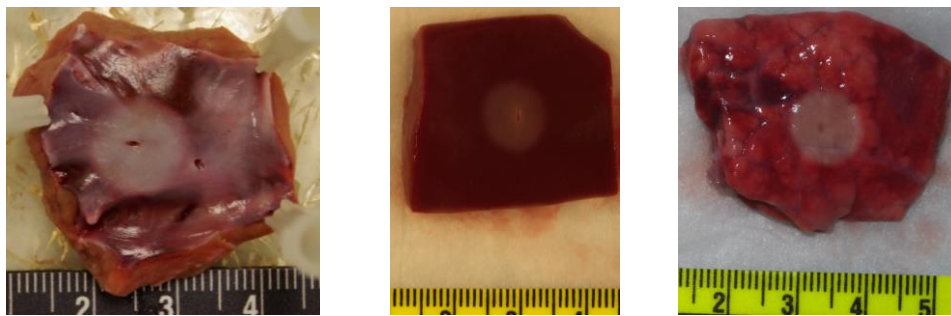


Figure 26: Examples of TTC stained myocardium (left), kidney (center), and lung (right) with central ablation lesions.

The first 6 samples for this study had a .040" gauge T-type thermocouple placed in a 1 mm superficial slit on the surface of the sample just under the endocardium. The IR

thermographic data and thermal profiles were compared to ensure environmental and sample parameters were being appropriately set in the IR software. It was found that the IR thermography and thermocouple data differed by less than the manufacturer published resolution (i.e., less than +/- 2°C or 2% of measurement).

Data analysis

After incubation the samples were photographed in a photo booth with ruler for image size calibration. The photographs were then analyzed using Matlab (MathWorks, Natick, MA) to determine the radial distance from cryoprobe to where the lesion ended and a zone of injured and live tissue began. This was done by plotting the gray values from the cryo probe edge outward radially and normalizing these values to clearly live and dead tissue areas. This yields a sigmoid like curve from 0 to 1 (i.e., dead to live, Figure 27). A single operator then selected two critical points on the curve where the transition from dead, injured, and live tissue occurs as determined by TTC intensity. Samples that did not yield clear sigmoid curves, indicating non-axis symmetric lesions, were removed from analysis.

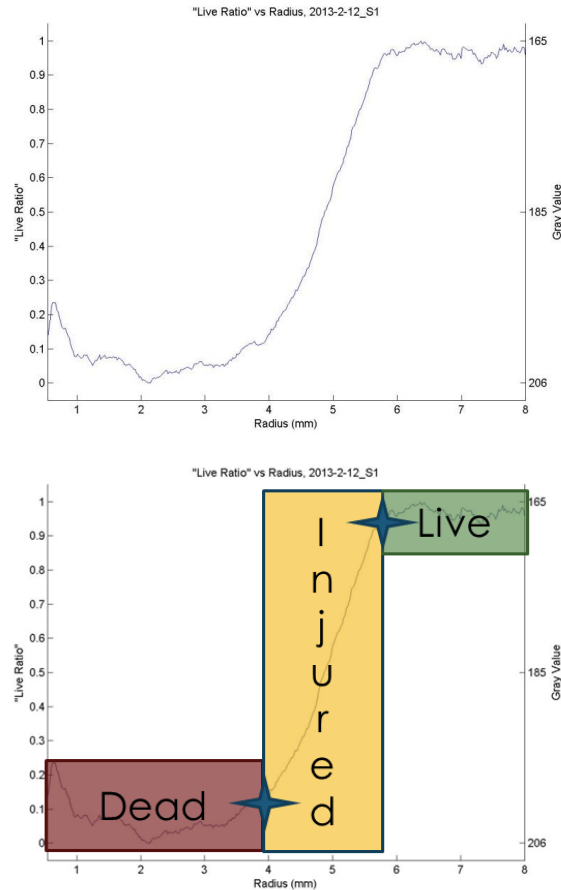


Figure 27: Shown left is a plot of the normalized gray values of a TTC stained image plotted radially outward from the cryoprobe. Shown right is how the data is classified after picking the two critical points (blue stars) on the sigmoid curve.

The raw IR data was analyzed with a Matlab program that could extract the temperature data of a region of interest using user specified radial distances as determined by the sigmoidal staining intensity curves (Figure 27). These were then categorized into a database of thermal profiles that lead to completely dead tissue, injured tissue, and live tissue. Cooling rates and nadir temperatures were extracted from the thermal profiles.

Results

The resultant categorical tissue response (i.e., live, injured or transition zone, dead) to the thermal ablation was plotted against the cooling rate and minimum temperature reached. The kidney results shown in Figure 28 were found to agree with previously published data on thermal injury. Comparing Figure 29 to Figure 30 one can see that similar patterns arise in both the atria and the ventricle. To look at the effect of which cryoprobe

was used, Figure 31 versus Figure 32 displays the data for atrium and ventricular samples pooled. Human myocardium and lung responses are shown in Figure 33 and Figure 35, respectively.

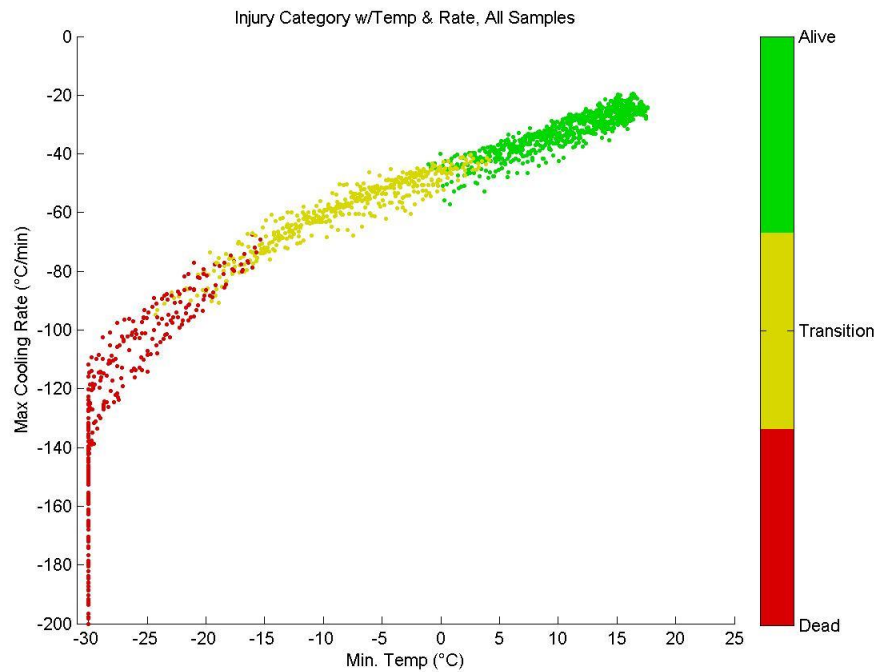


Figure 28: Swine kidney tissue viability response to ablation with Galil Seednet probe. (n=6)

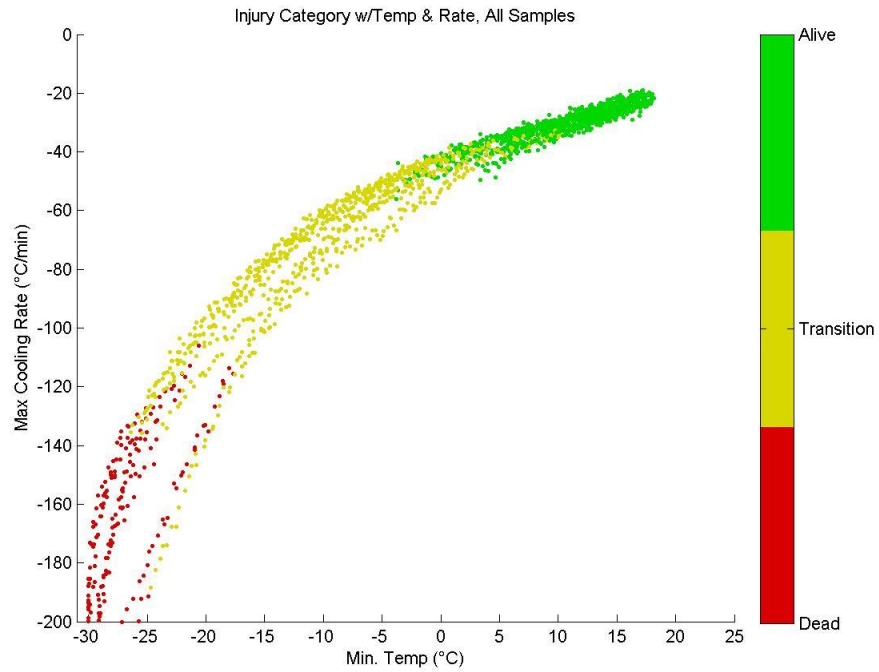


Figure 29: Swine atrium tissue viability response to ablation with Medtronic FreezorMax. (n=8)

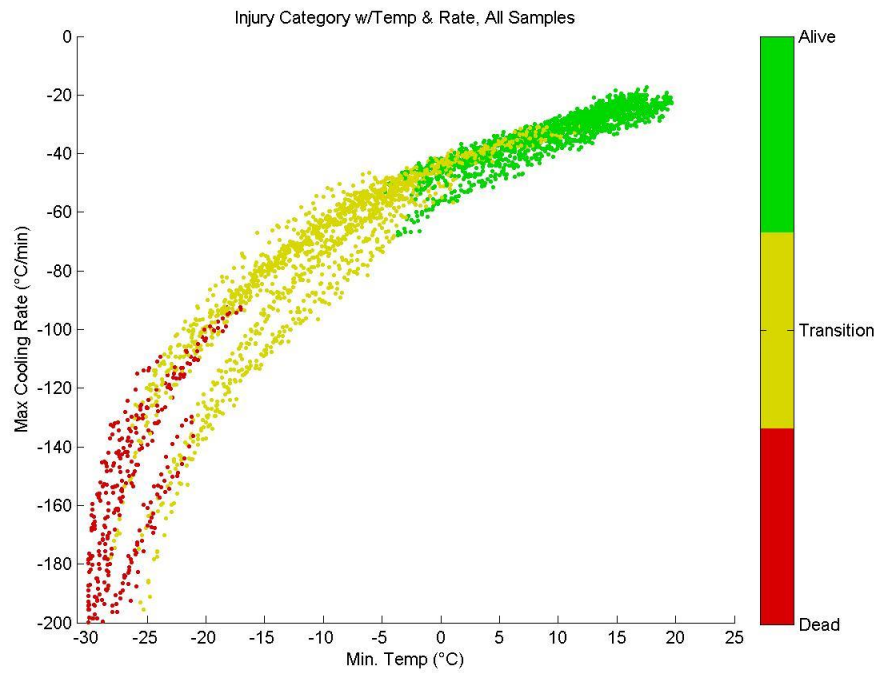


Figure 30: Swine ventricle tissue viability response to ablation with Medtronic FreezorMax. (n=14)

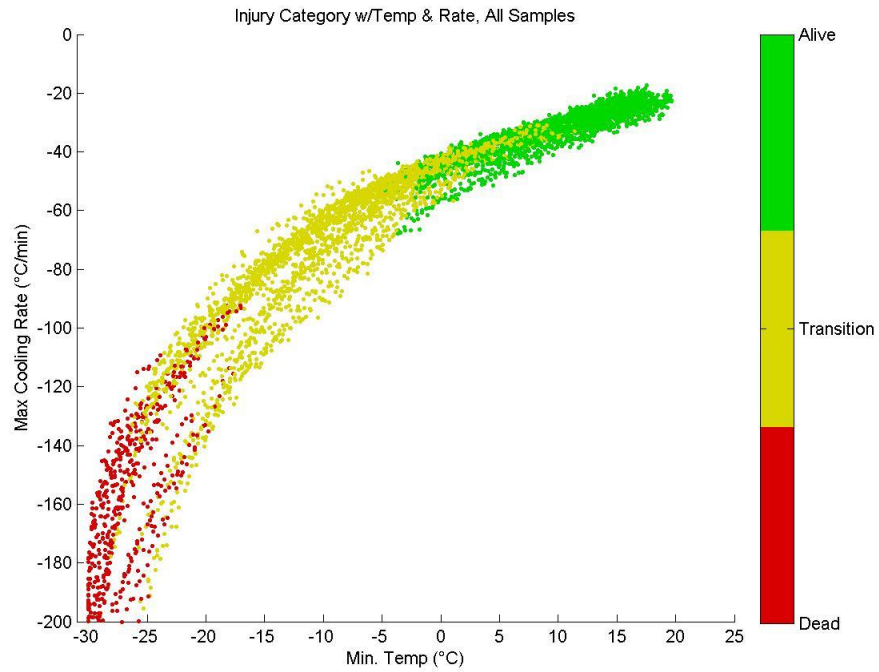


Figure 31: Swine myocardium tissue viability response to ablation with Medtronic FreezorMax. (n=22)

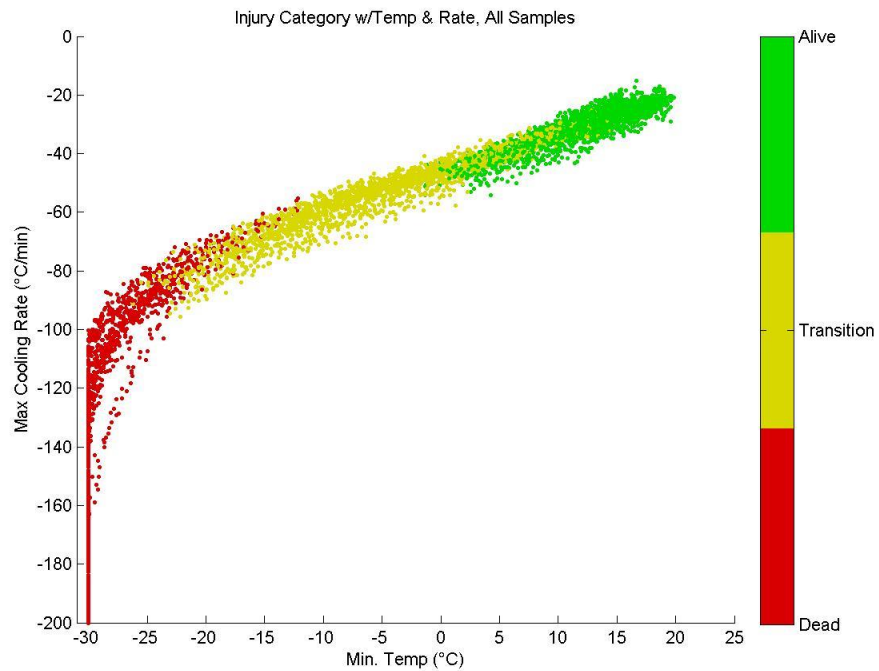


Figure 32: Swine myocardium tissue viability response to ablation with Galil Seednet. (n=17)

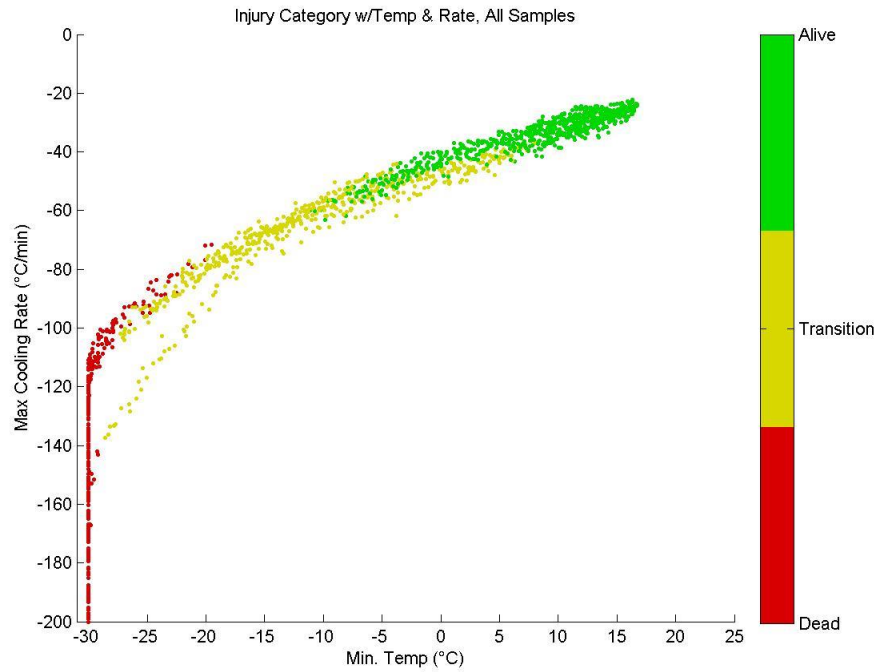


Figure 33: Human myocardium tissue viability response to ablation with Medtronic and Galil cryoprobes. (n=6)

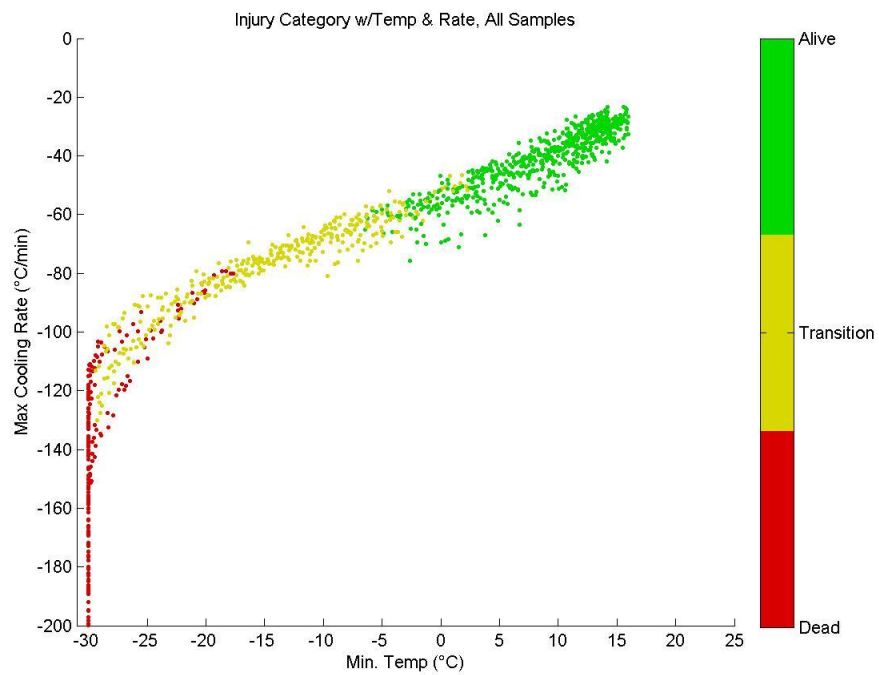


Figure 34: Swine lung tissue viability response to ablation with Medtronic and Galil cryoprobes. (n=5)

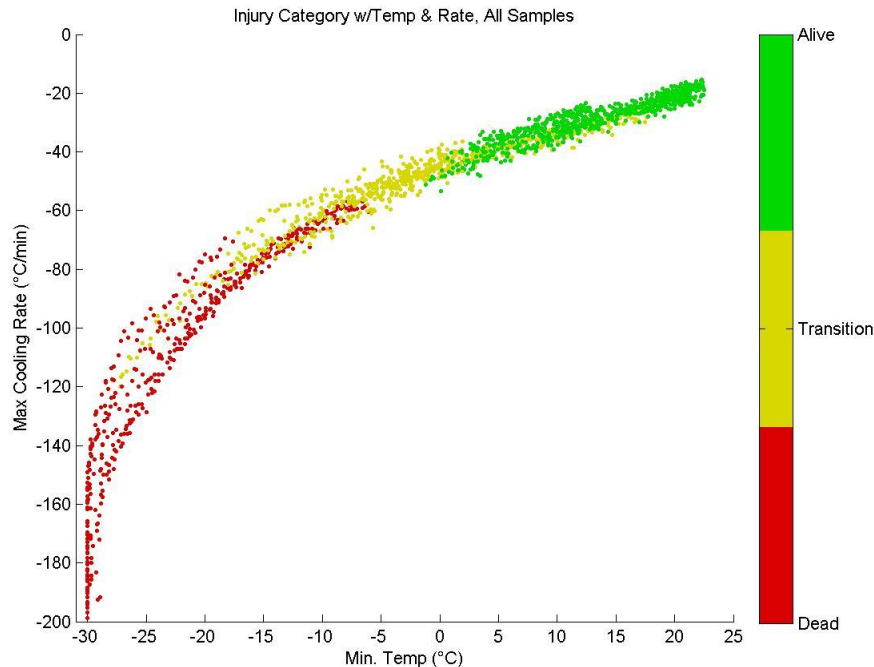


Figure 35: Human lung tissue viability response to ablation with Medtronic and Galil cryoprobes. (n=6)

Discussion

Reported here is the first study on cardiac tissue cryothermal tolerance to the author's knowledge. This novel approach may be adapted to many tissues types, as demonstrated here in small sample studies. This methodology may also be used to study the effects of multiple freeze-thaw cycles or complex cooling regimes. Data presented here suggest that myocardium needs to be cooled to -22.0 ± 3.4 °C for the atria and -22.1 ± 4.1 °C for ventricular tissue to obtain complete thermal lesions. The cooling regime is more complex than just these two parameters so the authors suggest caution and conservative use of these numbers.

Data presented here suggest that kidney tissues need to be cooled to -19.4 ± 3.6 °C at cooling rates of -82 °C/min to obtain complete lesions. This data agrees with previously published data on kidney cryothermal tolerance¹³². Benchmarking the system against previous literature data on kidney tissue demonstrates the ability of the system to determine injury thresholds accurately.

Interestingly, the lung data suggests that there may be significant differences between swine and human cryothermal tolerance. The human data suggests that cooling to -14.8

± 7.9 °C at cooling rates of -76.9 °C/min may be required for complete lesions (Figure 34). The data presented here also suggest that the temperature necessary to destroy healthy swine lung tissue are lower than human tissue. Temperatures of -26.0 ± 5.1 °C at -103 °C/min (Figure 34) were required for complete lung lesions which are approaching the limit of the current infrared camera (i.e., -30 °C). The discrepancy may be due to age, disease state, species variation, and/or pre-procurement sample treatment (e.g., human samples were transported at near zero temperatures for up to several hours before experiments). Nevertheless, these rare human specimens provide unique and translational insight to cryothermal injury thresholds of the lung.

This work is not without limitations, as is the case with any in-vitro, animal tissue based model. The effect of the tissue being perfused is not fully understood. However, work by other groups in the kidney¹³² have found similar temperatures necessary for complete necrosis in experimental groups that were perfused or non-perfused. The effect of shrinkage or swelling was examined on a subset of ten samples by measurement of the distance between two distinct points pre-incubation and post-incubation. The average change and standard deviation was found to be an increase of 0.2 ± 1.1 mm. The TTC stain is an indicator of metabolic activity and therefore not truly a direct indicator of live versus dead tissue. It was considered in this experiment as an acceptable surrogate for viability based upon the wealth of previously published literature using it as such in cardiac tissues.

Conclusions

We report here the first tissue level experiments to elucidate the myocardial tolerance of cryothermal treatments. The data presented here suggest there not significant differences between swine and human myocardial response, but that there may be differences between swine and human lung cryothermal tolerance. The novel system may be used in future experiments on multiple tissue types to study the viability response to simple or complex cooling regimes.

II.II- Chapter 6: Development of a high-throughput, in-vitro model to assess ablation parameters and modalities.

Ryan P. Goff, BS^{17,18,19}; Charles L. Soule MS¹⁸, Mark A. Benscoter MS^{17,18,19}; Paul A. Iaizzo PhD^{17,18}

Introduction

The field of cardiac ablation is highly complex due to the vast array of products, modalities, and treatment techniques available to the electrophysiologist. In the past decade, medical device designers have flooded the market with a glut of new products, all aimed to better treat the disease, primarily targeting atrial fibrillation due to the fact that it is the most prevalent arrhythmia, as stated previously. On the most basic level, the duration and “power” (i.e., wattage, depth of cooling, ultrasonic amplitude, etc.) applied during an ablation application may be modulated and cause significantly varied outcomes¹⁴⁰. Further, differing modalities may cause lesion formation by completely different biophysical mechanisms^{141,142} and the physiological environment may have contrasting effects¹⁴³. Therefore, objective experimental methods are necessary to compare existing and new modalities and devices for the proper evaluation of their safeties and efficacies.

The ablation parameters that may be varied during an applied therapy are numerous and the full design space is most likely rarely explored due to the number of variables. For example, parameters of radiofrequency ablation modality may include: frequency, phasing between electrodes, grounding, wattage, duration of application, device geometry, irrigation of device, size of electrodes, electrode surface treatment and modification¹⁴⁴, contact force, contact angle, etc. Yet to date, to this point, there are virtually no high-throughput experimental test methods to allow one to evaluate ablation parameters and their resultant injuries and/or physiological effects. Currently, the gold standard for testing of cardiac devices is an in-situ irrigated thigh model¹⁴⁰. It should be noted that this model requires a dedicated animal for these investigations and this

¹⁷ Department of Biomedical Engineering, University of Minnesota (Minneapolis, MN)

¹⁸ Department of Surgery, University of Minnesota (Minneapolis, MN)

¹⁹ Medtronic Inc., Mounds View, MN

approach is also limited by the number of ablation areas dictated by the given animal size.

The desire for a higher-throughput technique to evaluate multiple parameters is clearly of value to the device designer and scientist. A method is presented here which is derived from techniques that have been used previously for the study of skeletal¹⁴⁵ and cardiac¹⁴⁶ muscle physiology and the response of vascular tissues to cryoablation¹⁴⁷. The method was also used to assess how adjuvants may enhance cryoablation. Specifically, high salt concentrations have been shown to modify ice formation dynamics¹⁴⁸ and a high salt concentration buffer was compared to normal buffers. This work was accepted for presentation at the 2011 European Cardiac Arrhythmia Society congress¹⁴⁹.

Methods

Fresh rectus abdominis skeletal muscle biopsies and whole excised hearts were obtained from Yorkshire-Cross male castrated swine of approximately 75-90 kg as described in detail previously^{145,146}. Specimens were placed on cold Krebs-Ringer buffer for skeletal muscle or modified Krebs-Henseleit buffer for cardiac tissues. Samples were dissected to be between 3-5 mm in cross-sectional area. A silk suture was attached to each end of the sample and then placed within the experimental chamber shown in Figure 36. The apparatus consists of a water jacketed glass chamber with oxygenator, platinum electric field stimulation panels, and a force transducer by which the bundle is suspended and developed force measured. Specimens were stimulated at a rate of 0.1 Hz and allowed to recover until contraction force had plateaued.

Length-tension and voltage stimulation optimizations were performed for each study sample. Briefly, the tension was increased until resting tension was stable approximately between 1-3 grams of baseline force and developed twitch forces were maximal.

Voltages were increased until the developed twitch forces were no longer increased by voltage steps. The study voltage was then set supra-maximal so to ensure maximal stimulations of a given muscle bundle.

Ablations were performed for varying durations using a clinically available FreezorMax® (Medtronic, Inc., Minneapolis, MN) catheter. The catheter was placed in contact with the tissue in the mid-section of each bundle: electrical stimulus was turned off during the

ablation application. Bundle physiological performances were measured post-ablation for a minimum of four hours. After which, each bundle was weighed and as desired stained with a viability dye, triphenyltetrazolium chloride (TTC). A 1% solution of TTC in phosphate buffered saline (PBS) was used and bundles were incubated at 37°C for one hour to demonstrate the area of ablated tissue.

To investigate this experimental approach's ability to detect changes in ablation parameters, high salt concentration buffers were also tested. As stated previously, higher salt concentrations modulate ice formation characteristics and thereby increase injury. Thus, the salt concentration of the buffer was increased to 5% sodium chloride versus the standard 0.69%. The high salt buffer was only in used during the ablation and immediately after thawing it was replaced with normal buffer. A control group for the high sodium chloride group was utilized that consisted of replacing the normal buffer with the high salt buffer for 5 minutes.

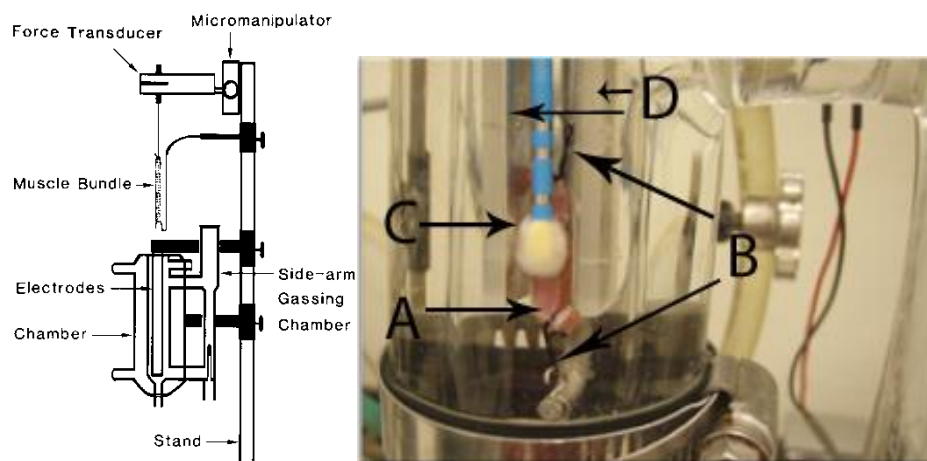


Figure 36: Shown left an illustrated schematic of experimental apparatus consisting of a water jacketed chamber, force transducer, platinum field stimulation panels, and gassing chamber. Shown right is a photograph of the actual system while a muscle bundle (A) is held in place by the force transducer and lower ring (B) during an ablation (C). The field stimulation panels (D) are used to elicit contraction.

Results

The physical characteristics of the muscle bundles size and length are detailed in Table 7. For the study on ablation duration effects (groups 1-5) there were no statistical differences between any of these parameters as discerned by a one-way ANOVA. The

same is true for the high sodium chloride study groups (groups 6 and 7): although note that these groups were quite small.

The effect of differing ablation durations on the peak force developed is shown in Figure 37. Figure 38 details the effect of extracellular or buffer salt concentration on ablation performance and thus peak twitch force developed. Preliminary data comparing the physiological response to ablation of cardiac tissues versus skeletal tissue is shown in Figure 39. Data are presented as averages with error bars displayed as standard error. An example of pre- and post-TTC stained control and treated samples is shown in Figure 40.

Table 7: Muscle bundle length and mass characteristics between treatment groups.

Group Number	Treatment Group	Length (mm)	Mass (mg)
Group 1: n = 12	Control	30.9±5.9	209±93
Group 2: n= 17	1/2 Minute	23.9±3.3	226.6±61
Group 3: n = 12	1 Minute	30.9±6.6	233±64
Group 4: n = 12	2 Minute	29.5±3.9	231±71
Group 5: n = 12	3 Minute	30.9±6.9	228±70
Group 6: n = 5	NaCl Control	25.4±1.4	174±79
Group 7: n = 5	1 Minute + 5% NaCl	26.1±3.4	192±40

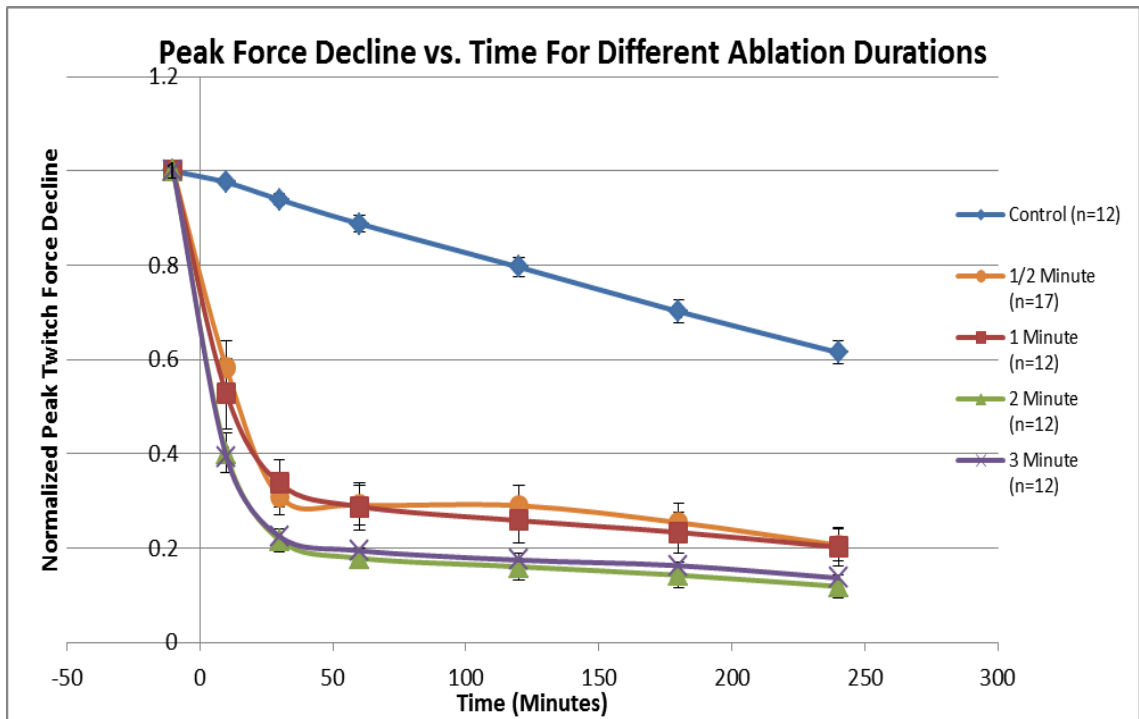


Figure 37: Effect of varying duration cryoablation treatments on normalize maximum force generated.

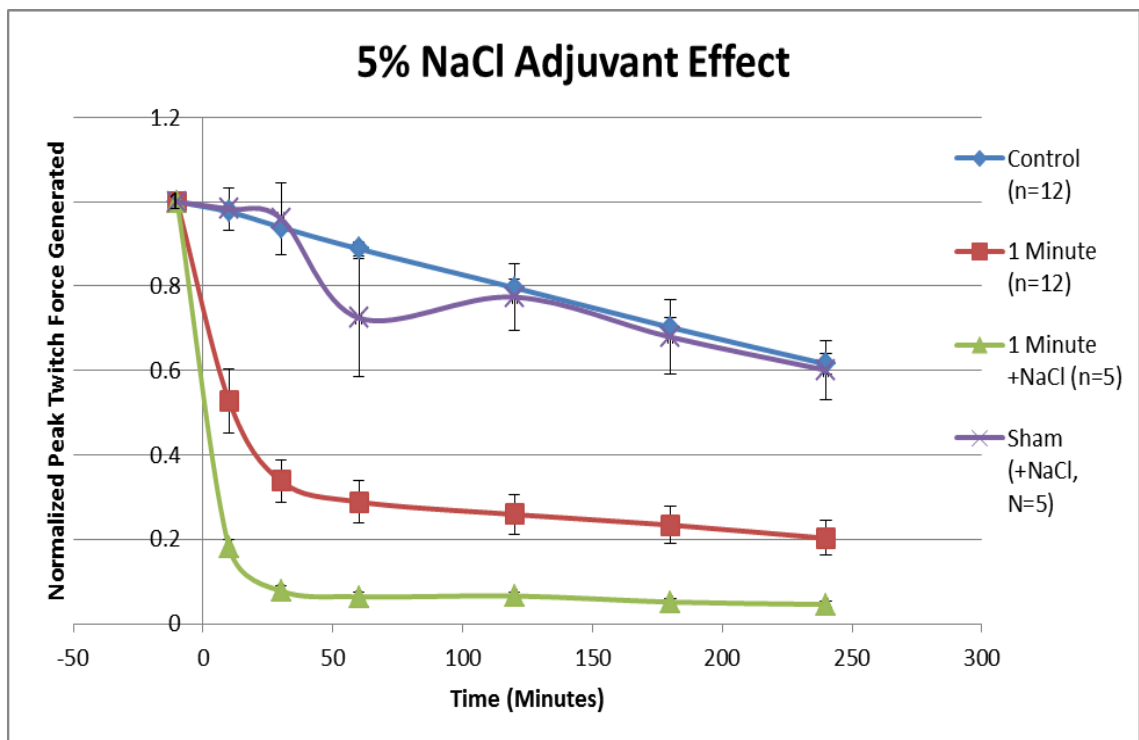


Figure 38: Effect of high NaCl buffer during ablation application as a proposed adjuvant therapy.

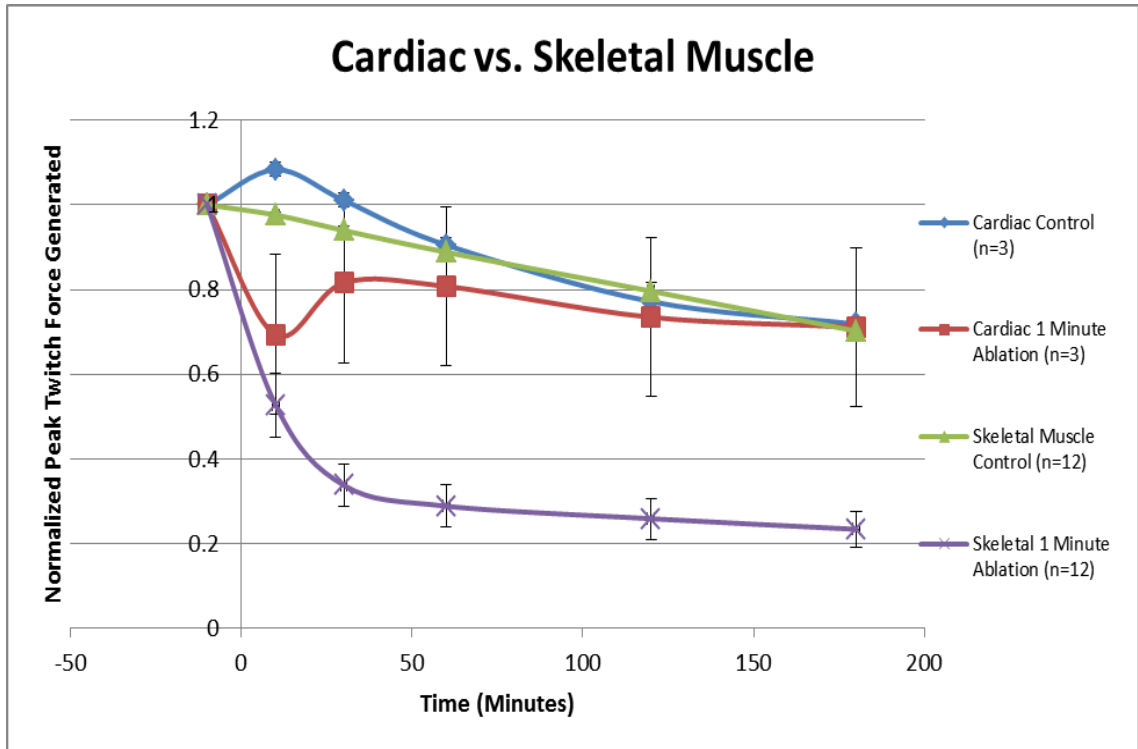


Figure 39: Performance of cardiac tissue compared to skeletal muscle tissue.

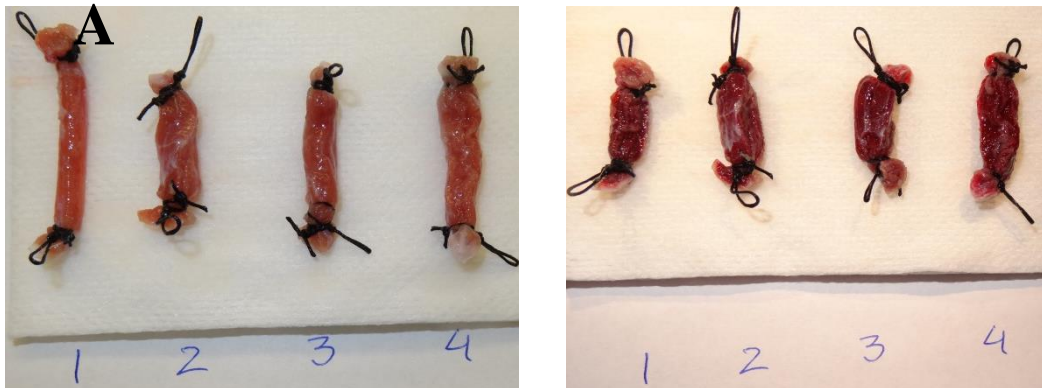




Figure 40: Example of pre- (Left) and post-TTC stained (Right) control (Top) and ablated tissues (Bottom). Samples 5, 6,7, and 8 were ablated for 2, 1.5, 1, and 0.5 minutes respectively.

Discussion

The experimental paradigm presented here provides a controlled environment for testing of cryo-ablation parameters in a systematic approach. Further, it is feasible to use with multiple modalities and preliminary data was presented on different tissues and adjuvants. As expected, with increasing ablation durations the degree of peak twitch force generated decreases as demonstrated in Figure 37. It is supposed that the degree of injury was well correlated to the reduction in peak twitch force.

As one means to test the methodological sensitivity of this approach, a high NaCl buffer that will act as an adjuvant, was piloted. This effect has been mechanistically explained previously and was employed only during the ablation period. The results in Figure 38 indicate the effects of the high NaCl buffer: note that during a sham procedure, the effects of the buffer changes alone were temporary. When applying the cryoablation therapy (freezing) in this high NaCl buffer, the resultant injuries appeared to be significantly increased, as judged by the reduction in peak twitch force. More specifically, when comparing Figure 37 to Figure 38 it can be observed that the effects of high salt buffer application during a 1 minute ablation reduces the developed force below that of even a 3 minute ablation. These data may suggest that significantly higher injuries were elicited due to the additions of the high salt concentration: thus clinically treatment times may be reduced or the zones of injury made larger if ablations are performed in high salt environments.

For the primary development of this experimental methodologies rectus abdominis tissue was utilized: it is quite easy to isolate uniform bundles of this muscle and these tissues are readily available in our laboratory. Nevertheless, experiments to ultimately characterize cardiac ablation catheters should be performed on these respective tissues, both from animal models and humans. Therefore, in a preliminary small pilot study, we employed cardiac tissue and these results were shown in Figure 39. Interestingly, the reduction in force between tissue types for the same duration ablation is quite large. We suspect that this is due to differing tissue structures. In cardiac tissue the cells have a more network structure (smaller cells making up a syncytium of tissue), whereas in the rectus abdominus muscle bundles, the fibers spanned the entire length of the bundle (tendon to tendon). Therefore, when an ablation is performed on cardiac tissue, the injury is local, but when performed on skeletal muscle, if the lesion encompasses the entire cross-section, potentially all fibers in the entire bundle could be injured. In other words, this is due to the fact that membrane integrity will have been lost throughout the bundle in the central region, lesion area thereby damaging virtually every cell. This highlights the importance of using the proper tissue for experimentation.

The experimental approach described here is not without limitations, as is the case with all in-vitro systems. Firstly, it is important to note that the studied tissues were not perfused, but oxygen was being supplied through superstation of the buffer (diffusion). Thus, depending on muscle bundle diameters, there may be differences in tissue necrosis at the core of a given bundle: i.e., where oxygen levels would be lowest. Yet, all attempts were being made in the present study to have samples dissected to consistent sizes, in an attempt to control for this. Secondly, ablation catheter contact forces were not controlled for: yet, because these muscle bundles were suspend from a moving cantilevered beam (force transducer) it was predicted that there should not have be a significant difference in the catheter forces applied (i.e., compared to applying the ablation on a hard surface the force applied can vary significantly). It should also be noted that an attempt was made to place the ablation catheter tip in contact with the tissue in an “end on” fashion, such that the catheter tip was perpendicular to the tissue, but in most cases the catheter experienced a slight incidence angle.

To conclude, the work described here details preliminary development of a novel system for evaluation of ablation parameters. As mentioned previously this work has been presented to a peer group, the European Cardiac Arrhythmia Society and has been accepted for publication in Heart Rhythm pending revisions. At this presentation there was much interest in further work with cardiac tissues to better understand how nuances in ablation applications may influence lesion formation and muscle physiology.

***II.III- Chapter 7: In Vitro Assessment of Induced Phrenic Nerve
Cryothermal Injury***

Accepted pending revision to Heart Rhythm (impact factor: 5.045)

Ryan P. Goff, BSE^{20,21}, Stephanie Bersie²², Paul A. Iaizzo, PhD^{20,21}

Short Title: Assessment of phrenic nerve cryothermal injury

Financial Support: This research was supported by a research agreement with Medtronic, Inc.

Conflict of Interest: Dr. Iaizzo has a research agreement with Medtronic, Inc; Ryan Goff has an internship with Medtronic, Inc.

Corresponding Author:

Paul A. Iaizzo, PhD

420 Delaware St. SE

B172 Mayo, MMC 195

Minneapolis, MN 55455

T: 612-624-7912

F: 612-624-2002

Email: iaizz001@umn.edu

²⁰ Department of Biomedical Engineering, University of Minnesota

²¹ Department of Surgery, University of Minnesota

²² Department of Genetics, Cell Biology and Development, University of Minnesota

Executive Summary:

Background: Phrenic nerve injury, both left and right, is considered a significant complication of cryoballoon ablation for treatment of drug refractory atrial fibrillation, and functional recovery of the phrenic nerve can take anywhere from hours to months.

Objective: This study focused on short periods of cooling to determine the least extreme temperatures that may terminate nerve function related to cryoballoon ablation.

Methods: Left and/or right phrenic nerves were dissected from the pericardium and connective tissue of swine (n=35 preparations). Nerves were placed in a recording chamber modified with a thermocouple array; this apparatus was placed in a digital water bath to maintain an internal chamber temperature of 37°C. Nerves were stimulated proximally with a 1V, 0.1 mS square wave. Bipolar compound action potentials were recorded proximal and distal to the site of ablation both before and after ablation, then analyzed to determine changes in latency, amplitude, and duration. Temperatures were recorded at a rate of 5 hertz, and maximum cooling rates were calculated.

Results: Phrenic nerves were found to elicit compound action potentials upon stimulation for periods up to four hours minimum. Average conduction velocity was 56.7±14.7 m/S pre-ablation and 49.8±16.6 m/S post- ablation (p=0.17). Cooling to mild subzero temperatures ceased production of action potentials for greater than one hour

Conclusion: Taking into account data presented here, previous publications, and a conservative stance: during cryotherapy applications cooling of the nerve to below 4 °C should be avoided whenever possible.

Key words (5-10): Phrenic nerve injury; atrial fibrillation; cryoballoon ablation; phrenic thermal tolerance; compound action potential

List of abbreviations:

AF=atrial fibrillation

CAP=compound action potential

Introduction

Recently shown in the pivotal US trial STOP-AF¹⁷ and other multi center trials³⁴, phrenic nerve injury was noted as the highest non-access site related complication of cryoballoon

ablation for the treatment of drug refractory atrial fibrillation (AF). Further, this form of injury is not unique to cryoballoon ablation, yet a recent systematic literature review suggests it may occur more frequently in cryoballoon ablation than in radiofrequency ablation³⁵.

The right phrenic nerve (PN) in general follows the posterior or posterolateral aspect of the vena cava and the left phrenic nerve passes over the marginal veins of the left ventricle (Figure 1). Both the right and left phrenic nerves (PN) terminate on the superior surface of the diaphragm, thus injury to either phrenic nerve may result in diaphragmatic hemi-paralysis or palsy^{36,37}. Usually, only the right phrenic nerve has been reported to be injured during cryoballoon ablation and most frequently during ablation of the right superior PV^{38,39}. However, recent case reports have also been published on left PN injury^{36,40} and such occurrences may only rise with increased cryoballoon adoption.

Reported rates of phrenic nerve injury varies in the literature: in the range of 4% to 17% (see Table 1). The reported time course of phrenic nerve functional recovery also varied considerably in the literature. The shortest recovery time periods reported are on the order of hours³⁸ and the longest on the order of months.

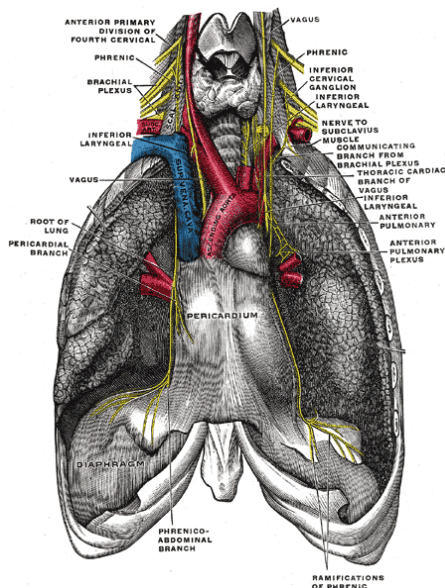


Figure 41: General anatomical course of the phrenic nerve. (Image from Gray's Anatomy33, public domain).

Injury of the phrenic nerve by hyperthermal methods (i.e., radiofrequency) has been investigated previously in the context of cardiac ablation¹⁵⁰. The effect of hypothermal

treatments has also been investigated in the context of topical cooling during open surgical procedures. However, these studies were performed on longer time scales relevant to surgery. In contrast, Dureuil and colleagues applied topical cooling to canine phrenic nerves to 0°C for either 5 or 30 minutes¹⁵¹. At this level of cooling they found recovery of all nerves, but the thirty minute treatment group experienced initial reductions in diaphragmatic electrical activity and transdiaphragmatic pressure. It is important to note that most tissues undergo phase change at temperatures slightly below zero due to salts and other solutes being present. It is thought that the majority of injury during cryo treatments occurs at such a phase change which leads to both extracellular and intracellular ice formations¹⁴². It is therefore not surprising that all nerves recovered from these treatments. Further, Robicsek and colleagues also have investigated cooling PNs for a period of thirty minutes¹⁵² they observed: 1) in mixed breed canines they found that conduction terminated by cooling to 10-12°C; 2) cooling to temperatures between 10-4°C the PNs recovered within an hour; and 3) cooling below 4°C caused the majority of nerves to not recover within the 4 hour monitoring period. These authors noted that the “cold resistant” preparations had a high degree of fatty tissue. Therefore, it may be the case that the nerves were not actually experiencing the temperatures produced by the probe. Nevertheless, the authors of these studies should be commended for their efforts in elucidation of PN thermal tolerance; however, again two sources of error may have influenced the studies. One potential error is that the cooling device temperatures were monitored and not the nerve temperatures themselves. Therefore, the exact temperatures that the nerves reached were unknown, but more than likely close to the probe temperatures. The second to consider is that in many experimental apparatuses thermal contact resistances (i.e., microscopic air pockets from surface roughness etc.) can significantly alter the degree of heat actually exchanged between two objects and may play a role.

From a clinical perspective, due to the fact that a phrenic nerve is typically not in direct contact with an intracardiac ablation catheter and there is a large degree of convective warming from blood flow occurring, these nerves are most likely experiencing cooling excursions to damaging temperatures for short durations. Yet, one has to consider the following clinical aspects, the treatments are generally for 3-4 minutes and there is lag

time associated with conduction of the cooling to the nerve, indicating the nerve will only be cooled for a fraction of the treatment time. Therefore, the study we performed and presented here was focused on short periods of cooling in an attempt to determine the least extreme temperatures that may terminate nerve function.

Table 8: Published incidences of PN injury occurring clinically. Studies are ordered from greatest number of patients to least. Entries left blank were not specified in the journal publication.

Cryoballoon Studies	Incidence of PNP per procedure	Phrenic Pacing	Resolution	Vein
Vogt, et al. ⁴¹	2%(12 of 605)		3 to 9 months	
Neumann, et al. ³⁴	8% (26 of 346)	Yes	Less than one year, two before procedure end	
Packer, et al. ¹⁷	11% (29 of 259)		25 of 28 within 144 ± 27 days	
Jackson, et al. ¹⁵³	8% (15 of 200)	Yes, SVC	2 hours to 12 months. 9 before procedure end	
Dorwarth, et al. ¹⁵⁴	9% (13 of 141)	Yes, SVC	One persistent at discharge	12 RSPV, 1 RIPV
Kuck, et al. ¹⁶	4% (6 of 136)	Yes, SVC	5 within 12 months, 1 present after 10 months	5 RSPV, 1 RIPV
Ghosh, et al. ¹⁵⁵	17% (22 of 130)	Yes, Right Innominate Vein	Before procedure end	
Casado-Arroyo, et al. ¹⁵⁶	11% (13 of 121)	Yes, SVC	No resolution in one case	RIPV of 3, RSPV of 10
-Artic Front	6% (5 of 80)		Resolution before discharge	
-Artic Front Advance	20% (8 of 41)		Resolution by 7 months, except one	
Defaye, et al. ¹⁵⁷	3% (4 of 117)	Yes	Within a few minutes	RSPV
Bitter, et al. ¹⁵⁸	3% (2 of 82)		Within 3 months	
Guiot, et al. ⁴⁴	8% (5 of 66)	Yes, SVC	"A few days". 1 patient longer than procedure duration. Normal chest x-ray at 2 weeks.	
Kuhne, et al. ³⁸	6% (4 of 65)	Yes, SVC	30 seconds in 3 cases, 24 hours in the fourth.	
Mandell, et al. ¹⁵⁹	2% (1 of 62)	Yes, SVC	Before procedure end	RSPV

Furnkranz, et al. ¹⁶⁰	3% (2 of 60)	Yes, SVC		
-Artic Front	3% (1 of 30)		By 3 month follow-up	Right sided
-Artic Front Advance	3% (1 of 30)		1 day post procedure, not related to ablation	Left sided
Peyrol, et al. ¹⁶¹	5% (3 of 55)	Yes, SVC	By 1 month follow-up	RSPV and RIPV
Chun, et al. (2012) ⁴³	6% (3 of 51)	Yes, SVC	Days 1, 172, 212 post ablation	RSPV
Rao, et al. ³⁹	6% (3 of 51)	Yes, SVC	Before procedure end	
Malmberg, et al. ¹⁶²	5% (2 of 40)	Yes, SVC	1 within the hour, 1 over 6 months	
Pokushalov, et al. ¹⁶³	8% (3 of 40)	Yes, SVC	2 within 1 week, 1 after cessation of cryoablation	RSPV
Schmidt, et al. ¹⁶⁴	3% (1 of 33)	Yes, SVC	Within 2 minutes post freeze	RSPV
Chun, et al. ¹¹⁹	3% (1 of 32)	Yes, SVC	By 3 month follow-up	RSPV
Catanzariti, et al. ¹⁶⁵	0% (0 of 30)	Yes, SVC		
Chun, et al. (2009) ¹⁶⁶	11% (3 of 27)	Yes, SVC	Before procedure end	2 RSPV, RIPV
Tang, et al. ¹⁶⁷	4% (1 of 23)	Yes, SVC	1 month post ablation	RSPV
Klein, et al. ⁴⁵	14% (3 of 21)	Yes, SVC	6 and 9 months. One persistent at 2 months	RSPV
Linhart, et al. ¹⁶⁸	15% (3 of 20)	Yes, SVC	Before procedure end	RSPV
Van Belle, et al. ¹¹⁸	0% (0 of 18)	Yes, SVC		
Namdar, et al. ¹⁶⁹	6% (1 of 18)	Yes, SVC	20 minutes	"large RSPV"

Kuhne, et al. ¹⁷⁰	0% (0 of 14)	Yes, SVC		
Multi Balloon Studies				
Bordignon, et al. ¹⁷¹ (Total)	5% (7 of 140)	Yes, SVC	Recovered by 6 month follow up	RSPV
-Cryo	6% (4 of 70)			
-Laser	4% (3 of 70)			
Horton, et al. ⁴⁷ (Total)	19% (7 of 37)	Yes, SVC		RSPV
-Cryo	16% (1 of 6)			
-HiFU	22% (4 of 18)			
-Laser	15% (2 of 13)			
Sohara, et al. ¹⁷² (Hot Balloon)	1% (1 out of 100)	Not in this patient, otherwise yes.	Within 3 months.	

Methods

Castrated male Yorkshire Cross swine being used for IACUC approved studies, weighing approximately 85 ± 10 kg, were used for this study. Anesthesia was induced with telazol and thiopental, animals were then intubated and mechanically ventilated, maintaining a PaCO_2 of 40 ± 2 mmHg, with a surgical level of anesthesia maintained with isoflurane (>1.2 MAC). Access to the thoracic cavity was achieved via a medial sternotomy. The left and/or right phrenic nerves were carefully dissected from the pericardium and connective tissue and placed in modified Krebs-Henseleit buffer at room temperature. The fatty sheaths and remaining connective tissues were dissected from the nerves using a stereomicroscope. Nerves were then placed in a nerve-recording chamber (MLT016,

ADInstruments, Dunedin, New Zealand) that was modified by the addition of a thermocouple array: the array consisted of a Styrofoam block with four, 40 gauge T-type thermocouples (#5SRTC, Omega Engineering, Stamford, CT) embedded 2.5 mm apart. The apparatus was placed in a digital water bath set to maintain an internal chamber temperature of 37°C (See Figure 1).

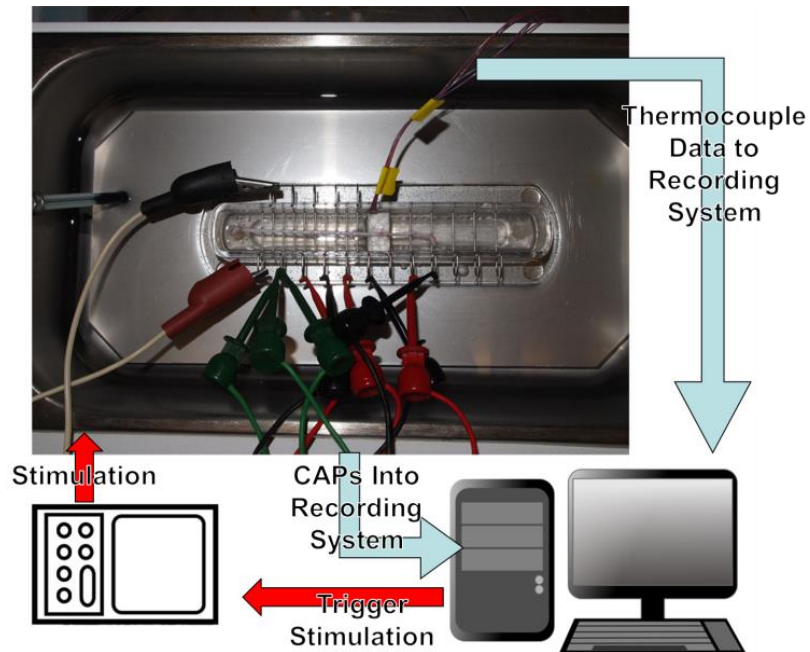


Figure 42: Nerve recording chamber displaying recording and stimulating electrode configuration. The white Styrofoam thermocouple array can be seen in the middle of the chamber. The nerve is stimulated at the left of the picture and evoked CAPs are recorded along the length of the nerve as they travel towards the right.

Nerves were stimulated proximally (i.e., cranially) with a 1V, 0.1 mS square wave (S48, Grass Technologies, Middleton, WI). Bipolar compound action potentials (CAPs) were recorded proximal and distal to the site of ablation both before and after ablation (Powerlab 16/30 with LabChart 7 software, ADInstruments). The characteristic parameters of the nerve CAPs that were analyzed are shown in Figure 43. This figure also demonstrates changes that occur as CAPs travel down the nerve, specifically: a broadening of the CAP waveform and the peak of the CAP magnitude shifted later in time as it takes longer for the signal to travel through the nerve with greater distance.

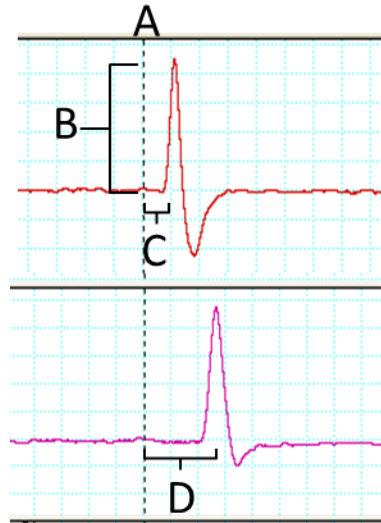


Figure 43: An example of a CAP recorded proximal (top) and distal to ablation (bottom). The dotted line (A) indicates time at which stimulus was applied. The magnitude (B) and latency to peak (C) were determined and average conduction speed (D) calculated based upon the distance the signal traveled.

The cooling power of the cryoprobe (FreezorMAX, Medtronic Inc., Minneapolis, MN) is such that, it is generally considered, that the nerve will be permanently injured with every application if the probe is placed in direct contact with the nerve. To weaken the amount of cooling the nerve receives, and act as a pseudo-atrial wall, a piece of fresh-viable skeletal muscle, dissected to 8 by 10 mm with thickness of 3.2 ± 0.4 mm, was placed over the nerve between the cryoprobe and nerve (See Figure 2). CAPs were recorded with before and after placement of the muscle.

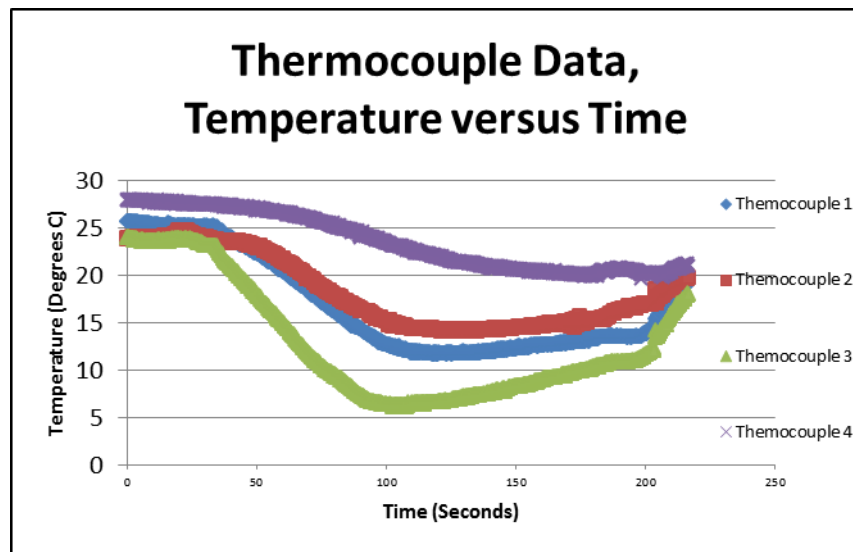
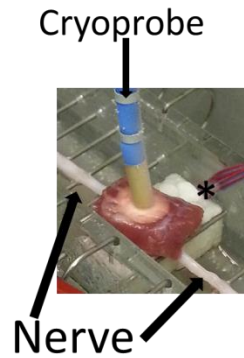


Figure 44: Shown left is the cryoprobe relation to the nerve, thermocouple array (*), and skeletal muscle segment to reduce cooling power experienced by the nerve. On the right is an example of the cooling profile experienced by the nerve.

The thermal profile of the thermocouple that recorded the lowest temperature was further analyzed to determine the maximum cooling rate. Temperatures were recorded at a rate of 5 hertz and the maximum cooling rate was calculated on a second-by-second basis using the average temperature per second. The CAPs were analyzed pre- and post-ablation to determine changes in latencies, amplitudes, and durations: as defined by Figure 4. Nerves were also categorically grouped as to whether or not the CAPs recovered distal to the ablation within an hour or failed to be produced.

Results

Phrenic nerves were found to elicit CAPs upon stimulation using this methodology for periods up to four hours. Thirty-five nerve preparations were studied using this approach and the figures below detail the cooling profile (Figure 45), magnitude (Figure 46), and latency (Figure 47) results for these collective studies. A graph of conduction velocities would be identical to Figure 47 because the latencies were used to calculate conduction rates: i.e., this would be simply a scaling of the latency. The average conduction velocity was calculated to be 56.7 ± 14.7 m/S pre-ablation and 49.8 ± 16.6 post-ablation ($p=0.17$) which agrees with values reported in the literature for that of human phrenic nerves¹⁷³. The dwell time of the cooling treatments was 102 ± 93 seconds as defined as the amount of time within 5 degrees of the nadir temperature. The dwell time in general was shorter for the colder thermal profiles due to higher thermal gradients causing faster rewarming.

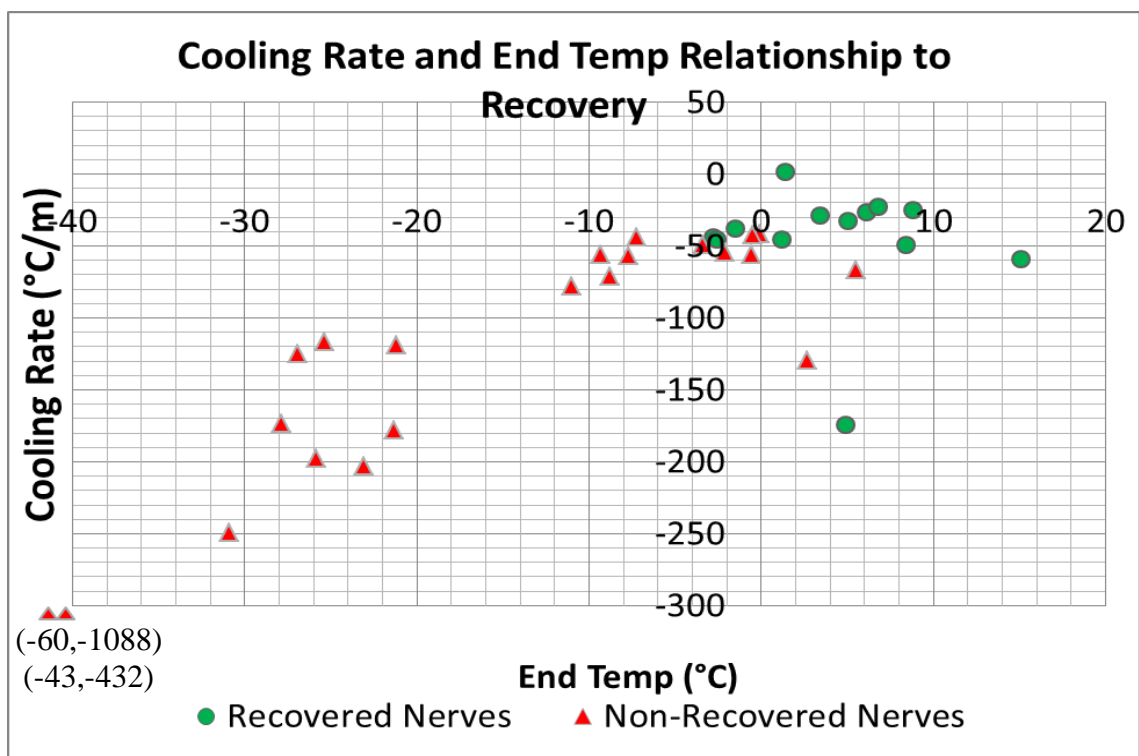


Figure 45: Relationship between cooling and recovery of phrenic nerve CAPs. Note that two extreme cooling cases are shown bottom left and off the scale of this graph to enable better visualization of the data.

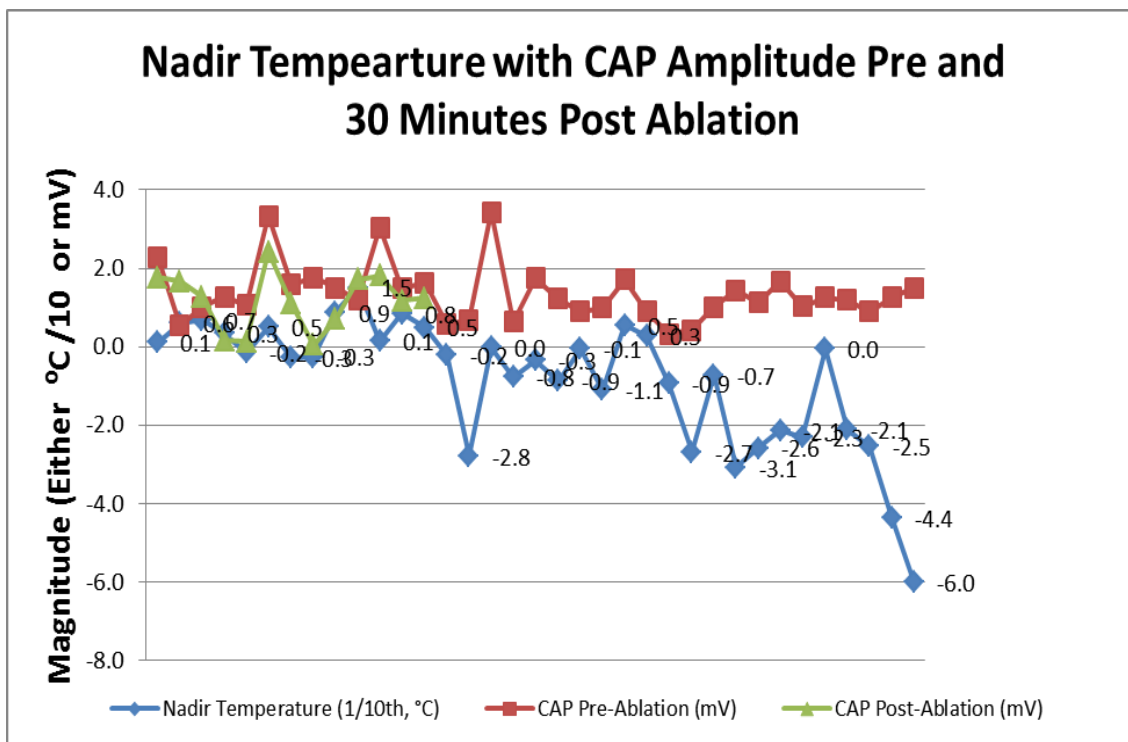


Figure 46: Phrenic nerve pre- and post-ablation CAP magnitude and nadir temperature relationship. Note that temperature is displayed as 1/10th the actual temperature to fit within the scale of the CAP magnitude.

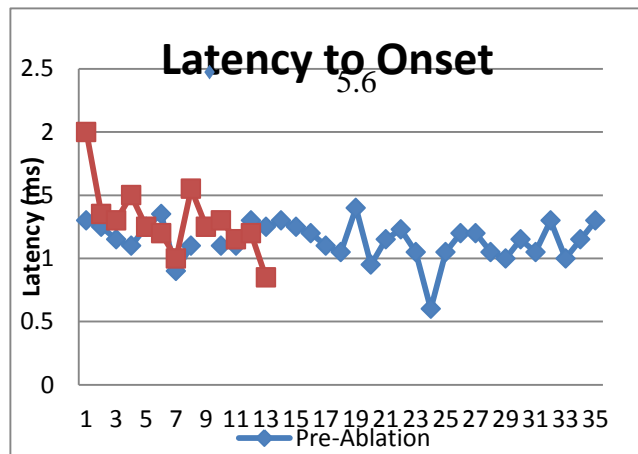


Figure 47: Latency to CAP onset pre- and post-ablation.

Discussion

The methodology presented here allowed us to reliably record compound nerve action potentials for several hours in vitro, but is not without noted limitations. The data suggest that cooling to mild subzero temperatures will affect nerve CAPs, but it did not necessarily damage them irreversibly. The relative temperatures we observed to cause acute termination of CAPs fall in line with longer cooling protocols that have been published previously. This suggests that an in vitro experimental approach may be employed to accurately predict acute in vivo or in situ therapeutic responses. Importantly, we observed that the phrenic nerves that did not recover within the one hour monitoring period were those that were cooled at significantly faster rates and to lower temperatures. Clinically, although mild subzero cooling may not prove to be a long-term detriment to the patient, it may or should alter the course of clinical action, likely causing an ablation to be ended earlier than planned. This, in turn, may affect atrial lesion durability and long-term outcomes.

Conclusions

Taking into account data presented here, previous publications, and a conservative stance, during cryotherapy applications cooling of the nerve to below 4°C should be avoided whenever possible. Data presented here support the notion that cooling to below zero Celsius will significantly alter nerve function for a minimum of one hour. In the future, ultrasound or magnetic resonance thermography may be utilized by the physician to monitor and avoid altering nerve function induced by thermal therapies as described here.

II.IV- Concluding remarks

To summarize the findings of these novel works I have:

- Developed a method to determine physiologic responses to ablation of vary modalities and benchmarked the system using myocardium and skeletal tissues.
- Further quantified the cryothermal tolerance of the phrenic nerve.
- Quantified myocardial and lung viability response to cryothermal treatments, which to my knowledge has not been performed previously.

These studies required fabrication of experimental apparatuses and development of novel methodologies for viability assessment. The data provided here may be used for predictive modeling of viability after an ablation treatment or possibly during preoperative planning. Taken in conjunction with data from cell studies performed by our collaborators in the Bischof laboratory we have covered a wide range of cooling regimes. If future modeling of the procedure is performed and the relative range of cooling the target tissue may experience determined, these data may be referred back to in order to optimize procedural dosing. This may increase procedural efficacy and reduce procedural complications.

One tissue in which I was unable to characterize the viability response to thermal treatments is the esophagus. Using the fore mentioned techniques was not successful, but this is not to say it is not possible. A modified TTC staining protocol can be used with esophageal tissue. The problem encountered was that esophageal tissue drastically changed shape upon ablation. With some fiducial tracking of shape changes and complex computer programs to correlate infrared data with viability data and/or strain tracking these studies are feasible.

III- Section 3 Investigation of Device-Tissue Interactions

One of the great benefits of the Visible Heart® Laboratory is its ability to routinely use reanimated human and swine hearts for experimentation. These studies are therefore translational in nature through the use of human hearts. The goal of this section of my thesis is to better quantify what is happening during a cardiac cryoablation procedure using our technically advanced in-vitro models.

The first chapter of the section details the creation and characterization of a novel, large mammalian reanimated heart-lung bloc model for novel device tissue interaction studies. This latest in vitro model builds upon previous isolated heart work pioneered by our laboratory. Briefly, it was determined that to best study the effects of cryoablation it was important to have the native pulmonary veins present. This inspired the creation of heart-lung bloc reanimation methodologies and its utilization.

The second chapter utilizes this isolated heart-lung bloc preparation to uniquely quantify to what degree transmural cooling is occurring during a typical cryoballoon ablation procedure performed within the ostia of the pulmonary veins. It is believed the transmural lesions are required for effective pulmonary vein isolation. To our knowledge this is one of the most advanced experimental approaches employed so to obtain the first human data on epicardial cryoablation temperatures. This work also compared the resultant cooling between the first and second generation balloon cryoablation catheters.

Interestingly, the identified temperature profiles determined epicardially are more than likely in the range of those experienced by collateral tissues (i.e., adjacent tissues such as esophagus, lung, etc.).

The third chapter explains a novel model for imaging ice dynamics to determine what extent ice can potentially form within the cardiac and non-cardiac tissues. This approach will allow for precise study of the effects of varying cooling regimes and the extent of ice formation in collateral tissues. Further, truly opens the door to the study of wide range of other parameters effects on ice freeze-thaw dynamics (e.g., catheter contact force, distal/inappropriate placement, poor occlusion, varying cardiac output, varying myocardial perfusion, novel intraprocedural ice monitoring, etc.).

III.I- Chapter 8: The Novel In-vitro Reanimation of Isolated Human and Large Mammalian Heart-Lung Blocs

This chapter is in the submission process to Nature.

Ryan P. Goff, BS^{23,24,25}; Brian Howard MS^{23,24}; Steve Quallich BS^{23,24,25}; Julianne Spencer PhD^{23,24,25};
Tinen Iles²⁴; Paul A. Iaizzo PhD^{23,24}

Executive Summary

Introduction: In-vitro isolated heart preparations are an invaluable tool for the study of cardiac anatomy, physiology, and device testing. Such preparations afford the investigator a high level of control, independent of host or systemic interactions, and high throughput if desired. We present here that isolated human and swine preparations with the lung(s) attached are particularly valuable for the study of device tissue interaction and anatomy. Detailed here is our laboratory's experience developing these heart/lung bloc in vitro methodologies.

Methods: Four human and 18 swine heart-lung preparations were procured using techniques analogous to those of cardiac transplant. Specimens were then rewarmed and reperfused using modifications of a previously developed apparatus and methodologies by our laboratory: positive pressure mechanical ventilation was also employed. Epicardial defibrillation was applied to elicit native sinus rhythm after rewarming. Videoscapy, fluoroscopy, ultrasound, and infrared imaging were performed for anatomical and experimental study.

Results: Systolic and diastolic pressures observed for human and swine specimens, respectively, were $68/2 \pm 11/7$ and $74/3 \pm 17/5$ mmHg, with heart rates of 80 ± 7 and 96 ± 16 BPM. High resolution imaging within functioning human pulmonary vasculature was obtained, among other anatomy of interest.

²³ Department of Biomedical Engineering, University of Minnesota (Minneapolis, MN)

²⁴ Department of Surgery, University of Minnesota (Minneapolis, MN)

²⁵ Medtronic Inc., Mounds View, MN

Conclusion: To the authors' knowledge, this is the first report of dynamic images of the pulmonary vasculature during cardiopulmonary function in isolated reanimated heart/lung blocs. This experimental approach provides unique in-vitro opportunities for the study of novel medical therapeutics applied to both human and large mammalian heart-lung specimens.

Background

In-vitro, isolated heart preparations have been a cornerstone of cardiac research since Langendorff's original methodology was described in the 1890s¹⁷⁴. The benefits of isolated heart research are numerous and can be remarkable depending on the investigator's goal. Isolated hearts offer a high degree of control over the system including, but not limited to: perfusate selection, flow control, and pre- and after-load variability. For a thorough historic summary of these aforementioned studies the reader is referred to a review by Hill *et al.* Furthermore, numerous pharmacological studies using such approaches can help elucidate the direct action of agents on the isolated cardiac tissues, i.e., while avoiding systemic interactions of other agents or breakdown products (e.g., cardiac-nervous system, hepatic metabolism, etc.)¹⁷⁵.

Additionally, high-throughput cardiac perfusion systems can be designed, or now even purchased off the shelf, in which multiple small mammalian hearts can be experimented on simultaneously. Isolated heart preparations have garnered notable insights to mechanisms of arrhythmias¹⁷⁶ and have been reviewed elsewhere¹⁷⁷. Depending upon the system configuration, a wide range of equipment and modalities are available to the investigator including: electrophysiologic monitoring and stimulus, ultrasonography, ultrasonic stimulation, fluoroscopy, infrared thermography, direct visualization via videoscopes, and anatomical mapping systems. Furthermore, the utilization of large mammalian isolated hearts allows for critical pre-clinical testing of device-tissue interactions in an environment highly similar to human anatomy and physiology, i.e. if the proper animal model is selected for the investigation¹⁷⁸. Comparative imaging of normal versus pathologic conditions, or interspecies comparisons, to determine optimal approaches, models, and designs are critical to development of novel therapeutics¹¹⁵. To

the medical device designer, engineer, or clinician, these insights have proven to be of high educational value^{179,180}.

Despite isolated heart preparations being a valuable tool, proper anatomical relationships can be considered lost when the lungs are removed. In particular, the pulmonary veins and their native ostia are of interest in the context of pulmonary vein isolation ablation treatments for atrial fibrillation. Heart-lung preparations have been utilized previously to elucidate the release of atrial natriuretic peptide¹⁸¹ and expand the pool of lung transplants to non-beating donors¹⁸²; they have also been used in numerous pharmacologic studies. Interestingly, the first heart-lung preparations are often attributed to Knowlton and Starling¹⁸³, however, their work acknowledges the methods of Martin¹⁸⁴ which were presented in lecture at Johns Hopkins in 1883. The first publication by Martin of his heart-lung bloc preparation was in 1881¹⁸⁵, therefore predating Langendorff's work by fourteen years. In short, this preparation cannulates in-situ the superior vena cava and one of the branches coming off the aortic arch. A closed loop is created by which pressure can be monitored, a compliance chamber incorporated, and pre- and afterloads varied.

It is also possible for human hearts from non-viable organ donors to be successfully reanimated using an isolated experimental apparatus⁹⁵. The Visible Heart® methodologies have been previously described by our laboratory⁹⁶, but more recently we have expanded these novel experimental approaches to incorporate whole large mammal heart-lung blocs, i.e., including both human and swine studies. To the authors' knowledge, this is the first description of such experimental results.

Method

The technique developed by our laboratory has been used successfully to reanimate human and swine hearts with right, left, or both lungs attached and functioning. Swine studies were approved by the Internal Animal Care and Use Committee at the University of Minnesota. Human hearts were approved for study by the Human Subject Committee Internal Review Board. Consent for use of the hearts for research purposes was received from the donors' family before explantation via LifeSource (St. Paul, MN).

The detailed procurement procedure has been described previously^{95,96}. Briefly, a median sternotomy was performed and an aortic root cannula implanted for delivery of cardioplegia. The inferior vena cava (IVC) was ligated and, just prior to cardioplegia delivery, the IVC for human preparations was removed with the liver if it was being recovered for transplant, and the superior vena cava (SVC) and aorta were cross-clamped. Cardioplegia was then delivered under pressure to rapidly cool and arrest the heart. The heart and lungs were then dissected and the heart-lung bloc removed by transection of the major vessels, trachea, and esophagus. The human specimens were then transported on ice to the laboratory within 6 hours of cross-clamp. An analogous procedure was performed on swine hearts in our laboratory: mean animal weights of 84 ± 14 Kg ($n=18$). We most commonly have performed these studies with just one lung attached, but the method has been adapted to include both lungs.

Upon arrival of human, or after explantation of swine, specimens, hearts were placed in an ice slurry of modified Krebs-Henseleit buffer while cannulation of the great vessels was performed (i.e., IVC, SVC, and Aorta). If a one lung preparation was desired, the left/right pulmonary veins and artery were dissected from the left/right lung and the lung was removed. These vessels were cannulated as well and a hemostasis valve was fitted for access. If both lungs were desired in the preparation, the pulmonary trunk was cannulated to allow control of the buffer flow, either directing all flow through the lungs or allowing some flow to the reservoir (i.e., a parallel path through the lungs and to the reservoir). An intubation tube was placed in the trachea and connected to a ventilator to control flow through the airway. Preparations were ventilated at a respiration rate of 11-15 per minute and a volume of 150-250 milliliters per lung.

The heart-lung blocs were then connected to the apparatus described in detail previously⁹⁶ that has been adapted for such use. A schematic of this system can be found in Figure 48. The system was altered to vary the aforementioned parameters of other isolated heart research systems and functions in either partial or four-chamber working mode. Partial working mode is similar to a Langendorff apparatus function, but fluid flow continues through an isolated lung. The system utilized a cardiovascular bypass oxygenator and heated water jacketed fluid reservoirs to maintain the proper physiologic environment. Seven to eight liters of modified Krebs-Henseleit buffer were contained in

the system and buffer changes of approximately four liters were performed regularly to wash out metabolites and maintain visualization as desired.

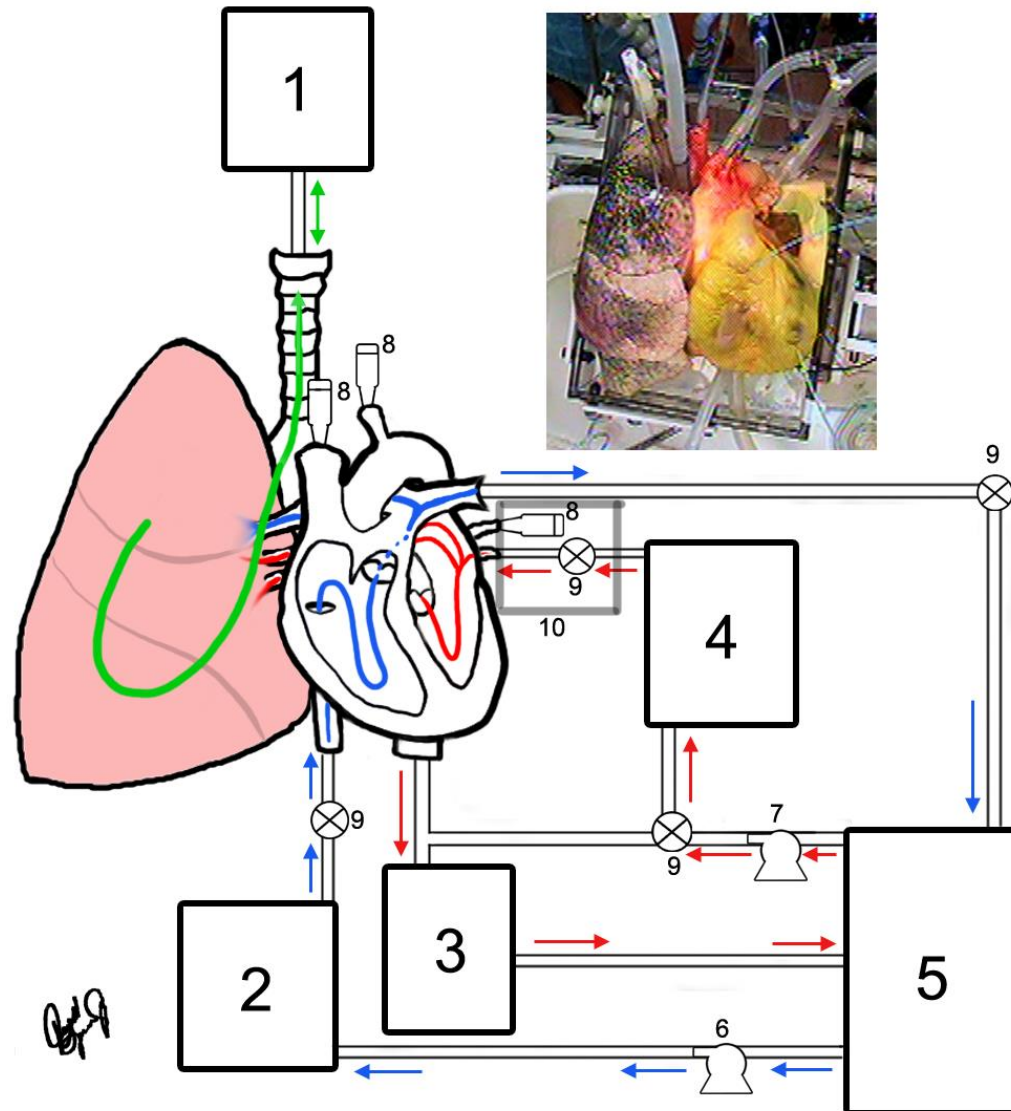


Figure 48: An external view of human heart 277 in systole and attached to the system is shown inset top right. Displayed center is a flow diagram for a functional heart and lung reanimation consisting of: (1) a respirator connected to the cannulated trachea and thus attached to the lung(s), (2) a pre-load chamber for the right side of the heart, (3) an aortic after-load chamber which mimics the resistance that the left ventricle works against, (4) a left pre-load chamber employed when only one lung is present, and (5) an oxygenator reservoir for pooling fluid expelled by any cannulated branch of the pulmonary artery. (6 & 7) fluid pumps to maintain the pre-load pressures, (8) hemostasis valves that allow access for delivery of cameras, instruments, and assorted devices, (9) valves that may also be used to redirect flow as physiologically appropriate, while (10) cannulation of the pulmonary vein(s) are shown here for a right lung preparation, but are absent or translated when either both lungs or the left alone respectively are used.

Once the specimen was re-warmed to 37°C, dobutamine was added to the system and the heart was defibrillated with 34 joules of energy supplied by a programmer-analyzer unit (#88345 Medtronic, Inc., Minneapolis, MN) via a pair of external patches (#6721, Medtronic, Inc.) placed epicardially above and below the ventricles. These hearts generally began beating in native sinus rhythm after a single defibrillation. It should be noted that one human heart developed heart block at two hours post-reanimation, and was then paced by a temporary pacing lead at 60 beats per minute; all specimens can be paced as desired. Hemodynamics of the left and right ventricle were recorded by Utah Medical pressure transducers (Model DPT-200, lot#1101991, Midvale, UT) via water columns from venogram balloon tipped catheters (Attain 6215, Medtronic, Inc.). High-resolution Olympus commercial endoscopes (Model 1V8200T, Model 1V8420, Center Valley, PA) were then placed within these heart and/or lungs to capture functional anatomy. To our knowledge, these are the first images of the pulmonary veins and arteries within the lung of functioning human heart-lung blocs.

Results

Using this novel experimental approach, to date, all attempts to reanimate hearts have been successful; eighteen swine and four human heart-lung blocs have been reanimated. Hemodynamic functioning of these in vitro reanimated specimens can be augmented by the delivery of inotropic agents and/or by increased dosing with extracellular calcium. Prior to heart recovery, the mean heart rates and blood pressures for the swine were: 91 ±13 beats per minute and 105/56±13/9 mmHg, respectively. Table 1 provides partial cardiac medical histories for the organ donors from which the human hearts were recovered. Table 2 provides the relative hemodynamic performance data for these reanimated heart-lung preparations.

Table 1: Summary of donor information and their hemodynamic status prior to organ recovery.

Human Specimens							
Specimen	Gender	Age (yrs)	Weight (kg)	Cause of Death	HR (bpm)	BP (mmHg)	CVP (mmHg)
HH 277	M	60.0	113.4	Head Trauma	71.0	105/61	15.0
HH 284	F	78.0	54.4	CVA	103.0	118/70	11.0
HH 291	F	58.0	114.7	Stroke	70.0	100/50	12.0
HH 295	M	34	68	Cardiac Arrest	92	130/75	-
Average		69	83.9		87		13
Standard Dev.		12.7	41.7		22.6		2.8

BP=blood pressure; HR=heart rate; CVP=central venous pressure

Table 2: Hemodynamic performances of each reanimated swine and human heart/lung bloc specimen.

Swine Specimens							
Specimen	HR (bpm)	LVSP (mm Hg)	LVEDP (mm Hg)	+dLVP/dt (mm Hg/s)	-dLVP/dt (mm Hg/s)	Tau	Lung
1	95.8	91.2	12.4	982.8	-903.0	31.2	Right
2	91.0	25.0	-2.0	430.8	-343.8	36.2	Right
3	100.0	77.0	-4.0	961.0	-462.0	30.0	Right
4	81.7	73.5	2.3	772.3	-354.5	37.7	Right
5	91.8	85.7	1.3	927.0	-509.8	33.2	Right
6	99.5	62.8	11.3	574.0	-435.0	30.2	Right
7	55.8	82.0	5.7	600.2	-358.2	63.0	Right
8	90.3	79.3	-4.3	842.5	-618.0	33.5	Left
9	92.7	75.7	12.0	623.3	-771.7	32.5	Left
10	102.5	67.5	1.2	637.8	-513.2	29.7	Right
11	76.7	101.7	10.7	786.5	-501.5	39.7	Right
12	123.3	76.3	1.3	729.0	-624.5	26.0	Right
13	124.8	58.7	2.7	762.5	-532.7	24.0	Right
14	84.5	87.2	0.7	888.8	-646.0	54.0	Right
15	114.0	91.7	-2.7	922.3	-808.0	27.5	Right
16	105.0	70.8	0.0	607.7	-446.3	28.8	Right

17	101.3	56.5	3.8	529.8	-317.7	29.8	Right
18	91.2	75.7	7.0	618.3	-810.2	33.0	Right
Average	95.7	74.3	3.3	733.2	-553.1	34.4	
Standard Dev.	16.3	17	5.4	163.6	177.6	9.7	
Human Specimens							
HH 277	85.8	65.7	-7.3	624.5	-475.5	37.2	Right
HH 284	81.2	79.5	1.7	848.2	-377.7	37.5	Right
HH 291	70.3	53.3	8.0	341.3	-273.7	45.3	Both
HH 295	81.3	72.5	4.2	415.7	-343.0	37.7	Right
Average	79.7	67.8	1.6	557.4	-367.5	39.4	
Standard Dev.	6.6	11.1	6.5	227.9	84	3.9	

HR=heart rate; LVSP=left ventricular systolic pressure; LVEDP=left ventricular end-diastolic pressure; +dLVP/dt= maximal positive derivative of left ventricular pressure with respect to time; -dLVP/dt= maximal negative derivative of left ventricular pressure with respect to time

It should be noted that one of the early reanimated swine heart-lung specimens (#2) elicited poor hemodynamic performance from the beginning of reanimation. We suspect that injury occurred during isolation and/or that emboli caused poor coronary perfusion. It should be noted that recorded data from several hearts elicited negative values for end-diastolic pressures; we suspect that this is due to drift in the sensors or a vacuum or syphoning effect, potentially occurring in the current system modification to incorporate the lungs.

Interestingly, compared to our long-term experience with lone heart reanimation using endscopes, a large degree of remaining particulate and blood within the lung has complicated our initial imaging during certain studies. Therefore, more frequent buffer changes have been required to obtain clear, high-fidelity images and video.

As previously mentioned the main benefit of this model is the maintenance of proper pulmonary ostia and vessel anatomy. A selected anatomical image series of a videoscope being retracted from either the pulmonary arteries or veins is shown in Figure 49; a corresponding video can be accessed via supplemental materials or online (<http://www.vhlab.umn.edu/atlas/>). The study of cryoballoon ablation procedures

motivated much of the development of this model, and a series of cryoballoon procedures have been performed, e.g., as viewed from within the vein as displayed in Figure 50, panel C. The supplemental video of the pulmonary arteries and veins functioning gives the reader an appreciation of the truly dynamic nature of these vessels which are usually thought to be relatively passive structures.

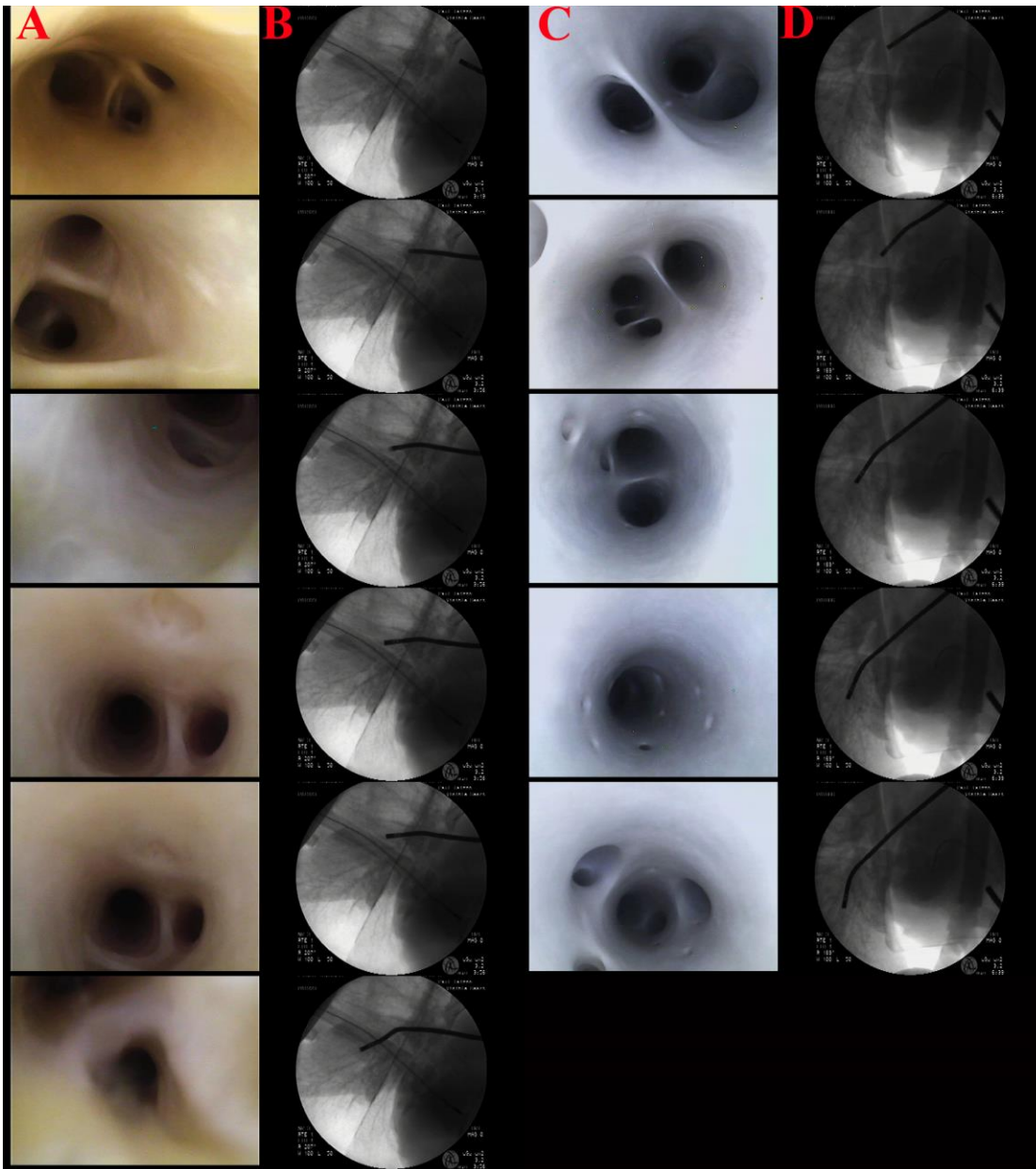


Figure 49: An image series obtained from reanimated human heart-lung bloc 284 (A,B) and 277 (C,D) showing the path through the distal pulmonary arteries and veins, respectively. The corresponding fluoroscopic images (B,D) in each case show the relative locations of the videoscopes (A,C). A supplemental video of the journey through the vasculature can be viewed as well.

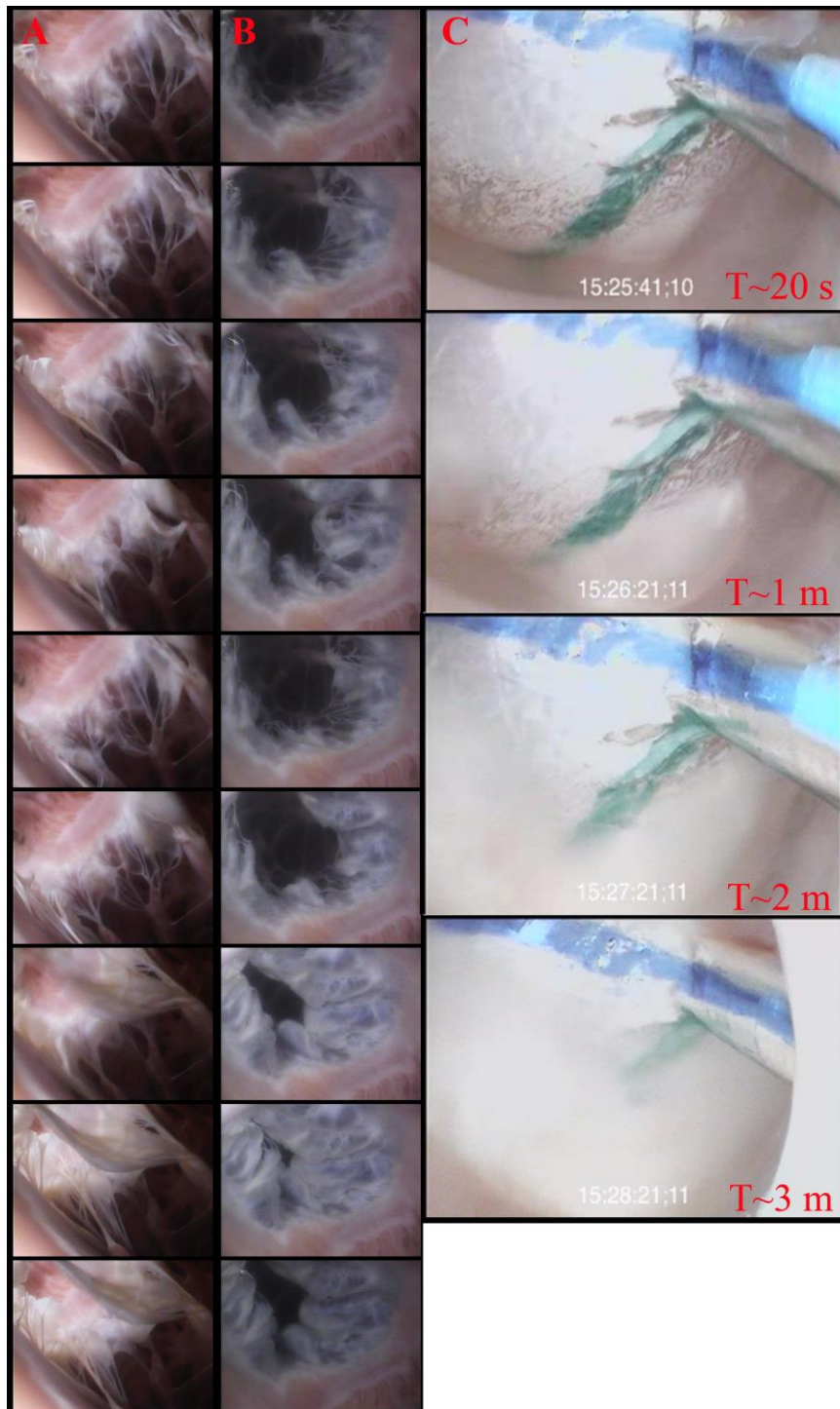


Figure 50: Provided here is a time series of images from human heart 277 showing tricuspid valve closure from the right ventricle (A) and right atria (B). Images are displayed 1/15th per second apart in time. Panel C displays ice formation on the distal portion of a cryoballoon ablation catheter (Artic Front, Medtronic, Inc., Minneapolis, MN) as seen from within the pulmonary vein. The images are spaced post-ablation 30 seconds, 1, 2, and 3 minutes apart.

Discussion

To the authors' knowledge, this report has provided first time dynamic images of the pulmonary vasculature during normal cardiac function in both reanimated human and swine heart-lung blocs. This model provides a unique in-vitro approach for the study of novel medical therapeutics from both human and large mammalian heart-lung specimens. In a similar embodiment (i.e., without the lungs), this reanimated heart model has been utilized in numerous cardiac studies. In the electrophysiologic area, these studies have included the use of endocardial noncontact mapping, pacemakers, defibrillators, leads, and catheters¹⁸⁶. The Visible Heart® model has also been employed to study the dynamic nature of valves and transcatheter valve deployment⁹⁴. Importantly these methodological approaches also allow for use of echocardiography and fluoroscopy to guide procedures, i.e., comparative imaging¹⁸⁷. Most recently, this approach has proven to be quite valuable for the study of novel cardiac treatments, such as leadless pacing devices¹⁸⁸. Nevertheless, the novel addition of a lung(s) to this paradigm still allows for any of the prior studies to be conducted, but may in turn reduce the number of hemostasis valve access points that were previously available.

Our continued use and enhancement of Visible Heart® methodology has also facilitated the creation of an open-access educational website, The Atlas of Human Cardiac Anatomy (<http://www.vhlab.umn.edu/atlas>)¹⁸⁹. The anatomical images and videos on the website are free to download and use for presentations and teaching; we request that proper citations be used. In other words, the novel images and/or comparative imaging of functional cardiac anatomy are of high value in teaching the nuances of cardiac anatomy, especially of active, complex structures, such as valves. It should be noted that this website also provides instructional tutorials on cardiac anatomy and physiology and full cadaveric thoracic cavity dissections. Finally, a cardiac device tutorial is available as well, which has been well noted as being beneficial in the explanation of therapies to patients.

The model described here is not without limitations, as is true with all in-vitro systems. Despite supersaturating the buffer with oxygen, there remains a significant difference in the oxygen content of the buffer compared to blood. For this reason, the function of the heart slowly declines over time from the initial reanimation. Yet reasonable physiologic

function to perform such aforementioned investigations is generally elicited for up to 4 to 8 hours, in our previous experiences. It is possible that the addition of the lungs may extend the functionality, which we tend to believe at this point but need more data to substantiate such. Most recently, we are employing a full anesthesia suite ventilator to more closely control the ventilation parameters (e.g., provide positive end expiratory pressure, PEEP). In such experimentation, one also needs to consider that although it is also known that hypothermal transport of organs protects them, global ischemic injury still occurs to some degree. Further, our current system is designed to replicate physiologic pre- and after-loads, but there potentially are important physiological effects that are not completely replicated, such as vessel compliance. Likewise, in our studies the heart-lung blocs are cradled on soft foam sponges, which may focally alter perfusion compared to the natural state. Finally, due to the nature of acquiring non-viable donor human heart-lung specimens, there are numerous differences between their inherent cardiac statuses that cannot be controlled. Such differences in status include, but are not limited to: method of cardiac arrest, transport time before arriving in the laboratory, inotropic support, potential air or other emboli in the coronary vasculature, and prior pathologies. Despite being unable to control for these parameters, the described system produced comparable pressures to other isolated human heart alone preparations^{95,190}. As reviewed in Table 2, despite these variances the hemodynamic data are fairly comparable from specimen to specimen. It should be specifically noted that we are extremely grateful and privileged to obtain these donated human heart-lung preparations as gifts for research.

To conclude, this extension of Visible Heart® methodologies has garnished novel, functional anatomical heart-lung anatomical visualization. Further, unique abilities to image the device-tissue interactions using this approach are unparalleled. Therefore, we consider that these obtained images are of high value to the medical device designer, educators, and clinicians for both training and educational purposes. The lab will continue to reanimate hearts and heart-lung blocs using these methodologies and thereby enable: the study of dynamic anatomy, insights into the device-tissue interface, and creation of new materials for the free-access Atlas of Human Cardiac Anatomy website.

Acknowledgements

The authors would like to thank the generous individuals and families that donated hearts for research and LifeSource for facilitation of this research. This research was supported in part by Medtronic Inc., the Lillehei Heart Institute, and the Institute for Engineering in Medicine at the University of Minnesota. A special thank you to Gary Williams for his computer assistance and Monica Mahre in preparation of this manuscript.

III.II- Chapter 9: Infrared imaging of cryoballoon ablation therapy applied to reanimated swine and human heart-lung blocs

This section is in the submission process to Heart Rhythm.

Ryan P. Goff, BS^{26,27,28}; Steve Quallich BS^{26,27,28}; Benjamin Troness BS²⁷; Paul A. Iaizzo PhD^{26,27}

Introduction

Cardiac balloon cryoablation for the treatment of atrial fibrillation has been gaining attention as an approach for isolation of the pulmonary veins (PV): i.e., since its first reported use in 2003¹⁵ and in the current clinical form in 2005¹¹⁶. Yet, it should be noted that focal cryoablation has been used surgically for many more years¹¹⁷ with transcatheter devices becoming available in more recent decades. An advantage of cryoballoon ablation of a pulmonary vein ostium, is that it is a ‘single-shot’ approach, which aids in accelerating the slow nature of freezing compared to RF energy (i.e., not point-by-point ablation). Further, the currently available ArticFront (Medtronic, Minneapolis, MN) cryoballoon has been shown to have comparable success rates to RF ablation with lower adverse events^{34,118}. The recent STOP-AF trial concluded similar findings to the observational European studies: that being an acceptable safety profile and superiority to antiarrhythmic drugs in those who have failed to respond to them¹⁷.

Despite widespread and growing clinical use there are still questions regarding dosing and treatment times for optimal cryoablation therapy, which in turn may affect both efficacy and collateral tissue injury^{119,120}. Conversely, parameters affecting RF ablation lesions have been investigated in numerous preclinical and clinical studies, and temperatures of 50°C or higher are required for the creation of necessary myocardial scars¹²¹. Additionally, although many open scientific questions remain, the effects of power, ablation durations, catheter orientations, catheter sizes, usage of irrigation, and

²⁶ Department of Biomedical Engineering, University of Minnesota (Minneapolis, MN)

²⁷ Department of Surgery, University of Minnesota (Minneapolis, MN)

²⁸ Medtronic Inc., Mounds View, MN

contact forces on lesion size have been investigated for RF¹²²⁻¹²⁵. Furthermore, the release of a second generation cryoablation device with a different cooling profile merits additional research to compare to both the previous versions of these devices and also to ablation using RF energy¹²⁶. It should be noted, to date, the highest regularly detected clinical complication for ablation with the cryoballoon is phrenic nerve palsy with rates of 4-8%^{17,118}. Yet, it remains unknown, the impact on esophageal cooling may also differ for the second generation balloon: importantly, esophageal injury is not normally detectable unless specifically searched for using endoscopy^{44,127}. Reports of hemoptysis are also reported in patient series of cryoballoon ablation, indicating the lung may be injured during these treatments as well^{41,161,191}. It is currently recommended by the manufacturer that two separate four minute ablations are applied per PV: yet, several clinicians have recently suggested that only one may be adequate. In other words, given that the phrenic nerve and esophagus are in intimate contact with the right PVs and posterior wall of the LA, respectively, optimization of dosing is important to both ensure permanent isolation of the pulmonary vein tissue while minimizing the impact to these structures.

It is well accepted that in order for cardiac ablation lesions to be effective long-term, it is necessary that they are transmural. In the present study through the use of infrared (IR) imaging, the epicardial surface temperatures were monitored as well as the relative times to reach those temperatures. Due to the anatomical relation of the aforementioned collateral tissues that might be impacted during treatment, these epicardial thermal profiles should be in the range of those experienced collaterally. That is to say that since the tissues that have been reported to be injured collaterally are in intimate contact with the epicardial surfaces, that the epicardial temperature profiles measured here are in the range of the most extreme temperatures the collateral tissues may encounter. This novel infrared imaging data, with additional information regarding the thermal thresholds of injury of the tissues of interest, may help guide decisions on dosing. Uniquely, we were able to collect these data from reanimated human and swine heart/lung blocs.

Methods

Isolated Heart-Lung Preparation

The technique developed by our laboratory has successfully reanimated human and swine hearts with right, left, or both lungs attached and functioning. Swine studies were approved by the Internal Animal Care and Use Committee at the University of Minnesota. The use of human specimens for research were approved for study by Human Subjects Institutional Review Board: consent for use of the hearts for research purposes was received from the donor's closest relative(s) via LifeSource (St. Paul, MN). Note, the detailed procurement procedures have been described previously⁹⁵. The human specimens were then transported on ice to the laboratory within 8 hours of cardiac arrest. For isolation of the swine specimens, a median sternotomy was performed and an aortic root cannula implanted for delivery of cardioplegia. The inferior vena cava (IVC) was ligated and just prior to cardioplegia delivery the IVC was removed with the liver and the superior vena cava (SVC) and aorta were cross-clamped. Cardioplegia was then delivered under pressure to cool and arrest the heart/lung blocs. The heart and one or both lungs were then dissected and the bloc then removed by transection of the major vessels, trachea, and esophagus. Note, we most commonly have performed these studies with just one lung attached, but the method has been easily adapted to have both lungs attached. The heart-lung blocs were then connected to an apparatus described in detail previously⁹⁶ that has been modified to accommodate the lung. The system can vary standard parameters of other isolated heart research systems (i.e., pre-load, after-load, perfusates, see Hill et al.⁹⁵) and functions in either partial or four-chamber working mode. Partial working right-side mode allows fluid flow to continue through the isolated lung(s), but without added flow directed into the left atrium. Four-chamber working mode is analogous to the native function of the heart and was used during all ablation procedures and throughout the thawing phase. Hemodynamic performance of these hearts is summarized in Table 9. Note, that as best as possible, the reanimated lung(s) were ventilated at a respiration rate of 11-15 per minute and a volume of 150-250 milliliters per lung. To do so, the remaining airway (the distal main trachea) was intubated by placement of an endotracheal tube (if only one lung was isolated the other primary branch

bronchus was tied off) and subsequently attached to the ventilator. Video endoscopes (IPLEX FX series, Olympus Corp., Tokyo, Japan) were employed so to observe the proper placements of the cryoballoons within the pulmonary vein ostia as previously described. A supplemental video provided here, shows an anterior view of a specimen and then the simultaneous multimodal imaging performed during the experiments.

Infrared Imaging and Data Analysis

A FLIR SC620 (FLIR Systems, Inc., Boston, MA) infrared (IR) camera was used to capture thermographic data at a minimum rate of one hertz. The emissivity and appropriate environmental parameters were input to the infrared software (ThermaCAM Researcher Pro 2.9, FLIR Systems, Inc., Boston, MA). Emissivity was determined by comparison of IR temperatures to a 0.040" T-type thermocouple (Omega Engineering) being read by a digital thermometer (Fluke 51II, Everett, WA). It should be noted that this IR system is only capable of measuring temperatures as low as -30 Celsius, below this level the accuracy of the measurements are reduced.

Measured parameters using FLIR software include: lowest epicardial temperature reached, epicardial area cooled to 10, 5, 0, and -5 °C, and time from start of an ablation until epicardial temperatures of 10, 5, 0, -5, and -10 °C were achieved. If required, the heart was held in a more lateral position to best view with the IR camera, the area being treated/cooled.

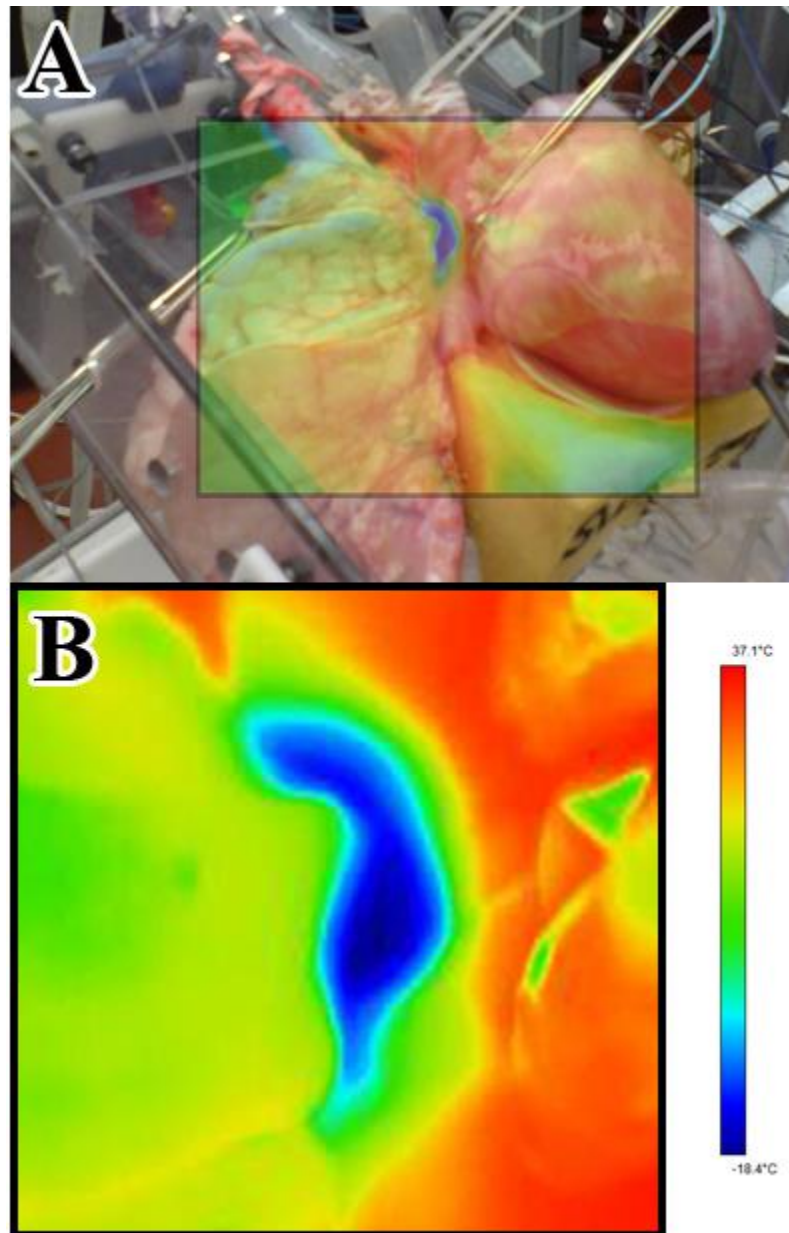


Figure 51: Shown above (A) the heart-lung bloc, with overlaid thermograph, attached to the Visible Heart ® apparatus with heart held laterally to best image area of therapy. Panel B shows a close up view of the resultant thermograph with the temperature scale ranging from -18 to 37 °C in this example.

Ablation Procedure

A steerable outer catheter (FlexCath, Medtronic, Inc.) was placed into the left atria (LA) by either a transseptal puncture via the inferior vena cava or directly via the contralateral PV cannulated with a fixture containing a hemostasis valve. Using direct endoscopic visualization and a 0.035" guidewire (PV tracker, Medtronic, Inc.) the ablation catheter was then inserted over the wire into the LA. Once the preparation and catheter delivery

sheath were in place the IR camera was setup and not moved throughout that given experimental procedure. The cryo-catheters investigated here were 28 mm ArticFront and ArticFront Advance (Medtronic, Inc.). The catheters were marked along the length of the balloon with colored fiducial markers, so to ensure that the clocking of the catheters in between exchanges or ablations were consistent (see Figure 2 and supplemental video).

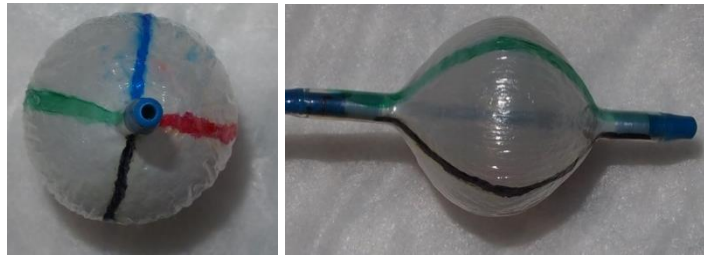


Figure 52: ArticFront 28 mm balloon cryoablation catheter with colored markings for optimizing the alignments of catheter position between ablations. The blue band corresponds to the top of the catheter handle and the red band corresponds to the left side of the handle (i.e., the operator's perspective).

Data were presented as the means \pm standard deviations. These results were compared on a day-by-day basis using a paired T-test ($\alpha=0.05$) to determine if there were statistical differences between the various parameters of interest and between the catheters employed.

Results

Swine data

Using these methods a total of 8 heart-lung blocs were reanimated and studied. In most cases, two or three ablations per catheter (ArticFront and ArticFront Advance) were performed per day; note in one instance only one ablation was performed due to technical difficulties. The daily results of the cooling measurements were averaged by catheter type. This approach was chosen to compare the differences between catheters without the influence of daily variabilities such as: camera position, atmospheric conditions, cardiac outputs, and differing anatomy. The relative hemodynamic performances of these specimens during these applied thermal therapies were provided below in Table 9.

Table 9: Hemodynamic performance of reanimated swine heart-lung blocs.

Specimen	HR (bpm)	LVSP (mm Hg)	LVEDP (mm Hg)	+dLVP/dt (mm Hg/s)	-dLVP/dt (mm Hg/s)	Tau	Lung
1	94.0	77.8	-2.3	857.5	-553.5	32.0	Right
2	106.5	85.5	1.8	838.2	-664.2	28.3	Right
3	76.8	89.3	-1.0	893.3	-640.7	40.0	Left
4	105.2	70.7	12.0	715.8	-682.2	30.2	Left
5	108.0	79.2	1.5	683.3	-564.0	28.5	Right
6	119.7	74.0	9.0	716.5	-622.3	25.0	Right
7	90.8	96.3	5.0	853.8	-681.0	37.7	Right
8	105.0	82.0	-3.5	809.2	-662.2	31.3	Right
Average	100.8	81.9	2.8	796.0	-633.8	31.6	
Standard Dev.	13.1	8.4	5.5	79.3	50.4	5.0	
Human Specimens							
HH 277	63.7	71.8	-3.0	485.3	-428.2	50.7	Right
HH 284	104.5	83.0	0.8	836.0	-641.0	28.8	Right

The temperature area measurements were made using the time point at which the most extreme cooling had occurred. A total of 24 and 26 ablations for ArticFront and the ArticFront Advance were measured, respectively. When all the data were examined, including cases in which the ablation had not reached the indicated temperatures (i.e., an area value of zero), Figure 53 demonstrates that ArticFront Advance cooled greater areas and in most cases achieved lower temperatures. However, when the subset of data in which only ablations which reached the measured temperature were plotted in Figure 54, one can see that the differences were less pronounced.

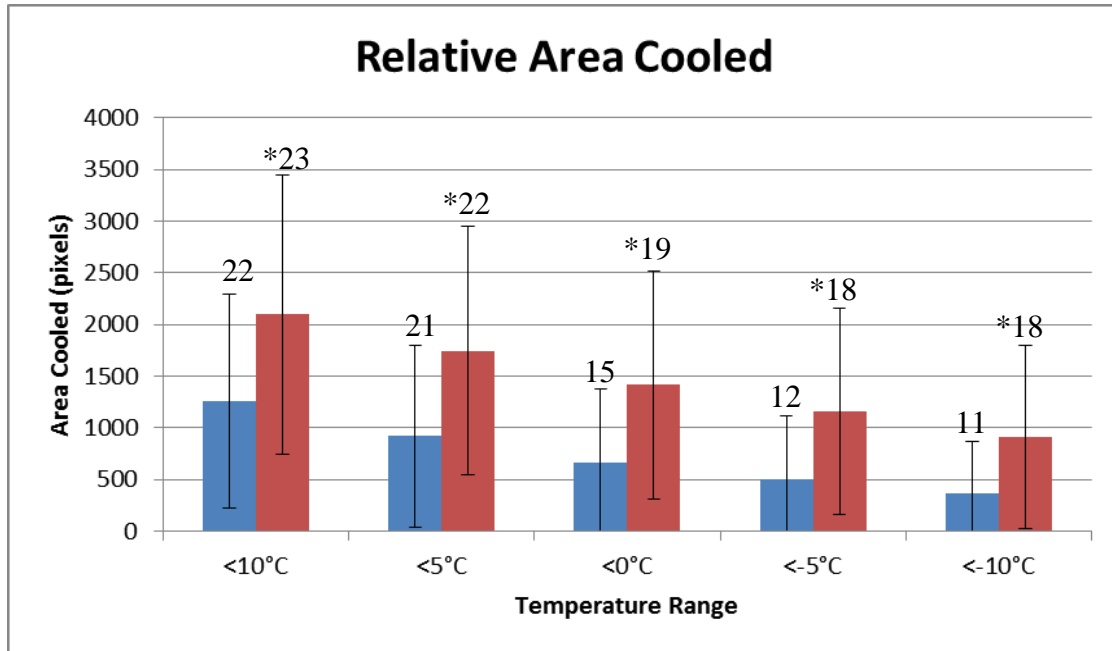


Figure 53: Relative area cooled by employing ArticFront (blue) and ArticFront Advance (red) catheters. Above each bar is the number of ablations in which the indicated level of cooling was achieved. For each the ArticFront and ArticFront Advance catheters, 24 and 25 ablations were analyzed, respectively. Ablations which did not achieve cooling to the measured temperature were averaged with the other ablations performed that day as zero area cooled. (*= $p < .05$)

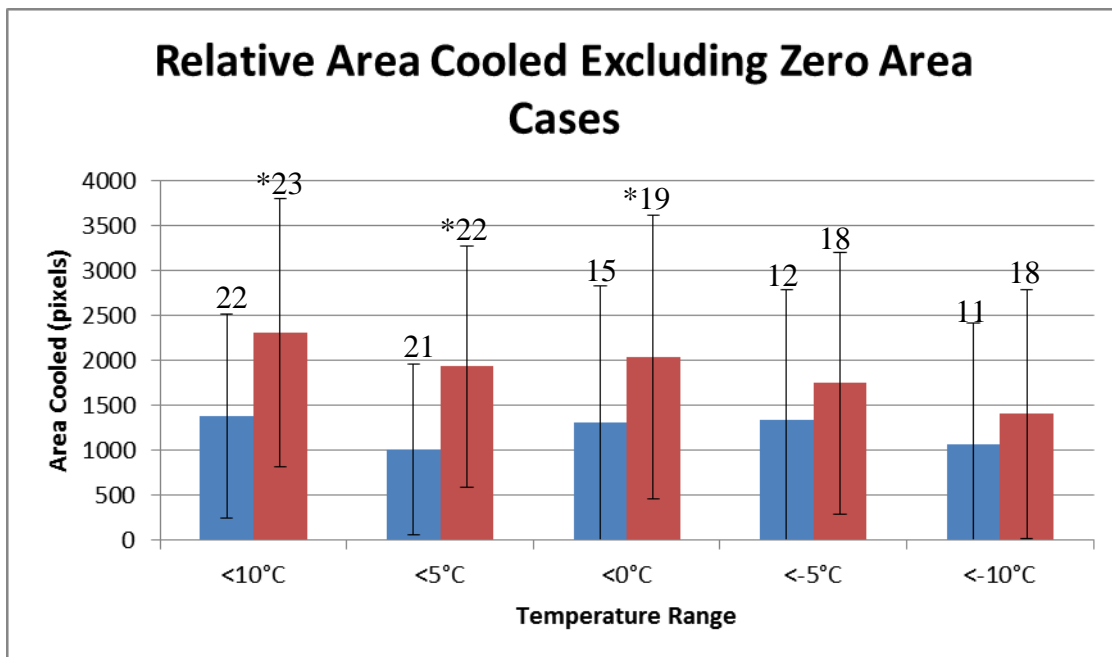


Figure 54: Relative area cooled during therapy application by ArticFront (blue) and ArticFront Advance (red) catheters excluding cases in which the measured temperature was not achieved (e.g., if -5°C was not achieved, that ablation was not analyzed in the -5°C group). The number of ablations measured is displayed above the error bars. (*= $p < .05$)

The cooling time to epicardial temperatures of 10, 5, 0, -5, and -10°C were measured in 16 ablations delivered using ArticFront and 20 ablations for ArticFront Advance catheters. Note, that these Ns differ from the area measurements, due to subsequent technical problems during which the digital video recording system was damaged, thus making the syncing of multiple timed systems not possible (e.g., IR computer and CryoConsole).

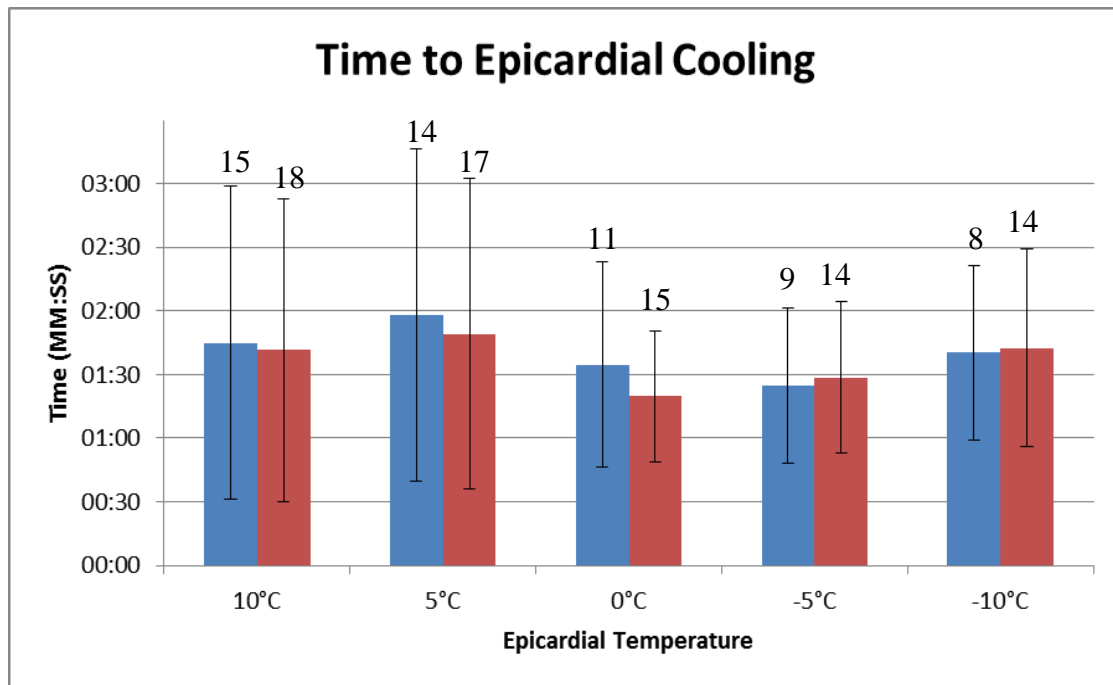


Figure 55: Time to reach indicated epicardial temperatures from beginning of ablation. Note that differences between treatments delivered with ArticFront (blue, n=16) versus ArticFront Advance (red, n=20) catheters were not found to be significant.

The lowest temperature achieved during these series of ablations were measured for each application. Again, it should be noted that the limitations of IR imaging somewhat complicated this analysis, because of the considered reduced accuracy of this specific camera for temperatures less than -30°C: therefore ablations that demonstrated very low temperatures (i.e., reading less than -40°C) were considered to be not lower than -40°C for the results shown in Figure 57 to take a conservative measurement approach. This occurred once for an ArticFront ablation and four times during ArticFront Advance treatments, suggesting that the ArticFront Advance catheters allow for greater cooling potential. The histogram shown in Figure 56 displays the distribution of nadir

temperatures: temperatures less than -30°C are denoted by an * to indicate that they may not be reliable.

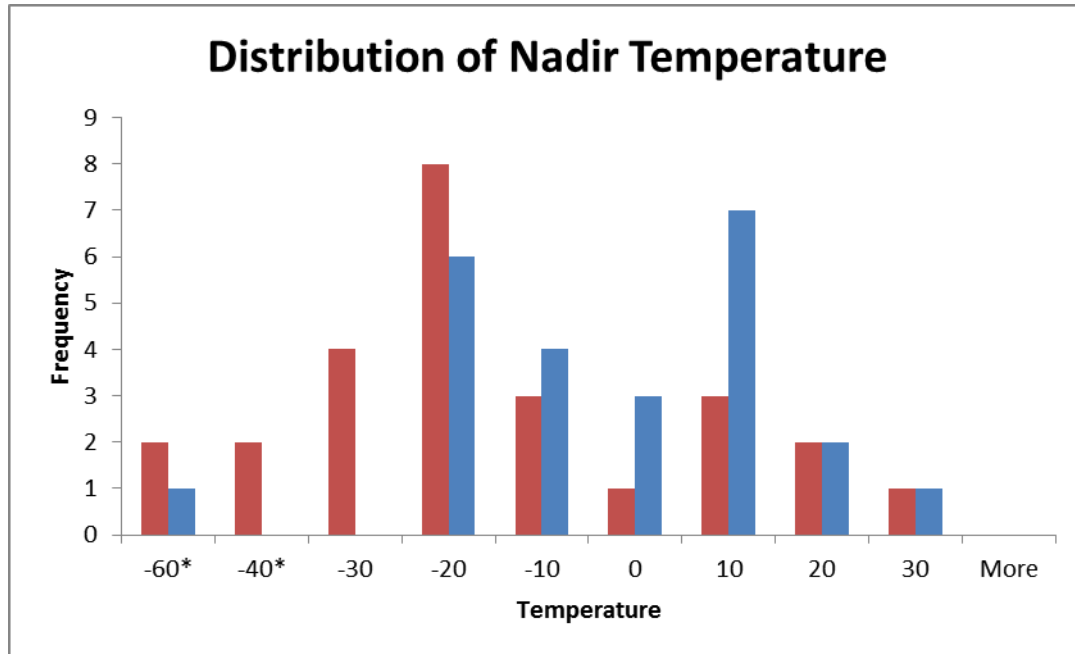


Figure 56: Distribution of nadir temperatures achieved following treatments with either catheter system: ArticFront (blue) and ArticFront Advance (red). Note, accuracy of temperatures less than -30°C may be decreased as denoted by an *. No temperatures fell within the 50°C bin and therefore it was omitted.

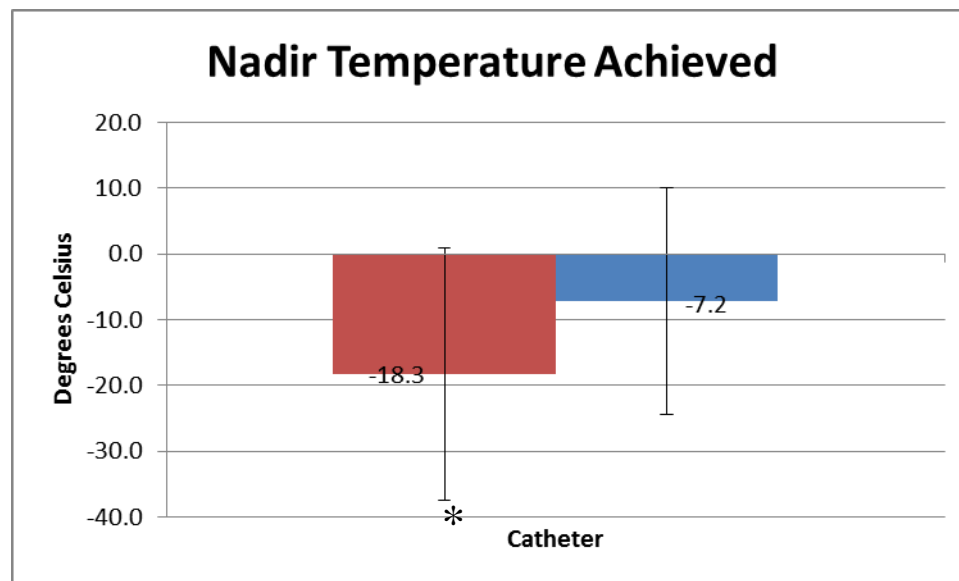


Figure 57: Minimum temperature achieved by treatment applications with ArticFront (blue) and ArticFront Advance (red) catheters ($p=0.036$).

Human data

Two human specimens became available to our lab during the course of these experiments. In each specimen two ablations with the ArticFront Advanced 23 mm catheter were performed. To compare the results of the 23 mm catheter in human versus swine, one swine experiment with six ablations using the 23 mm catheter was performed. The data is included due to the unique opportunity to study human versus swine specimens, thus making these studies of high translational value.

Since it is not feasible to compare different human samples or human to swine samples on the same day, with the same setup, anatomy, etc. a ruler was included in the recording to scale the images. However, the ruler was not held perfectly planar to the lens by an apparatus, but was approximated. The results suggest that a smaller area is cooled in human samples as indicated by Figure 58. However, as can be seen there are very large standard deviations. Data on cooling speeds were not able to be calculated due to syncing technical difficulties mentioned previously. Comparing the data on the lowest temperature achieved the differences are minimal, with swine achieving $-17.9 \pm 18.9^\circ\text{C}$ and human samples reaching $14.2 \pm 16.6^\circ\text{C}$.

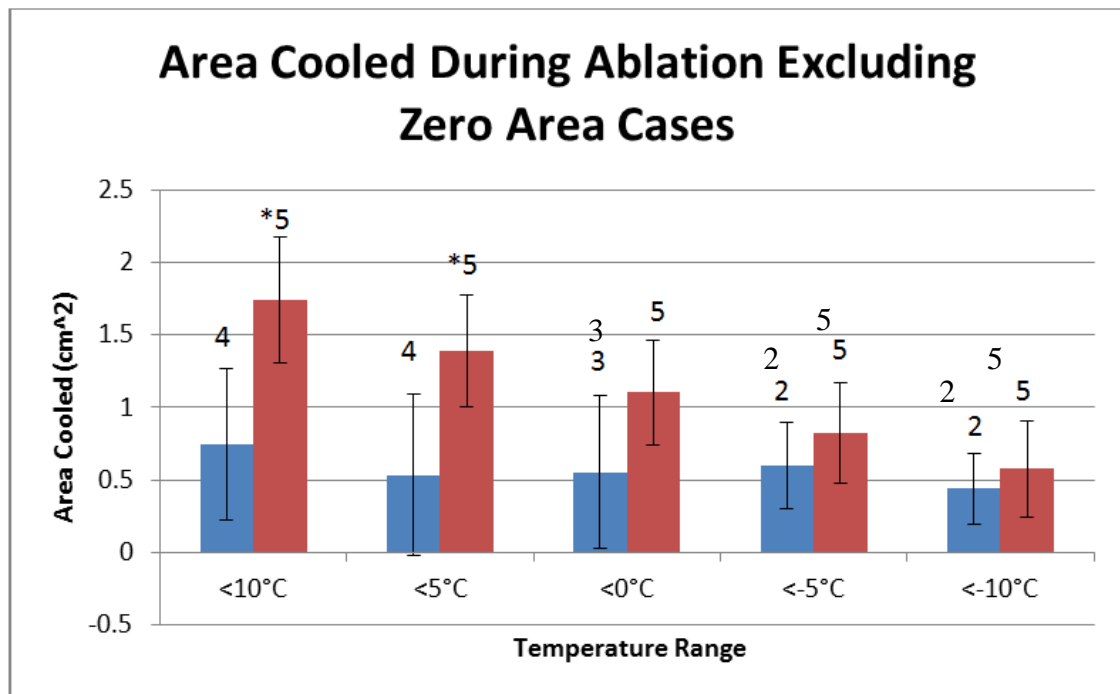


Figure 58: Area cooled by ArticFront 23 mm catheter in human (blue) and swine (red). The number of ablations measured is displayed above the error bars. (*= p<.05)

Discussion

Here we present a novel, technically challenging study utilizing external infrared imaging data obtained during cryoablation treatments applied employing ArticFront (blue) and ArticFront Advance (red) catheters. We uniquely performed these studies employing both reanimated human and swine heart/lung blocs and believe this to be the first report of thermal ablation studies using such a method. Yet, one must also consider that the translational experimental methodology presented here, may be considered as possible worst case scenarios or extreme cases, in the sense that the measured temperatures are expected to be colder than what would be measured in-vivo. This is due to the fact that the reanimated heart and lung(s) were surrounded by air. Note that this experimental design was required so to be able to obtain these real time infrared measurements of the resultant tissue temperatures. Therefore, the metabolic heat generated by surrounding organs is not being transferred to the isolated block. Additionally, air is a superior insulator compared to tissues by orders of magnitude and will in effect keep the cooling within in the tissue, having very little warming effects from the air. It should be noted, attempts by our laboratory to utilize IR imaging in-situ open chest models proved difficult to obtain direct visualization of the zone of ablation. The use of isolated hearts is already well established in cardiac research^{95,96} and this methodology incorporates native sinus rhythm with physiologically relevant hemodynamics.

The results of the cooling area measurements suggest that AFA will cool a larger area and more frequently to colder temperatures. However, there may be other influencing parameters that will dictate how large an area is cooled, such as, anatomical variance and catheter pressure. This is suggested by the differences between Figure 53 and Figure 54. The time to cool the epicardium to a particular temperature did not vary much between catheters. This is expected because rate of heat transfer transmurally is most likely governed by the thermal conductivity of tissue, which should remain relatively constant between samples. The fact that it varies little between catheters may speak to the robustness of this methodology. The depth of cooling appears to be greater for AFA than AF based upon the distribution of nadir temperatures. This technique is not limited to the

use of cryoablation catheters. Any thermally based ablation targeting the pulmonary veins, or even other structures, may be studied using these approaches. The authors believe that this is one of the most translational methodologies available for study, especially when human heart specimens are available.

The data presented here suggests that differences exist between human and swine cryoballoon ablation cooling profiles. The differences may be due to tissue thickness, age, disease state, fibrosis, and relative mass. It should be noted that we have observed that the pulmonary veins in aged human samples that our laboratory has received are thicker than the relatively young swine. The lungs of the human samples were also larger than those of the swine. The fact that only some of the area measurements were statistically different, and the end temperatures not significantly different, suggests that the translational aspect of the swine data is valid. The human data translates to the clinical case, but as mentioned previously the temperatures are most likely colder, and/or the rate of cooling faster, than those experienced in-vivo.

Reviews of cryosurgical injury are readily available in the literature¹⁴² and it is accepted that differing tissues and cells have varying thermal tolerance. Unfortunately, the thermal tolerance of myocardium, esophagus, and lung is not fully understood. In our lab efforts are underway to further characterize some of these tissues. However, it is accepted in the cancer field that if the vascular supply is damaged a lesion will eventually result. The vascular susceptibility to cooling also differs by tissue, but has been generally reported to be in the range of -20 to -30°C¹⁴². Whether or not this applies to tissues that are in contact with blood (i.e., myocardium and PV) is unclear, but may guide the community until better data is published. However, taking this into account with the aforementioned data suggests that shorter treatments may be necessary to avoid collateral injury. As a precaution, shorter treatment times are already being proposed in the literature¹⁹².

Work done on the swine phrenic nerve in our lab suggests that cooling to mild subzero temperatures will acutely, irreversibly cease conduction¹⁹³ in most cases. This data is in agreement with previous studies^{151,152}. Taken into account with the findings presented here, an operator should be particularly careful to avoid placing a cryoballoon deep within the pulmonary veins and phrenic nerve monitoring should be used, as is standard now. However, certain patients may possess atypical phrenic anatomy that is less

compatible with cryoballoon and/or RF ablation of the pulmonary veins, such as: close right superior PV and superior vena cava relationship³⁸ or the right upper PV ostium to the right pericardiacophrenic artery¹⁹⁴.

To the author's knowledge this is the first publication of such an experimental methodology to investigate the effects of cardiac thermal ablation. The data from these experiments may aid in the guidance of dosing. Future experiments using these methodologies could be performed to determine the characteristics of novel ablation devices and how they may impact the myocardium and surrounding tissues.

III.III- Chapter 10: Magnetic Resonance Imaging of Ice Dynamics During Cryoballoon Ablation

Ryan P. Goff, BS^{29,30,31}; Devashish Shrivastava PhD³²; Jean-Pierre Lalonde³; Paul A. Iaizzo PhD^{1,2}

Introduction:

As has been stressed many times throughout this thesis the full extent of collateral injury occurring to tissues due to cardiac ablations remains largely unknown. Ice formation may serve somewhat as a surrogate for the extent of collateral injury. Although, it has been established in many tissues and supported in this thesis that temperatures below phase change (i.e., $\sim -0.5^{\circ}\text{C}$ for most tissues) are necessary for complete destruction of tissue. However, this data is still useful through either computer modeling to back calculate thermal profiles, estimation based upon thermal injury thresholds, or even just as a quasi-quantitative examination of the extent of collateral injury.

In order to better understand the extent to which ice from cryoballoon ablations is entering collateral tissues a technique utilizing high-resolution MR (magnetic resonance) imaging during cryoballoon ablation was developed. This methodology allows the quantification of where ice is forming and on what timescales it is entering other tissues. To the author's knowledge this is the first report of a cardiac cryoablation system being used in MR environment and that we are the first collaboration to accomplish such in the summer of 2012.

Methods:

For isolation of the swine specimens, a median sternotomy was performed and an aortic root cannula implanted for delivery of cardioplegia. The inferior vena cava (IVC) was ligated and just prior to cardioplegia delivery the IVC was removed with the liver and the superior vena cava (SVC) and aorta were cross-clamped. Cardioplegia was then delivered

²⁹ Department of Biomedical Engineering, University of Minnesota (Minneapolis, MN)

³⁰ Department of Surgery, University of Minnesota (Minneapolis, MN)

³¹ Medtronic Inc., Mounds View, MN

³² ⁴Center for Magnetic Resonance Research, University of Minnesota (Minneapolis, MN)

under pressure to cool and arrest the heart/lung blocs. The heart and one or both lungs were then dissected and the bloc then removed by transection of the major vessels, trachea, and esophagus. Human specimens may be utilized by acquisition using the same methods or dissection from fresh cadavers.

The IVC and the brachiocephalic artery off of the arch of the aorta was then cannulated. The descending aorta and SVC were tied off. The pulmonary artery was cannulated with Y connector that allows buffer to flow into the lung or bypass the lung. The distal left pulmonary vein was cannulated with a Y connector in which one end is connected to a hemostasis valve for catheter placement and the other connected to the pulmonary artery (i.e., to perfuse the left side while bypassing the lung if the lung were to become edematous).

The specimens were then imbedded in approximately 10-15 liters of ultrasound gel. Ultrasound gel was chosen because the thermal properties have been found to be highly similar to that of myocardium¹³⁶. This serves to act as a pseudo thoracic cavity and has benefits over liquid buffers (e.g., lungs will float in liquids and liquid in the MRI bore are undesirable). A ~20-30 mmHg static pressure head was applied and then the brachiocephalic, followed by the IVC, clamped shut to maintain static dilation of the chambers. The experiment was performed at room temperature.

Cryoballoon catheters (ArcticFront product line, Medtronic, Inc., Minneapolis, MN) were modified by removal of electronics and other ferrous materials from the catheter to make them suitable for use in the MRI suite. The patient safety systems on the Cryo Console were turned off to allow ablations to be performed. A ten meter refrigerant delivery umbilical was fabricated such that the Cryo Console could be outside of the MRI suite and fed through a pass through for connection to the catheter. A 2.4 mm endoscope (IPLEX TX series, Olympus Corp., Tokyo, Japan) was used to place a .030" carbon fiber rod as a guidewire or to place the ArcticFront catheter directly in the right pulmonary vein ostia.

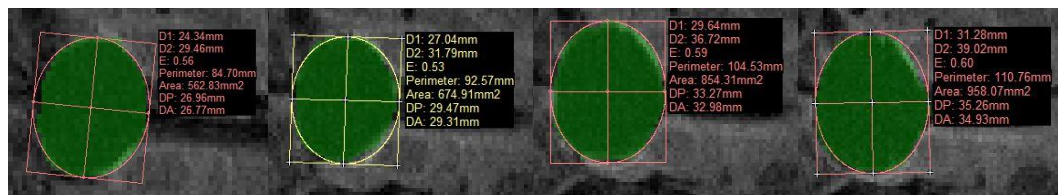
After dilation of the cardiac chambers and placement of the catheter, the first scan was started as the ablation began and the balloon inflated. A four minute ablation was performed and sequential scans were taken until the ablation was complete and for several minutes after. A gradient T2 weight scan with in plane resolution of 1 mm and 2

mm between slices was performed. The scan sequence was one minute long resulting in four scans during refrigerant injection.

Datasets were analyzed using Mimics (Materialise, Leuven Belgium) to derive anatomical measurements. To do so, each cardiac image set was imported using the native DICOM data files generated from the MRI scan and then converted into 3 dimensional renditions (i.e., each 2D DICOM image was layered together to create a 3D model). A baseline (i.e., no ice present) scan was performed immediately after balloon inflation. This is performed due to the fact that the ice and balloon both show up as black on the MRI scans due to the fact that the balloon is filled with gas, which has very little water content, and that once phase change in a material occurs there is also very little detectable MR signature.

Results:

Three ablations using the ArticFront 28mm catheter were performed and imaged. The balloon/ice were reconstructed and compared over time. The difference between the first and second ablation were negligible, but it appears that ablation three may have delayed beginning by approximately one minute (Figure 61). Ablation three also appears to have delayed fully inflating the balloon or had a lower degree of ice formation.



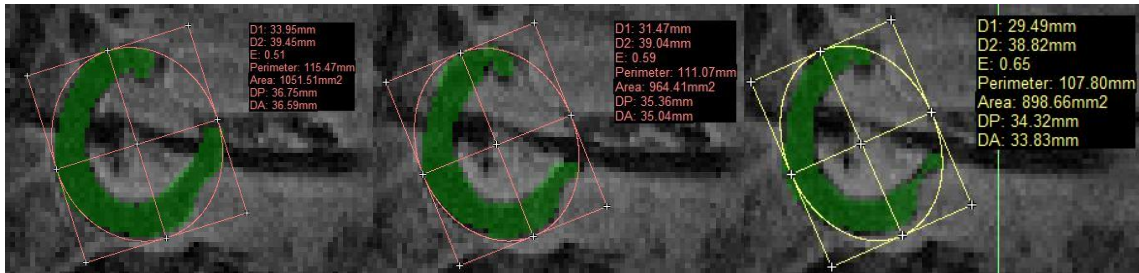


Figure 59: Time progression of ablation at MRI slice number 24. The top four images are during the active ablation period. The bottom three images are after the balloon has deflated and coolant injection has stopped. Measurements are displayed because the images are not the same magnification.

Upon reconstruction of the sequential scan sequences it is apparent when the ablation ends and the balloon deflates (see Figure 59 and Figure 60). This is also clearly seen in Figure 61 and Figure 62 as the volume peaks at the fourth scan for ablations one and two and then drops sharply. Ablation three does not behave the same as ablation one and two, and appears to be delayed in time.

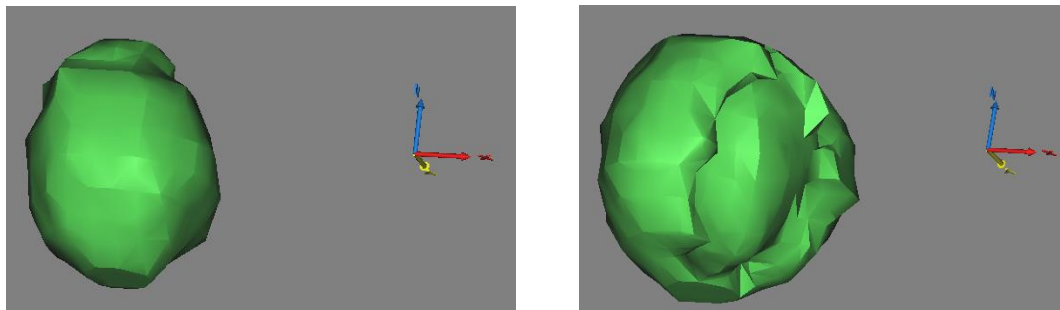


Figure 60: Three dimensional reconstruction of the first scan at the beginning of ablation and following deflation of the balloon. These reconstructions are from scan one and scan five from Figure 59.

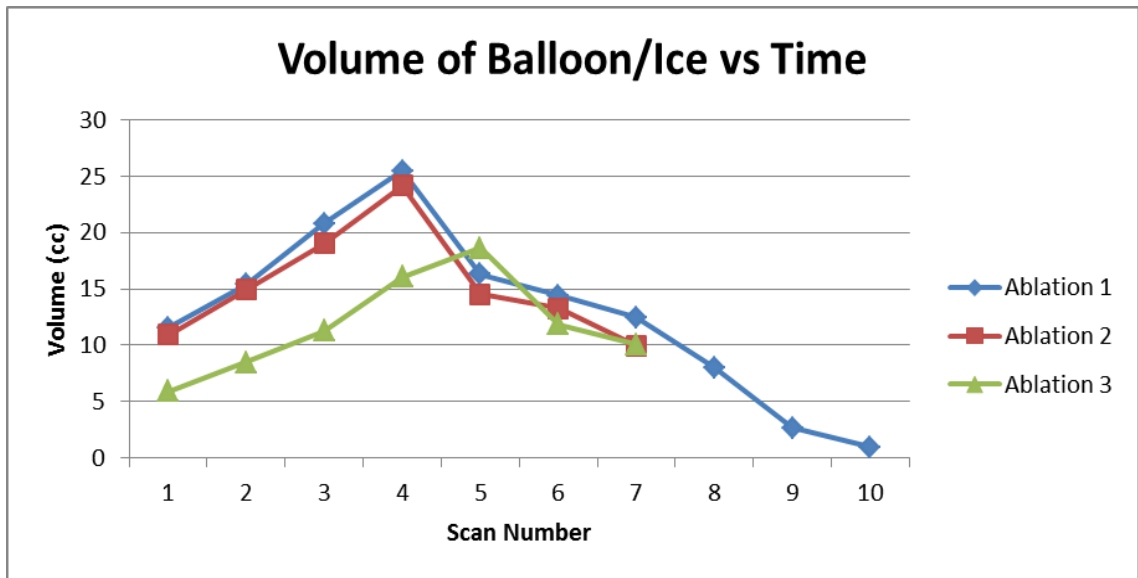


Figure 61: Volume of balloon and ice reconstruction over time. Ablation 3 was slightly delayed in time. Each scan is one minute.

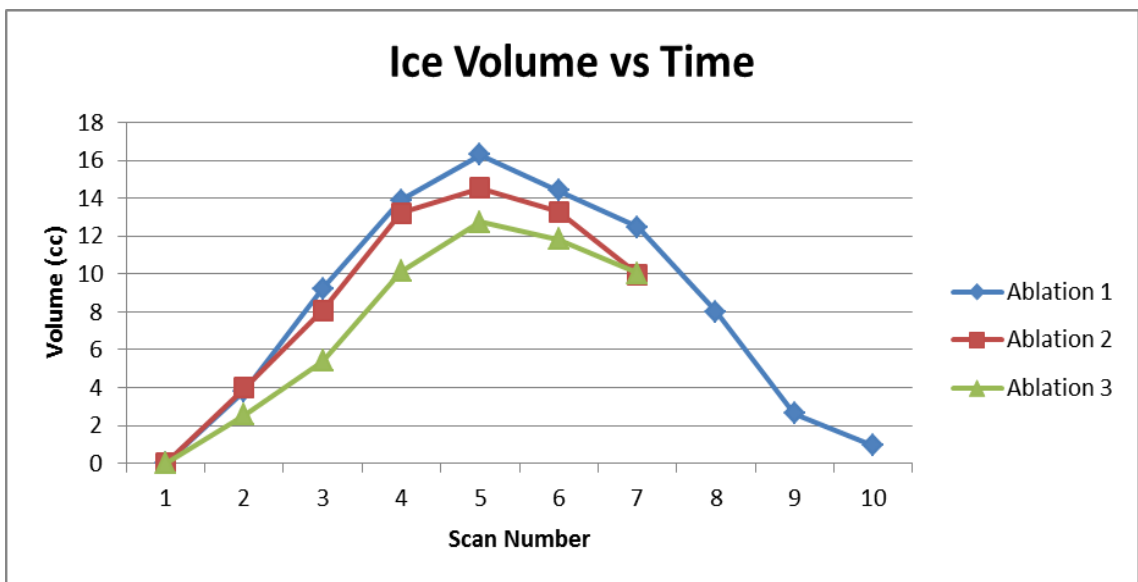


Figure 62: Volume of ice versus time. The balloon volume was subtracted from the balloon/ice reconstruction for the time points at which the balloon was inflated. Scan sequence time of 1 minute

The central slice of the balloon along the axis running from the distal tip to the shaft was located and an ellipse was fit to the ice/balloon area (see Figure 59). The major and minor axes were measured and the results are displayed as mean \pm standard deviation in Figure 63.

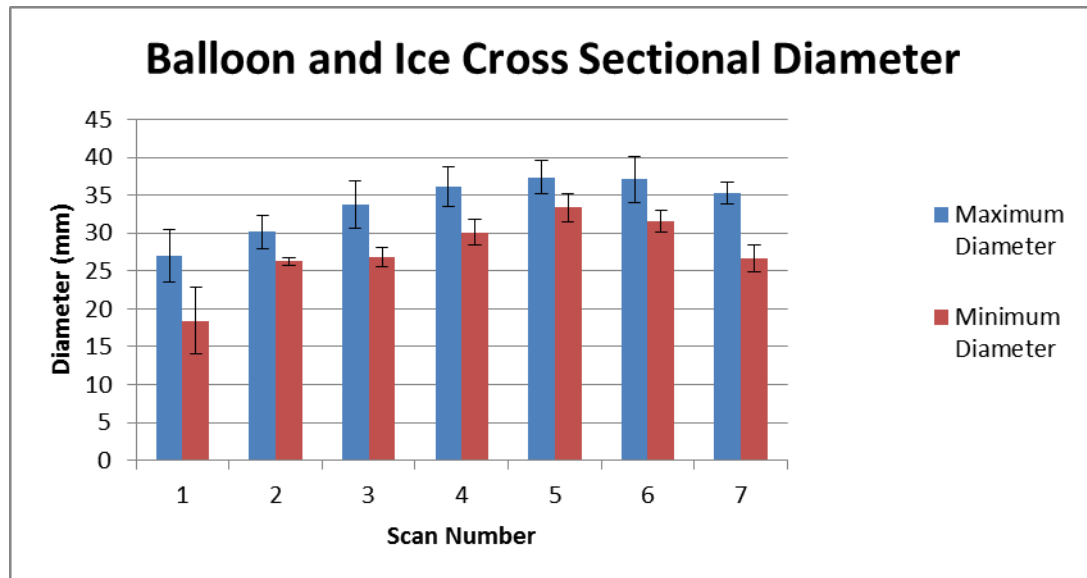


Figure 63: Results from fitted ellipse measurements from a cross section slice in center of balloon running from distal tip to the shaft. Examples of the measurements can be seen in Figure 59.

Discussion:

Presented here is the first cardiac cryoablation performed in an MR environment to author's knowledge. This technical feat has yielded novel insights to the temporal and spatial progression of ice dynamics caused by cryoballoon ablation. This opens up a new avenue of research regarding collateral injury, ice dynamics, and the device tissue interaction of balloon cryoablation.

As noted, ablation three did not behave the same as ablations one and two. The discrepancy in volume, from ablation three, apparent in Figure 61 may be due to refrigerant delivery line clogging. However, Figure 62 shows that the amount of ice formation between ablations was relatively the same. A clog would explain the delayed effect and smaller volume of ice formation overall. This may also explain that when peak volume occurred later if there was a clog in the refrigerant line, pressure in the line may have still been significant even though the ablation had ended on the console. This could lead to an extended cooling time beyond four minutes.

Interestingly, the differences in volumes between ablation one and two were minimal.

This is somewhat expected when one looks to the literature on changes in thermal properties pre- and post-freeze. For many tissues similar to myocardium (e.g., skeletal muscles) the properties change little pre- and post-freeze¹⁹⁵, but the lung properties may

change significantly¹⁹⁶. This is due to the fact that freezing of the lung is suspected to allow fluid into the alveolar spaces, thereby significantly changing the fluid density of the lung tissues. This seems to have had little effect between the first and second ablations. The novel method presented here is quite technically demanding, but can yield insights that are not possible using other methods. In the future, using modified scan sequences MR thermography may be performed using this methodology. The incorporation of constant flow is technically feasible as well. This is the ultimate method to help determine tissue tolerances of thermal treatments and for possible thermal model validations. The results to date are quite impressive and improvements to the methodology will be continued in our laboratory.

III.IV- Concluding Remarks

To summarize the results of this section of my thesis, by designing and employing several unique experimental approaches to quantify the device-tissue interactions I have:

- Aided in developing and characterizing a novel in vitro model incorporating reanimated human and swine heart-lung blocs. This approach and model system which allows for multimodal imaging within both the heart and lung may be used in the Visible Heart Laboratory for many years to come.
- Further elucidated the thermal and cellular effects of cryoballoon ablation procedures on function human and swine heart-lung blocs and quantified differences in catheter generations. Many of the multimodal images collected during these investigations have strong educational benefits for clinicians, design engineers and patients themselves.
- Developed a novel methodology for the three-dimensional imaging of ice dynamics employing MRI, thereby opening the door for complex future studies of parameters effecting cryoballoon ablation.

In summary, these three studies are novel, creative, and require a high degree of technical understanding. I believe that the studies I presented here pave the way for future experimentation, which can further expand the field of cardiac cryoablation.

Thesis Summary

A translational research approach was utilized for my thesis project, hence at first review of the contents it may seem that the works of this thesis are somewhat fragmented, but I believe upon further consideration one will determine that the experimental work was performed at multiple levels of complexity as required to obtain the desired knowledge and also which ultimately complemented each other. In organization of this work I chose to group it into three study categories: anatomy, thermal injury, and device-tissue interactions. Throughout these three categories there are the common, interwoven themes of the phrenic nerve, myocardium, lung, thermal imaging, and three dimensional data sets (i.e., MRI, CT).

The studies on anatomy relate to the investigations on thermal injury because anatomy is the basis of understanding of device-tissue interaction and is necessary for simulation. I believe that the three-dimensional computer models made of the phrenic nerve and coronary sinus associated anatomy can in the future be used for computer simulations/computational modeling. For example, simulations of an ablative procedure could incorporate the determined thermal injury thresholds of the lung, phrenic nerve, and myocardium, in a better attempt to predict and optimize: lesion size, collateral injury, and/or lesion transmuralty.

The investigations on device-tissue interaction brings together the work within the other two chapters and were performed to answer research questions on a more complex system approach. If a simulation were made as mentioned previously, it could be validated using the MRI ice imaging studies. Using the anatomy of those studies computer simulated cryoballoon ablations could be performed and the degree of ice formation compared between the model and the actual data for validation. The MRI ice study and the IR Visible Heart studies are also complementary to the aforementioned injury work. I believe that it was until this point unknown what temperatures the external surface of the heart reach (i.e., the surface contacting surround tissues) and to what extent ice travels outside of the heart. In order for collateral injury to occur ice must be traveling outside of the heart and as I have described here, this is now better understood and

quantified. The IR Visible Heart ablations may also be used to help validate a thermal model of the heart by confirming similar epicardial temperatures are reached by a model and the actual isolated heart situation.

To conclude, the works included in my thesis were highly collaborative and novel pursuits that were designed and executed to answer numerous basic and applied research questions surrounding cardiac cryoablation. These translational studies included herein have yielded several publications to date and more are in the submission process, thereby disseminating the findings to both the scientific and clinical communities. I believe that the knowledge attained through this work should aid in development and optimization of ablation technologies and the methods adapted to the study of modalities, if so desired. Additional studies using the methodologies developed within may also be used to better understand all facets of cryoablation (e.g., multiple freeze-thaw cycles, distinct anatomic variances, etc). Also, as mentioned previously, future work in this area may include the creation of thermal models of the procedures and would thus complement this thesis well because the data presented within may be vital for their validations.

References

1. Go AS, Hylek EM, Phillips KA, et al. Prevalence of diagnosed atrial fibrillation in adults. *JAMA J Am Med Assoc.* 2001;285(18):2370.
2. Feinberg W, Blackshear J, Laupacis A, Kronmal R, Hart R. Prevalence, Age Distribution, and Gender of Patients With Atrial Fibrillation. *Arch Intern Med.* 1995;155:469–473.
3. Wijffels M, Kirchhof C, Dorland R, Allessie M. Atrial fibrillation begets atrial fibrillation. A study in awake chronically instrumented goats. *Circulation.* 1995;92(7):1954–68.
4. Rostock T, Steven D, Lutomsky B, et al. Atrial Fibrillation Begets Atrial Fibrillation in the Pulmonary Veins:: On the Impact of Atrial Fibrillation on the Electrophysiological Properties of the Pulmonary Veins in Humans. *J Am Coll Cardiol.* 2008;51(22):2153–2160.
5. ACC/AHA/ESC 2006 Guidelines for the Management of Patients With Atrial Fibrillation: A Report of the American College of Cardiology/American Heart Association Task Force on Practice Guidelines and the European Society of Cardiology Committee for Practice Guidelines (Writing Committee to Revise the 2001 Guidelines for the Management of Patients With Atrial Fibrillation): Developed in Collaboration With the European Heart Rhythm Association and the Heart Rhythm Society. *Circulation.* 2006;114(7):e257–e354. doi:10.1161/CIRCULATIONAHA.106.177292.
6. Bonanno C, Paccanaro M, La Vecchia L, Ometto R, Fontanelli A. Efficacy and safety of catheter ablation versus antiarrhythmic drugs for atrial fibrillation; a meta-analysis of randomized trials. *J Cardiovasc Med.* 2010;11(6):408–18.
7. Haissaguerre M, Clementy J. SPONTANEOUS INITIATION OF ATRIAL FIBRILLATION BY ECTOPIC BEATS ORIGINATING IN THE PULMONARY VEINS. *N Engl J Med.* 1998;339(10):659–666.
8. Katritsis D, Giazitzoglou E, Zografos T, Pokushalov E, Po S, Camm J. Rapid pulmonary vein isolation combined with autonomic ganglia modification: A randomized study. *Heart Rhythm.* 2011;8(5):672–678.
9. Aliot EM, Stevenson WG, Almendral-Garrote JM, et al. EHRA/HRS expert consensus on catheter ablation of ventricular arrhythmias. *Europace.* 2009;11(6):771.
10. Coad JE, Kosari K, Humar A, Sielaff TD. Radiofrequency ablation causes “thermal fixation” of hepatocellular carcinoma: a post-liver transplant histopathologic study. *Clin Transplant.* 2003;17(4):377–384.
11. Khairy P, Chauvet P, Lehmann J, et al. Lower incidence of thrombus formation with cryoenergy versus radiofrequency catheter ablation. *Circulation.* 2003;107(15):2045.
12. Matsumoto N, Miyake F. Experimental Study on the Effectiveness and Safety of Radiofrequency Catheter Ablation With the Cooled Ablation System. *Circ J.* 2003;67:154–158.
13. Taylor GW, Kay GN, Zheng X, Bishop S, Ideker RE. Pathological effects of extensive radiofrequency energy applications in the pulmonary veins in dogs. *Circulation.* 2000;101(14):1736.
14. Zrenner B, Dong J, Schreieck J, et al. Transvenous cryoablation versus radiofrequency ablation of the slow pathway for the treatment of atrioventricular nodal

- re-entrant tachycardia: a prospective randomized pilot study. *Eur Heart J*. 2004;25(24):2226.
15. Avitall B, Urboniene D, Rozmus G, Lafontaine D, Helms R, Urbonas A. New Cryotechnology for Electrical Isolation of the Pulmonary Veins. *J Cardiovasc Electrophysiol*. 2003;14:281–286.
 16. Kuck K-H, Füllkrantz A. Cryoballoon Ablation of Atrial Fibrillation. *J Cardiovasc Electrophysiol*. 2010;21(12):1427–1431. doi:10.1111/j.1540-8167.2010.01944.x.
 17. Packer DL, Kowal RC, Wheelan KR, et al. Cryoballoon Ablation of Pulmonary Veins for Paroxysmal Atrial Fibrillation: First Results of the North American Arctic Front (STOP AF) Pivotal Trial. *J Am Coll Cardiol*. 2013. doi:10.1016/j.jacc.2012.11.064.
 18. Sanchez-Quintana D, Cabrera JA, Climent V, Farre J, Weiglein A, Ho SY. How Close Are the Phrenic Nerves to Cardiac Structures? Implications for Cardiac Interventionalists. *J Cardiovasc Electrophysiol*. 2005;16(3):309–313. doi:10.1046/j.1540-8167.2005.40759.x.
 19. Lemola K. Computed Tomographic Analysis of the Anatomy of the Left Atrium and the Esophagus: Implications for Left Atrial Catheter Ablation. *Circulation*. 2004;110(24):3655–3660. doi:10.1161/01.CIR.0000149714.31471.FD.
 20. Cummings JE. Assessment of Temperature, Proximity, and Course of the Esophagus During Radiofrequency Ablation Within the Left Atrium. *Circulation*. 2005;112(4):459–464. doi:10.1161/CIRCULATIONAHA.104.509612.
 21. Ripley KL, Gage AA, Olsen DB, Van Vleet JF, Lau C-P, Tse H-F. Time Course of Esophageal Lesions After Catheter Ablation with Cryothermal and Radiofrequency Ablation: Implication for Atrio-Esophageal Fistula Formation After Catheter Ablation for Atrial Fibrillation. *J Cardiovasc Electrophysiol*. 2007;18(6):642–646. doi:10.1111/j.1540-8167.2007.00790.x.
 22. Gage AA, Baust JM, Baust JG. Experimental cryosurgery investigations in vivo. *Cryobiology*. 2009;59(3):229–243.
 23. Bischof JC, Smith D, Pazhayannur PV, Manivel C, Hulbert J, Roberts KP. Cryosurgery of Dunning AT-1 Rat Prostate Tumor: Thermal, Biophysical, and Viability Response at the Cellular and Tissue Level. *Cryobiology*. 1997;34:42–69.
 24. Mazur P. Freezing of living cells: mechanisms and implications. *Am J Physiol-Cell Physiol*. 1984;247(3):C125.
 25. Singh SM, d'Avila A, Doshi SK, et al. Esophageal Injury and Temperature Monitoring During Atrial Fibrillation Ablation. *Circ Arrhythm Electrophysiol*. 2008;1(3):162–168. doi:10.1161/CIRCEP.107.789552.
 26. Nakagawa H, Seres KA, Jackman WM. Limitations of Esophageal Temperature-Monitoring to Prevent Esophageal Injury During Atrial Fibrillation Ablation. *Circ Arrhythm Electrophysiol*. 2008;1(3):150–152. doi:10.1161/CIRCEP.108.805366.
 27. Cummings JE, Barrett CD, Litwak KN, et al. Esophageal Luminal Temperature Measurement Underestimates Esophageal Tissue Temperature During Radiofrequency Ablation Within the Canine Left Atrium: Comparison Between 8 mm Tip and Open Irrigation Catheters. *J Cardiovasc Electrophysiol*. 2008;19(6):641–644. doi:10.1111/j.1540-8167.2008.01130.x.
 28. Deneke T, BüNZ K, Bastian A, et al. Utility of Esophageal Temperature Monitoring During Pulmonary Vein Isolation for Atrial Fibrillation Using Duty-Cycled

- Phased Radiofrequency Ablation. *J Cardiovasc Electrophysiol*. 2011;22(3):255–261. doi:10.1111/j.1540-8167.2010.01916.x.
29. McDannold NJ, King RL, Jolesz FA, Hynynen KH. Usefulness of MR Imaging-Derived Thermometry and Dosimetry in Determining the Threshold for Tissue Damage Induced by Thermal Surgery in Rabbits1. *Radiology*. 2000;216(2):517.
 30. Cernicanu A, Lepetit-Coiffe M, Roland J, Becker CD, Terraz S. Validation of fast MR thermometry at 1.5 T with gradient-echo echo planar imaging sequences: phantom and clinical feasibility studies. *NMR Biomed*. 2008;21(8):849–858. doi:10.1002/nbm.1267.
 31. Ballard JR, Casper AJ, Ebbini ES. Monitoring and Guidance of HIFU Beams with Dual-Mode Ultrasound Arrays. In: ; 2009:137–140.
 32. Will K, Krug J, Jungnickel K, et al. MR-compatible RF ablation system for online treatment monitoring using MR thermometry. In: ; 2010:1601–1604.
 33. Gray H. *Anatomy of the Human Body*. 20th ed. Philadelphia: Lea & Febiger; 1918.
 34. Neumann T, Vogt J, Schumacher B, et al. Circumferential pulmonary vein isolation with the cryoballoon technique results from a prospective 3-center study. *J Am Coll Cardiol*. 2008;52(4):273–278. doi:10.1016/j.jacc.2008.04.021.
 35. Andrade JG, Khairy P, Guerra PG, et al. Efficacy and safety of cryoballoon ablation for atrial fibrillation: a systematic review of published studies. *Heart Rhythm Off J Heart Rhythm Soc*. 2011;8(9):1444–1451. doi:10.1016/j.hrthm.2011.03.050.
 36. Andrié RP, Schrickel JW, Nickenig G, Lickfett L. Left Phrenic Nerve Injury during Cryoballoon Ablation of the Left Superior Pulmonary Vein. *Pacing Clin Electrophysiol PACE*. 2012. doi:10.1111/j.1540-8159.2012.03470.x.
 37. Ahsan SY, Flett AS, Lambiase PD, Segal OR. First report of phrenic nerve injury during pulmonary vein isolation using the Ablation Frontiers pulmonary vein ablation catheter. *J Interv Card Electrophysiol Int J Arrhythm Pacing*. 2010;29(3):187–190. doi:10.1007/s10840-010-9517-1.
 38. Kühne M, Knecht S, Altmann D, et al. Phrenic nerve palsy during ablation of atrial fibrillation using a 28-mm cryoballoon catheter: predictors and prevention. *J Interv Card Electrophysiol Int J Arrhythm Pacing*. 2013;36(1):47–54; discussion 54. doi:10.1007/s10840-012-9740-z.
 39. Rao JY, Chierchia G-B, de Asmundis C, et al. Cryoballoon ablation as index procedure for paroxysmal atrial fibrillation: long-term results from a single center early experience. *J Cardiovasc Med Hagerstown Md*. 2013. doi:10.2459/JCM.0b013e3283623838.
 40. Hermida J-S, Traullé S, Kubala M. Left phrenic nerve injury after cryoballoon ablation of the pulmonary veins. *Eur Eur Pacing Arrhythm Card Electrophysiol J Work Groups Card Pacing Arrhythm Card Cell Electrophysiol Eur Soc Cardiol*. 2012. doi:10.1093/europace/eus296.
 41. Vogt J, Heintze J, Gutleben KJ, Muntean B, Horstkotte D, Nölker G. Long-Term Outcomes After Cryoballoon Pulmonary Vein Isolation: Results From a Prospective Study in 605 Patients. *J Am Coll Cardiol*. 2012. doi:10.1016/j.jacc.2012.09.033.
 42. Martins RP, Hamon D, Césari O, et al. Safety and efficacy of a second-generation cryoballoon in the ablation of paroxysmal atrial fibrillation. *Heart Rhythm Off J Heart Rhythm Soc*. 2014. doi:10.1016/j.hrthm.2014.01.002.

43. Chun KRJ, Fürnkranz A, Köster I, et al. Two versus one repeat freeze-thaw cycle(s) after cryoballoon pulmonary vein isolation: the alster extra pilot study. *J Cardiovasc Electrophysiol*. 2012;23(8):814–819. doi:10.1111/j.1540-8167.2012.02315.x.
44. Guiot A, Savouré A, Godin B, Anselme F. Collateral Nervous Damages After Cryoballoon Pulmonary Vein Isolation. *J Cardiovasc Electrophysiol*. 2011. doi:10.1111/j.1540-8167.2011.02219.x.
45. Klein G, Oswald H, Gardiwal A, et al. Efficacy of pulmonary vein isolation by cryoballoon ablation in patients with paroxysmal atrial fibrillation. *Heart Rhythm Off J Heart Rhythm Soc*. 2008;5(6):802–806. doi:10.1016/j.hrthm.2008.02.014.
46. Matsumoto Y, Krishnan S, Fowler SJ, et al. Detection of phrenic nerves and their relation to cardiac anatomy using 64-slice multidetector computed tomography. *Am J Cardiol*. 2007;100(1):133–137.
47. Horton R, Di Biase L, Reddy V, et al. Locating the right phrenic nerve by imaging the right pericardiophrenic artery with computerized tomographic angiography: Implications for balloon-based procedures. *Heart Rhythm*. 2010;7(7):937–941. doi:10.1016/j.hrthm.2010.03.027.
48. Okumura Y, Henz BD, Bunch TJ, Dalegrave C, Johnson SB, Packer DL. Distortion of Right Superior Pulmonary Vein Anatomy by Balloon Catheters as a Contributor to Phrenic Nerve Injury. *J Cardiovasc Electrophysiol*. 2009;20(10):1151–1157. doi:10.1111/j.1540-8167.2009.01495.x.
49. Van Belle Y, Janse P, Rivero-Ayerza MJ, et al. Pulmonary vein isolation using an occluding cryoballoon for circumferential ablation: feasibility, complications, and short-term outcome. *Eur Heart J*. 2007;28(18):2231–2237. doi:10.1093/eurheartj/ehm227.
50. Anderson SE, Hill AJ, Iaizzo PA. Microanatomy of human left ventricular coronary veins. *Anat Rec Hoboken NJ* 2007. 2009;292(1):23–28. doi:10.1002/ar.20766.
51. Anderson SE, Quill JL, Iaizzo PA. Venous valves within left ventricular coronary veins. *J Interv Card Electrophysiol Int J Arrhythm Pacing*. 2008;23(2):95–99. doi:10.1007/s10840-008-9282-6.
52. Eggen M, Bateman M, Iaizzo PA. Methods to Prepare Perfusion Fixed Cardiac Specimens for Multimodal Imaging: The Use of Formalin and Agar Gels. *J Med Devices*. 2011;5(2):027539–027539. doi:10.1115/1.3591396.
53. Noheria A, Desimone CV, Lachman N, et al. Anatomy of the Coronary Sinus and Epicardial Coronary Venous System in 620 Hearts: An Electrophysiology Perspective. *J Cardiovasc Electrophysiol*. 2012. doi:10.1111/j.1540-8167.2012.02443.x.
54. Wittkampf FHM, van Oosterhout MF, Loh P, et al. Where to draw the mitral isthmus line in catheter ablation of atrial fibrillation: histological analysis. *Eur Heart J*. 2005;26(7):689–695. doi:10.1093/eurheartj/ehi095.
55. Berrueto A, Bisbal F, Fernández-Armenta J, et al. Transthoracic epicardial ablation of mitral isthmus for treatment of recurrent perimitral flutter. *Heart Rhythm Off J Heart Rhythm Soc*. 2014;11(1):26–33. doi:10.1016/j.hrthm.2013.10.030.
56. Calvo N, Nadal M, Berrueto A, et al. Improved outcomes and complications of atrial fibrillation catheter ablation over time: learning curve, techniques, and methodology. *Rev Esp Cardiol Engl Ed*. 2012;65(2):131–138. doi:10.1016/j.recesp.2011.08.015.

57. Jaïs P, Hocini M, Hsu L-F, et al. Technique and results of linear ablation at the mitral isthmus. *Circulation*. 2004;110(19):2996–3002. doi:10.1161/01.CIR.0000146917.75041.58.
58. Yokokawa M, Sundaram B, Garg A, et al. Impact of mitral isthmus anatomy on the likelihood of achieving linear block in patients undergoing catheter ablation of persistent atrial fibrillation. *Heart Rhythm Off J Heart Rhythm Soc*. 2011;8(9):1404–1410. doi:10.1016/j.hrthm.2011.04.030.
59. Wong KCK, Jones M, Sadarmin PP, et al. Larger coronary sinus diameter predicts the need for epicardial delivery during mitral isthmus ablation. *Eur Eur Pacing Arrhythm Card Electrophysiol J Work Groups Card Pacing Arrhythm Card Cell Electrophysiol Eur Soc Cardiol*. 2011;13(4):555–561. doi:10.1093/europace/eur019.
60. Chae S, Oral H, Good E, et al. Atrial tachycardia after circumferential pulmonary vein ablation of atrial fibrillation: mechanistic insights, results of catheter ablation, and risk factors for recurrence. *J Am Coll Cardiol*. 2007;50(18):1781–1787. doi:10.1016/j.jacc.2007.07.044.
61. Wong KC, Betts TR. A review of mitral isthmus ablation. *Indian Pacing Electrophysiol J*. 2012;12(4):152–170.
62. Matsuo S, Wright M, Knecht S, et al. Peri-mitral atrial flutter in patients with atrial fibrillation ablation. *Heart Rhythm Off J Heart Rhythm Soc*. 2010;7(1):2–8. doi:10.1016/j.hrthm.2009.09.067.
63. Deisenhofer I, Estner H, Zrenner B, et al. Left atrial tachycardia after circumferential pulmonary vein ablation for atrial fibrillation: incidence, electrophysiological characteristics, and results of radiofrequency ablation. *Eur Eur Pacing Arrhythm Card Electrophysiol J Work Groups Card Pacing Arrhythm Card Cell Electrophysiol Eur Soc Cardiol*. 2006;8(8):573–582. doi:10.1093/europace/eul077.
64. Schmidt B, Ernst S, Ouyang F, et al. External and endoluminal analysis of left atrial anatomy and the pulmonary veins in three-dimensional reconstructions of magnetic resonance angiography: the full insight from inside. *J Cardiovasc Electrophysiol*. 2006;17(9):957–964. doi:10.1111/j.1540-8167.2006.00548.x.
65. Takatsuki S, Extramiana F, Hayashi M, et al. High take-off left inferior pulmonary vein as an obstacle in creating a conduction block at the lateral mitral isthmus. *Eur Eur Pacing Arrhythm Card Electrophysiol J Work Groups Card Pacing Arrhythm Card Cell Electrophysiol Eur Soc Cardiol*. 2009;11(7):910–916. doi:10.1093/europace/eup151.
66. Wongcharoen W, Tsao H-M, Wu M-H, et al. Morphologic characteristics of the left atrial appendage, roof, and septum: implications for the ablation of atrial fibrillation. *J Cardiovasc Electrophysiol*. 2006;17(9):951–956. doi:10.1111/j.1540-8167.2006.00549.x.
67. Hocini M, Shah AJ, Nault I, et al. Mitral isthmus ablation with and without temporary spot occlusion of the coronary sinus: a randomized clinical comparison of acute outcomes. *J Cardiovasc Electrophysiol*. 2012;23(5):489–496. doi:10.1111/j.1540-8167.2011.02248.x.
68. Wong KCK, Jones M, Qureshi N, et al. Balloon occlusion of the distal coronary sinus facilitates mitral isthmus ablation. *Heart Rhythm Off J Heart Rhythm Soc*. 2011;8(6):833–839. doi:10.1016/j.hrthm.2011.01.042.

69. Chiang S-J, Tsao H-M, Wu M-H, et al. Anatomic characteristics of the left atrial isthmus in patients with atrial fibrillation: lessons from computed tomographic images. *J Cardiovasc Electrophysiol*. 2006;17(12):1274–1278. doi:10.1111/j.1540-8167.2006.00645.x.
70. Hall B, Jeevanantham V, Simon R, Filippone J, Vorobiof G, Daubert J. Variation in left atrial transmural wall thickness at sites commonly targeted for ablation of atrial fibrillation. *J Interv Card Electrophysiol Int J Arrhythm Pacing*. 2006;17(2):127–132. doi:10.1007/s10840-006-9052-2.
71. Wong KCK, Qureshi N, Jones M, Rajappan K, Bashir Y, Betts TR. Mitral isthmus ablation using steerable sheath and high ablation power: a single center experience. *J Cardiovasc Electrophysiol*. 2012;23(11):1193–1200. doi:10.1111/j.1540-8167.2012.02380.x.
72. Becker AE. Left atrial isthmus: anatomic aspects relevant for linear catheter ablation procedures in humans. *J Cardiovasc Electrophysiol*. 2004;15(7):809–812. doi:10.1046/j.1540-8167.2004.03651.x.
73. Hamer ME, Blumenthal JA, McCarthy EA, Phillips BG, Pritchett EL. Quality-of-life assessment in patients with paroxysmal atrial fibrillation or paroxysmal supraventricular tachycardia. *Am J Cardiol*. 1994;74(8):826–829.
74. Perret-Guillaume C, Briancon S, Wahl D, Guillemin F, Empereur F. Quality of Life in elderly inpatients with atrial fibrillation as compared with controlled subjects. *J Nutr Health Aging*. 2010;14(2):161–166.
75. Dąbrowski R, Smolis-Bąk E, Kowalik I, Kazimierska B, Wójcicka M, Szwed H. Quality of life and depression in patients with different patterns of atrial fibrillation. *Kardiologia Pol*. 2010;68(10):1133–1139.
76. Park H, Hildreth A, Thomson R, O’Connell J. Non-valvular atrial fibrillation and cognitive decline: a longitudinal cohort study. *Age Ageing*. 2007;36(2):157.
77. Puccio D, Novo G, Baiamonte V, et al. Atrial fibrillation and mild cognitive impairment: what correlation? *Minerva Cardioangiol*. 2009;57(2):143–150.
78. Jozwiak A, Guzik P, Mathew A, Wykretowicz A, Wysocki H. Association of atrial fibrillation and focal neurologic deficits with impaired cognitive function in hospitalized patients ≥ 65 years of age. *Am J Cardiol*. 2006;98(9):1238–1241. doi:10.1016/j.amjcard.2006.05.058.
79. Rastas S, Verkkoniemi A, Polvikoski T, et al. Atrial fibrillation, stroke, and cognition: a longitudinal population-based study of people aged 85 and older. *Stroke J Cereb Circ*. 2007;38(5):1454–1460. doi:10.1161/STROKEAHA.106.477299.
80. Kato R, Lickfett L, Meininger G, et al. Pulmonary vein anatomy in patients undergoing catheter ablation of atrial fibrillation: lessons learned by use of magnetic resonance imaging. *Circulation*. 2003;107(15):2004–2010. doi:10.1161/01.CIR.0000061951.81767.4E.
81. Reant P, Lafitte S, Jaïs P, et al. Reverse remodeling of the left cardiac chambers after catheter ablation after 1 year in a series of patients with isolated atrial fibrillation. *Circulation*. 2005;112(19):2896–2903. doi:10.1161/CIRCULATIONAHA.104.523928.
82. Beukema WP, Elvan A, Sie HT, Misier ARR, Wellens HJJ. Successful radiofrequency ablation in patients with previous atrial fibrillation results in a significant decrease in left atrial size. *Circulation*. 2005;112(14):2089–2095. doi:10.1161/CIRCULATIONAHA.104.484766.

83. Leung DY, Chi C, Allman C, et al. Prognostic implications of left atrial volume index in patients in sinus rhythm. *Am J Cardiol.* 2010;105(11):1635–1639. doi:10.1016/j.amjcard.2010.01.027.
84. Abecasis J, Dourado R, Ferreira A, et al. Left atrial volume calculated by multi-detector computed tomography may predict successful pulmonary vein isolation in catheter ablation of atrial fibrillation. *Europace.* 2009;11(10):1289.
85. Sunderland N, Maruthappu M, Nagendran M. What size of left atrium significantly impairs the success of maze surgery for atrial fibrillation? *Interact Cardiovasc Thorac Surg.* 2011;13(3):332–338. doi:10.1510/icvts.2011.271999.
86. Marchese P, Bursi F, Delle Donne G, et al. Indexed left atrial volume predicts the recurrence of non-valvular atrial fibrillation after successful cardioversion. *Eur J Echocardiogr J Work Group Echocardiogr Eur Soc Cardiol.* 2011;12(3):214–221. doi:10.1093/ejechocard/jeq176.
87. Lee Y-S, Hyun DW, Jung BC, et al. Left atrial volume index as a predictor for occurrence of atrial fibrillation after ablation of typical atrial flutter. *J Cardiol.* 2010;56(3):348–353. doi:10.1016/j.jjcc.2010.07.006.
88. Ayirala S, Kumar S, O’Sullivan DM, Silverman DI. Echocardiographic predictors of left atrial appendage thrombus formation. *J Am Soc Echocardiogr Off Publ Am Soc Echocardiogr.* 2011;24(5):499–505. doi:10.1016/j.echo.2011.02.010.
89. Beinart R, Heist EK, Newell JB, Holmvang G, Ruskin JN, Mansour M. Left Atrial Appendage Dimensions Predict the Risk of Stroke/TIA in Patients With Atrial Fibrillation. *J Cardiovasc Electrophysiol.* 2011;22(1):10–15. doi:10.1111/j.1540-8167.2010.01854.x.
90. Wittkamp FHM, Vonken E-J, Derksen R, et al. Pulmonary vein ostium geometry: analysis by magnetic resonance angiography. *Circulation.* 2003;107(1):21–23.
91. Beinart R, Abbara S, Blum A, et al. Left atrial wall thickness variability measured by CT scans in patients undergoing pulmonary vein isolation. *J Cardiovasc Electrophysiol.* 2011;22(11):1232–1236. doi:10.1111/j.1540-8167.2011.02100.x.
92. Nikitin NP, Witte KKA, Thackray SDR, Goodge LJ, Clark AL, Cleland JGF. Effect of age and sex on left atrial morphology and function. *Eur J Echocardiogr J Work Group Echocardiogr Eur Soc Cardiol.* 2003;4(1):36–42.
93. Thomas L, Levett K, Boyd A, Leung DYC, Schiller NB, Ross DL. Compensatory changes in atrial volumes with normal aging: is atrial enlargement inevitable? *J Am Coll Cardiol.* 2002;40(9):1630–1635.
94. Quill JL, Laske TG, Hill AJ, Bonhoeffer P, Iaizzo PA. Images in cardiovascular medicine. Direct visualization of a transcatheter pulmonary valve implantation within the visible heart: a glimpse into the future. *Circulation.* 2007;116(22):e548. doi:10.1161/CIRCULATIONAHA.107.728667.
95. Hill AJ, Laske TG, Coles JA Jr, et al. In vitro studies of human hearts. *Ann Thorac Surg.* 2005;79(1):168–177. doi:10.1016/j.athoracsur.2004.06.080.
96. Chinchoy E, Soule CL, Houlton AJ, et al. Isolated four-chamber working swine heart model. *Ann Thorac Surg.* 2000;70(5):1607–1614.
97. Marino P. *The ICU Book.* 3rd ed. Philadelphia: Lippincott Williams & Wilkins; 2007.

98. Swan HJ, Ganz W, Forrester J, Marcus H, Diamond G, Chonette D. Catheterization of the heart in man with use of a flow-directed balloon-tipped catheter. *N Engl J Med*. 1970;283(9):447–451. doi:10.1056/NEJM197008272830902.
99. Chatterjee K. The Swan-Ganz catheters: past, present, and future. A viewpoint. *Circulation*. 2009;119(1):147–152. doi:10.1161/CIRCULATIONAHA.108.811141.
100. Sandham JD, Hull RD, Brant RF, et al. A randomized, controlled trial of the use of pulmonary-artery catheters in high-risk surgical patients. *N Engl J Med*. 2003;348(1):5–14. doi:10.1056/NEJMoa021108.
101. Harvey S, Harrison DA, Singer M, et al. Assessment of the clinical effectiveness of pulmonary artery catheters in management of patients in intensive care (PAC-Man): a randomised controlled trial. *Lancet*. 2005;366(9484):472–477. doi:10.1016/S0140-6736(05)67061-4.
102. Shah MR, Hasselblad V, Stevenson LW, et al. Impact of the pulmonary artery catheter in critically ill patients: meta-analysis of randomized clinical trials. *JAMA J Am Med Assoc*. 2005;294(13):1664–1670. doi:10.1001/jama.294.13.1664.
103. National Heart, Lung, and Blood Institute Acute Respiratory Distress Syndrome (ARDS) Clinical Trials Network, Wheeler AP, Bernard GR, et al. Pulmonary-artery versus central venous catheter to guide treatment of acute lung injury. *N Engl J Med*. 2006;354(21):2213–2224. doi:10.1056/NEJMoa061895.
104. Dalen JE, Bone RC. Is it time to pull the pulmonary artery catheter? *JAMA J Am Med Assoc*. 1996;276(11):916–918.
105. Ramsay J. Pro: Is the pulmonary artery catheter dead? *J Cardiothorac Vasc Anesth*. 2007;21(1):144–146. doi:10.1053/j.jvca.2006.12.001.
106. Murphy GS, Vender JS. Con: Is the pulmonary artery catheter dead? *J Cardiothorac Vasc Anesth*. 2007;21(1):147–149. doi:10.1053/j.jvca.2006.11.001.
107. Gwak MS, Kim JA, Kim GS, et al. Incidence of severe ventricular arrhythmias during pulmonary artery catheterization in liver allograft recipients. *Liver Transplant Off Publ Am Assoc Study Liver Dis Int Liver Transplant Soc*. 2007;13(10):1451–1454. doi:10.1002/lt.21300.
108. Thomson IR, Dalton BC, Lappas DG, Lowenstein E. Right bundle-branch block and complete heart block caused by the Swan-Ganz catheter. *Anesthesiology*. 1979;51(4):359–362.
109. Karanikas ID, Polychronidis A, Vrachatis A, Arvanitis DP, Simopoulos CE, Lazarides MK. Removal of knotted intravascular devices. Case report and review of the literature. *Eur J Vasc Endovasc Surg Off J Eur Soc Vasc Surg*. 2002;23(3):189–194. doi:10.1053/ejvs.2001.1591.
110. O’Quin R, Marini JJ. Pulmonary artery occlusion pressure: clinical physiology, measurement, and interpretation. *Am Rev Respir Dis*. 1983;128(2):319–326.
111. Ganter CC, Ganter CG, Jakob SM, Takala J. Pulmonary capillary pressure. A review. *Minerva Anesthesiol*. 2006;72(1-2):21–36.
112. Abreu AR, Campos MA, Krieger BP. Pulmonary artery rupture induced by a pulmonary artery catheter: a case report and review of the literature. *J Intensive Care Med*. 2004;19(5):291–296. doi:10.1177/0885066604265255.
113. Foote GA, Schabel SI, Hodges M. Pulmonary complications of the flow-directed balloon-tipped catheter. *N Engl J Med*. 1974;290(17):927–931. doi:10.1056/NEJM197404252901702.

114. Bossert T, Gummert JF, Bittner HB, et al. Swan-Ganz catheter-induced severe complications in cardiac surgery: right ventricular perforation, knotting, and rupture of a pulmonary artery. *J Card Surg*. 2006;21(3):292–295. doi:10.1111/j.1540-8191.2006.00235.x.
115. Bateman MG, Iaizzo PA. Comparative imaging of cardiac structures and function for the optimization of transcatheter approaches for valvular and structural heart disease. *Int J Cardiovasc Imaging*. 2011;27(8):1223–1234. doi:10.1007/s10554-011-9807-4.
116. Sarabanda AV, Bunch TJ, Johnson SB, et al. Efficacy and safety of circumferential pulmonary vein isolation using a novel cryothermal balloon ablation system. *J Am Coll Cardiol*. 2005;46(10):1902–1912. doi:10.1016/j.jacc.2005.07.046.
117. Smith JJ, Fraser J. An estimation of tissue damage and thermal history in the cryolesion. *Cryobiology*. 1974;11(2):139–147.
118. Van Belle Y, Janse P, Theuns D, Szili-Torok T, Jordaens L. One year follow-up after cryoballoon isolation of the pulmonary veins in patients with paroxysmal atrial fibrillation. *Eur Eur Pacing Arrhythm Card Electrophysiol J Work Groups Card Pacing Arrhythm Card Cell Electrophysiol Eur Soc Cardiol*. 2008;10(11):1271–1276. doi:10.1093/europace/eun218.
119. Chun KJ, Bordignon S, Gunawardene M, et al. Single Transseptal Big Cryoballoon Pulmonary Vein Isolation using an Inner Lumen Mapping Catheter. *Pacing Clin Electrophysiol PACE*. 2012. doi:10.1111/j.1540-8159.2012.03475.x.
120. Drago F, Silveti MS, Santis A, Grutter G, Andrew P. Lengthier cryoablation and a bonus cryoapplication is associated with improved efficacy for cryothermal catheter ablation of supraventricular tachycardias in children. *J Interv Card Electrophysiol*. 2006;16(3):191–198. doi:10.1007/s10840-006-9028-2.
121. Haines DE. The biophysics of radiofrequency catheter ablation in the heart: the importance of temperature monitoring. *Pacing Clin Electrophysiol PACE*. 1993;16(3 Pt 2):586–591.
122. Joseph JP, Rajappan K. Radiofrequency ablation of cardiac arrhythmias: past, present and future. *QJM Mon J Assoc Physicians*. 2012;105(4):303–314. doi:10.1093/qjmed/hcr189.
123. Hashimoto K, Watanabe I, Okumura Y, et al. Comparison of endocardial and epicardial lesion size following large-tip and extra-large-tip transcatheter cryoablation. *Circ J Off J Jpn Circ Soc*. 2009;73(9):1619–1626.
124. Parvez B, Pathak V, Schubert CM, Wood M. Comparison of Lesion Sizes Produced by Cryoablation and Open Irrigation Radiofrequency Ablation Catheters. *J Cardiovasc Electrophysiol*. 2008;19(5):528–534. doi:10.1111/j.1540-8167.2007.01072.x.
125. Yokoyama K, Nakagawa H, Wittkampf FHM, Pitha JV, Lazzara R, Jackman WM. Comparison of electrode cooling between internal and open irrigation in radiofrequency ablation lesion depth and incidence of thrombus and steam pop. *Circulation*. 2006;113(1):11–19. doi:10.1161/CIRCULATIONAHA.105.540062.
126. Bordignon S, Fürnkranz A, Schmidt B, Chun KRJ. Remaining ice cap on second-generation cryoballoon after deflation. *Circ Arrhythm Electrophysiol*. 2012;5(5):e98–99. doi:10.1161/CIRCEP.112.975516.
127. Ahmed H, Neuzil P, d' Avila A, et al. The esophageal effects of cryoenergy during cryoablation for atrial fibrillation. *Heart Rhythm*. 2009;6(7):962–969.

128. Pearce J, Thomsen S. Thermal Damage Processes in Myocardium. *Conf Proc IEEE Eng Med Biol Soc.* 1998;20(1):256.
129. Han A, Pearce J. Kinetic Model For Thermal Damage in the Myocardium. *Adv Meas Comput Temp Biomed Therm Tomogr Tech Bio-Heat Transf Models.* 1990;147:59–66.
130. He X, Bischof JC. Quantification of temperature and injury response in thermal therapy and cryosurgery. *Crit Rev Biomed Eng.* 2003;31(5-6):355–422.
131. Han B, Bischof JC. Direct cell injury associated with eutectic crystallization during freezing. *Cryobiology.* 2004;48(1):8–21. doi:10.1016/j.cryobiol.2003.11.002.
132. Rupp CC, Hoffmann NE, Schmidlin FR, Swanlund DJ, Bischof JC, Coad JE. Cryosurgical changes in the porcine kidney: histologic analysis with thermal history correlation. *Cryobiology.* 2002;45(2):167–182. doi:10.1016/S0011-2240(02)00125-6.
133. Rivoire ML, Voiglio EJ, Kaemmerlen P, et al. Hepatic cryosurgery precision: evaluation of ultrasonography, thermometry, and impedancemetry in a pig model. *J Surg Oncol.* 1996;61(4):242–248. doi:10.1002/(SICI)1096-9098(199604)61:4<242::AID-JSO2>3.0.CO;2-A.
134. Goel R, Swanlund D, Coad J, Paciotti GF, Bischof JC. TNF-alpha-based accentuation in cryoinjury--dose, delivery, and response. *Mol Cancer Ther.* 2007;6(7):2039–2047. doi:10.1158/1535-7163.MCT-06-0676.
135. Ogan K, Roberts WW, Wilhelm DM, et al. Infrared thermography and thermocouple mapping of radiofrequency renal ablation to assess treatment adequacy and ablation margins. *Urology.* 2003;62(1):146–151.
136. Etheridge ML, Choi J, Ramadhyani S, Bischof JC. Methods for characterizing convective cryoprobe heat transfer in ultrasound gel phantoms. *J Biomech Eng.* 2013;135(2):021002. doi:10.1115/1.4023237.
137. Klein HH, Puschmann S, Schaper J, Schaper W. The mechanism of the tetrazolium reaction in identifying experimental myocardial infarction. *Virchows Arch A.* 1981;393(3):287–297. doi:10.1007/BF00430828.
138. Sigg DC, Coles JA Jr, Oeltgen PR, Iaizzo PA. Role of delta-opioid receptor agonists on infarct size reduction in swine. *Am J Physiol Heart Circ Physiol.* 2002;282(6):H1953–1960. doi:10.1152/ajpheart.01045.2001.
139. Fishbein MC, Meerbaum S, Rit J, et al. Early phase acute myocardial infarct size quantification: validation of the triphenyl tetrazolium chloride tissue enzyme staining technique. *Am Heart J.* 1981;101(5):593–600.
140. Nakagawa H, Yamanashi WS, Pitha JV, et al. Comparison of in vivo tissue temperature profile and lesion geometry for radiofrequency ablation with a saline-irrigated electrode versus temperature control in a canine thigh muscle preparation. *Circulation.* 1995;91(8):2264–2273.
141. Nath S, Haines DE. Biophysics and pathology of catheter energy delivery systems*. *Prog Cardiovasc Dis.* 1995;37(4):185–204.
142. Hoffmann NE, Bischof JC. The cryobiology of cryosurgical injury. *Urology.* 2002;60(2):40–49.
143. PILCHER TA, Saul JP, HLAVACEK AM, Haemmerich D. Contrasting effects of convective flow on catheter ablation lesion size: cryo versus radiofrequency energy. *Pacing Clin Electrophysiol.* 2008;31(3):300–307.

144. Balázs T, Laczkó R, Bognár E, et al. Ablation time efficiency and lesion volume - in vitro comparison of 4 mm, non irrigated, gold- and platinum-iridium-tip radiofrequency ablation catheters. *J Interv Card Electrophysiol Int J Arrhythm Pacing*. 2013;36(1):13–18; discussion 18. doi:10.1007/s10840-012-9743-9.
145. Bandschapp O, Ginz HF, Soule CL, Girard T, Urwyler A, Iaizzo PA. In vitro effects of propofol and volatile agents on pharmacologically induced chloride channel myotonia. *Anesthesiology*. 2009;111(3):584–590. doi:10.1097/ALN.0b013e3181b05f23.
146. Marshall MT, Liao KK, Loushin MK, Iaizzo PA. The effects of temperature on cardiac pacing thresholds. *Pacing Clin Electrophysiol PACE*. 2010;33(7):826–833. doi:10.1111/j.1540-8159.2009.02681.x.
147. Venkatasubramanian RT, Wolkers WF, Shenoi MM, et al. Freeze–Thaw Induced Biomechanical Changes in Arteries: Role of Collagen Matrix and Smooth Muscle Cells. *Ann Biomed Eng*. 2010;38(3):694–706. doi:10.1007/s10439-010-9921-9.
148. Goel R, Anderson K, Slaton J, et al. Adjuvant Approaches to Enhance Cryosurgery. *J Biomech Eng*. 131(7):074003.
149. Goff RP, Benscoter M, Iaizzo PA. Functional In-Vitro Cardiac Tissue Model For The Evaluation of Ablation. In: *Journal of Interventional Electrophysiology*. Vol 30. 2. Springer; 2011:188–189.
150. Bunch TJ, Bruce GK, Mahapatra S, et al. Mechanisms of Phrenic Nerve Injury During Radiofrequency Ablation at the Pulmonary Vein Orifice. *J Cardiovasc Electrophysiol*. 2005;16(12):1318–1325. doi:10.1111/j.1540-8167.2005.00216.x.
151. Dureuil B, Viirès N, Pariente R, Desmots JM, Aubier M. Effects of phrenic nerve cooling on diaphragmatic function. *J Appl Physiol Bethesda Md 1985*. 1987;63(5):1763–1769.
152. Robicsek F, Duncan GD, Hawes AC, Rice HE, Harrill S, Robicsek SA. Biological thresholds of cold-induced phrenic nerve injury. *J Thorac Cardiovasc Surg*. 1990;99(1):167–170.
153. Jackson N, Barlow M, Leitch J, Attia J. Treating Atrial Fibrillation: Pulmonary Vein Isolation with the Cryoballoon Technique. *Heart Lung Circ*. 2012. doi:10.1016/j.hlc.2012.03.123.
154. Dorwarth U, Schmidt M, Wankerl M, Krieg J, Straube F, Hoffmann E. Pulmonary vein electrophysiology during cryoballoon ablation as a predictor for procedural success. *J Interv Card Electrophysiol Int J Arrhythm Pacing*. 2011;32(3):205–211. doi:10.1007/s10840-011-9585-x.
155. Ghosh J, Sepahpour A, Chan K, Singarayay S, McGuire MA. Immediate Balloon Deflation for Prevention of Persistent Phrenic Nerve Palsy During Pulmonary Vein Isolation by Balloon Cryoablation. *Heart Rhythm Off J Heart Rhythm Soc*. 2013. doi:10.1016/j.hrthm.2013.01.011.
156. Casado-Arroyo R, Chierchia G-B, Conte G, et al. Phrenic nerve paralysis during cryoballoon ablation for atrial fibrillation: A comparison between the first- and second-generation balloon. *Heart Rhythm Off J Heart Rhythm Soc*. 2013. doi:10.1016/j.hrthm.2013.07.005.
157. Defaye P, Kane A, Chaib A, Jacon P. Efficacy and safety of pulmonary veins isolation by cryoablation for the treatment of paroxysmal and persistent atrial fibrillation. *Eur Eur Pacing Arrhythm Card Electrophysiol J Work Groups Card Pacing Arrhythm*

- Card Cell Electrophysiol Eur Soc Cardiol.* 2011;13(6):789–795.
doi:10.1093/europace/eur036.
158. Bitter T, Nölker G, Vogt J, Prinz C, Horstkotte D, Oldenburg O. Predictors of recurrence in patients undergoing cryoballoon ablation for treatment of atrial fibrillation: the independent role of sleep-disordered breathing. *J Cardiovasc Electrophysiol.* 2012;23(1):18–25. doi:10.1111/j.1540-8167.2011.02148.x.
159. Mandell J, Amico F, Parekh S, Snow J, Germano J, Cohen TJ. Early experience with the cryoablation balloon procedure for the treatment of atrial fibrillation by an experienced radiofrequency catheter ablation center. *J Invasive Cardiol.* 2013;25(6):288–292.
160. Fürnkranz A, Bordignon S, Schmidt B, et al. Improved procedural efficacy of pulmonary vein isolation using the novel second-generation cryoballoon. *J Cardiovasc Electrophysiol.* 2013;24(5):492–497. doi:10.1111/jce.12082.
161. Peyrol M, Sbragia P, Quatre A, et al. Pulmonary vein isolation using a single size cryoballoon chosen according to transesophageal echocardiography information. *Int J Cardiol.* 2012. doi:10.1016/j.ijcard.2012.09.063.
162. Malmberg H, Lönnerholm S, Blomström-Lundqvist C. Acute and clinical effects of cryoballoon pulmonary vein isolation in patients with symptomatic paroxysmal and persistent atrial fibrillation. *Eur Eur Pacing Arrhythm Card Electrophysiol J Work Groups Card Pacing Arrhythm Card Cell Electrophysiol Eur Soc Cardiol.* 2008;10(11):1277–1280. doi:10.1093/europace/eun286.
163. Pokushalov E, Romanov A, Artyomenko S, et al. Cryoballoon versus radiofrequency for pulmonary vein re-isolation after a failed initial ablation procedure in patients with paroxysmal atrial fibrillation. *J Cardiovasc Electrophysiol.* 2013;24(3):274–279. doi:10.1111/jce.12038.
164. Schmidt M, Dorwarth U, Straube F, et al. A novel double cryoballoon strategy in persistent atrial fibrillation: a pilot study. *Clin Res Cardiol Off J Ger Card Soc.* 2012. doi:10.1007/s00392-012-0456-y.
165. Catanzariti D, Maines M, Angheben C, Centonze M, Cemin C, Vergara G. Usefulness of Contrast Intracardiac Echocardiography in Performing Pulmonary Vein Balloon Occlusion during Cryo-ablation for Atrial Fibrillation. *Indian Pacing Electrophysiol J.* 2012;12(6):237–249.
166. Chun K-RJ, Schmidt B, Metzner A, et al. The “single big cryoballoon” technique for acute pulmonary vein isolation in patients with paroxysmal atrial fibrillation: a prospective observational single centre study. *Eur Heart J.* 2009;30(6):699–709. doi:10.1093/eurheartj/ehn570.
167. Tang M, Kriatselis C, Nedios S, et al. A novel cryoballoon technique for mapping and isolating pulmonary veins: a feasibility and efficacy study. *J Cardiovasc Electrophysiol.* 2010;21(6):626–631. doi:10.1111/j.1540-8167.2009.01668.x.
168. Linhart M, Bellmann B, Mittmann-Braun E, et al. Comparison of cryoballoon and radiofrequency ablation of pulmonary veins in 40 patients with paroxysmal atrial fibrillation: a case-control study. *J Cardiovasc Electrophysiol.* 2009;20(12):1343–1348. doi:10.1111/j.1540-8167.2009.01560.x.
169. Namdar M, Chierchia G-B, Westra S, et al. Isolating the pulmonary veins as first-line therapy in patients with lone paroxysmal atrial fibrillation using the Cryoballoon. *Europace.* 2012;14(2):197–203. doi:10.1093/europace/eur299.

170. Kühne M, Schaer B, Ammann P, Suter Y, Osswald S, Sticherling C. Cryoballoon ablation for pulmonary vein isolation in patients with paroxysmal atrial fibrillation. *Swiss Med Wkly*. 2010;140(15-16):214–221. doi:smw-12977.
171. Bordignon S, Chun KJ, Gunawardene M, et al. Comparison of Balloon Catheter Ablation Technologies for Pulmonary Vein Isolation: The Laser Versus Cryo Study. *J Cardiovasc Electrophysiol*. 2013. doi:10.1111/jce.12192.
172. Sohara H, Takeda H, Ueno H, Oda T, Satake S. Feasibility of the Radiofrequency Hot Balloon Catheter for Isolation of the Posterior Left Atrium and Pulmonary Veins for the Treatment of Atrial Fibrillation. *Circ Arrhythm Electrophysiol*. 2009;2(3):225–232. doi:10.1161/CIRCEP.108.817205.
173. Morélot-Panzini C, Fournier E, Donzel-Raynaud C, Dubourg O, Willer J-C, Similowski T. Conduction velocity of the human phrenic nerve in the neck. *J Electromyogr Kinesiol Off J Int Soc Electrophysiol Kinesiol*. 2009;19(1):122–130. doi:10.1016/j.jelekin.2007.06.017.
174. Langendorff O. Untersuchungen am überlebenden Säugethierherzen. *Arch Für Gesamte Physiol Menschen Tiere*. 1895;61(6):291–332. doi:10.1007/BF01812150.
175. Sigg DC, Iaizzo PA. In vivo versus in vitro comparison of swine cardiac performance: induction of cardiodepression with halothane. *Eur J Pharmacol*. 2006;543(1-3):97–107. doi:10.1016/j.ejphar.2006.06.011.
176. Baker LC, London B, Choi B-R, Koren G, Salama G. Enhanced Dispersion of Repolarization and Refractoriness in Transgenic Mouse Hearts Promotes Reentrant Ventricular Tachycardia. *Circ Res*. 2000;86(4):396–407. doi:10.1161/01.RES.86.4.396.
177. Efimov IR, Nikolski VP, Salama G. Optical Imaging of the Heart. *Circ Res*. 2004;95(1):21–33. doi:10.1161/01.RES.0000130529.18016.35.
178. HILL AJ, IAIZZO PA. Comparative Cardiac Anatomy. In: *Handbook Of Cardiac Anatomy, Physiology And Devices*. 3rd ed. Springer; 2005.
179. Eggum JH, Howard SA, Goff RP, Iaizzo PA. Imaging of a Coronary Artery Stent Implantation Within an Isolated Human Heart. *J Cardiovasc Transl Res*. 2011;5(1):73–74. doi:10.1007/s12265-011-9322-y.
180. Bandschapp O, Goff R, Mallin G, Loushin M, Iaizzo PA. The Path of a Pulmonary Artery Catheter Visualized through a Beating Human Heart. *Am J Respir Crit Care Med*. 2012;186(4):385. doi:10.1164/rccm.201112-2227IM.
181. Dietz JR. Release of natriuretic factor from rat heart-lung preparation by atrial distension. *Am J Physiol - Regul Integr Comp Physiol*. 1984;247(6):R1093–R1096.
182. Inokawa H, Sevala M, Funkhouser WK, Egan TM. Ex-Vivo Perfusion and Ventilation of Rat Lungs From Non-Heart-Beating Donors Before Transplant. *Ann Thorac Surg*. 2006;82(4):1219–1225. doi:10.1016/j.athoracsur.2006.05.004.
183. Knowlton FP, Starling EH. The influence of variations in temperature and blood-pressure on the performance of the isolated mammalian heart. *J Physiol*. 1912;44(3):206–219.
184. Martin HN. The Direct Influence of Gradual Variations of Temperature upon the Rate of Beat of the Dog's Heart. *Philos Trans R Soc Lond*. 1883;174:663–688. doi:10.1098/rstl.1883.0021.
185. Martin HN. A New Method of Studying the Mammalian Heart. In: *Studies from the Biological Laboratory: V.1 -5; 1877/78-1891/93*. Vol 2. J. Murphy & Company; 1881:119–130.

186. ANDERSON SE, SKADSBERG ND, LASKE TG, BENDITT DG, IAIZZO PA. Variation in Pacing Impedance: Impact of Implant Site and Measurement Method. *Pacing Clin Electrophysiol.* 2007;30(9):1076–1082. doi:10.1111/j.1540-8159.2007.00816.x.
187. Iaizzo PA, Hill AJ, Laske TG. Cardiac device testing enhanced by simultaneous imaging modalities: the Visible Heart, fluoroscopy and echocardiography. *Expert Rev Med Devices.* 2008;5(1):51–58. doi:10.1586/17434440.5.1.51.
188. Eggen M, Bonner M, Sheldon T, Williams E, Iaizzo PA. Implantation of a Leadless Pacemaker within Reanimated Human Hearts using Direct Visualization. In: Heart Rhythm Society 2013; 2013.
189. Spencer JH, Quill JL, Bateman MG, et al. The benefits of the Atlas of Human Cardiac Anatomy website for the design of cardiac devices. *Expert Rev Med Devices.* 2013;10(6):729–734. doi:10.1586/17434440.2013.843449.
190. Slater JP, Lipsitz EC, Chen JM, Levin HR, Oz MC, Burkhoff D. Use of explanted human hearts as a model for the study of cardiac pathophysiologic conditions. *J Thorac Cardiovasc Surg.* 1995;110(1):239–247.
191. Van Opstal JM, Timmermans C, Blaauw Y, Pison L. Bronchial erosion and hemoptysis after pulmonary vein isolation by cryoballoon ablation. *Heart Rhythm Off J Heart Rhythm Soc.* 2011;8(9):1459. doi:10.1016/j.hrthm.2010.06.024.
192. Andrade JG, Dubuc M, Guerra PG, et al. Pulmonary vein isolation using a second-generation cryoballoon catheter: a randomized comparison of ablation duration and method of deflation. *J Cardiovasc Electrophysiol.* 2013;24(6):692–698. doi:10.1111/jce.12114.
193. Goff RP, Iaizzo PA. In vitro assessment of phrenic nerve cryothermal injury. In: *Scientific Sessions of the American Heart Association.* Dallas, TX; 2013. Available at: <http://www.aievolution.com/aha1301/index.cfm?do=abs.viewAbs&abs=3576>.
194. Canpolat U, Aytémir K, Hizal M, et al. Imaging before cryoablation of atrial fibrillation: is phrenic nerve palsy predictable? *Eur Eur Pacing Arrhythm Card Electrophysiol J Work Groups Card Pacing Arrhythm Card Cell Electrophysiol Eur Soc Cardiol.* 2013. doi:10.1093/europace/eut155.
195. Bowman HF, Cravalho EG, Woods M. Theory, Measurement, and Application of Thermal Properties of Biomaterials. *Annu Rev Biophys Bioeng.* 1975;4(1):43–80. doi:10.1146/annurev.bb.04.060175.000355.
196. Nakatsuka S, Yashiro H, Inoue M, et al. On freeze-thaw sequence of vital organ of assuming the cryoablation for malignant lung tumors by using cryoprobe as heat source. *Cryobiology.* 2010;61(3):317–326. doi:10.1016/j.cryobiol.2010.10.157.

Appendices

Appendix A: Published or Accepted Conference Abstracts

Listed in chronological order beginning with most recent

In-Vitro Assessment of Phrenic Nerve Cryothermal Injury

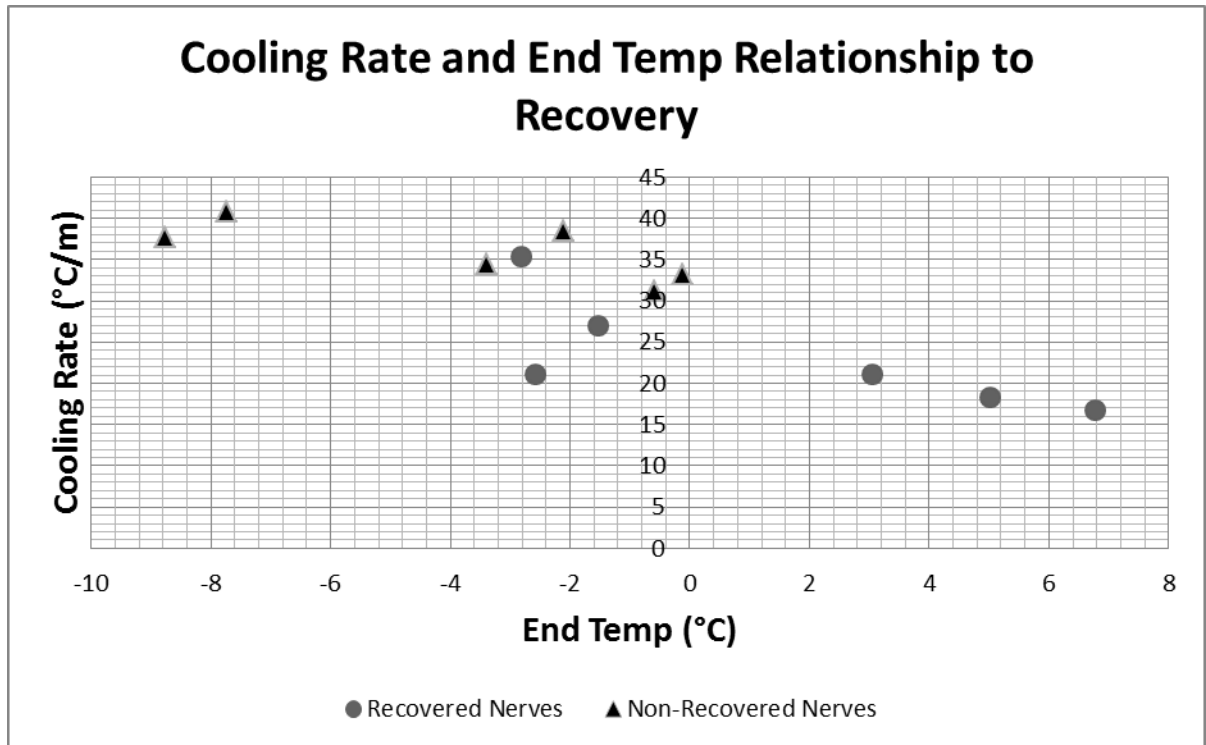
Selected for poster presentation at American Heart Association 2013 Scientific Sessions, Dallas, TX

Authors: Ryan P. Goff, Paul A. Iaizzo

Background: Phrenic nerve (PN) injury may result from transcatheter ablations for the treatment of arrhythmias. Cryoballoon ablation has been reported to cause phrenic nerve (PN) injury: occasionally resulting in diaphragmatic hemi-paralysis. To date, the tolerance of the phrenic nerve to cold energy on short timescales is largely unstudied.

Methods: Swine phrenic nerves (n=12) were harvested and the fatty sheath dissected from the nerve. The PNs were then placed in a nerve recording chamber (ADInstruments, Colorado Springs, CO) with a custom built thermocouple array. Stimulus of 1 V and 0.1 mS were applied to the proximal end of the nerve. Propagated compound action potentials (CAPs) were recorded pre- and one hour post-ablation. A 3-5 mm thick section of striated muscle was placed on top of the nerve/thermocouple array to reduce the cooling power of the catheter. A Freezor Max (Medtronic, Minneapolis, MN) catheter was placed in contact with the muscle and a one minute ablation applied while nerve temperatures being recorded.

Results: The figure below displays cooling profile and recovery relationship. The table summarizes characteristics of the CAPs pre- and post-ablation for nerves that recovered. The p-values were calculated using a paired t-test.



Phrenic Nerve CAP Parameter Analysis +/- Standard Deviation				
Parameter	Pre-Ablation Average	Post-Ablation Average	Average Paired Percent Change	P Value
Latency to Onset (ms)	0.115 +/- 0.015	0.13 +/- 0.020	15.0%	0.15
Amplitude (mV)	1.54375 +/- 0.940	0.866 +/- 0.920	-50.0%	0.02
Duration (ms)	0.065 +/- 0.013	0.063 +/- 0.011	10.3%	0.77
Conduction Speed (m/s)	57.25 +/- 7.80	51.07 +/- 8.35	-10.7%	0.12

Conclusion: The data suggests that cooling to subzero temperatures will often cause PN CAPs to cease, indicating injury/death. For nerves that elicited post-ablation CAPs, reduction in amplitude was the recorded parameter with the greatest change. These data support the notion that cooling a PN to low, suprazero temperatures, may cause clinically relevant changes in diaphragmatic function.

In-Vitro Characterization of Myocardial Cryothermal Injury

Selected for oral presentation at Cryobiology Conference 2013, Washington D.C.

Ryan P. Goff [1,2], Stephen G. Quallich [1,2], Robert A. Buechler [1,3], Jeunghwan Choi PhD[4], John C. Bischof PhD [1,4], Paul A. Iazzo PhD [1,2]

- 1) Department of Biomedical Engineering, University of Minnesota
- 2) Department of Surgery, University of Minnesota
- 3) Medtronic, Inc., Minneapolis, MN
- 4) Mechanical Engineering, University of Minnesota

Background: Cardiac balloon and catheter cryoablations for the treatment of atrial fibrillation have been gaining attention as approaches for treating arrhythmias, in particular for isolation of the pulmonary veins (PV). Despite widespread clinical use of cardiac cryoablation, there are still questions regarding dosing and treatment time, which may affect both efficacy and collateral injury. To date injury thresholds for therapy of cardiac tissues are largely unreported in the literature.

Methods: Slices of ventricular myocardium (n=11) and left atrial tissue (n=6) from female Yorkshire Cross swine hearts were dissected including the native endocardial surface. Samples were placed in an infrared imaging apparatus consisting of a plastic petri dish with central ablation probe (1.5 mm IceSeed, Galil Medical, Arden Hills, MN) and 2 millimeters of Sylgard polymer formed to the bottom. The tissue slices were impaled on the central cryoprobe and infrared thermography was captured using a Flir A20 looking from the top down. Subsequently, samples were cultured for 24 hours in a cell culture incubator (myocardium) at 37°C or 4 hours at room temperature (PV) for optimal lesion identification with 1% TTC in Trizma buffer for 1 hour at 37°C. Photographs of the resultant TTC staining of each sample were captured and a custom Matlab program was used to normalize staining intensity and correlate the average staining intensity with the average thermal profile at any radial distance from the cryoprobe. The relationship between the staining intensity and end temperature was fit with a sigmoidal curve. Samples with a fit of greater than $R^2 > 0.99$ were analyzed. The transition from dead to injured tissue was defined as the point on the curve fit where the staining ratio was 10% of the range between the lower and upper asymptotes of the sigmoid (i.e., 10% of the grayscale value change at the lesion margin closest to the lesion). The maximum cooling rate correlated to this ratio and end temperature was then calculated from the thermal profiles. Eight thermal profiles at different radii were averaged to obtain a characteristic thermal profile for each sample. This approach has led to the creation of a database of thermal profiles that results in either completely or partially injured tissues.

Results: Initial results suggest that cooling rates of -103 ± 49 and -72 ± 9 °C/min and end temperatures of approximately -21 ± 6 and -17.2 ± 3.2 °C are necessary for complete necrosis of ventricular and left atrial tissue, respectively. Using a two-tailed t-test assuming equal variance the difference in end temperature and cooling rate between ventricular and left atrial tissue were non-significant ($p=.21$, $p=.20$ respectively).

Conclusions: Experiments are ongoing to determine cryothermal injury thresholds of tissues associated with cardiac ablation, such as: lung and esophagus. The TTC staining protocol is in the process of being validated by comparison to H&E stain. Cellular viability assays are being performed to compare to these findings.

Acknowledgment/Funding: The author's sincerely thank Dr. Jim Coad for advising on staining protocols. This work was supported by the GAANN program, the Institute for Engineering in Medicine, and a contract with Medtronic, Inc.

Direct Visualization of Pulmonary Vein Ablations within Reanimated Swine Hearts to Investigate Recent Advances in Cryo-balloon Technologies

Selected for poster presentation at Transcatheter Therapeutics Conference 2013, San Francisco, CA.

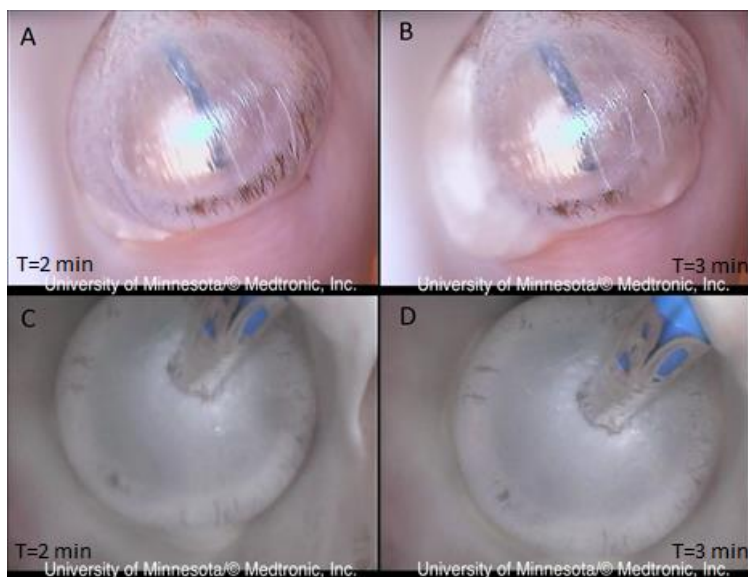
Authors: Ryan Goff B.S., D. Wyn Davies M.D., Stephen Howard B.S., Mark Benscoter M.S., Paul A. Iaizzo PhD

Background: The use of cryo-balloon ablation for pulmonary vein (PV) isolation has led to questions as to how best to optimize single procedure success. Specifically, what new indicators can be identified to better determine ideal ablation durations as well as the best catheter orientations and catheter placements in the PV antra. Here we present unique data obtained by observing PV antral cryo-balloon ablation under direct vision.

Methods: Swine hearts were reanimated using Visible Heart ® methodologies as described previously via direct visualization capabilities. The device-tissue interface was viewed with videoscopes within the left atria. These images were obtained simultaneously with fluoroscopy of the PV occlusions. The effects of different cooling profiles, catheter orientations, and impact of ablation durations on ice propagation were compared.

Results: Images shown in the figure demonstrate an ablation with an Arctic Front Advance™ (Medtronic, Minneapolis, MN) catheter (C,D) versus a previous generation (A,B). Note, the advance catheter elicited a more circumferential, ice formation. Ice appears to be more evenly distributed for the newer generation catheter shown by a visible ring of ice at the balloon/tissue interface (D).

Conclusion: This method provides unique insights into the rates and sites of ice propagation/formation in ways that fluoro and temperature feedback cannot. This information can be utilized to show several features of balloon cryo-therapy and serve as a foundation for advances in balloon catheter technologies.



External Infrared Visualization of an Endocardial Cryoablation: Performed on a Reanimated Swine Heart

Selected for oral presentation at the 2013 International Mechanical Engineering Conference and Expo, Houston, TX.

Ryan P. Goff BS, University of Minnesota, Minneapolis, Minnesota, U.S.A.

Stephen G. Quallich BS, University of Minnesota, Minneapolis, Minnesota, U.S.A.

Paul A. Iaizzo PhD, University of Minnesota, Minneapolis, Minnesota, U.S.A.

Today, clinical electrophysiologists still considered cryoablation a relatively new treatment modality for cardiac arrhythmias. Interestingly, the bioheat transfer in this environment has been largely unstudied. Furthermore, during the clinical applications of cryotherapy, adjacent tissues may become injured from the induced cooling. These facts, along with the desire to validate models of cryotherapy, to potentially increase efficacy and safety, warrants the study in reanimated large mammalian hearts where visualization of heat transfer is feasible. Specifically, cryoballoon catheters (ArticFront, Medtronic Inc.) were positioned in the superior vena cava and the clinically recommended ablation duration of four minutes was applied. Similarly, focal cryo-catheters (FreezorMax, Medtronic Inc.) were placed in the right atrial appendages and spot ablations were performed for four minutes. We believe that this novel model allows for both high spatial and temporal resolutions for the study of these treatments. More specifically, multi-modal imaging can be performed, with: intracardiac videoscopes, externally with IR and video cameras, with fluoroscopy and/or echocardiography and all while hemodynamic monitoring of the heart (Fig. 1). Time from beginning of ablation is displayed in the top left corner and temperature scale to the right.

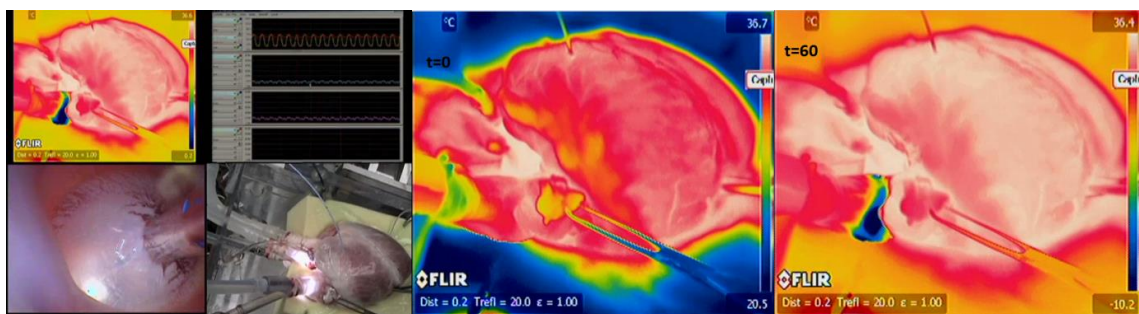
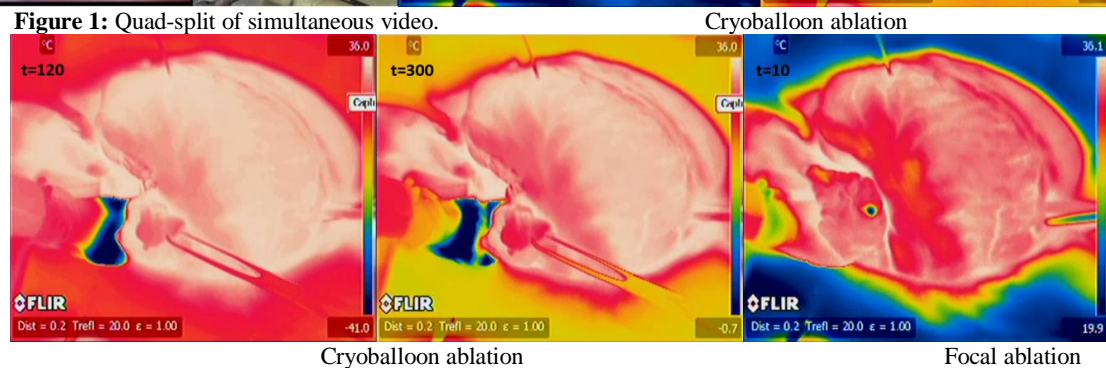
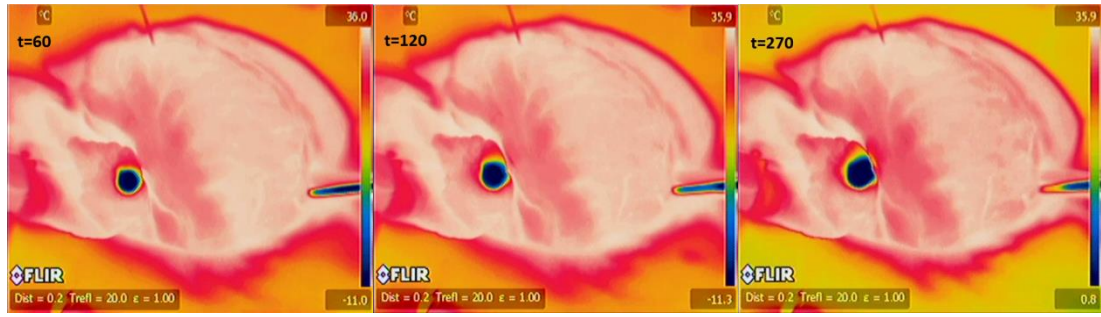


Figure 1: Quad-split of simultaneous video.



Cryoballoon ablation

Focal ablation



Focal ablation

Novel visualization of iatrogenic atrial septal defects and ablation lesions in a reanimated human heart

Selected for poster presentation at Experimental Biology 2013, San Diego, CA.

Published in *The Journal of the Federation of American Societies for Experimental Biology*, April 1, 2012

Ryan P. Goff^{1,2}, Stephen A. Howard^{1,2}, Paul A. Iaizzo^{1,2,3}

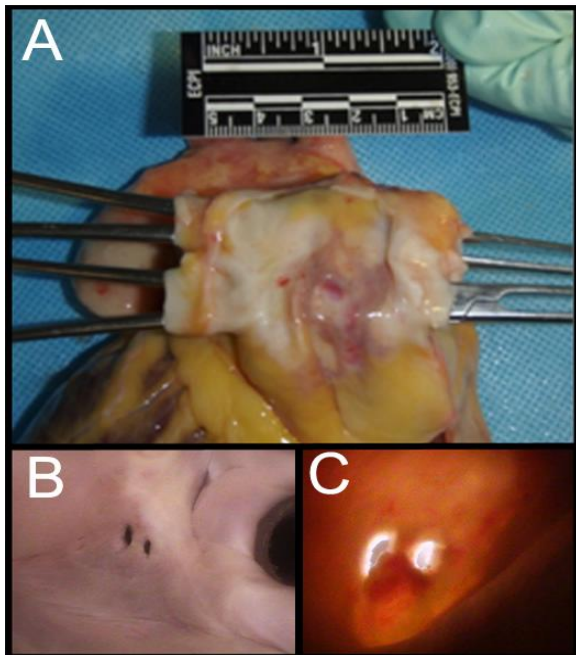
Departments of Biomedical Engineering¹, Surgery², and Integrated Physiology and Biology³

Using methods previously published, we reanimated a donated human heart from a 72 year old female that was deemed not viable for transplantation. The patient's cardiac history indicated that several months prior, she had undergone a cardiac ablation procedure. Photographs were taken of the lesions as well as internal functional images of the ablation and transseptal punctures sites.

This heart contained two iatrogenic atrial septal defects (iASD) presumably from two transseptal punctures (through the fossa ovalis) for application of ablation therapy within the left atrium. Using an endoscope, video of the ablation lesions was captured and tissue around the pulmonary veins appeared pale: indicating fibrous scar. It was of interest to note, that although the procedure was performed months prior, the iASDs (> 7F) were still prominent within the anatomy.

Example images of the ablation procedure effects on the cardiac anatomy are shown below. (A) External image of the left atrium where the pulmonary vein lesions are noticeably lighter than the other musculature. iASDs are seen through the fossa ovalis from the left (B) and right (C) atrium. A pulmonary vein is seen in B with an ablation lesion between the fossa ovalis and the right pulmonary veins and the left atrium is backlit to show the iASDs in C.

This work has been supported by the NIH training grant 5T32AR007612-10 and the Medtronic Professorship for Visible Heart Research.



MRI Reconstruction of Human Hearts and Their Relationship to Direct Measurements taken from Hypertensive Specimens

Selected for poster presentation at Experimental Biology 2013, San Diego, CA.

Published in *The Journal of the Federation of American Societies for Experimental Biology*, April 1, 2012

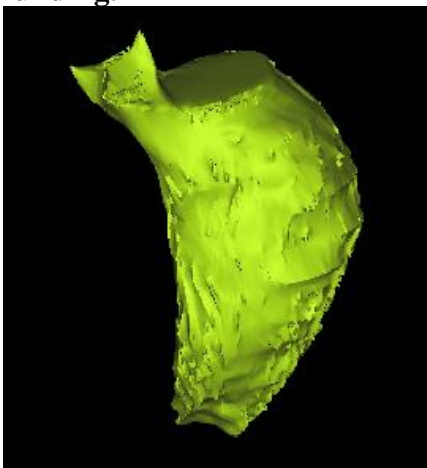
Stephen A Howard^{1,2}, Ryan Goff^{1,2} and, Paul A. Iaizzo^{1,2,3}

Departments of Biomedical Engineering¹, Surgery², and Integrated Physiology and Biology³

MRI is a very useful tool to examine the blood volume in patients. However one downside is that generally it is as an approximation based on an assumed volume shape using 3 to 10 individual measurements of the chamber of interest. In this study we are examining the blood volume of perfusion fixed human hearts via direct measurements and 3D reconstruction of the heart's chambers.

The perfusion fixed hearts were suspended in agar gel and imaged with 1.5T or 3T MRI. From the images we are able to analyze the blood volume in the chambers of the hearts using 3D reconstructions produced with image processing software. This tool allows us to obtain very precise volumes of the chambers of the heart and compare them to direct, physical measurements of the blood volume by filling and assessing the fluid capacity of each chamber of the heart. This allows us to compare the usefulness of the 3D reconstructions and its ability to quantify variables within clinically diagnosed hypertensive patients compared to control hearts.

Funded by NIH training grant 5T32AR007612-10 and Medtronic professorship funding.



Left-sided Epicardial Pacing Via A Transvenous Lead Delivery

Selected for poster presentation Design of Medical Devices Conference 2013, Minneapolis, MN.

Published in the ASME Journal of Medical Devices.

Julianne H. Eggum

Ryan P. Goff

David G. Benditt

Paul A. Iaizzo

Departments of Surgery, Biomedical Engineering, and Medicine

University of Minnesota

1 Background

Cardiac Resynchronization Therapy (CRT) is considered a useful therapy for heart failure patients with electromechanical dyssynchrony. To date, it has been reported that approximately 10-20% of heart failure patients (570,000-1.14 million people) will benefit from the placement of CRT [1]. The current approach of CRT is to pace the site of latest left ventricular activation [2-3]. The LV lead is typically implanted in a cardiac vein.

However, approximately 30% of CRT patients do not clinically respond to the treatment [4-5]. In many cases, this is considered to be a result of suboptimal lead placement due to limitations of the cardiac venous anatomy. We propose here that it may be possible to overcome such limitations by perforating through the wall of the coronary sinus or great cardiac vein to gain access to the epicardial surface for optimal lead placement.

2 Methods

In order to test our proposed method, we employed the Visible Heart ® methodologies, which allows for a four chamber working swine heart preparation as described previously [6]. The University of Minnesota's Animal Care and Use Committee approved all experimental protocols involved in this study.

First, we cannulated a given coronary sinus (CS) with a CS catheter (Attain, Medtronic Inc., Mounds View, MN). We then advanced a steerable inner catheter (Prevail, Medtronic Inc., Mounds View, MN) through the CS catheter and identified a target perforation site. The target perforation site will be the location within the CS or great cardiac vein that is close to the site of latest activation. Next, we advanced a stylet (Medtronic Inc., Mounds View, MN) through the lumen of the inner steerable catheter until it perforated the target venous perforation site. Then we advanced the inner steerable catheter over the stylet through the perforated vein and steered the catheter to the target pacing site.

3 Results

Figure 1 exhibits our proposed method. Figure 1(a) demonstrates perforation of the great cardiac vein with a stylet followed by the advancement of the inner catheter 1(b). Figure 1(c) displays access to the target pacing site with a steerable inner catheter. Figure 1(d) demonstrates a subsequent lead placement.

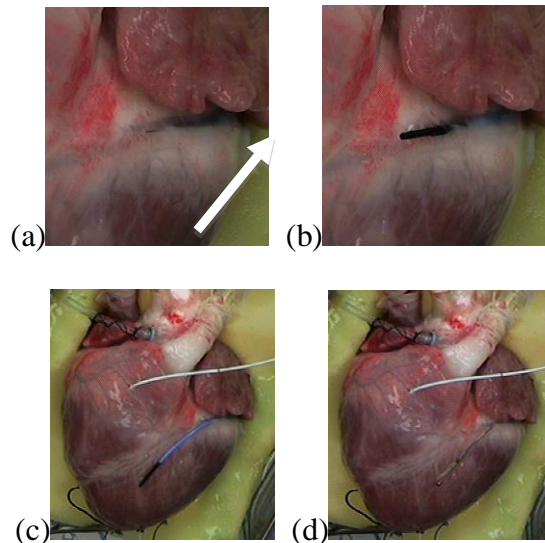


Figure 1

4 Interpretation

We believe that these preliminary tests provide evidence that this epicardial lead placement technique is a feasible method to obtain access to optimal CRT pacing sites.

There are a few factors that must be considered as we continue to develop this method. It is important to ensure that the stylet will perforate outwardly into the pericardial fluid and not into any nearby arteries. The use of fluoroscopy should reduce this risk. There is also a risk for pericardial perforation; however, our preliminary *in situ* studies indicate that this risk is low. The risk of cardiac tamponade is minimized due to the low pressures in the veins and right atrium, but we plan to investigate this risk further.

We will continue to perform further testing in an *in situ* swine model, with the pericardium intact. We will also look into various epicardial lead anchoring techniques once the optimal pacing position has been obtained.

References

- [1] Lu, F., 2009, "Cardiac Resynchronization Therapy," Handbook of cardiac physiology and anatomy., 2nd ed., pp. 475-497.
- [2] Dekker, A. et al, 2004, "Epicardial Left Ventricular Lead Placement for Cardiac Resynchronization Therapy: Optimal Pace Site Selection with Pressure-Volume Loops," J Thorac Cardiovasc Surg., 127, pp. 1641-1647.
- [3] Ypenburg, C. et al, 2008, "Optimal left ventricular lead position predicts reverse remodeling and survival after cardiac resynchronization therapy," J Am Coll Cardiol., 52, pp. 1402-1409.
- [4] Khan N. et. al, 2008, "Do the Official Guidelines for Cardiac Resynchronization Therapy Need to Be Changed?" Devices for Cardiac Resynchronization; Technologic and Clinical Aspects, New York: Springer Science, pp. 3-16.
- [5] Vardas P. et. al, 2007, "Guidelines for Cardiac Pacing and Cardiac Resynchronization Therapy," European Heart Journal, 28, pp. 2256-2295.

[6] Chinchoy E. et. al, 2000, "Isolated Four-Chamber Working Swine Heart Model," Ann Thorac Surg., 70, pp. 1607-1614.

Functional In-Vitro Cardiac Tissue Model For The Evaluation of Ablation Parameters and/or The Use of Adjuvant Therapies.

Selected for poster presentation at European Cardiac Arrhythmia Society 2011, Paris, France.

Published in the *Journal of Interventional Cardiac Electrophysiology*, March 2011.

Ryan P. Goff, Mark Bencoter, Paul A. Iaizzo

Cardiac cryoablation is expanding with novel uses of minimally invasive procedures and endocardial tools. This in-vitro model allows one to uniquely investigate, four parameters that will alter contractility, to describe the thermal history of a treatment: cooling rates, end temperatures, hold times, and/or thaw rates. Multiple tissue baths provide for a higher throughput analysis of novel ablative products and adjuvant therapies (versus in situ or in vivo animal models).

Methods:

Swine trabeculae muscle bundles were hung from a force transducer and bathed in oxygenated Krebs's buffer at 37 degrees C. Care was taken during dissection to keep constant cross sections of approximately 3 mm by 3 mm. Field stimulation was applied every 10 seconds and maximum twitch force generated was measured. After a control period, ablative treatments of varying time were applied to the segments and decline in contractility was measured. To visualize lesion size a TTC assay was performed. As shown in the figure, the test method is able to accurately characterize the decrease in contractility when using ablation therapy. The photo inset in the graph shows the muscle bath, catheter (blue), and iceball formation on muscle bundle.

Conclusion:

The model simulates an environment similar to that found endocardially, with convective movement of constant temperature fluid in which ablative parameters can be varied their effect on contractility measured. The model is able to vary lesions as evidenced by the TTC assay and reduced contractility. An active fixation pacing/sensing system can be applied to examine local versus field stimulation and conduction block with relation to the therapy applied. Using this system new treatment regimens can be evaluated in a highly controlled environment without varying anatomy or physiology. Future work involves evaluation adjuvant treatment (such as local delivery of high NaCl or glycine solutions) effect on human muscle and lesion formation.

**Development of an Endocardial Cryoablation Catheter for
Concomitant Delivery of Cryogenic Treatments and Adjuvants**

Selected for poster presentation Design of Medical Devices Conference 2013,
Minneapolis, MN.

Published in the ASME Journal of Medical Devices.

**Proceedings of the 2011 Design of Medical Devices Conference
DMD2011**

April 12-14, 2011, Minneapolis, MN, USA

DMD2011-5263

Ryan P. Goff

University of Minnesota

Departments of Surgery and Biomedical
Engineering

Minneapolis, MN, United States

Paul A. Iaizzo

University of Minnesota

Department of Surgery and the Institute for
Engineering in Medicine

Minneapolis, MN, United States

John C. Bischof

University of Minnesota

Department of Mechanical Engineering
Minneapolis, MN, United States

ABSTRACT

This paper presents the preliminary development of a novel cryoablation catheter for the delivery of cryo energy and complimentary pharmacological agents selected to improve lesion formation. The described prototype uses a commercially available cryoablation catheter with a deployable needle injection catheter grafted onto it. The device would be used in endocardial ablation of thick structures and would inject an adjuvant at the desired depth prior to cryo-therapy delivery. Adjuvants have been investigated previously to increase the “kill zone” of an ablation lesion and can minimize the zone of incomplete death near the iceball edge. This makes visualization of the iceball via ultrasound a better predictor for lesion size and progression. Transmurality of a lesion can be essential for a clinical ablation procedure to have long-term effectiveness. The secondary goal of such a device may be to increase energy transfer via the metal needle in the myocardium, so to further aid in the creation of transmural lesions in thick tissues (e.g., the ventricles).

Added embodiments of such therapeutic devices would be to also have electrical pacing/sensing capabilities and/or temperature monitoring capabilities at the tip of the needle. Such features would likely provide a physician with more precise information regarding lesion progressions and efficacies. One potential device design could therefore have two temperature sensors, one at the ablative tip and one at the needle tip. This will allow the user to monitor how far and how fast the lesion has advanced into the myocardium at the preset depth of the needle. After the lesion is formed, entrance and exit block tests could then be used to evaluate the ability of the lesion to block electrical propagation.

A unique feature of this catheter design approach is the method of active deployment. The physician will pre-set a desired needle deployment depth and then navigate the catheter to the location of treatment. Next, the cryocatheter would be positioned and frozen to the desired location of the endocardium, when appropriate, the needle would then be deployed, perhaps by first applying a RF energy to warm the system within the created iceball so to allow needle to be actively plunged into the myocardium. Subsequently, the contact of the needle to the cryo-catheter system will rapidly cool the needle within the engaged myocardium. This approach could potentially reduce the risks of perforations and ensure consistent deployment depths.

As found in the literature, and during preliminary testing, lesion size can be readily increased using the focal delivery of a high NaCl infusion, prior to energy application. We consider here that it should be possible to create the final embodiments of such devices with additional pacing/sensing, temperature monitoring, and active deployment: this should be technologically feasible using commercially available products and SLA rapid prototyping.

INTRODUCTION

The field of cryo therapy is rapidly expanding with many novel devices and associated procedures currently under development or in clinical trials [1] [2] [3] [4]. For example, recent search of the clinical trials database for *cryoablation* yielded over sixty

results. The most common application of cryoablation is the destruction of tumors in the lung, liver, breast, kidney, and prostate. Use of cryoablation in the cardiovascular system is gaining popularity due to the inherent advantages over conventional ablation energy sources and novel therapies, such as peripheral vasculature cryoplasty. Nevertheless, one of the unique problems associated with ablation of the myocardium, it that fact that the heart is moving, it has very non-homogeneous wall thicknesses and it is associated with the potentials for causing stroke. This paper will discuss the development of a novel catheter for endocardial ablative procedures that allows for the targeted delivery of adjuvant drugs selected to increase efficacy of cryoablation lesions.

Recently, there are several touted benefits that cryoablation has been found to have over conventional RF energy ablation. In the eyes of most, relative to inducing lesions with the heart, the highest importance is patient safety. Cryoablation for the treatment of cardiac arrhythmias has been found to have a 5.6 fold lower risk of thrombus formation versus RF energy [5]. This is of great concern when performing procedures in the left side of the heart. In the right side of the heart emboli are essentially filtered out by the lungs, causing blockage of blood flow to a portion of the lung and eventually necrosis of the part of the lung being supplied by the blocked artery. This is usually asymptomatic because the majority of the lung is still functioning. In the left side of the heart emboli can have much graver consequences by traveling to the brain or coronary vasculature causing strokes and/or myocardial infarctions, respectively. Interestingly, the use of cryoablation has also been associated with lower immune responses, even being described as immunosuppressive [7].

Most current systems used to deliver cryoenergy also have the ability to perform cryomapping. Generally, a short period of -30°C energy, versus -70°C for permanent ablation, is used to “stun” the myocardium temporarily (Jensen-Urstad). This can be beneficially exploited during procedures requiring ablation near the conduction system of the heart, such as the AV node [8]. This allows the physician to test the location of a lesion before making it permanent and also to observe the electrophysiological effects of placing a lesion in that exact position. It is important to note that, to date, the other energy modalities (e.g., RF) cannot offer this assurance to the physician.

The iceball formation associated with cryoablation also offers the benefit of stabilizing the catheter. The natural motion of a beating heart can cause catheters to move around substantially within it. To maintain the desired position, physicians must apply pressure against the endocardial surface with the catheter, which in some anatomic locations may be difficult to achieve. Furthermore with using such energy sources, the pressure must be maintained by the physician and it has been found that higher pressures on the wall can lead to charring, crater formation, and perforation [9]. One can imagine a physician wanting to be absolutely sure that their catheter will not move during the application of energy and applying more force than necessary. This can lead to the negative effects of emboli, as discussed earlier, or perforation which can cause cardiac tamponade, which will lead to death if not remedied. . In contrast, when using a cryogenic based catheter, after a few seconds the catheter is anchored to the desired

location of endocardium by the iceball and added pressure during localizing the catheter can be released.

Of utmost importance to the success of cardiac ablative procedures is the creation of transmural lesions. A lesion that is not transmural in some patients will not completely block conduction and may therefore immediately or over time be clinically ineffective. Thus it is important to note, that near the edge of a formed iceball there is an intermediate zone where incomplete destruction exists, leading to ineffective lesions [10]. Often such an iceball boundary can be visualized using ultrasound. However, the value of this imaging is limited because it is known that a zone close to the outside of the iceball is often not completely ablated and these zone can be difficult to visualize clinically in a beating heart. Hence, to aid in the effectiveness of placed lesions, adjuvant therapies have been investigated by several authors [12] [7] [11]. Importantly, these therapies have been shown to reduce the size of the incomplete kill zone and beneficially make the visualization of iceballs better predictors of lesion sizes, while simultaneously creating more complete lesions.

Adjuvant therapies can also lead to enhanced destructions of tissues at warmer temperatures. This can even lead to the ablative region being outside of the iceball. It is considered that with some tuning of concentration and delivery dosage, cryoablation with adjuvant therapy should make the lesion size match the iceball size. This could be of great benefit with the growing use of 3D echocardiography (reducing fluoroscopy times during such procedures), allowing for real-time visualization of lesion formation. This could also allow for effective ablation lesions to be created at higher temperatures and reduction in damage to adjacent anatomy.

It has been reported that adjuvant therapies can work via substantially different pathway and can be generally classified into four groups: thermophysical, chemotherapeutic, cytokine/vascular agents, and immunomodulators [7]. More specifically, TNF- α has been investigated to increase the immune and inflammatory response after a cryoablation [11]. Yet, this type of treatment will probably meet some opposition from clinicians in the cardiac arena, due to concern over of the actions of TNF- α on “healthy” tissue; but may be of great use in the field of oncology. Thus we propose here that the initial focus of novel ablation devices, like the one described here, will be on the delivery of thermophysical adjuvants: due to their relatively benign methods of action. Nevertheless, we believe that the proposed device designs could be used to deliver any class of adjuvant.

In general, thermophysical adjuvants work primarily by modulating physical ice formation. Examples of these agents include salt solutions (NaCl, KCl, etc.) [11], amino acids [11], and proteins. The salt and amino acid adjuvants can cause secondary, or eutectic ice formation which has been shown to enhance cell death in the warmer temperature range of -21 to -5°C [7]. More specifically, NaCl eutectic ice formation has also been shown to cause a decrease from 64 to 18 percent cell viability at -25 °C with all other parameters being constant (the only difference was formation of eutectic ice) [11].

Another interesting thermophysical adjuvant is a class of proteins called antifreeze proteins (AFP). In high concentration they have been shown to modulate ice formation into a sharper, needle-like shape. This causes greater damage to cell membranes and tissue structures. In lower concentration they actually have cryo protective action which could be particularly useful when ablating near areas such as the AV node.

The device approach described here is primarily intended to increase lesion creation efficacy and/or intraprocedural evaluation. It is proposed that such an injectable catheter will have greatest utility in situations with larger tissue mass, like the ventricles, versus thin walled structures, like the atria. Therefore, ventricular or septal ablative procedures are envisioned as the primary application for this device.

So to increase intraprocedural evaluation and monitoring of lesions the next generation versions of such catheters could also employ sensing/pacing capabilities and temperature monitoring at the catheter tip and/or at the adjuvant delivery needle. Such capabilities have been incorporated in many types of thermal specific ablation catheter so to provide the physician with additional information and capabilities. For example, one can imagine a situation where an adjuvant was delivered into the middle of the myocardium. After delivery, the energy application begins and the controller can then monitor the catheter tip (endocardial) temperatures as well as the mid myocardial temperatures (needle tip), hence to better assess lesion progression. As such it is predicted that the user will be then better informed as to the length of time that the energy should be applied. After the lesion is assumed complete, entrance and exit block testing could be performed using the pacing and sensing capabilities of the delivery needle. Entrance and exit block testing is standard electrophysiological testing to evaluate lesion sets and their electrical isolation abilities. In other words, this will provide more accurate evaluations of transmural of formed lesions, if the pacing and sensing are performed within the tissue. The needle/catheter approach will also provide higher thermal transfer within the tissue and that alone should aid in the creation of transmural lesions.

Methods

A prototype catheter was created by grafting an injectable catheter onto a CryoCath Freezor Xtra 5mm catheter as seen in Fig. 1. The grafting allowed the prototype to perform ablation and articulation uninhibited. The needle catheter had the capability to allow the user to define the final needle depths.



Figure 1: A functional catheter prototype with injection needle pre-deployed at 5 mm.

To test the ability of the catheter to create lesions, ablations were performed on freshly isolated swine skeletal muscle: which was selected as a test tissue because of its homogeneity and the fact that the heart itself has similar composition. This skeletal muscle biopsy was submerged in 37°C Krebs's buffer to help simulate a physiologic environment. Ablations were performed for a three minute period with a one minute infusion of 14.6% NaCl at 1 mL/min by syringe pump started 30 seconds prior to ablation, similar to what is described by Bhowmick *et al.* A photo of the setup appears in Fig. 2. In this protocol, the optimal time to display a detectable lesion was found to be a three minute ablation treatment. Therefore, three minute cryoablation periods were used for subsequent testing. The injection catheter was set for a depth of 5 mm for all tests. For the control group, the procedures and needle punctures were performed exactly as in the treatment group but without NaCl infusions. It should be noted that this concentration of NaCl alone, was found to not cause a significant level of direct tissue damage by itself [13].



Figure 2: Experimental setup with Cryo Console, syringe pump, and test sample in 37°C Krebs buffer.

To macroscopically examine lesion size a standardized triphenyltetrazolium chloride (TTC) assay was [14] [12]. TTC stains for intracellular dehydrogenase activity;

therefore, viable tissue stains red and nonviable tissue remains gray or white. Fig. 3 shows the sample with high concentration NaCl before stain and Fig. 4 shows the same sample after staining and sectioning. For analysis, tissue was sliced parallel to the injection to yield lesion cross sections and immersed in 1% TTC in phosphate buffer solution for 45 minutes at 37°C. Slices were then photographed with a caliper set to 20 mm included for reference and placed in formalin for storage. Images were analyzed for area and depth using ImageJ (NIH) software. If an area was questionably part of a lesion it was included regardless, therefore results more accurately represent the area at risk rather than the “kill zone”. One tailed paired T-tests were performed with statistical significance set at $p < 0.05$.

Results

As seen when comparing Fig. 4 to Fig.5, the sample with the adjuvant therapy showed a much larger lesion. Both Fig. 4 and Fig. 5 are tissue slices at a depth of approximately 5 mm perpendicular to the needle, which is also the injection depth of the infusion needle. Although these are preliminary results, it is clear that the adjuvant did induce a significant increase in lesion dimensions. In Fig. 5 the lesions are barely evident versus Fig. 4 it is clear that there are large lesion areas. Effectiveness of adjuvants is already supported in the literature, but a small sample of lesions were created to support the proof concept (N=3).



Figure 3: High NaCl treatment clearly shows large lesions even prior to staining with TTC.

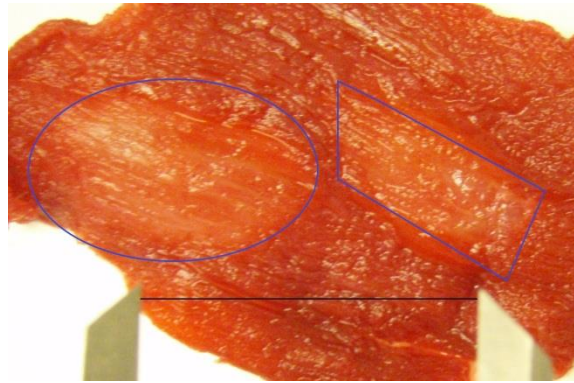


Figure 4: TTC stained three minute ablation sample with 1 ml high NaCl infusion. Lesions are outlined in blue to delineate for the reader. The black scale bar between the calipers is 20 mm.

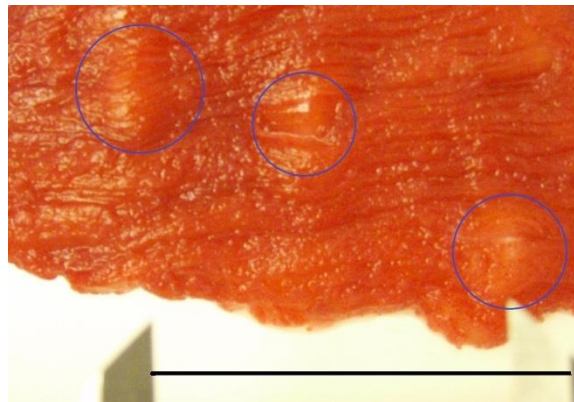


Figure 5: Control sample with three minute ablation and no infusion. Lesions are outlined in blue to delineate for the reader. The black scale bar between the calipers is 20 mm.

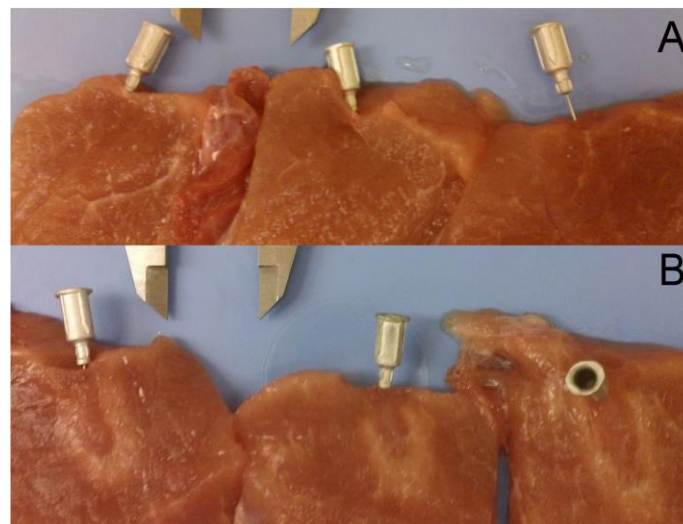


Figure 6: Cross sections of ablation lesions perpendicular to injection needle. Calipers are set to 20 mm and needles are indicating where injection catheter was positioned. The control group is on top labeled A and the 1 minute NaCl infusion is on bottom labeled B.

In Fig. 6 it is clear that even prior to staining the high NaCl infusion group created much larger lesions, whereas the non-infusion group appeared almost unchanged. To quantify the difference, TTC staining of cross sectional area perpendicular to the depth of the needle was performed and analyzed using image J. The high NaCl infusion group showed statistically significant deeper and larger lesions than the control as seen in Fig. 7 and Fig. 8.

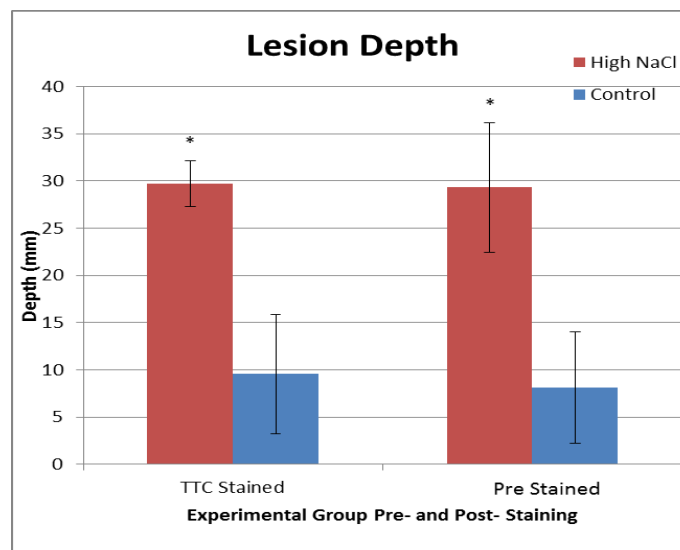


Figure 7: Graph of lesion depth between experimental groups. The high NaCl infusion had significant impact on both pre- and post stained analysis.

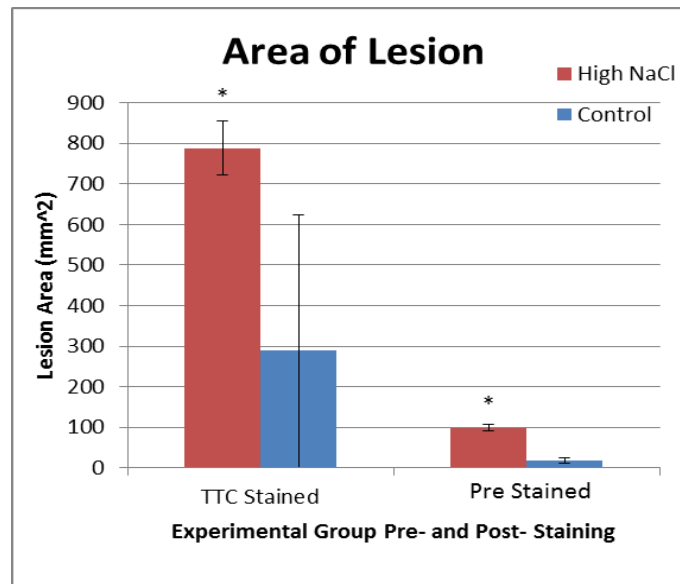


Figure 8: Graph of lesion perpendicular area between experimental groups. The high NaCl infusion had significant impact on both pre- and post stained analysis.

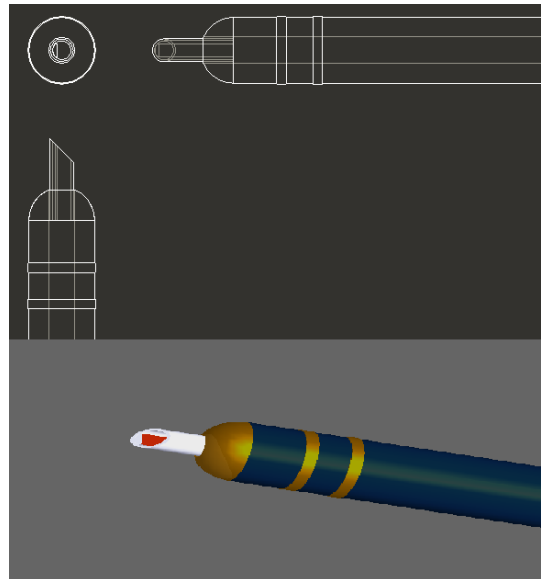


Figure 9: An envisioned future prototype consisting of a retractable, concentric needle. The gold tip is the main ablative segment of the catheter. The gold rings are pacing electrodes. The small red area within the needle represents a resistive style heating element designed to melt through the iceball prior to injection of needle. Pacing/sensing from the needle could be achieved by insulating the entire needle except for the very distal surface (beveled surface) .

Discussion/Future work

As the results of this preliminary study and support of previously publications show, adjuvants can have significant impact on the modulation of lesion size and depth. The reason for the large variation in the control group lesion depth is because only one of the lesions actually showed virtually any depth. The other two were hardly visible. The same is true for the TTC stained area of lesion for the control group. In that case, two samples showed virtually no destruction of tissue and one sample showed large destruction. It is the author's opinion that this is actually due to connective tissue not being stained well in that sample by the TTC assay. The author believes this because the lesion, as shown by lack of red staining, was not evident at the surface, but at depth of approximately 5 mm. Indicating that the lack of stain was not due to the ablation, but another factor. Nevertheless, it was included because the protocol called for including any regions of possible damage.

Although the underlying concepts discussed herein have been proven at the bench, until now there has been no discussion of leveraging the concept of adjuvants in the cardiovascular area. The results show that it is feasible to deliver agents via catheter and with the proper tuning of adjuvant concentration and volume ice formation can be modulated however the user desires.

As described here, we envision that the design and use of such adjuvant/ablation catheter could be of high utility for electrophysiologist performing cardiac cryo-ablation procedures. Ideally, the user would initially map the area and determine exactly where lesions are needed. Such a catheter design may have its maximal utility if focal lesions are needed in the ventricular or septal myocardial areas. In such a procedure, the catheter would be navigated under fluoroscopy to the desired position and then the needle would be deployed to the desired depth. This deployment could also be aided by prior iceball formation: i.e., an initial cryo treatment could be turned on for a short period to anchor the catheter to the endocardial surface and then the needle plunged into the myocardium: the needle may need to be distally heated to allow for advancement (see Fig. 9). This in turn may help prevent transmural perforations, because the physician is not pushing on the entire catheter to insert the needle; only the needle portion is being extended. This is also envisioned being deployed actively, meaning the physician would set the desired depth, push a button, a small iceball would form to anchor the tip to the endocardial surface, and the needle would extend through the ice ball deeper within the myocardial tissue. Provided the depth was set correctly, and the catheter anchored to the myocardium by an iceball, there would be virtually no chance of perforation.

Once the needle was deployed the adjuvant could be delivered and again cryo therapy applied, but this time for a therapeutic duration. During such, the temperatures could then be monitored at both the cryo and needle tips (endocardial surface and within the myocardium, respectively). This should provide the physician a better idea of how far and how fast the lesion is progressing within the myocardium. After the lesion is made, it would then be evaluated for completeness by performing entrance and exit block testing using this same catheter system. This could also be facilitated by pacing and sensing from the tip of the needle to determine electrical isolation. Performing such test at known

depths within the myocardium should provide for better transmural lesion evaluation, versus testing at the endocardial surface alone.

For complete utilization of such a described device, a computer controlled temperature sensing, electrical sensing, and pacing system should be specifically designed or an application program developed for existing systems. This would require electrical isolation of the needle tip from the main cryocatheter, which should be technologically feasible using electrically insulated coatings to control electrical routing and small thermocouples available commercially. A system for active deployment of the needle also needs to be developed.

To ideally test early prototypes of such a device, animal models with histologic assays would be required. The author also proposes to use the Visible Heart preparation for evaluation. The Visible Heart preparation uses an isolated swine heart on a modified double pump system which circulates a clear buffer perfusate. Advantages of this setup include a thermodynamic environment very similar to that found physiologically, ease of endocardial access, and the ability to visualize tissue/device interaction using endoscopes. The lesion size can then be evaluated macroscopically using methods similar to those described above and subsequent histological studies can also be performed.

The primary goal of this novel design of a cryoablation catheter system is to create a more well defined lesion and also to provide physicians more intraprocedural information and hence more treatment options. Hopefully, this will lead to fewer follow up treatments, as stated by multiple professional bodies in the document titled *EHRA/HRS Expert Consensus on Catheter Ablation of Ventricular Arrhythmias*, "Inability to create a sufficiently deep lesion to ablate VT is an important cause of ablation failure...". We consider that such a system should provide for better realtime assessments and more procedural options, so to allow the electrophysiologist more confidence in their treatment, hence in turn minimize secondary procedures, and lowering risks of damaging adjacent cardiac structure also leading to fewer complications.

NOMENCLATURE

RF- Radiofrequency

AFP-Antifreeze Proteins

ACKNOWLEDGMENTS

The author would like to thank the Visible Heart Laboratory staff and Medtronic for the use of a CryoConsole and spare CryoCath Freezor catheter for prototyping. Funding for the author's research assistantship was provided partially by the GAANN fellowship and Medtronic Visible Heart research contract.

REFERENCES

- [1] Abboud M. "Wide area ablation of myocardial tissue." USA: Patent 7794455 B2. 14 September 2010.
- [2] Joyce J. "Cryogenic angioplasty catheter." USA: Patent 6428534 B1. 6 August 2002.

- [3] Wittenberger D. "Variable geometry tip for a cryosurgical ablation device." USA: Patent 6106518. 22 August 2000.
- [4] Khairy P, *et al.* "A novel hybrid transcatheter ablation system that combines radiofrequency and cryoenergy." *Journal of Cardiovascular Electrophysiology*, 2008, **19**(2): pp. 188-193.
- [5] Khairy P, *et al.* "Lower incidence of thrombus formation with cryoenergy versus radiofrequency catheter ablation." *Circulation*, 2003, **107**(15): pp. 2045-2050.
- [6] Jensen-Urstad M, *et al.* "High success rate with cryomapping and cryoablation of atrioventricular reentry tachycardia." *Pacing Clinical Electrophysiology*, 2006, **29**(5):487-489
- [7] Goel R, *et al.* "Adjuvant approaches to enhance cryosurgery." *Journal of Biomechanical Engineering*, 2009, **131**(7): 074003.
- [8] Perez-Castellano N, *et al.* "High resistance of atrioventricular node to cryoablation: a great safety margin targeting perinodal arrhythmic substrates." *Heart Rhythm*, 2006, **3**(10): pp. 1189-1195.
- [9] Di Biase L, *et al.* "Relationship between catheter forces, lesion characteristics, "popping", and char formation: experience with robotic navigation system." *Journal Cardiovascular Electrophysiology*, 2009, **20**(4): pp. 436-440.
- [10] Hoffmann NE, Bischof JC. "The cryobiology of cryosurgical injury." *Urology*, 2002, **60**(2 supplement): pp. 40-49.
- [11] Han B, *et al.* "Improved cryosurgery by use of thermophysical and inflammatory adjuvants." *Technol. Cancer Res. Treatment* 2004, **3**(2): pp. 103-111.
- [12] Wang CL, *et al.* "An amino acid adjuvant to augment cryoinjury of MCF-7 breast cancer cells." *Cryobiology*, 2008, **57**(1): pp. 52-29.
- [13] Bhowmick S, *et al.* "Evaluation of thermal therapy in a prostate cancer model using a wet electrode radiofrequency probe." *Journal of Endourology*, 2001, **15**(6): pp. 629-640.
- [14] Xiao YF, *et al.* "Pericardial delivery of omega-3 fatty acid: a novel approach to reducing myocardial infarct sizes and arrhythmias." *American Journal of Physiology Heart and Circulatory Physiology*, 2008, **294**(5): pp. 2212-2218.